



The University of  
**Nottingham**

UNITED KINGDOM • CHINA • MALAYSIA

# **Exploration and development of domestic thermoelectric cogeneration system**

**Xiaofeng Zheng, BEng. MEng**

**Thesis submitted to the University of Nottingham  
for the degree of Doctor of Philosophy**

**October 2013**

## ABSTRACT

Due to quiet operation, no moving parts, long lifespan and compact structure, the thermoelectric application has become a potential green technology which has been used in different areas in the efforts of contributing to achieve simplified and compact system structures and environmental friendliness. Its applications cover a wide range from the earliest application on kerosene lamp to aerospace applications, transportation tools, industrial utilities, medical services, electronic devices and temperature detecting & measuring facilities. Its disadvantage lies in the low conversion efficiency which only converts small amount (for  $\text{Bi}_2\text{Te}_3$ , up to 5%) of harvested energy to electrical power. It makes the use of the TEG system far from being economically feasible due to long cost recovery period. Consequently, its use is limited to specialised area where it is unnecessary to consider the cost of the thermal energy input and system cost recovery.

This research aims to explore a way of widening the application range of thermoelectric generation based on introducing a potential direction of improving energy utilisation efficiency to a higher level by adopting thermoelectric cogeneration concept in residential house. It focuses on investigating the practicality of using thermoelectric applications in domestic sectors where the large amount of heat is exhausted to environment without being used and developing thermoelectric cogeneration system to generate electricity and produce pre-heated water for domestic use by recovering the waste heat from the domestic boiler and utilising the on-site solar energy. With the conversion efficiency given by the current commercially available thermoelectric modules, the optimised heat exchanging regimes and systems for thermoelectric applications have been comprehensively studied from the aspects of system design, integration, experimental study, numerical simulation and modification. The importance and necessity of effective heat exchanging methods have been emphasised by the experimental and numerical proofs for the development of a domestic thermoelectric cogeneration system with higher thermal efficiency. The impacts of this domestic energy solution have been evaluated from the aspects of the improvement for outdoor environment and indoor energy profile, as well as economic benefit.

For the flue gas heat exchanger, the model with sudden expansion and gradual constriction has been identified gives in terms of overall performance. The model with sudden expansion, gradual constriction and staggered pipe layout and the one with sudden expansion, gradual constriction and inline pipe layout show better overall performance than other models. Among these two models, the one with staggered pipe layout shows better performance than the one with inline pipe layout in the velocity range of 3.6m/s-5m/s, whilst the one with inline pipe layout shows better performance between 0-3.6m/s. For the cold side heat exchanger, the one with four  $\phi 5\text{mm}$  branch channel angled at 90 against the main channel delivers the best overall performance out of 9 cooling plates built according to three variables. Experimental studies show the one-stage TCS produces more power than the two-stage TCS does when the heat input is supplied at 47W and 60W. As the heat input increases, the power output of two-stage TCS gets closer to that of one-stage TCS.

In the system construction and assembly, uneven assembly can lead to a 20% drop in conversion efficiency. The pressure load at 181psi gives the highest power output out of five load values, which are 136psi, 159psi, 181psi, 204psi and 227psi, respectively. In comparison with individual assembly, module thickness difference in whole



assembly degrades the system conversion efficiency. The cost recovery period of deploying this system in a residential house installed with a 24kW boiler and a 1m<sup>2</sup> solar collector has been evaluated. Based on the conversion efficiency and thermal efficiency that is 4% and 67% at 130°C temperature difference, the house can produce 98W electricity and 1640W useable heat when the boiler is running and the contribution from the solar energy is included. It takes less than 4.2 years to recover the system cost.

**Key words:** *Thermoelectric co-generation, domestic, electrical power, thermal energy, conversion efficiency, thermal efficiency*

## **PUBLICATIONS**

- X.F. ZHENG, C.X. LIU, R. BOUKHANOUF, Y.Y. YAN, W.Z. LI, 2014. Experimental study of a domestic thermoelectric cogeneration system. *Applied Thermal Engineering*, 62(1), 69-79.
- X F Zheng *et al* 2012. Investigations on an oriented cooling design for thermoelectric cogenerations. *J. Phys.: Conf. Ser.* 395 012062.
- Zheng XF, Yan YY, Simpson K. A potential candidate for the sustainable and reliable domestic energy generation-Thermoelectric cogeneration system. *Applied Thermal Engineering*, 53 (2013) 305-311.
- X.F. ZHENG, Y.Y. YAN, 2010. A biomimetic smart control of viscous drag reduction. *Advances in Natural Science*,3(2), 139-151.
- N. GAO, Y.Y. YAN, X.Y. CHEN, X.F. ZHENG, 2010. Superhydrophobic composite films based on THS and nanoparticles. *Journal of Bionic Engineering*, 7(Suppl), 59-66.
- G. WANG, X.F. ZHENG, S.T HU, "Study on Effect of Fresh Air Mode on Indoor Pollutant Dispersion," *iceet*, vol. 3, pp.115-118, 2009 International Conference on Energy and Environment Technology, 2009.

## ACKNOWLEDGEMENTS

I would like to express my gratitude to Professor Yuying Yan for his kind support, encouragement and valuable advice on my research work during my PhD study period in the University of Nottingham. Together with the patient supervision, his constant support from international conferences, academic publication to workshop training, enabled me to gain confidence, accumulate important experience and build up network, which all together made this whole PhD journey clear, positive and enjoyable for me. Also thanks to Dr. Rabah Boukhanouf and Dr. Jie Zhu for their patient help on publication review and valuable advice on my research work, and to the technicians such as Dave-s for their help on building test rigs as well as Nan and Bo for their friendship and advice on various aspects.

I would like to pay my gratitude and respect to the Division of Energy and Sustainability and the University of Nottingham for partially funding my PhD study and the consistent efforts in involving itself with tackling the global issues such as food security, energy crisis and sustainability. I feel deeply fortunate and proud that I can conduct my PhD study in this special environment, that I can be part of this mission and “grow” up at the same time.

Many thanks go to my great friends that I have got to know in the UK in the last more than three years, who have given me immense support and help in different aspects during my PhD study, such as Zeny, Lyn and Sophie, who have also brightened my time in this department.

Also many thanks to my great friends in China such as CC, Junru, Shaoqing, Xianyin and Jie and other friends for their financial and mental support to my PhD study. My sincere gratitude also goes to great friends that I have known since 2006, such as Anne, Derek, Martin, Vanessa, Clive and many other friends for their great friendship and support.

At last but not the least, my love and gratitude goes to my dear loving parents, brother and sister in law, family Zhu and also others in the big family for this countless love, support and care in encouraging me to chase my dreams. Without them, I would not be where I am now. I feel guilty to my family that I have been away from them for so long. However, I feel extremely grateful for their understanding and support, especially for my brother who has been taking such a great care of the family.

# CONTENTS

ABSTRACT.....	i
PUBLICATIONS.....	iii
ACKNOWLEDGEMENTS.....	iv
CONTENTS.....	v
LIST OF TABLES.....	viii
LIST OF FIGURES.....	ix
NOMENCLATURE.....	xvi
<b>Chapter 1 Introduction.....</b>	<b>1</b>
1.1 Background.....	1
1.2 Fundamentals of Thermoelectrics.....	3
1.3 Aims and objectives.....	7
1.4 Research Methodology.....	9
1.5 Outline of thesis.....	11
<b>Chapter 2 Literature review.....</b>	<b>13</b>
2.1 Material development.....	13
2.1.1. Commercialization.....	13
2.1.2. Development of high efficiency thermoelectric modules.....	15
2.2 Applications.....	24
2.2.1. Heat engines.....	24
2.2.2. Thermoelectric generators.....	27
2.3 Summary.....	33
<b>Chapter 3 Domestic house energy analysis.....</b>	<b>34</b>
3.1. Energy consumption analysis.....	34
3.2. Profile of heating demand.....	36
3.3. Heating methods.....	36
3.3.1 Solar power.....	36
3.3.2 Boiler.....	37
3.3.3 Wood burning/biomass stove.....	38
3.3.4 Furnaces.....	38
3.4. Previous research.....	39
3.5. Material selection.....	40
3.6. Availability.....	40
3.7. Summary.....	43
<b>Chapter 4 Heat sourcing.....</b>	<b>44</b>
4.1 Background.....	44
4.2 System description.....	45

4.3	Solar heat exchanger .....	47
4.4	Boiler flue heat exchanger.....	49
4.4.1	Design and investigation plan .....	49
4.4.2	Identification of the suitable models .....	55
4.4.3	Identification of the modified models .....	77
4.4.4	Detailed modification.....	80
4.4.5	Other considerations .....	82
4.5	Summary .....	83
<b>Chapter 5 Heat dissipation.....</b>		<b>84</b>
5.1.	Design.....	84
5.2.	Experiment methodology .....	89
5.3.	Hydraulic performance.....	91
5.4.	System performance .....	93
5.4.1	Effect of coolant flow velocity .....	96
5.4.2	Effect of cooling temperature .....	100
5.4.3	Dynamic thermal response of the system .....	101
5.5.	Further modifications based on CFD .....	104
5.5.1	Individual assembly .....	104
5.5.2	Whole assembly .....	131
5.5.3	Integration .....	134
5.6.	Summary .....	134
<b>Chapter 6 Experimental investigations.....</b>		<b>136</b>
6.1.	Theoretical analysis.....	136
6.1.1	One-stage TCS .....	136
6.1.2	Two-stage TCS .....	140
6.2.	Experimental study for one stage TCS.....	142
6.2.1	System description .....	142
6.2.2	Measurement .....	146
6.2.3	Electric performance .....	147
6.2.4	Thermal performance.....	150
6.3.	Experimental study of Two-stage TCS .....	151
6.3.1	System introduction .....	151
6.3.2	Performance .....	152
6.4.	Energy management .....	154
6.4.1	Thermal energy .....	154
6.4.2	Electrical power .....	155
6.5.	Mechanical assembly .....	158

6.5.1	Assembly introduction.....	158
6.5.2	The optimum pressure load.....	161
6.5.3	Washer configuration.....	162
6.5.4	Uneven assembling .....	163
6.5.5	Conclusion .....	165
6.6.	Summary .....	165
<b>Chapter 7 Discussion, conclusion and future work .....</b>		<b>167</b>
7.1.	Discussion .....	167
7.1.1.	Candidate designs .....	167
7.1.2.	Economic analysis .....	171
7.1.3.	Environmental impact.....	178
7.2.	Conclusion.....	179
7.3.	Future work .....	181
<b>Reference .....</b>		<b>183</b>

## **LIST OF TABLES**

Table 2-1 Comparison of PV and TE	15
Table 3-1 Yearly sum of gas consumption per consumer in the UK [1]	37
Table 3-2 Furnace combustion performance	39
Table 4-1 Physical properties of flue gas ( <a href="http://www.pipeflowcalculations.com/tables/flue-gas.php">http://www.pipeflowcalculations.com/tables/flue-gas.php</a> )	55
Table 5-1 Power output after heat input is cut off from 53W, 80W, 100W and 133W	103
Table 5-2 Specifications of the thermoelectric generators	109
Table 5-3 Average temperature of the module cold side (°C)	133
Table 5-4 Mass flow rate of each sub-channel (kg/s)	133
Table 5-5 Minimum flow rate through boiler (L/min)	134
Table 6-1 Seebeck coefficient of semiconductor elements of TE module	149
Table 6-2 Power generation performance of one stage and two stage thermoelectric cogeneration system	153
Table 6-3 Specifications of torque wrench	160
Table 6-4 The pressure loads used for the test	161
Table 7-1 Cost estimation of a TCS with 16 thermoelectric modules	174
Table 7-2 Hourly availability of solar energy and boiler waste heat in the two-bedroom bungalow of each month in a whole year in Northampton (kW)	176
Table 7-3 Hourly output of electrical power of each month in a whole year in Northampton (kWh)	177

## **LIST OF FIGURES**

Figure 1-1 Energy consumption of different sectors in the UK (1980-2010)	1
Figure 1-2 Energy consumption chart in different industrial sectors	2
Figure 1-3 Schematic diagram of thermoelectric generation	3
Figure 1-4 Cooling/Heating and Power Generation Thermoelectric Heat Engines	5
Figure 1-5 Typical thermoelectric module construction	5
Figure 1-6 Thermocouple for power generation	7
Figure 1-7 Top view of flue heat exchanger section of 3D models for numerical simulations conducted at two stages	9
Figure 2-1 TE Material Market, 2023 Projection: A. Power generation; B. Cooling/Heating	14
Figure 2-2 ZT values of state of the art and JPL improved thermoelectric materials as a function of temperature A. N-type; B. P-type	16
Figure 2-3 Dimensionless figure of merit ZT for Bi <sub>2</sub> Te <sub>3</sub> /Sb <sub>3</sub> Te <sub>3</sub> superlattices, PbTe-based quantum dot superlattices	17
Figure 2-4 Examples of results of surface treatment by plasma	18
Figure 2-5 Concept of surface treatment of powder	18
Figure 2-6 Relationship between oxygen concentration and performance	18
Figure 2-7 Shifting Z value [52]	19
Figure 2-8 Schematic of a segmented thermoelectric generator using segmented thermoelectric material developed at JPL	20
Figure 2-9 Schematic of segmented material	20
Figure 2-10 Efficiencies of different TE materials	21
Figure 2-11 Calculated thermoelectric materials conversion efficiency as a function of ZT for various segmented generators operating at different $\Delta T$	21
Figure 2-12 Schematic diagram of thin film thermoelectric module	
Figure 2-13 Schematic diagram of Peltier effect for cooling and heating	24
Figure 2-14 Vehicular Climate Control System amounted in seat and installation rate	25
Figure 2-15 Schematic diagrams of an integrated thermoelectric microcooler with infrared components integrated onto cooled central region (a) Plane view and (b) cross-sectional view.	27
Figure 2-16 Temperatures of exhaust system components for a gasoline engine and a diesel engine	28
Figure 2-17 Energy consumption distribution of industry sectors in the UK	31
Figure 2-18 Chart of energy consumption in different industrial sectors	31
Figure 3-1 Saving in space heating due to better insulation and heating efficiency in the UK between 1970 and 2007	34
Figure 3-2 Hourly heating demand of a UK two-bed bungalow in a year	35
Figure 3-3 Purposefully designed fuel-powered furnace for central heating system integrated with thermoelectric generation [131]	38
Figure 3-4 Thermal cycle of thermoelectric cogeneration system	41
Figure 4-1 Heat exchange types in thermoelectric applications	44
Figure 4-2 Concept diagram of domestic thermoelectric cogeneration system	46
Figure 4-3 Schematic diagram of hot side heat exchanger	48
Figure 4-4 Rating chart of domestic boiler by SEDBUK	50
Figure 4-5 Roof installation and wall installation of boiler flue pipe (A. Roof installation; B. Wall installation.)	50



Figure 4-6 Typical boiler flue pipe	50
Figure 4-7 Investigated models of flue heat exchanger	52
Figure 4-8 Concept of thermoelectric cogeneration system for domestic use	53
Figure 4-9 Inline layout and staggered layout	54
Figure 4-10 Flow patterns observed by Brauer [145] for (a) staggered and (b) inline finned tube banks	54
Figure 4-11 Schematic of flue heat exchanger integrated in boiler exhaust pipe	56
Figure 4-12 Computational domain of flue heat exchanger	58
Figure 4-13 Mesh details of flue heat exchanger	59
Figure 4-14 Velocity contour in the flow direction of flue heat exchanger	60
Figure 4-15 Staggered layout (0) and Inline layout (3) ( $S=2.5d$ )	60
Figure 4-16 Velocity contour of central horizontal plane at different flue gas velocity	61
Figure 4-17 Temperature contour of central horizontal plane at different flue gas velocity	62
Figure 4-18 Outlet temperature when the flue gas is exhausted at different velocities	62
Figure 4-19 Effectiveness of flue heat exchanger with staggered and inline layout at different velocities	63
Figure 4-20 Heat transfer coefficient of flue heat exchanger with staggered layout and inline layout	63
Figure 4-21 Transferred heat of staggered layout and inline layout at different flue gas velocity	64
Figure 4-22 Pressure drop of staggered layout and inline layout at different flue gas velocity	64
Figure 4-23 Fan power of staggered layout and inline layout under different flue gas velocity	64
Figure 4-24 Net energy gain under different flow velocity	65
Figure 4-25 Cross sectional area ( $A_0=0.91A$ , $A_2=1.19A$ , $S=2.5d$ )	65
Figure 4-26 Pressure drop of models with cross section at 0.91A and 1.19A at different flue gas velocity	66
Figure 4-27 Velocity contour of central horizontal plane at different flue gas velocity	66
Figure 4-28 Fan power of the models with cross section at 0.91A and 1.19A at different flue gas velocity	67
Figure 4-29 Effectiveness of flue heat exchanger with different cross sections	67
Figure 4-30 Temperature contour of central horizontal plane at different flue gas velocity	68
Figure 4-31 Heat transfer rate of flue heat exchanger with 0.91A and 1.19A cross section	68
Figure 4-32 Net energy gain of flue heat exchanger with 0.91A and 1.19A cross section	69
Figure 4-33 Net energy gain of flue heat exchanger with different cross section area	69
Figure 4-34 Velocity contour of central horizontal plane at different flue gas velocity	70
Figure 4-35 Staggered layout with different pitch (A: $S_1=S_2=2.5d$ ; B: $S_1=S_2=2d$ )	71

Figure 4-36 Temperature contour of central horizontal plane at different flue gas velocity	71
Figure 4-37 Pressure drop of flue heat exchanger with different pitch	72
Figure 4-38 Pressure drop of flue heat exchanger with different pitch	72
Figure 4-39 Effectiveness of flue heat exchanger with different pitch	72
Figure 4-40 Heat transfer rate of pitch 2.0d and 2.5d	73
Figure 4-41 Net energy gain of flue heat exchanger with different pitch	73
Figure 4-42 Sudden junction (A) and gradual junction (B)	73
Figure 4-43 Velocity contour of central horizontal plane at different flue gas velocity	74
Figure 4-44 Pressure drop of models with sudden and gradual junction at different flue gas velocity	74
Figure 4-45 Temperature contour of central horizontal plane at different flue gas velocity	75
Figure 4-46 Effectiveness and heat transfer rate of flue heat exchanger with sudden junction and gradual junction at different flue gas velocity	75
Figure 4-47 Net energy gain of flue heat exchanger with sudden junction and gradual junction	76
Figure 4-48 Fan power need of all the investigated models of flue heat exchanger	77
Figure 4-49 Net energy gain of all the investigated models of flue heat exchanger	77
Figure 4-50 Modified models based on the previous numerical results	77
Figure 4-51 Velocity contour on the central horizontal plane of modified flue heat exchanger	78
Figure 4-52 Temperature contour on the central horizontal plane of modified cooling plates	79
Figure 4-53 Heat transfer coefficient between the heat pipes and flue gas of modified models	79
Figure 4-54 Heat transfer rate between the heat pipes and flue gas of modified models	80
Figure 4-55 Net energy gain of the five modified models	80
Figure 4-56 Temperature distribution on the exterior surface of fins and pipes	81
Figure 4-57 Pressure drop of M4 model before and after finned under different flow velocity	81
Figure 4-58 Cooling capacity of M4 before finned and after under different flow velocity	82
Figure 5-1 Typical fan cooling for thermoelectric power generation	84
Figure 5-2 Passive heat dissipating method- heat pipe sink (a. heat pipe; b. thermosyphonic heat sink)	85
Figure 5-3 Schematic diagram of individual assembly (a) and whole assembly (b)	86
Figure 5-4 Module damages caused by uneven and excessive pressure load	86
Figure 5-5 Thickness of 20 random thermoelectric modules	87
Figure 5-6 Single module performance in whole assembly (WA) and individual assembly (IA)	87
Figure 5-7 Cooling plate for thermoelectric cogeneration	88
Figure 5-8 The photo and schematic diagram of the single thermoelectric cogeneration block	89
Figure 5-9 Fabrication schematic diagram of multi channel cooking plate	89
Figure 5-10 Pressure drop test of cooling plates at different inlet velocity	90
Figure 5-11 Pressure drop and heat transfer test of the cooling plate	91

Figure 5-12 Hydraulic performance of the cooling plate	92
Figure 5-13 Pressure drop comparison of single channel (SC) and multi-channel (MC) cooling plates	92
Figure 5-14 Schematic diagram of test rig	93
Figure 5-15 Water temperature at the inlet of three cooling plates	94
Figure 5-16 Measurement of the system stabilizing time	94
Figure 5-17 Thermal efficiency with the heat inputs at 47W and 93W	94
Figure 5-18 Power output of three cooling plates	95
Figure 5-19 Conversion efficiency	95
Figure 5-20 Heat output	95
Figure 5-21 Thermal efficiency	96
Figure 5-22 Voltage output at different load resistance of the system integrated with 3mm, 4mm and 5mm cooling plate	96
Figure 5-23 Power output at different inlet velocity	97
Figure 5-24 Cold side temperature at different inlet velocity	97
Figure 5-25 Pressure drop and thermal resistance (TR) at different inlet velocity	97
Figure 5-26 Heat output and pressure drop vs. Inlet velocity (m/s) (PD represents pressure drop)	98
Figure 5-27 Conversion efficiency at different inlet velocity	98
Figure 5-28 Thermal resistance at different water velocity	98
Figure 5-29 Thermal efficiency at different inlet velocity	99
Figure 5-30 Temperature of inlet water (IWT) and TE cold side (CST) against fan operation	100
Figure 5-31 Temperature of TE hot side under different cooling condition	100
Figure 5-32 Thermal efficiency (SE) and conversion efficiency (CE) vs. Fan operation	101
Figure 5-33 Power output (PO) and heat output (HO) vs. Fan condition	101
Figure 5-34 Dynamic thermal response of the system	102
Figure 5-35 Power output and heat output in a test cycle	102
Figure 5-36 Storing performance at 53W, 80W, 100W and 133W heat input	103
Figure 5-37 Correlation between heat input and heat storing coefficient	104
Figure 5-38 Problem schematic of cooling plate on the module cold side	104
Figure 5-39 Physical models of investigated multi-channel cooling plates	107
Figure 5-40 Single channel cooling plate	108
Figure 5-41 Temperature result of multi-channel cooling plate attached with the module	108
Figure 5-42 Slots on the heat exchangers for the thermocouples (left to right: hot side, cold side)	109
Figure 5-43 The experimental result of TE module thermal conductivity	109
Figure 5-44 Cooling capacity and pressure drop of single channel cooling plate	110
Figure 5-45 Surface heat transfer coefficient (SHC) of flow channel, temperature at outlet and TE cold side surface	110
Figure 5-46 Schematic diagram of computing domain and meshing of cooling plate	112
Figure 5-47 Pressure drop against velocity of cooling water of single channel cooling plate	112
Figure 5-48 Cooling capacity and Surface heat transfer coefficient against velocity of cooling water (SC vs. MC)	113

Figure 5-49 Velocity distribution in flow channel of cooling plates with 5mm, 4mm and 3mm branch channel	113
Figure 5-50 Pressure drop of cooling plates with different branch channel dimensions	114
Figure 5-51 Temperature distribution on cold side surface of TE module attached with 5mm, 4mm and 3mm cooling plates	114
Figure 5-52 Temperature distribution in flow channel of cooling plates with 5mm, 4mm and 3mm branch channel	115
Figure 5-53 Cooling capacity of cooling plates with different branch channel dimension by numerical simulations	115
Figure 5-54 Cooling capacity of cooling plates with different branch channel dimension measured in experiment	115
Figure 5-55 TE hot side temperature using cooling plate with 3mm, 4mm and 5mm branch channel	116
Figure 5-56 TE cold side temperature using cooling plate with 3mm, 4mm and 5mm branch channel	116
Figure 5-57 Pumping power of the cooling plates with 3mm, 4mm and 5mm branch channel	117
Figure 5-58 Net energy gain of the cooling plates with 3mm, 4mm and 5mm branch channel	117
Figure 5-59 Surface heat transfer coefficient and HPPD of cooling plate with 3mm, 4mm and 5mm branch channel	118
Figure 5-60 Cooling plates with 4, 6 and 8 branch channels	118
Figure 5-61 Velocity contour of flow channel in cooling plates with 4, 6 and 8 branch channels (5mm)	119
Figure 5-62 Turbulence contour of water flow in cooling plates with 4, 6 and 8 branch channels (5mm)	119
Figure 5-63 Pressure drop of cooling plates with 4, 6 and 8 branch channels	120
Figure 5-64 Temperature contour of water flow in cooling plates with 4, 6 and 8 branch channels (5mm)	120
Figure 5-65 Temperature contour of water flow in cooling plates with 4, 6 and 8 branch channels (5mm)	121
Figure 5-66 Cooling capacity of cooling plate with 4, 6 and 8 branch channels	121
Figure 5-67 TE cold side temperature when using cooling plate with 4, 6 and 8 channels	121
Figure 5-68 Advanced modification of the cooling plate	122
Figure 5-69 Cooling plates with branch channels at angle 90°, 60° and 45°	123
Figure 5-70 Velocity contour of flow channel in cooling plates with branch channel (5mm) angle at 45°, 60° and 90°	123
Figure 5-71 Turbulence contour of flow channel in cooling plates with branch channel (5mm) angle at 45°, 60° and 90°	124
Figure 5-72 Pressure drop of cooling plates (5mm) with branch channel angle at 45°, 60° and 90°	124
Figure 5-73 TE cold side temperature contour using cooling plates with branch channel (5mm) angle at 45°, 60° and 90°	125
Figure 5-74 Temperature contour of flow channel in cooling plates with branch channel (5mm) angle at 45°, 60° and 90°	125
Figure 5-75 TE cold side temperature for cooling plates with branch channel (5mm) angle at 45°, 60° and 90°	126

Figure 5-76 Cooling capacity of cooling plates (5mm) with branch channel angle at 45°, 60° and 90°	126
Figure 5-77 Cooling capacity vs. TE hot side temperature	126
Figure 5-78 Cooling capacity of the cooling plates	127
Figure 5-79 Pumping power of the cooling plates	127
Figure 5-80 Pumping power plotted against thermal resistance	128
Figure 5-81 Net energy gain of the cooling plates against Reynolds number	128
Figure 5-82 Net energy gain level of the plates with different configuration	129
Figure 5-83 The Colburn j factor plotted against Reynolds number (Re is calculated according to the main channel)	129
Figure 5-84 The local resistance coefficient plotted against Reynolds number	130
Figure 5-85 Cooling plate concepts for whole assembly	131
Figure 5-86 Schematic diagram of channel structure and dimension at the inlet corner	132
Figure 5-87 Numbering of channel and module positions	132
Figure 5-88 Domain and temperature distribution of the module cold side	133
Figure 5-89 Standard deviation of the cold side temperature of each thermoelectric module	134
Figure 6-1 Schematic diagram and photo of TCS with single module	137
Figure 6-2 Schematic diagram of heat flux distribution in single-stage TCS	138
Figure 6-3 Schematic diagram of TCS working mechanism, A. Single-stage TCS; B. Multi-stage TCS	140
Figure 6-4 Schematic diagram of hot side heat exchanger	143
Figure 6-5 Whole assembly and individual assembly	143
Figure 6-6 Schematic diagram and photo of the single TE block system	144
Figure 6-7 Photo and specifications of the electric heater	144
Figure 6-8 Acquisition data unit	145
Figure 6-9 Photos and specifications of thermocouples	145
Figure 6-10 Photo and specifications of inline flow transmitter	146
Figure 6-11 Cooling loop for single-stage TCS	146
Figure 6-12 Circuit for measuring the maximum power output and internal resistance	147
Figure 6-13 Maximum power output	148
Figure 6-14 System open voltage output and power output at different temperature difference	148
Figure 6-15 Maximum power output and conversion efficiency Vs. Heat source temperature	149
Figure 6-16 Experimental voltage output and theoretical voltage output under different temperature difference	150
Figure 6-17 Experimental power output and theoretical power output under different temperature difference	150
Figure 6-18 Thermal efficiency and conversion efficiency under different temperature differences	151
Figure 6-19 Heat output (HO) and corresponding temperature rise of coolant that flows through the cooling plate at different inlet coolant velocity	151
Figure 6-20 Test rig of two stage thermoelectric cogeneration system (the image at the right bottom corner shows the insulated two-stage TCS)	152
Figure 6-21 Schematic diagram of two stage thermoelectric cogeneration system	152
Figure 6-22 Temperature difference developing trend under 47W, 60W and 93W	153

Figure 6-23 Natural air cooling for domestic TCS	154
Figure 6-24 Schematic of Single-ended primary inductance converter (SEPIC)	156
Figure 6-25 Schematic of typical battery charging setting	156
Figure 6-26 Schematic diagram of battery charging by TE power generator	158
Figure 6-27 Torque wrench for thermoelectric assembly	159
Figure 6-28 The most common thermoelectric assembly method (left to right: crinkle washer, flat metal washer and fibre washer)	160
Figure 6-29 Maximum voltage output under different pressure load	161
Figure 6-30 Power output under different pressure load	162
Figure 6-31 Heat output under different pressure load	162
Figure 6-32 Washer configurations in the assembling procedure (from left to right, crinkle washer, flat metal washer and fibre washer)	162
Figure 6-33 Conversion efficiency change caused by the removal of fibre washer and flat metal washer	163
Figure 6-34 Thermal efficiency when the unit is assembled with one crinkle washer and three washers	163
Figure 6-35 The impact on conversion efficiency from uneven pressure load	164
Figure 6-36 The impact on thermal efficiency from uneven pressure load	164
Figure 6-37 Efficiency drop caused by uneven assembling	165
Figure 7-1 Improved system concept for domestic TCS	168
Figure 7-2 Schematic diagram of hot side heat exchanger	169
Figure 7-3 Cooling unit of thermoelectric cogeneration system	169
Figure 7-4 3D model of cold side heat exchanger	170
Figure 7-5 3D printed sample of cold side heat exchanger	170
Figure 7-6 Schematic diagram of the integration with domestic boiler, A: distant view; B: near view;	171
Figure 7-7 Photos of TEG building block, A: Cooling side; B: Heat source side	171
Figure 7-8 Comparison of energy recovery period	172
Figure 7-9 Average daily solar irradiance of each month in Northampton	173
Figure 7-10 Hourly heating demand of a UK two-bed bungalow in a year	173
Figure 7-11 Open voltage and power output of a single cell thermoelectric cogeneration system	174
Figure 7-12 Open voltage and power output of a single cell thermoelectric cogeneration system	174

## **NOMENCLATURE**

$A$	exterior surface area of heat source	$m^2$
$A_{con}$	area of solar concentrator	$m^2$
$A_{fhx}$	heat transfer area of flue heat exchanger	$m^2$
$A_{ins}$	Area of insulation around heat source	$m^2$
$C$	torque coefficient	
$c$	specific heat capacity of water	$j/kg \cdot K$
$c_p^{bw}$	specific heat capacity of boiler waste	$j/kg \cdot K$
$c_o$	specific heat capacity of heat transfer oil ( 2500)	$j/kg \cdot K$
$D$	duty cycle	
$d$	heat pipe diameter	$m$
$d_b$	diameter of branch channel	$m^2$
$d_m$	diameter of main channel	$m^2$
$E_n$	net energy gain	$W$
$g$	gravitational constant	$m/s^2$
$G$	water flow rate in cooling plate	$m^3/s$
$G_{bw}$	mass flow rate of flue gas	$kg/s$
$h$	heat transfer coefficient	$W/m^2K$
$h_p^{bw}$	average heat transfer coefficient between the boil flue and ambient air	$W/m^2K$
$h_{fhx}$	surface heat transfer coefficient of flue heat exchanger	$W/m^2K$
$h_{ins}$	heat transfer coefficient between ambient environment and insulated heat source	$W/m^2K$
$j$	colburn j factor	
$k_T$	specific thermal conductivity	$W/mK$
$k_w$	thermal conductivity of water	$W/mK$
$k_{Al}$	thermal conductivity of aluminium	$W/mK$
$M$	Ratio of voltage output	
$n$	quantity of branch channel	
$N$	pairs of thermoelectric elements	
$P$	power output	$W$
$P_{max}$	maximum power output	
$Q_2^*$	solar input at 2 <sup>nd</sup> stage	$W$
$Q_a$	absorbed heat from flue heat exchanger	$W$

$Q_{as}$	absorbed solar power	W
$Q_{bw}$	heat content in flue gas	W
$Q_{cp}$	captured heat from boiler exhaust	W
$Q_e$	heat loss in the flue gas	W
$Q_w$	available boiler waste heat	W
$Q_{input}$	heat input	W
$Q_{loss}$	system heat loss to the ambient environment	W
$Q_n$	heat output at nth stage	W
$Q_{output}$	heat output	W
$Q_{solar}$	available solar power	W
$Q_{sys}$	effective heat to the system	W
$r_{cp}$	area ratio of branch channels to main channel	
$Re_d$	Reynolds number based on the heat pipe diameter	
$R$	system thermal resistance	$m^2K/W$
$R_{cp}$	thermal resistance of cooling plate on the module side	$m^2K/W$
$R_{int h}$	thermal resistance of hot side heat exchanger	$m^2K/W$
$R_{int c}$	thermal resistance of cold side heat exchanger	$m^2K/W$
$R_{ins}$	thermal resistance of insulation	$m^2K/W$
$R_{ex}$	electrical resistance of external load	$\Omega$
$R_m$	module electrical resistance	$\Omega$
$R_{te}$	module thermal resistance	$m^2K/W$
$R_{tb}$	thermal resistance of screw fit	$m^2K/W$
$R_{2/1}$	power output ratio of two-stage TCS to one-stage TCS	
$S$	Seebeck coefficient	V/K
$S_p$	Seebeck coefficient of p-type element	$\mu V/K$
$S_n$	Seebeck coefficient of n-type element	$\mu V/K$
$S1$	transverse pitch	mm
$S2$	longitudinal pitch	mm
$T$	torque per screw	Nm
$t$	heated time	s
$t_{op}$	boiler operation time	s
$T_a$	ambient temperature	$^{\circ}C$
$T_{ac}$	flue gas temperature after passes	$^{\circ}C$



	through flue heat exchanger	
$T_{bc}$	flue gas temperature before passes through flue heat exchanger	°C
$T_c$	heat sink temperature	°C
$T_f$	flue gas temperature	°C
$T_h$	heat source temperature	°C
$T_o$	oil temperature	°C
$\bar{T}$	average operating temperature	°C
$T_1$	module hot side temperature	°C
$T_2$	module cold side temperature	°C
$U_{input}$	voltage input	V
$v$	water inlet velocity in cooling plate	m/s
$V_o$	volume of heat transfer oil	m <sup>3</sup>
$V_1$	open circuit voltage output	V
$V_2$	loaded voltage output	V
$V_{1st}$	voltage output at 1 <sup>st</sup> stage	V
$V_{2nd}$	voltage output at 2 <sup>nd</sup> stage	V
$V_{max}$	maximum voltage output	
$W$	equivalent fan power	W
$T_{outlet}$	outlet water temperature	°C
$T_{inlet}$	inlet water temperature	°C
$ZT$	dimensionless figure of merit	
$Z$	figure of merit	K <sup>-1</sup>
<b>Greek symbols</b>		
$\eta_2^*$	conversion efficiency at 2 <sup>nd</sup> when solar input is present	
$\eta_a$	effectiveness of flue heat exchanger	
$\eta_f$	fan efficiency	
$\eta_{hx}$	effectiveness of hot side heat exchanger	
$\eta_m$	module conversion efficiency	
$\eta_n$	conversion efficiency at the nth stage	
$\eta_{co}$	system thermal efficiency	
$\eta_p$	pump efficiency	
$\eta_s$	efficiency of solar collector	
$\lambda$	thermal conductivity of water	W/m K
$\lambda_{TE}$	equivalent thermal conductivity of TE module	W/m K

$\mu_{bw}$	dynamic viscosity of flue gas	Ns/m <sup>2</sup>
$\mu_w$	dynamic viscosity of water	Ns/m <sup>2</sup>
$\rho$	water density	kg/m <sup>3</sup>
$\rho_T$	specific electric resistivity	$\Omega$ m
$\rho_o$	density of heat transfer oil (0.888)	g/ml
$\sigma$	electrical conductivity	S/m
$\nu$	kinematic viscosity	m <sup>2</sup> /s
$\alpha$	thermal diffusivity of water	m <sup>2</sup> /s
$\zeta$	local resistance coefficient of cooling plate	
$\Delta P$	pressure drop caused by flue heat exchanger	Pa
$\Delta P_{cp}$	pressure drop of cooling plate	Pa
$\Delta T$	temperature difference between heat source and coolant	°C
$\Delta T_{te}$	temperature difference across thermoelectric module	°C
$\Delta T_{cp}$	temperature difference between cooling water and module cold side	°C
$\Delta T_{fh}$	temperature drop from flue gas to the module hot side	°C

# Chapter 1 Introduction

## 1.1 Background

Power generation using thermoelectric generators have been utilised in areas like aerospace facilities, transport tools and industry utilities, in which a considerable amount of waste heat offers a great opportunity for making direct use. Fig.1 shows the energy consumption in four major sectors [1], where a considerable amount of energy has been exhausted into environment without being used.

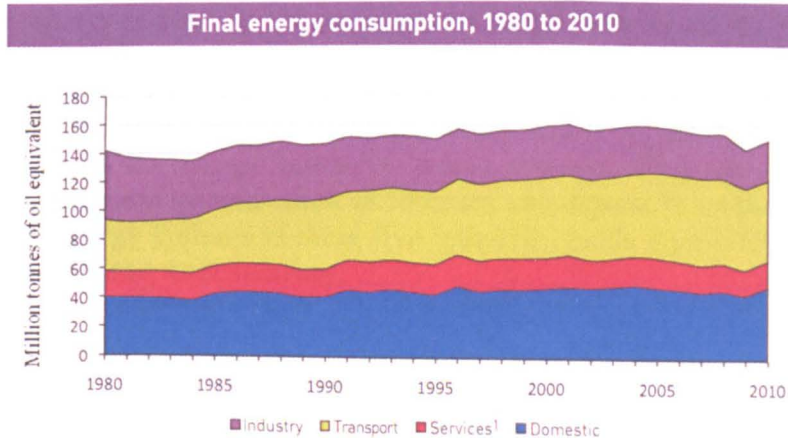


Figure 1-1 Energy consumption of different sectors in the UK (1980-2010)

In vehicles, over 50% of the total fuel energy escapes to the ambient environment as heat loss through the exhaust system and radiator. The possibility of recovering it with thermoelectric module was explored as early as 1914 [2]. Joint efforts by universities and industry used the most advanced available thermoelectric materials of the time to achieve an overall efficiency of 5-10% [3]. Due to the different temperature levels across the section between engine and exhaust, the optimum performance could be obtained by adopting specific modules for individual temperature level and applying segmented materials or multistage designs. Meanwhile, thermoelectric devices are also used to control temperature and produce cooling and heating from electrical power input in automobiles. This type of application avoids the use of environmentally harmful refrigerants.

Explorations in hostile and inaccessible locations, advances in medical physics, deployment of marine and terrestrial surveillance systems and earth resources require autonomous long-life sources of electrical power. Thermoelectric generators have more than 100,000 hours steady-state operation and precise temperature control [4]. Their developments were used by NASA to provide electrical power for spacecraft since 1961. The reliability of thermoelectric technology has been demonstrated in the Voyager spacecraft with Voyager 1 passing into the Heliosheath about 8.3 billion miles from Earth on May 24th 2006. The application normally involves using radioisotopes as the heat sources which are restricted in specialised applications where the advanced properties outweigh the low conversion efficiency. Early successful space applications of thermoelectric power generation were achieved by the development of systems for Nuclear Auxiliary Power in America in 1955 [5]. Similar applications on artificial satellites Cosmos-84 and Cosmos-90 in USSR were also recorded [6]. For the aircraft industry (both commercial and military),

thermoelectric devices can capture waste heat from the engine and operate over the entire aircraft flight envelope without affecting engine's performance.

The process industries include food, beverages, chemicals, pharmaceuticals, petroleum, ceramics, base metals, coal, plastics, rubber, textiles, tobacco, wood and wood products, paper and paper products. Industrial energy consumption represents a large contingent of energy consumption. For example, it accounted for more than a fifth of all UK energy consumption in 2001 consuming 35,152 thousand tonnes of oil equivalent [7], as shown in Figure 1-1. Due to the large scale in most cases, industries involve with a huge amount of energy consumption, in which a considerable amount escapes to the environment in the form of exhausting, radiation and cooling. Figure 1-2 compares the energy use and loss in energy systems across sixteen industrial sectors [8]. Five industrial sectors, which include petroleum refining, chemicals, forest products, iron and steel, and food and beverage, account for over 80% of all the energy inputs to energy systems. They are large users of steam systems and fired systems such as furnaces and dryers. In total, energy losses associated with energy systems in these five industries totals represents over 15% of the energy consumed by U.S. industry.

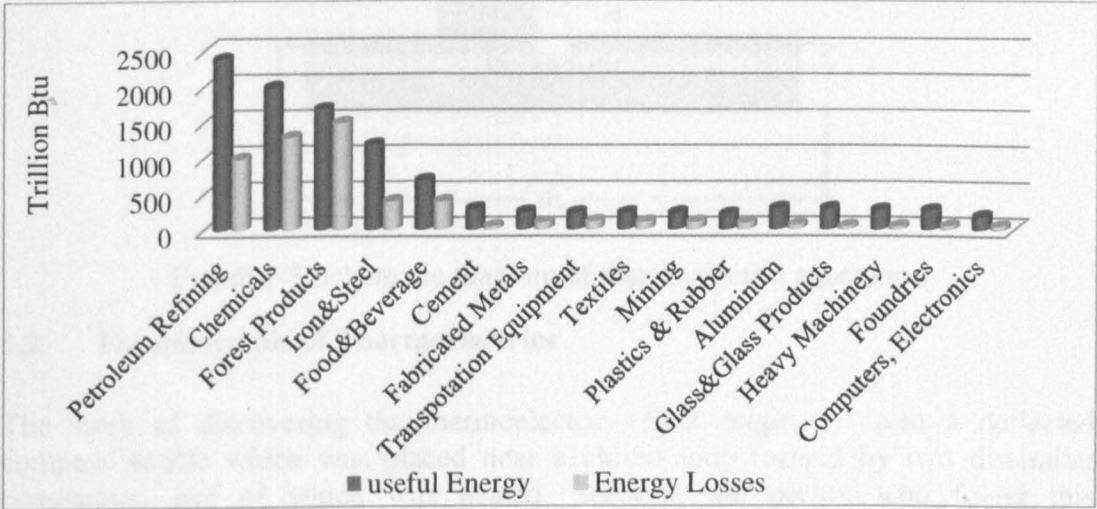


Figure 1-2 Energy consumption chart in different industrial sectors

This energy loss or waste heat, produced in the processes of fuel combustions and chemical reactions, is wasted by ending up in the environment rather in the product due to unnecessary processes, intensive drying, inefficient boilers and steam systems. The possibility of employing thermoelectric technology to generate electrical power from low temperature (80-100K) heat source on off-shore oil platforms was discussed in 1992 [9]. Applications in both small scale and large scale for recovering heat from combustible solid waste have been developed in Japan [10]. An estimated conversion efficiency of 4.36% was achieved in a small-scale on-site experiment using a 60W thermoelectric module installed near the boiler section of an incinerator plant [11].

Nowadays, the use of PV (photovoltaic) technology takes over the major role of domestic power generation in many countries and regions. It needs to be mentioned that PV delivers higher conversion efficiency compared to the thermoelectric generator. However, it has a small capacity factor due to its dependence on solar radiation. The disadvantage of PV is obvious especially in the regions where show a



lack of solar radiation. Due to multi-heat-sourcing, quiet, long period reliable and maintenance-free operation, thermoelectric generators have become an environmentally friendly and energy-saving star despite lower efficiency compared to solar PV power generation. Efforts have been continuously made to adopt thermoelectric technologies in many different areas. Relevant investigations have been carried out in the pursuit of optimum and sustainable ways of using them.

When a temperature difference is established between two ends of semiconductor material, a voltage is generated. This effect was discovered by Thomas Johann Seebeck over 180 years ago and called Seebeck effect. It is a conversion of temperature difference directly to electricity. Its construction consists of pairs of p-type and n-type semiconductor materials forming a pair of thermocouple, shown in Figure 1-3. They are then sandwiched between two electrical-insulating and thermal-conducting ceramic wafers.

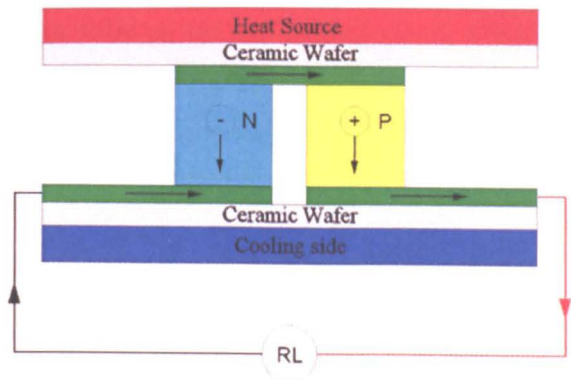


Figure 1-3 Schematic diagram of thermoelectric generation

1.2 Fundamentals of Thermoelectrics

The story of discovering the thermoelectric effect originates from a deflected compass needle which was placed near a closed loop formed by two dissimilar conductors, one of which was heated. Seebeck, the person who found this phenomenon, attributed it to an interaction of the Earth’s magnetism with the temperature difference between the equator and the Poles. Based on the current knowledge, the magnetic phenomenon discovered by Seebeck was because of the electricity generated in the presence of temperature difference across a thermocouple. Following this discovery, after 12 years a complementary effect was discovered by Peltier, who observed temperature changes in the vicinity of the junction between dissimilar conductors when a current passed. This is how the well known effect-Peltier effect came to our awareness. Thomson (Lord Kelvin) predicted the existence of a third thermoelectric effect (known as Thomson effect), which he subsequently observed experimentally on the basis of establishing a relationship between Seebeck and Peltier effect. However, since the discovery of these thermoelectric effects, the application of them didn’t attract much interest due to many more exciting discoveries were made during that time. Until 1850 when the interest was focused on all forms of energy conversion, attentions were tilted to thermoelectricity, which was considered in 1885 by Rayleigh who tried to calculate the efficiency of a thermoelectric generator. Following Rayleigh, Altenkirch gave a satisfactory theory of thermoelectric generation and refrigeration with a conclusion that a large Seebeck

coefficient should be possessed by good thermoelectric materials which also need to show low thermal conductivity [12].

The theory of thermoelectric transport is essentially the domain of transport in semiconductors [6]. All the essential features and complications of transport phenomena in solids are shown in semiconductors. It involves a flow of electric charge or energy or the combination of both. Due to the “forces” caused by external causes such as an electric field or temperature gradient, these “flows” or “transportation” occurs. The various transport coefficients that characterizes the electrons and phonons in the material are defined by the relationships between various “forces” and “flows” [13, 14, 15]. Basically, the flow can be driven by any force. A linear relationship can be obtained between “forces” and “flows” on the assumption that the electron and phonon systems depart only slightly from their equilibrium distributions. Assuming a solid semiconductor contacting with two reservoirs, one is energy and the other is electrons. In the steady state, a steady flow is maintained through the solid as are the differences in electrochemical potential ( $\mu$ ) and temperature ( $T$ ) between the two ends.

A good choice of the forces are  $grad(\mu/T)$  and  $grad(1/T)$ , the components of the flows of electrons ( $\vec{j}$ ) and of energy ( $\vec{w}$ ) are given by Eq.(1-1) and Eq.(1-2).

$$-j_i = \sum_{k=1}^3 L_{ik}^{(1)} \frac{\delta}{\delta x_k} \left( \frac{\mu}{T} \right) + \sum_{k=1}^3 L_{ik}^{(2)} \frac{\delta}{\delta x_k} \left( \frac{1}{T} \right) \quad (1-1)$$

$$w_i = \sum_{k=1}^3 L_{ik}^{(1)} \frac{\delta}{\delta x_k} \left( \frac{\mu}{T} \right) + \sum_{k=1}^3 L_{ik}^{(4)} \frac{\delta}{\delta x_k} \left( \frac{1}{T} \right) \quad (1-2)$$

The total energy flow can be written as a sum of  $W_e$  and  $W_p$ , where e and p refer to the electron and phonon systems, respectively. For example,  $L^{(3)} = L_e^{(3)} + L_p^{(3)}$ . The set of coefficients  $L_{ik}$  provide a complete description of the transport properties of the solid.

The electric current density ( $\vec{i} = -e\vec{j}$ ) and thermal current density ( $\vec{w}$ ) can be expressed by Eq.(1-3) and Eq.(1-4) in terms of  $grad(\mu)$  and  $grad(T)$ .

$$i_i = \frac{1}{e} a \cdot grad\mu - a \cdot a \cdot gradT \quad (1-3)$$

$$\vec{w} = \left( \pi - \frac{\mu}{e} \right) \vec{i} - \lambda \cdot gradT \quad (1-4)$$

Where,  $a$ ,  $\pi$  and  $\lambda$  are second order tensors which are related to the coefficient,  $L^{(n)}$ .

The theory of electronic transport has been described by Single Spherical Band Model, Two-Band Conduction, Multi-valley Effects and Intervalley Scattering. More details are given in the CRC handbook of Thermoelectrics [12].

Thermoelectric materials can be used for either heat pump or power generation, shown in Figure 1-4. Its construction consists of arrays of N & P type semiconductors in which, by applying a heat source on one side and a cooler heat

sink to the other side, electric power is produced and vice versa. Namely, electric power can be converted to cooling or heating by reversing the current direction.

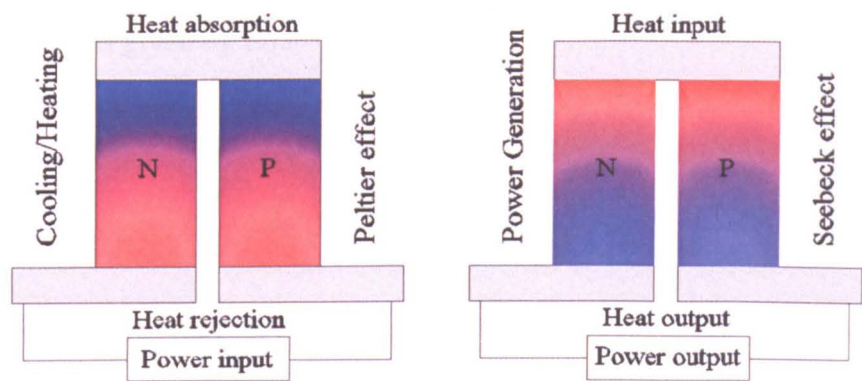


Figure 1-4 Cooling/Heating and Power Generation Thermoelectric Heat Engines

Despite the low conversion efficiency of around 10% when used as power generators, they are strongly advantageous as they have no moving parts and are therefore both more reliable and durable compared to conventional energy technologies. Apart from that, they are scalable without releasing any pollutant to the environment during the operations. Hence they would be ideal for applications in many areas at different scales replacing the traditional cooling and power generation methods.

In typical TE (thermoelectric) devices, the N & P materials are electrically connected in series and thermally connected in parallel in the form of flat arrays called modules, as shown in Figure 1-5.

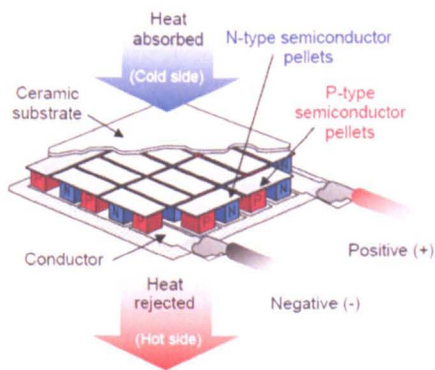


Figure 1-5 Typical thermoelectric module construction

Thermoelectric materials are evaluated by the figure-of-merit  $ZT$  , it is defined in terms of intrinsic material properties of both the N and P type materials and determined by three physical properties—Seebeck coefficient (  $S$  ), electrical conductivity(  $\sigma$  ), and thermal conductivity (  $\lambda$  ). It can be related to the physical properties by Eq.(1-5):

$$ZT = \frac{\sigma S^2}{\lambda} T \tag{1-5}$$

Where,  $T$  is the absolute temperature, the figure-of-merit  $ZT$  serves as a dimensionless parameter to evaluate the performance of a thermoelectric material.

The larger the value of  $ZT$ , the better is the thermoelectric material. Obviously, the materials with higher electrical conductivity and lower thermal conductivity have larger value of  $Z$  which contributes more to the enhancement of conversion efficiency  $\eta$ . It is given by Eq.(1-6):

$$\eta = \frac{\Delta T}{T_1} \left( \frac{\sqrt{ZT+1}-1}{\sqrt{ZT+1}+1-\frac{\Delta T}{T_h}} \right) \quad (1-6)$$

The conversion efficiency of electrical power to cooling is given in terms of  $COP$ , defined as:

$$COP = Q_c / P_{input} \quad (1-7)$$

Where,  $P_{input}$  is the electric power input and  $Q_c$  is the cooling thermal power produced by TE module. The  $COP$  of TE module measures the cooling effectiveness of thermoelectric cooler. In an ideal assembly, the optimum cooling effectiveness can be expressed by Eq.(1-8):

$$\beta_c = \frac{T_c}{\Delta T} \left( \frac{\sqrt{Z\bar{T}+1}-1-\frac{\Delta T}{T_c}}{\sqrt{Z\bar{T}+1}+1} \right) \quad (1-8)$$

Where,  $T_c$ ,  $\bar{T}$  and  $\Delta T$  are the cold side temperature, average temperature of hot and cold sides, and temperature differential.

Supposing a load of resistance  $R_{ex}$  is connected across the thermocouple at A and C shown in Figure 1-6, a heat source is supplied at the rate  $Q$  so as to maintain a temperature difference  $(T_1 - T_2)$  between the junctions. The produced voltage by the generator is  $(\alpha_p - \alpha_n)(T_1 - T_2)$  and this yields useful power across the load given by

$$W = \left[ \frac{(\alpha_p - \alpha_n)(T_1 - T_2)}{R_{ex} + R_m} \right] R_{ex} \quad (1-9)$$

Among the supplied heat by the heat source, most of the heat is conducted to the sink through the thermocouple branches, some is used to balance the Peltier effect which is associated with the current flow just as for the case of thermoelectric refrigeration, half of the Joule heating in the arms finds its way to the source. It can be described by Eq.(1-10):

$$Q = K(T_1 - T_2) + (\alpha_p - \alpha_n)IT_1 - I^2 R / 2 \quad (1-10)$$

Where the current  $I$  equals to  $(\alpha_p - \alpha_n)(T_1 - T_2) / (R_{ex} + R_m)$ .



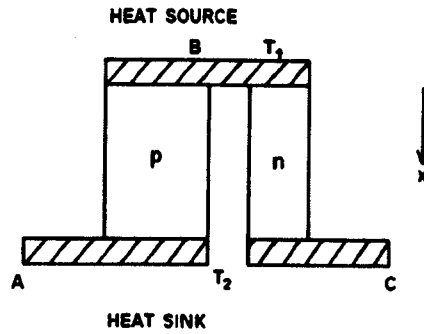


Figure 1-6 Thermocouple for power generation

The efficiency  $\eta$  is equal to  $w / Q$  and its value depends to some extent on the way that the load is matched to the resistance of the module. The condition for maximum power transfer is obtained if  $R_{ex}$  and  $R_m$  is made equal to one another. However, if this condition is satisfied, the efficiency can never exceed 50% of the ideal thermodynamic value  $(T_1 - T_2) / T_1$ . Therefore, it is assumed that the load resistance is chosen so as to yield maximum efficiency. If the ratio  $R_{ex} / R_m$  is denoted by  $m$ , it is required that  $d\eta/dm = 0$ .

### 1.3 Aims and objectives

The domestic power generation using thermoelectric technology has been mentioned in previous studies [16, 17, 18, 19]. However, the common disadvantage shown by these stove application designs lies in the use of a cooling fan which consumes electricity and has moving parts. Most of heat output is exhausted to the environment in an unorganised way except for [19] which uses the heat for space/water heating; only a small part of the absorbed heat is converted into electricity. This disadvantage is enlarged further when the conversion efficiency is low. The system concept introduced in this research intends to overcome the issue of low energy utilisation efficiency shown in conventional thermoelectric applications. Developing a thermoelectric cogeneration system for domestic use with the combination of experimental and numerical studies and pointing a potential direction of improving the energy utilisation efficiency in residential houses installed with combustion appliances by using this concept is the major task of this research. Additionally, it looks into the parameters that significantly affect the performance of thermoelectric system by understanding the correlation between the system performance and the variables including heat source, inlet coolant velocity, inlet coolant temperature, assembly method and pressure load, as well as developing the suited models of boiler flue heat exchanger and cooling plates to support the thermoelectric cogeneration system. This is intended to imply the possibility of widening the range of economically feasible thermoelectric application and provide general technical information for the engineers and researchers in practical applications and experimental studies.

In order to achieve this purpose, the following challenges need to be tackled:

#### 1. Heat sourcing

Capturing heat from the available heat sources in residential house is one of the primary issues that need to be tackled. It determines the amount of heat that can be

used by the thermoelectric system. Specifically designed for recovering the waste heat existing in the boiler flue, the flue heat exchanger plays two important roles in the system, including heat recovering and heat transportation. More details based on CFD are given in Section 4.3. The heat recovered from the heat sources is directed to the TE modules which converts part of the heat flux into electricity and leaves the rest, unconverted heat flux, to be dissipated into the cold side heat exchanger for other purposes, such as water preheating. It provides heat for the modules, which are mounted between heat exchangers. Numerical studies will be carried out to develop the suitable model for the flue heat exchanger.

## **2. System performance**

This includes the conversion, utilisation and management of converted heat and unconverted heat. DC electricity is produced from the heat converted by thermoelectric module. The parameter identification that affects the maximum power output under different thermal conditions is important to the design of the external electrical circuit for the sake of the maximal harvest of electrical power and good use and management of generated power in domestic environment. The unconverted heat, which is wasted to environment in conventional heat sink design, is re-used to heat the feed water for existing combustion appliances in residential house. The challenge lies in mitigating the increased pressure drop without significantly affecting the heat transfer performance between the feed water and thermoelectric cogeneration system. This is discussed in section 6.4.

## **3. Heat dissipation**

Cold side heat exchanger shoulders the responsibility of dissipating the unconverted heat. The design of heat dissipation, including the dissipating destination and consumed energy during heat dissipation, is the threshold for good overall energy utilisation efficiency. Conventional fan assisted heat dissipation only gives the energy utilisation efficiency of less than 5% because the unconverted heat is wasted by escaping to the environment without being used. Moreover, the use of fan represents extra electrical energy consumption. Heat dissipation by adopting fluid-based heat exchanger makes it more practical to utilise the unconverted heat in managing-friendly way due to compactness and effective characteristic. However, the transportation of thermal fluid involves the use of electrically-powered pump. The capacity of the pump is determined by hydraulic characteristic of heat exchanger. The design of a suitable heat dissipation method and the exploration of suitable operating regime, which determines the amount of net energy harvest, are introduced by conducting experimental and numerical studies in chapter 5.

## **4. System integration**

System integration determines how well the thermoelectric applications can be suitably fitted into the host facilities: It includes the design, construction and integration of thermoelectric cogeneration system to the residential environment without degrading the boiler performance. It includes two major tasks: thermoelectric system construction and domestic integration. The former one determines how well the thermoelectric system can perform with the given thermoelectric generators, details are given in section 6.5. The latter one decides the way that thermoelectric

cogeneration system can serve the host house in an efficient way, more details are discussed in section 6.4.

### 1.4 Research Methodology

The aim of this research is to develop a thermoelectric generation system concept to improve the energy efficiency in residential house in the countries/regions with temperate climate where the boiler is used to provide space/water heating. To achieve this purpose, the whole research problem is broken down to four major issues, heat sourcing, heat dissipation, system performance and system integration, which are introduced in section 1.3. Different approaches have been employed to tackle the issues.

#### Heat sourcing

Numerical approach has been used to develop a suitable model for flue heat exchanger, which recovers the heat from the boiler flue gas. An indirect heat exchange style is selected to achieve this purpose. Based on the previous researches and the requirements in this research, the initial structure has been proposed. 3D models with different configurations in terms of heat pipe layout, pitch, cross sectional area and joint style have been established to compare and identify the suitable model for flue heat exchanger.

The numerical simulation has been carried out at two stages: Stage 1. Identify the optimal structure for the flue heat exchanger enclosure in by investigating 7 models; Stage 2. Finalise the detailed design by comparing 5 models, which are built based on the results obtained from stage 1.

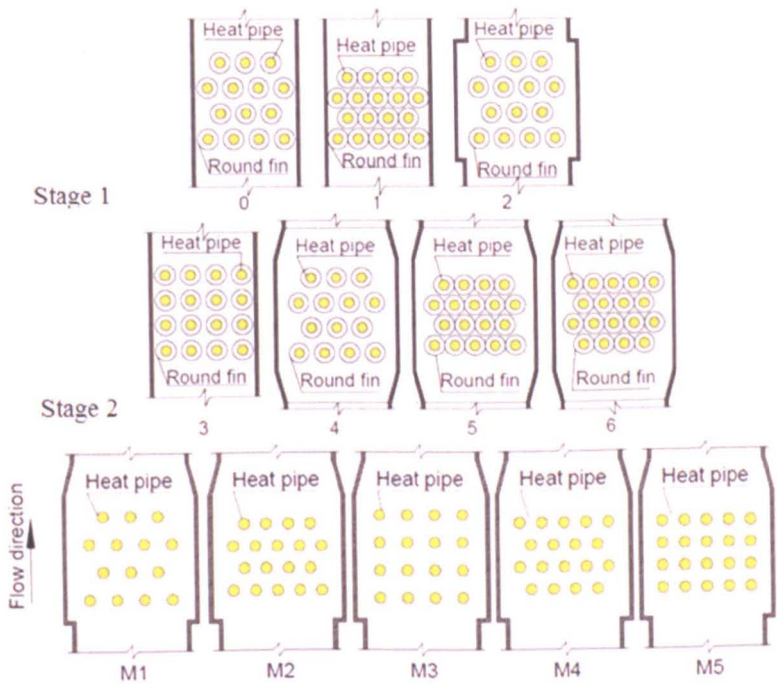


Figure 1-7 Top view of flue heat exchanger section of 3D models for numerical simulations conducted at two stages

Recovered heat and equivalent fan power, which reflects the thermal benefit and the penalty of increased pressure drop by using this flue heat exchanger to evaluate the

overall performance of the flue heat exchanger, more details can be referred in chapter 4.

### *Heat dissipation*

Both numerical and experimental studies have been used to investigate an oriented cooling plate for its contribution to the system performance. With the initial experimental verification, numerical method using CFD has been used to develop its optimal structure based on four major structural variables.

The thermal performance and hydraulic performance of the cooling plate have been studied in the system test. The cooling capacity is investigated by measuring the temperature and flow rate of the water flow that is supplied to the cooling plate to cool down the module cold side. The water temperatures before and after the cooling plate are measured by K-type thermocouples. The pressure drop is measured by a manometer which is connected to the inlet and outlet of cooling plate. It is reset to zero when the water does not flow. Each set of the test has been repeated three times to make sure the experimental results are reproducible.

The experimental results are used to verify the results obtained from numerical simulation to a 3D model of cooling plate. The verified 3D model is used to modify the current designs and develop the optimal structure for the system. The model is shown in Figure 5-38 and Figure 5-39. The net energy gain defined by the combination of recovered heat and consumed equivalent pumping power to evaluate the overall performance.

### *System performance*

The system performance has been investigated experimentally on a bench-scale experimental prototype to investigate its performance as a building block producing electrical power and preheated/hot water. The experimental study has been carried out at one-stage TCS and two-stage TCS separately to understand its system characteristic with different system structures. The test rigs of them can be referred in Figure 6-6 and Figure 6-20, respectively. The maximum power output has been used to evaluate the system performance. It has been measured by a data-taker under different external loads.

A few factors in system construction that determine the system performance have been investigated. They include pressure load, assembly method and washer configuration, respectively. The pressure on the module surface is loaded by torque wrench, whose specifications can be referred in Table 6-3.

### *System integration*

System integration determines how well the thermoelectric applications can be fitted into the host facilities: It includes the design, construction and integration of thermoelectric cogeneration system to the residential environment without degrading the boiler performance.

The major factors in system integration such as pressure load, assembly method and washer configuration are investigated to understand how they influence the overall system performance. The pressure onto the module surface is loaded by using a torque wrench, whose specifications can be referred in Table 6-3. Three output

parameters including open voltage output, maximum power output and heat output have been used to evaluate the impact. Experiment studies with whole assembly and individual assembly are carried out and compared with each other to find out the pros and cons of each method. The average power output of each module under different temperature differences is used to compare the performance of each method. Two types of washer configuration are compared to see its impact on the conversion efficiency and thermal efficiency. More details are introduced in chapter 6.

## **1.5 Outline of thesis**

The thesis, comprised of 7 chapters, is summarized as follow:

### **Chapter 2 Literature review**

This chapter reviews previous research on the thermoelectric material and module construction to demonstrate the current development on the discovery and development of advanced materials, the fabrication technologies and the difficulties in commercialization. It aims to show a full image of the research in the thermoelectric field for a better understanding of the position that this research stands at and the role in exploring the potential of more economically feasible and wider use of thermoelectric generation played by this research.

### **Chapter 3 Domestic energy profile**

This chapter takes the UK as an example to introduce the energy profile of domestic sector in the regions/countries with temperate climate which the domestic boiler plays the major role of supplying space and water heating in residential houses. The proportion of the energy used for space/water heating in the overall energy consumption of a residential house has been introduced together with the role of domestic boiler in space and water heating to show the importance and necessity of improving the thermal efficiency of domestic boiler. The thermoelectric material that is suitable to be used in domestic environment is introduced according to the available heat sources in residential house. The availability of solar energy and waste heat from domestic boiler has been discussed in different scenarios for a case study conducted in chapter 7.

### **Chapter 4 Heat sourcing**

This chapter introduces the system concept and breaks down the issues that are confronted by this research and need to be solved to improve the domestic energy efficiency by employing the domestic thermoelectric cogeneration system. The hot side heat exchangers including the solar heat exchanger and boiler flue heat exchanger have been discussed. For the boiler flue heat exchanger, harvesting the waste heat in boiler exhaust pipe by installing arrays of heat pipe heat exchangers has been proposed as an attempt of efficient and suitable method in this research due to the advanced heat transfer characteristic shown in heat pipe heat exchangers. A series of numerical simulations have been carried out to investigate four parameters that affect the performance to identify the suitable design of boiler flue heat exchanger using heat pipe.

### **Chapter 5 Heat dissipation**

This chapter reviews the heat dissipation methods that are used in the previous researches and applications. In comparisons with the disadvantages shown in the conventional heat dissipation, an oriented cooling method for the domestic TCS has been proposed on the basis of experimental study and numerical study. In this research, the cooling plates are supposed to be integrated between the main water supply and boiler. The water is preheated in the cooling plates before goes to the boiler. The goal of adopting this cooling plate is to cool down the thermoelectric generator cold side effectively with minimum penalty in pumping power. Numerical and experimental investigations have been carried out to test its performance in the system and modify its structure further according to three variables.

## **Chapter 6 Experimental investigations**

This chapter introduces the experimental investigations of one-stage thermoelectric cogeneration system and two-stage cogeneration system based on the use of a simulated heat source and purpose-designed heat dissipation-multi channel cooling plate. Insight is also shed on the investigation to the performance of one-stage cogeneration system and the parametric factors such as coolant flow rate, pressure load and assembling method that influence the system performance.

## **Chapter 7 Discussion, conclusion and future work**

This chapter introduces a potential candidate concept which, based on the result of current work, has been modified and extended. The economic impact of deploying the domestic TCS in residential house in the UK has been evaluated in a case study. The environmental impact has also been discussed. Final insight has been shed onto the conclusion of this current work and suggestions for future work.

## Chapter 2 Literature review

The overall performance of thermoelectric system is determined by two major factors: the material properties and the system. Although this research is mainly focused on the system wise, the research work on the thermoelectric material and module construction are also reviewed to show a full image of the research in the thermoelectric field for a better understanding of the position that this research stands at and the role in exploring the potential of more economically feasible and wider use of thermoelectric generation played by this research.

### 2.1 Material development

#### 2.1.1. Commercialization

The commercialization of thermoelectric materials involves the validation of a thermoelectric performance at the system level in commercial configuration. It is considered beyond the scope of the intended TE material research. The most famous commercialized thermoelectric material must go to  $\text{Bi}_2\text{Te}_3$ . It was recently reported that a material which is a promising candidate to fill the temperature range in the ZT spectrum between those based on  $\text{Bi}_2\text{Te}_3$  and  $\text{PbTe}$  is the semiconductor compound  $\beta\text{-Zn}_4\text{Sb}_3$ . It possesses an exceptionally low thermal conductivity and exhibits a maximum ZT of 1.3 at a temperature of 670K. This material is also relatively cheap and stable up to this temperature in a vacuum [20]. Other new types of materials are coming up to market as exclusive researches are ongoing to develop advanced modules. However, the commercialisation of those materials is experiencing difficulties. They are included in material research, development & fabrication of TE couple & module and also design & construction of TE system.

Due to the limitation of testing equipments and measurement methods, some of the materials with the claimed high ZT are not reproducible and the relevant experiments are unrepeatable. The properties change with time and exposure to test conditions which leads to insufficient accuracy. For fabrication of TE element and modules, the fabrication of TE couple requires time consuming procedures for fabricating the N and P type elements with the expected level of electrical and thermal resistance. The wrong fabrication would lead to the degradation of couple performance. However, the successful fabrication of TE couple has been proven to be difficult using the experimental materials produced in research laboratories. Furthermore, the fabrication of low thermal and electrical interface resistivity makes the metalizing process difficult since the current metallization procedures are immature. The measurements of interfacial resistances are also difficult and time consuming. For the fabrication of TE module, reliable, repeatable, economical and durable fabrication methods are needed for connecting large arrays of TE couples with the capability of accommodating thermal expansion, mechanical shock as well as other physical conditions and withstanding the necessary environmental conditions.

For the design and construction of TE system, design methods and construction tools for developing stable, durable and environmentally compatible TE system need to be standardized. The cost, performance, usage and final disposal of the system need to warrant commercial development [21]. Although TE materials have various applications in several areas, for the commercialization, there is still a long way to go. Most published announcements of improved TE materials note the commercial



need of better materials, with the implication that the materials described will enable, or at least constitute a significant step towards, meeting market needs. Figure 2-1 (A) [22],[23] presents projections for sales of power generation materials as a function of ZT, assuming materials are available with an average ZT of 2 by 2018 and are mass produced by 2023. Figure 2-1 (B) presents market projections for cooling/heating materials under the same assumptions. The results show that market size is a strong function of ZT, for device level values up to about 2.

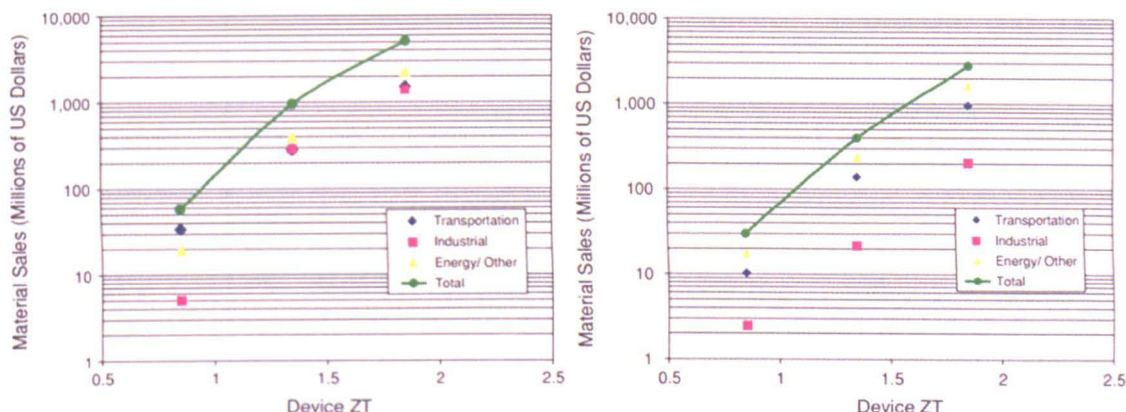


Figure 2-1 TE Material Market, 2023 Projection: A. Power generation; B. Cooling/Heating

However, there has been no breakthrough in developing new commercial material with superior ZT which can displace  $\text{Bi}_2\text{Te}_3$  or the other materials previously at the device level in the last two decades. Several causes can be identified as follow [24]:

1. Usually, materials are fabricated in a form factor suitable for testing by a particular, specialized type of equipment.
2. Samples fabricated as thin films (1  $\mu\text{m}$  to 10  $\mu\text{m}$  thick) tested in plane may have surface dislocations, substrate interactions, or stress-induced effects that skew results. Quantitative corrections for these effects are difficult and time consuming.
3. Inadequate test equipment or simple test errors, has (infrequently) resulted publication of erroneous or non-repeatable measurements.
4. Individual properties, if measured sequentially, can change with time or exposure to test conditions. The resulting computed ZT can be misleading.
5. In some cases, two material properties (e.g.  $\alpha$  and  $\rho$  in thin films) have been measured and the third property (e.g.  $\lambda$ ) extrapolated or inferred (erroneously) from the literature and used to compute artificially high values of ZT.

Commercialization is a key factor for thermoelectric research and development. In all of the Science and Nature magazine articles published since 2000, which have discussed development in TEs, the authors referenced the commercial need for better TE materials in their introductions [25]. However, the commercialization process is going to take a long time.

TE systems appear to be as green as another emerging solid state energy conversion technology, photovoltaics (PV). The comparison discloses that the research in each has been extending over about the same period of time, and in each case, the commercialization has been impeded by similar barriers of high cost per watt output and low efficiency. The comparison is showed in Table 2-1.



Table 2-1 Comparison of PV and TE

	<b>Photovoltaics( PV)</b>	<b>Thermoelectric (TE )</b>
<b>Fabricating</b>	Be fabricated using equipment generally available in semiconductor R&D facilities	Usually requires specialized equipment and specialized post production processing (consolidation, phase transformation, etc.), may take additional equipment and can introduce large variations into the manufacturing process.
<b>Performance</b>	can be measured using standard methodologies at or near room temperature, and with relatively high accuracy.	Often need to be taken over a broad temperature range.
<b>Material's operating</b>	PV devices operate over a temperature range far from material melting points, at temperatures for which the chemical and mechanical material stability can be predicted	Assuring stability requires lengthy experimental study and material development efforts because of TE materials' operating, especially for power generation application, often above 2/3 of their melting temperature.
<b>Environmental stability</b>	Can be controlled with coatings that operate near room temperature.	TE material protection and stability (for power generation applications) must be provided over a much broader range.
<b>Manufacturing equipment</b>	Has become somewhat standardized both because of similarities to semiconductor process equipment and methodology, and the benefits of the very recent large investment in production readiness.	Highly variable and dependent on the material system. Generally, the methods used are specialized and equipment is not commonly available.

Progress over the past two decades suggests that new TE material technology will be too slow to make significant commercial impact unless new approaches are taken to accelerate material development.

### 2.1.2. Development of high efficiency thermoelectric modules

Discovery of the Seebeck effect, thermoelectric modules have been studied for more than 180 years. Nevertheless, the thermoelectric module has not become widespread yet. The major reason for this is the low conversion efficiency of conventional thermoelectric modules. The development of new, more efficient materials and devices is the key to expanding the range of application of thermoelectric generators and coolers.

The discovery and development of advanced thermoelectric materials, which involves improving three physical properties: Seebeck coefficient, thermal conductivity and electrical resistivity, is needed to expand the range of applications of thermoelectric devices. A broad research and development for advanced thermoelectric has been conducted by JPL which has identified and retained several categories of materials by using several physical and chemical criteria. Among discovered materials, the skutterudite and  $\text{Zn}_4\text{Sb}_3$ -based materials are particularly promising and were developed and optimized by Fleurial et al [55]. The materials with figure-of-merit over 1 cover a wide range of temperatures [53]: p-type  $\text{Zn}_4\text{Sb}_3$ -based materials (375-675K), p-type Ce-based filled skutterudite (675-975K), and n-type heavily doped  $\text{CoSb}_3$  (525-975K), shown in Figure 2-2.

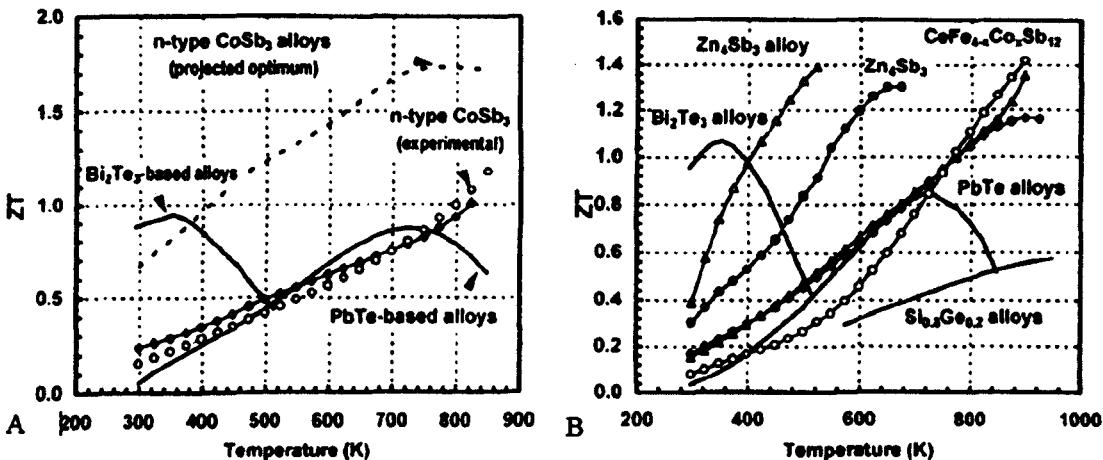


Figure 2-2 ZT values of state of the art and JPL improved thermoelectric materials as a function of temperature A. N-type; B. P-type

Since it was shown that further improvements in the thermoelectric performance are possible, an increasing effort in discovering and developing materials with figure-of-merit higher than 2.0 to 3.0 had been stimulated [26].

Here the following methods are introduced with regard to improving ZT value. They are superlattice, plasma treatment, segmented element, nanocomposite and nanostructure.

### 2.1.2.1. Superlattice

Due to the classical and quantum size effects on energy carriers, energy transport in nanostructures differs significantly from that in macrostructures. It was proved that [27] the thermal conductivity values of nanostructures such as superlattices are lower than that of their bulk constituent materials. This reduction leads to a large increase in thermoelectric figure-of-merit in several superlattice systems.

Superlattices are anisotropic. It improves ZT along the directions both parallel (in-plane) and perpendicular (cross-plane) to the film plane by the enhancement of the electron performance through taking advantage of sharp features in the electron density of state and reduction of phonon thermal conductivity through interface scattering [28]. The other involved mechanisms for the improvement of electron performance include electron energy filtering [29] and thermionic emission [30].

Experimental studies have demonstrated that a significant thermal conductivity reduction in a wide variety of superlattices can be achieved [31].

The idea of using superlattices to improve the figure-of-merit through the reduction of phonon thermal conductivity and enhancement of electronic conductivity was first discussed by M.S. Dresselhaus, T. Harman, and R. Venkatasubramanian [32]. In their publications, the quantum size effects on electrons drew wide attention and inspired intense theoretical and experimental researches on the thermoelectric properties of quantum wells and superlattices [33]. It has been applied on several materials ( $\text{Bi}_2\text{Te}_3/\text{Sb}_2\text{Te}_3$ , [34]), among which  $\text{Bi}_2\text{Te}_3$  superlattices and PbTe-based quantum dot superlattices showed the most impressive results [35], [36], which is shown in Figure 2-3 [35], [37]. A comprehensive summary of researches in superlattices has been done by Harald Boettner et al [38]. However, superlattices grown by thin film deposition are limited to niche applications.

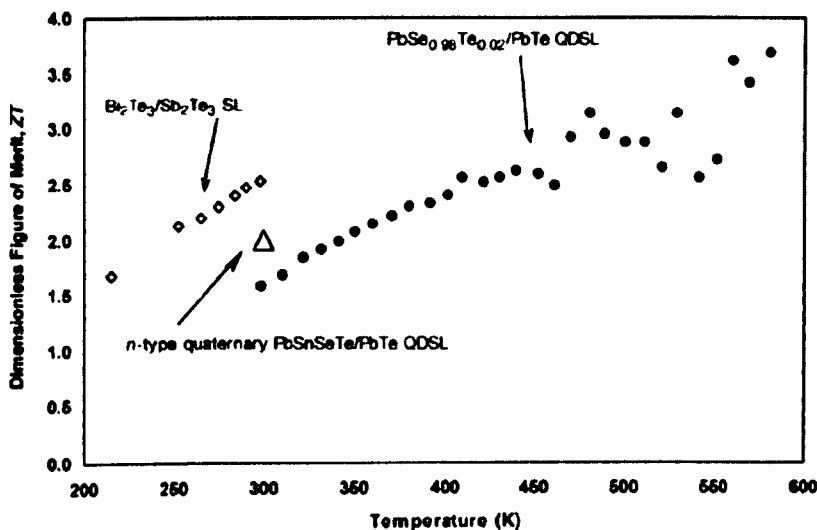


Figure 2-3 Dimensionless figure of merit ZT for  $\text{Bi}_2\text{Te}_3/\text{Sb}_2\text{Te}_3$  superlattices, PbTe-based quantum dot superlattices

Dresselhaus proposed the use of quantum wells to increase the power factor via quantum size effects of electrons in 1993 [39], the practical implementation of these quantum-well structures calls for superlattices or multiple quantum well structures. Meanwhile, there were also suggestions and experimental evidence that superlattices could be made into superior thermal insulators, promising a second route to improve the figure-of-merit [40]. Subsequent experimental studies have demonstrated significant thermal conductivity reduction in a wide variety of superlattices [41]. Most recently, significant enhancements of the thermoelectric figure-of-merit were reported in  $\text{Bi}_2\text{Te}_3/\text{Sb}_2\text{Te}_3$  superlattices along the cross-plane direction and PbTe/PbTeSe quantum dot superlattices along the film-plane direction [42], [43].

The method of molecular beam epitaxy (MBE) and vapour deposition which are utilized in the production of superlattice film are effective ways to improve the ZT value. Such research utilizes two known thermoelectric materials (well-performance but different band gap) to form a superlattice quantum well so as to confine the carrier in the potential well and improve the value of ZT by using its grain boundary scattering role on the phonon in the heat transfer process. Currently, the physical and chemical methods are used to grow superlattices on various substrates. The physical

method includes MBE, MOVCD, PVD, CVD, magnetron sputtering, successive ionic layer adsorption and reaction (SILAR), co-evaporation process, etc [44, , , , , 50]. The chemical method includes electro-deposition and chemical deposition [51].

### 2.1.2.2. Plasma treatment

Different methods have been adopted to improve the performance of thermoelectric element by Seiji [52]. For BiTe-based materials, two used methods include surface treatment and shifting Z value. Plasma treatment using various types of coating was applied to treat the raw material powder as it was predicted that reducing powder by hydrogen would improve the powder characteristics because of low oxygen concentration. Figure 2-4 shows examples of the results of powder treatment by hydrogen plasma and oxygen plasma, respectively. It proves that a lower oxygen concentration obtains a low oxidation of the powder surface and the figure-of-merit is improved as the oxygen concentration decreases, which is shown in Figure 2-6. It makes it clear that isolating the plasma treatment process from oxygen is necessary.

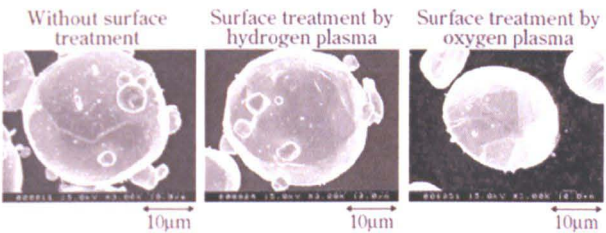


Figure 2-4 Examples of results of surface treatment by plasma

With the aim of improving the figure of merit of a thermoelectric element, they applied plasma treatment to the raw material powder. Figure 2-5 shows the possible effects of applying various types of coating to the raw material powder. It has been predicted that reducing powder by hydrogen will improve the powder characteristics because its oxygen concentration decreases. It can be seen that the plasma treatment removed many of micro-deposits from the powder surface. Figure 2-6 shows the relationship between oxygen concentration and figure of merit, obtained with a p-type, Bi-Te-based thermoelectric material. It can be seen that the figure-of-merit improves as the oxygen concentration decreases.

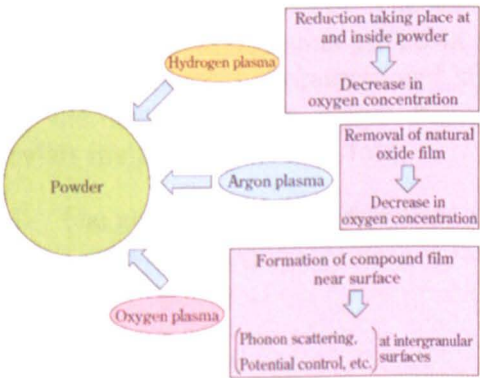


Figure 2-5 Concept of surface treatment of powder

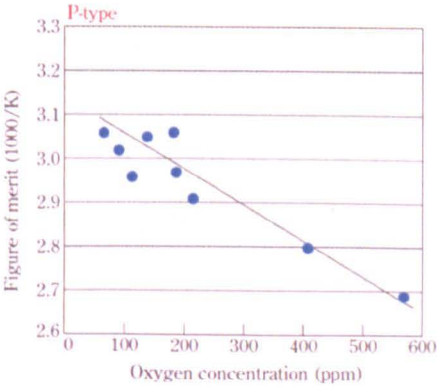


Figure 2-6 Relationship between oxygen concentration and performance

Shifting peak value of figure-of-merit was proposed in reference 52 to improve the performance of BiTe-based thermoelectric elements. By adjusting the carrier concentration to improve the high temperature characteristic and changing the composition to control the energy band gap, the peak Z could be shifted to high temperature side, the result is shown in Figure 2-7. They obtain a thermoelectric conversion thermal efficiency of 6% in view of the thermoelectric conversion efficiency of conventional waste incinerators is 3.6%.

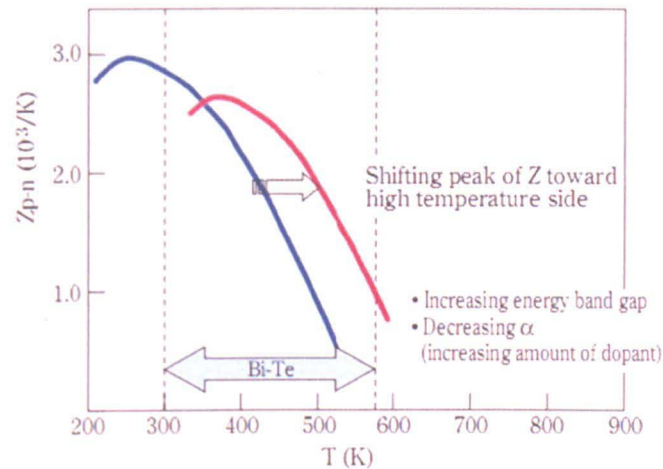


Figure 2-7 Shifting Z value [52]

N-type Bi-Te-based maintains an improved characteristics (large Z) in high-temperature region without a significant decrease in that of the low-temperature, whereas Z reduces remarkably in low-temperature region if it is p-type. Nonetheless, the average performance index is improved across the entire working temperature range.

### 2.1.2.3. Segmented material

No single thermoelectric material is suitable for operating over a very wide temperature range (-300-1000K). It brings about the problem of converting heat over a large temperature difference range. From material wise, segmented material can solve this problem by using different materials in each temperature range where they possess optimum performance. The segmented materials have p-type and n-type legs formed of different segments joined in series. The first generation was developed in JPL (Jet Propulsion Laboratory) and shown in Figure 2-8 [53]. Compared to those using the state-of-the-art single material, the benefits of using this segmented materials includes are double-fold:

1. The generator can operate over a large temperature difference range;
2. The average figure-of-merit is larger.



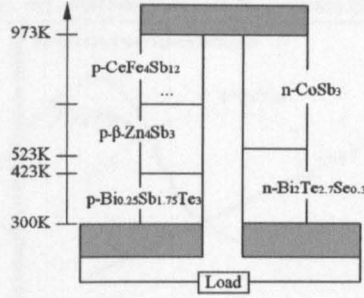


Figure 2-8 Schematic of a segmented thermoelectric generator using segmented thermoelectric material developed at JPL

The optimum design of the geometry of segmented materials involves primarily fine tuning the cross section and length of the different segments. With the given average thermoelectric properties (Seebeck coefficient, electrical resistivity and thermal conductivity) over the temperature range that each segment operates at, the optimum cross section, length and optimum current and efficiency can be calculated [54]. They can be calculated using the following equations:

$$\frac{\lambda_{p_i} \Delta T_{p_i}}{l_{p_i}} = \frac{\lambda_{p_{i+1}} \Delta T_{p_{i+1}}}{l_{p_{i+1}}} \quad (2-1)$$

$$\frac{\lambda_{n_i} \Delta T_{n_i}}{l_{n_i}} = \frac{\lambda_{n_{i+1}} \Delta T_{n_{i+1}}}{l_{n_{i+1}}} \quad (2-2)$$

$$L = \sum_{i=1}^m l_{p_i} = \sum_{j=1}^o l_{n_j} \quad (2-3)$$

Where  $\lambda$ ,  $l$  and  $\Delta T$  are the thermal conductivity, the length of each segment and temperature drop across each segment and  $L$  is the total length of the legs.

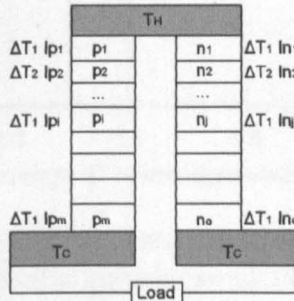


Figure 2-9 Schematic of segmented material

In the direction of current flow, different thermoelectric material forms segmented elements and each operates its superior performance over its temperature range. Materials of good electric conductors and poor thermal conductors are intended to be discovered to expedite the development of high-efficiency.

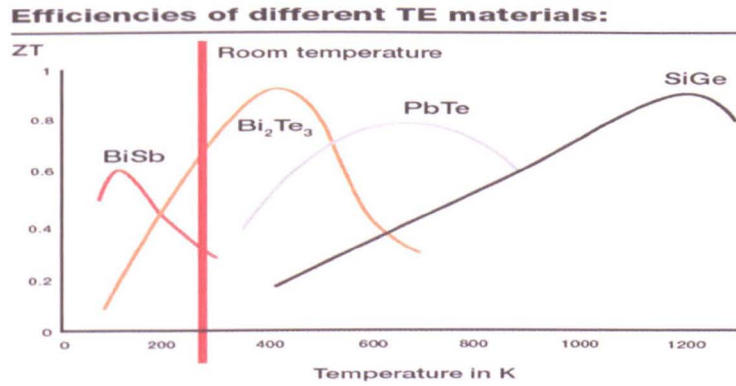


Figure 2-10 Efficiencies of different TE materials

Based on results achieved to date at the Jet Propulsion Laboratory (JPL) on novel materials, the performance of an advanced segmented generator design operating in a large 300-945K temperature gradient is predicted to achieve about 15% conversion efficiency. This would be a very substantial improvement over state-of-the-art thermoelectric power converters. Such a terrestrial power generator could be using waste heat or liquid fuels as a heat source [55]. Figure 2-11 shows the conversion efficiency as a function of ZT for a thermoelectric generator operating between different temperature differences with the advantages of using materials with better thermoelectric performance and of operating at larger  $\Delta T$ .

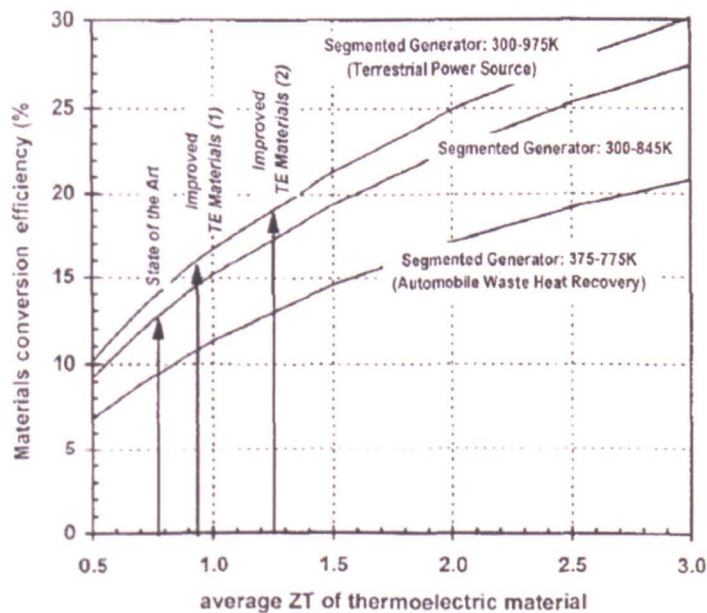


Figure 2-11 Calculated thermoelectric materials conversion efficiency as a function of ZT for various segmented generators operating at different delta T

#### 2.1.2.4. Nanocomposite

Nanocomposite structure thermoelectric material is the thermoelectric material mixed with impurity, such as nanoparticles (insulating, semiconductor or metal) or nanometer-sized hollow [56]. It was said to represent one promising approach that fabricates thermoelectric materials with high figure of merit. It is generally believed that the strong phonon scattering effect in the transmission caused by incorporation

of nanoparticles is the main reason of improving the thermoelectric properties of nanocomposite thermoelectric materials. In the semiconductor, electricity is carried by the electrons and holes, and energy is transmitted by lattice vibrations and phonon. However, currently there are little theoretical or modeling works that have been done in the literature regarding thermoelectric properties of nanocomposites that one can rely on to achieve good design of nanocomposites. The reason lies in the fact that there are a variety of challenges in simulation of both electron and phonon thermoelectric transport in nanocomposites and the inspection of the wave effect in transport processes in nanostructure [57]. Worlock [58] first studied the phonon scattering after mixing nanoparticles. Vining [59] presented his theoretical calculations which lead to a result that mixing free dispersed nanoparticles can reduce the thermal conductivity without affecting its electrical transmission performance. The idea of nanocomposites was inspired from the conclusion that the reduced thermal conductivity in superlattices comes from the sequential interface scattering of phonons rather than the coherent superposition of phonon waves. Hence, the nanocomposites can be a cheaper alternative of superlattices to obtain materials with high figure-of-merit [60], [61]. The challenge is choosing the mismatch in electronic properties properly between the constituent materials thus the electron transport properties can be maintained or even enhanced.

In the advances of nanotechnology leading to high efficiency, complex bulk materials including skutterudites, clathrates, and Zintl phases have been explored. By decoupling the conflicting properties, these complex high efficiency materials give way to further enhancement in cell arrangement such as diversifying array of complexity within the unit cell, of nano-structured bulk, or of thin-film multi-layer structures.

### **2.1.2.5. Nanowires and nanotubes**

Quantum wire can improve the density of states more than quantum well, theoretical calculations of the lower dimensional structure show that nanowires may have better thermoelectric properties than the superlattice [62]. It is theoretically expected that the diameter of quantum wire will be less than 10Å and the ZT value of material will be more than 10.

Current preparation methods for one-dimensional nanowire are mainly gas condensation method [63], electrochemical method [64, 65, 66, 67] and high-pressure injection method [68, 69, 70]. Zeolites, alumina template and the porous polymers are good template materials for nanowire growth. Bi [70], CoSb<sub>3</sub> [64], Bi<sub>2</sub>Te<sub>3</sub> or Bi<sub>1-x</sub>Sb<sub>x</sub> [66] nanowires can be obtained by the above methods and their Seebeck coefficients are superior to conventional materials. In addition to the previously mentioned ways, there are also examples which use silicon mold technology. Using micro-machined silicon wafer as the mold, micro thermoelectric devices are prepared and there are 10,000 pairs Bi<sub>2</sub>Sb<sub>2</sub>Te columnar array PN junction (depth about 300µm, side length about 40µm) arranged in one square centimeter on them. Silicon mold technology can take advantage of the mature silicon wafer micro-machining technology to produce complex shapes, ultra-fine silicon mold, combine micro-fabrication technology in micro-electromechanical systems (MEMS) and material forming technology together. Although the obtained nanowires have not yet been small enough in size, silicon mold technology has played a very good reference for future applications in micro-device.



Zhao's research team [71] used hydrothermal synthesis to obtain  $\text{Bi}_2\text{Te}_3$  compounds nanotubes and nanocapsules (diameter 100nm), then added them to the n-type  $\text{Bi}_2\text{Te}_3$  thermoelectric material to form nanocomposites. Comparing to traditional zone-melting method, the material's conductivity has been improved significantly, the thermal conductivity decreases significantly (only  $0.3\text{W}/(\text{m}\cdot\text{K})$  at  $473\text{K}$ ), the ZT value reaches 1.0 or more, more than the highest value of commercialization thermoelectric devices presented by Tritt et al [72].

The study of quantum line transmission performance shows that its diameter's being equal to or less than  $2\text{nm}$  is necessary [73]. The measurements of nanowire conductivity and thermal conductivity make it difficult to study nanowire thermoelectric materials.

### 2.1.2.6. Structure/geometry

In addition to the conventional method of improving the competitiveness of thermoelectric materials by improving the figure-of-merit, another direction to improve the competitiveness of thermoelectric materials is developing the novel thermoelectric module shapes. Thermoelectric modules have typically plate-like shapes and are fabricated from bulk semiconductors such as  $\text{Bi}_2\text{Te}_3$  and  $\text{PbTe}$ , making them rigid and unfit for non-flat surfaces (e.g. circular tubes) used in waste heat recovery applications where the heat flow is perpendicular to the ceramic plates. When heat flows in radial directions, the attachment of flat modules around a cylindrical heat source is often complicated. Hence, it is highly necessary to fabricate thermoelectric modules which can conform easily to the curved surface. Thin film thermoelectric module is an invention that overcomes this technical issue, one example is shown in Figure 2-12 [74]. It is a type of thermoelectric power generator that is based on thin film with flexible fiber substrates. Another novel tube-shape thermoelectric module for power generation has also been developed recently by Min and Rowe [75]. It is fabricated from four ring-shaped thermoelements and its performance in electrical power generation is evaluated by measuring the power output as a function of temperature difference across the device. It was concluded that a tube-shape thermoelectric module could achieve similar performance to that of a conventional flat module, and has an advantage in waste heat recovery applications where heat flows in a radial direction.

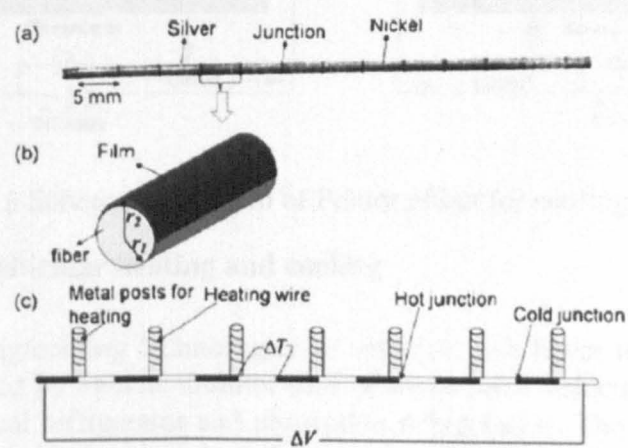


Figure 2-12 Schematic diagram of thin film thermoelectric module

Where, (a) is striped thin film thermoelectric fibre made with thermal evaporation of nickel and silver; (b) is fibre with thin film deposited on one side; (c) is experimental setup for applying a temperature difference and measuring the induced open circuit voltage

## 2.2 Applications

### 2.2.1. Heat engines

A conventional cooling system contains four fundamental parts which are evaporator, compressor, expansion valve and condenser. The evaporator or cold section is the part where the pressurized refrigerant expands, and evaporates. Energy is absorbed during this state change. The condenser dissipates the heat absorbed at the evaporator plus the heat produced during compression, into the environment or ambient.

For thermoelectric coolers based on the same fundamental laws of thermodynamics with the conventional heat pumps, they are solid-state heat pumps without moving parts, without using fluids or gases. They have compact and simple structure with quiet and maintenance-free operation. For heating and cooling applications, the TE energy conversion from electrical power to thermal energy is called “Peltier effect”, where a temperature difference is created across two dissimilar legs of semiconductor material by supplying an electric current through the legs, which are shown in Figure 2-13. At the cold junction, heat is absorbed by electrons as they pass from a low energy level in the p-type semiconductor element, to a higher energy level in the n-type semiconductor element. The power supply provides the energy to move the electrons through the system. At the hot junction, energy is expelled to a heat sink as electrons move from a high energy level element (n-type) to a lower energy level element (p-type).

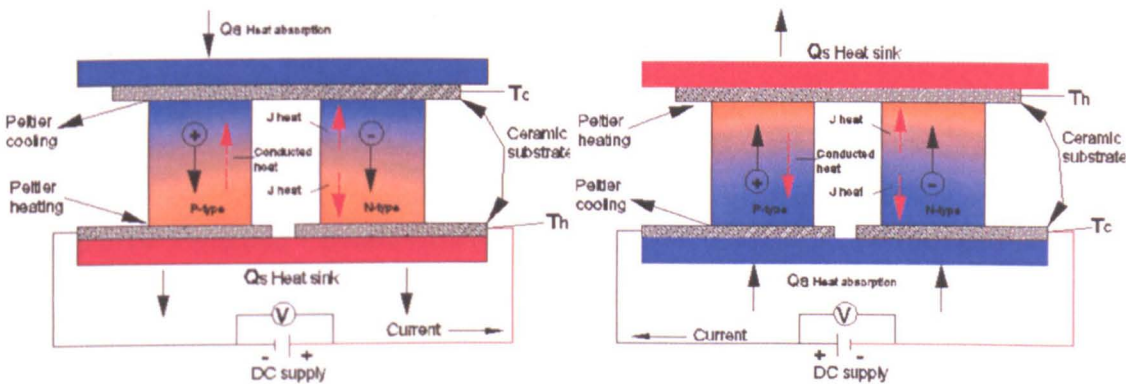


Figure 2-13 Schematic diagram of Peltier effect for cooling and heating

#### 2.2.1.1. Vehicular heating and cooling

Solid state heating/cooling technologies in vehicles with fewer moving parts if any are much favoured by vehicle architectures. Conventional vehicular HVAC systems include mechanical refrigerator and absorption refrigerators. The former one, which has notably high coefficients of performance and good reliability in spite of the moving parts, involves with complex system structure, noisy operation, usage of refrigerant and large vehicle space. Meanwhile, the latter one, which can operate



silently using almost any kind of heat sources, has a relatively low coefficient of performance due to the combination of heat pump and heat engine. Another problem is that it only works properly when installed without being tilted.

It has to be admitted that thermoelectric refrigerators are much less efficient than mechanical refrigerators when operated in the suited conditions. However, unlike mechanical refrigerators, thermoelectric coolers can maintain the efficiency down to very low cooling power, even at the order of milliwatts. In addition, they operate silently without any moving parts, with no working fluids to leak away. This fact gives these devices an extremely great advantage by providing long life time especially when the care is taken in the process of design and construction. The real benefit that comes from the flexibility is its operation in conjunction with a proportional control rather than the on-off style. Therefore, thermoelectric device is a candidate solution for vehicular HVAC.

They have been used to cool or heat car seats by several major car manufacturers including Ford, GM, Hyundai, Jaguar, Nissan, Range Rover and Toyota [76]. The boarder use has been enabled by the improved thermodynamic cycles and advancements in device architecture which enhances the cooling and heating efficiency and reduces the amount of used material, respectively. The current climate control system for vehicular heating and cooling, which has been widely used, is presented by Amerigon and shown in Figure 2-14 [77].

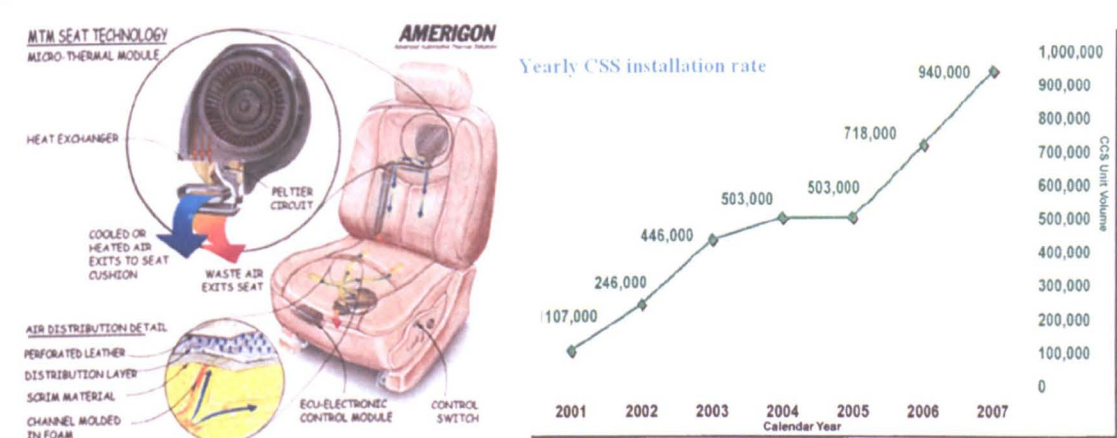


Figure 2-14 Vehicular Climate Control System amounted in seat and installation rate

Due to the role of TEC (Thermoelectric Cooling) in improving the fuel economy, the trend that it has been transforming from assistant HVAC device to the main cooling and heating provider in vehicle is becoming increasingly obvious. One advantage of TEC system is that the cooling and heating can both be achieved and switched by just simply reversing the current. When operating as heat pumps, TEC devices can readily have COP in the range of 2-3 without going through energy-consuming procedures, whilst the traditional HVAC system needs to pump the extracted thermal energy into working fluids to deliver to other component where another heat exchange procedure occurs to finish the passing with lower COP.

Cooling/heating using currently available thermoelectric materials could provide significant advantages compared with current systems for improved fuel economy, reduced toxic and greenhouse gas emissions. Thermoelectric HVAC systems could

be designed to take best advantages of thermoelectric. Compact thermoelectric units can be installed in the seats, dashboard and overhead for the driver and the front seat occupant. Units can be installed in the back of the front seats, the overhead, seats and floor. These units can be devised to only cool or heat the person, not the whole cabin. The driver can be cooled with less than 700 watts of cooling whereas current air conditioners have to provide up to 3,500 to 4,000 watts to achieve the same purpose [78]. Thermoelectric HVAC can be converted from cooling to heating by simply changing the polarity of DC power. The thermoelectric HVAC system can be remotely activated 50 meters or so from the vehicle. The thermoelectric modules are silent with no moving parts. However, the thermoelectric HVAC system would have fans or a coolant loop circulating pump to extract the heat from the modules to heat sinks to dissipate the heat. The possibility of using thermoelectric devices as heat pumps to produce cooling, heating and temperature control from electric power input has been discussed by Lon E. Bell [79].

Advances have been made in the performance, efficiency and cost of thermoelectric devices for cooling, heating, and power generation applications. These advances enable thermoelectrics, along with efficient thermal management systems, the potential to key the next wave of advances in the automotive industry, particularly in HVAC systems and later for waste power recovery. In the past few years the technology, used in military and aerospace applications since the early 1960's, has become cost-effective for mass production. It is of specific interest for automotive applications, an industry with sales of over 50 million units annually.

#### **2.2.1.2. Medical service and food industry**

In medical area, it is important to keep vaccination, blood serum and other biological products within certain temperature range for storage and transportation purpose. The properties will stabilise in the range of medical requirements. A portable thermoelectric medical cooling kit controlled by a microprocessor was developed for preserving human blood during transportation. It operates with 12V dc and 4A [80]. In remote regions in developing countries like India and China, this new method shows a trend of more flexible ways of transporting medical products. Also, it could make on-door medical visits and dealing urgent medical issues possible. This thermal requirements also apply to the food industry which needs temperature control during the process of food transportation and storage. Some patents have been issued on the concept of food cooler/warmer with the use of thermoelectric module [81]. The patent on icemaker and control was also made [82].

#### **2.2.1.3. Electronic device**

In electronic engineering areas, many electronic devices with high power, such as power amplifiers and microprocessors, operate at high temperatures close to the edge of reliability. This could cause severe impact on the performance and lifetime. Thus, cooling is needed to improve the performance and lifetime of the devices. The conventional devices are not well suited in these application areas due to their general large size. For the power device with high density structure, the difficulty becomes more obvious for the conventional cooling techniques due to the large heat fluxes. The thermoelectric coolers can deal with this problem by effective local cooling. Thermoelectric coolers operate quietly due to no moving parts. For example in Figure 2-15, an application has been used to improve the accuracy of electronic

instruments by reducing the thermal noise of the electric components and the leakage current of the electronic devices [83], [84], [85]. One of the examples is a cooled  $CdZnTe$  detector for X-ray astronomy. Cooling between  $30^{\circ}C$  and  $40^{\circ}C$  reduces the leakage current of detector and allows the use of a pulsed reset preamplifier and long pulse shaping times, significantly improving the energy resolution. Although the heat is conducted from the very low temperature  $40^{\circ}C$  to the chilled water of  $10^{\circ}C$ , it is only necessary to use 3W of electrical power for this small capacity application.

In the aforementioned applications, an electronic device to be cooled is usually mounted directly on the cold side of one or more thermoelectric devices allowing maximum thermal transfer between the electronic device and the cold side. The hot side is coupled to a fan or water heat sink. Natural convection is also used in some cases. A variable source of direct current connected to the thermoelectric coolers allows them to lower the temperature of the electronic devices. Applications of thermoelectric devices for cooling electric devices require very small and low current thermoelectric devices.

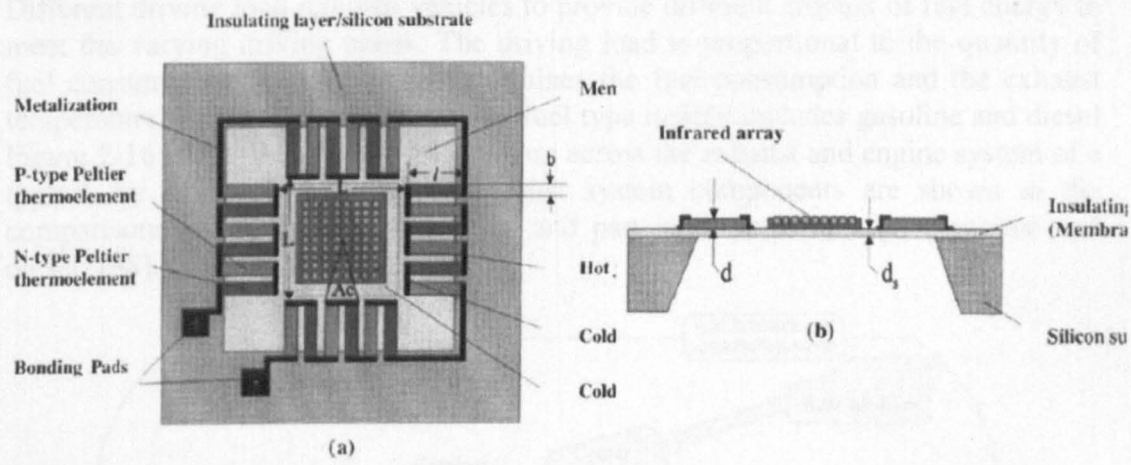


Figure 2-15 Schematic diagrams of an integrated thermoelectric microcooler with infrared components integrated onto cooled central region (a) Plane view and (b) cross-sectional view.

Thermoelectric cooling can also be used to work with solar PV for electrical power generation. Better performance and cheaper cost were obtained when thermoelectric modules are used to actively cool solar PV than when used to recover heat from solar PV panel [86].

### 2.2.2. Thermoelectric generators

Thermoelectric generators are solid-state devices that convert heat into electricity. Unlike traditional dynamic heat engines, they have no moving parts, long lifespan, compact size and silent operation. Due to these advantages, thermoelectric generators have been utilised in wide areas like aerospace, vehicle, industries and domestic environment.

#### 2.2.2.1. Automobile

With less than 25% of the energy content in the gasoline of most cars goes into actual vehicle propulsion, over 50% of the total fuel energy escapes to the ambient as



heat loss primarily through the vehicle exhaust system and radiator. Different from other waste heat sources, the vehicular exhaust lies in a wide temperature range which extends from 100°C to 800°C [87]. The temperature level depends on the driving conditions such as part loaded driving or full loaded driving. Therefore, developing vehicular thermoelectric generation system for recovering vehicle waste heat needs to take the following factors into account.

1. Varying thermal conditions caused by different driving conditions;
2. Wide exhaust temperature range;
3. Moving state;

Under general driving circumstances, the vehicle goes through different driving behaviours (such as acceleration, brake and stop) and varying road conditions (steep and bumpy) which make the engine and exhaust systems work in a varying condition to accommodate the changes.

The driving load and fuel category decide the temperature level of exhaust gas. Different driving load requires vehicles to provide different amount of fuel energy to meet the varying driving needs. The driving load is proportional to the quantity of fuel consumption. The fuel type determines the fuel consumption and the exhaust temperature. Currently, the commercial fuel type mainly includes gasoline and diesel. Figure 2-16 shows the exhaust temperature across the exhaust and engine system of a typical car. The temperatures of exhaust system components are shown in the comparisons of driving load (full load and part load) and fuel type (gasoline and diesel) [88].

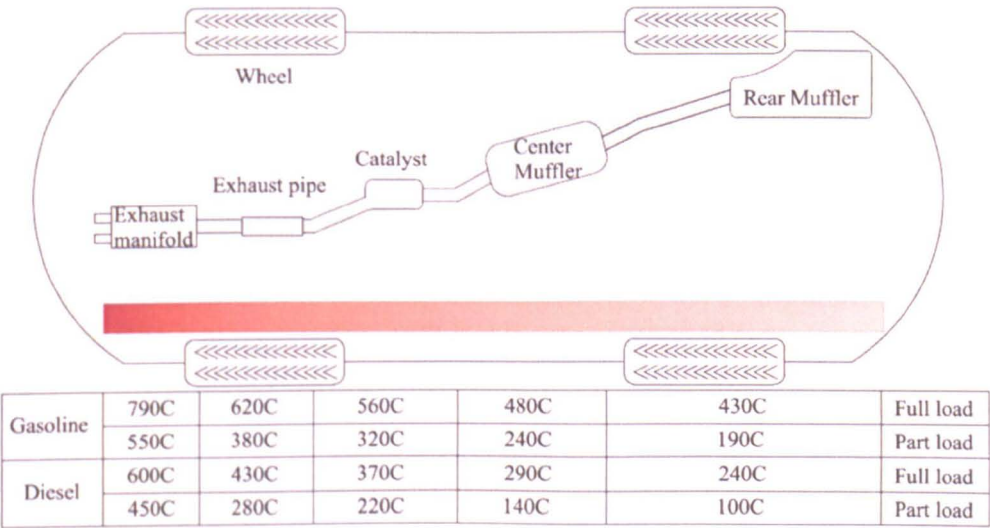


Figure 2-16 Temperatures of exhaust system components for a gasoline engine and a diesel engine

Waste heat is generated only in motion mode. The movement of vehicle necessitates the considerations of the impacts that the moving status imposes on TE modules enclosed in the thermoelectric generation system.

Considering the factors mentioned above, a successful design and construction of vehicular thermoelectric generation system must cover the following considerations:

1. Adopting temperature stabilizing method to eliminate excess temperature on the hot end of TE modules to avoid malfunctions (the welding points could be melted by excess temperature conditions caused by extreme driving conditions);
2. Selecting the technically and economically suitable thermoelectric materials for waste heat recovery for the corresponding sections in the exhaust system;
3. Accommodating the thermal and mechanical stresses under extreme driving conditions while maintaining an optimal thermal conductivity with TE modules as well as long cycle fatigue.

It was thought to be unattractive to employ thermoelectric power generation in automobile due to the high temperature thermal environment in automobile's exhaust/engine system. The high operating temperature requires high temperature standard material which turns out to be very high-cost. However, considering the fact that both cars and trucks consume a considerable amount of fuel at low mass flow rates, especially when the vehicles are experiencing city driving where the fuel efficiency is much lower than that of highway driving due to the energy-inefficient operating such as varying speed, frequent braking and accelerating, improved fuel saving and reduced greenhouse gas emissions become the major impetuses for thermoelectric applications in vehicles. Thermoelectric power generation by recovering waste heat from automobile has become a highly necessary and promising approach. Many studies have reviewed its application in automobile engine/exhaust system and developed effective ways to recover the waste heat in automobile in an economical and optimum way. The possibility of recovering the waste heat with thermoelectric power generation was explored as early as 1914 [89, 90]. The waste heat recovery application on automobile has been investigated for over 90 years [91, 92, 93, 94]. Some of them have developed thermoelectric generation systems which produce 0.5-1kW electrical power with 5-10% overall efficiency [95, 96]. Currently, there are a few major teams that are dedicated in thermoelectric application researches in automobile.

Thermoelectric applications on Porsche [97], truck [98, , 100, 101] and passenger cars [102, 103, 104] and military vehicle have been studied. Waste heat recovering at low temperature (250°C) and medium temperature (550°C) configurations have been discussed by BSST in partnership with BMW and Visteon [87].

#### **2.2.2.2. Aerospace**

Explorations in hostile and inaccessible locations such as space, advances in medical physics, deployment of marine and terrestrial surveillance systems and earth resources require autonomous long-life sources of electrical power. Due to the characteristic of no moving parts, no position dependence and the good adaptability for various heat sources, thermoelectric generators have more than 100,000 hours steady-state operation and precise temperature control [105]. Their developments first occurred in US space program, they have been used by NASA (National Aeronautics and Space Administration) to provide electrical power for spacecraft since 1961. Thermoelectric power generation system has a great application potential for a large number of different classes of space missions especially. As researches continue in power conversion field to improve configurations and specific designs, thermoelectric power generation keeps showing great strength for both short- and long-term space missions.

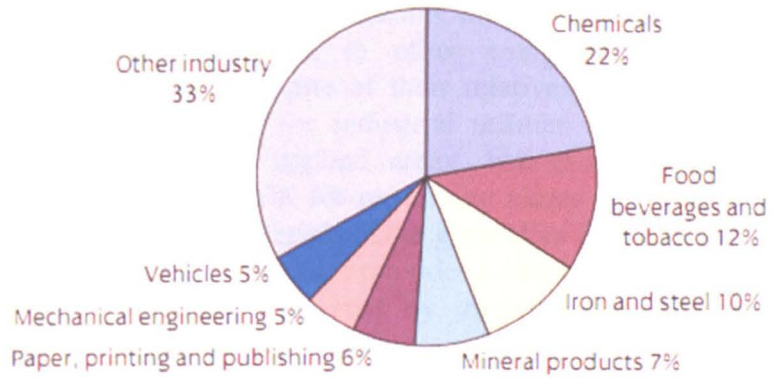
High performance radioisotope generators (RTG) are still of interest for deep space missions but the shift towards small, light spacecrafts has developed a need for advanced power sources. The development of thin film thermoelectric devices shows attractive potential. The development of light weight, high voltage devices with good performance is realisable with the employment of the combination of semiconductor technology, thermoelectric thin films and high thermal conductivity materials. The reliability of thermoelectric technology has been demonstrated in applications such as the Voyager spacecraft with Voyager 1 passing into the Heliosheath about 8.3 billion miles from Earth on May 24th 2006. The successful application also goes to TAGS-85 which has been used in numerous space and terrestrial applications<sup>12</sup>. These TAGS radioisotope thermoelectric generators (RTG) working over 20 years are still delivering enough power to support the Pioneer 11 (together with the Pioneer 10, the pioneer 11 was the first to traverse the asteroid belt and visit the giant gas planets) spacecraft onboard experiments and power the radio which is returning useful data back to earth. The overall power degradation rate, including fuel decay, helium buildup, and all other effects was approximately 0.00007 W/h per generator. As far as is known, these are the longest lived autonomous electrical power sources ever produced. The same type of applications also provided long-lasting power to the Viking Landers 1 and 2 and other devices used in inaccessible or hostile areas like meteorological data collection and transmission system in off-coast areas and seismic detectors in Alaska, more details can be referred to [12].

For aircraft industry (both commercial and military), thermoelectric device can capture waste heat from the engine and operate over the entire aircraft flight envelope and operates without affecting engine's performance. Fuel consumption can be cut down and consequently the cost for passenger and cargo airlines could be reduced.

#### **2.2.2.3. Industries**

Industrial processes are usually procedures involving chemical or mechanical steps in the manufacture of an item or items on a very large scale. The process industries include food, beverages, chemicals, pharmaceuticals, petroleum, ceramics, base metals, coal, plastics, rubber, textiles, tobacco, wood and wood products, paper and paper products, etc. Industrial energy consumption accounted for more than a fifth of all UK energy consumption in 2001 consuming 35,152 thousand tonnes of oil equivalent. For example, the energy consumption of different industry sectors in 2001 in the UK is shown in Figure 2-17 which is cited from the national statistics by the Department of Trade and Industry [106].





Source: DTI

Figure 2-17 Energy consumption distribution of industry sectors in the UK

Due to the large scale in most cases, industries involve with a huge amount of energy consumption, in which a considerable amount escapes to ambient through exhausting, radiation and cooling. Figure 2-18 compares the energy use and losses in energy systems (steam systems, fired systems, and motor drive) across sixteen industrial sectors [107]. Five industrial sectors which include petroleum refining, chemicals, forest products, iron and steel, and food and beverage, account for over 80% of all the energy inputs to energy systems. They are large users of steam systems and fired systems such as furnaces and dryers. In total, energy losses associated with energy systems in these five industries totals represents over 15% of the energy consumed by U.S. industry.

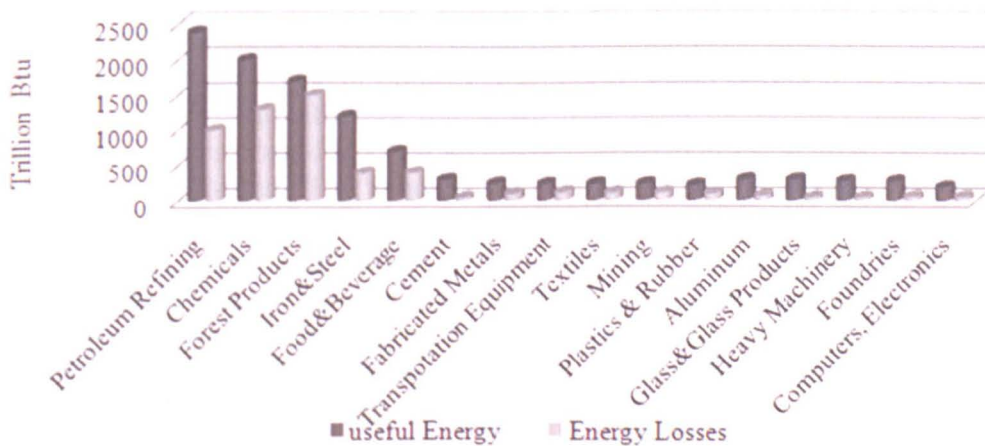


Figure 2-18 Chart of energy consumption in different industrial sectors

This unused energy is energy loss or waste heat, which is generated in the processes of fuel combustion and chemical reactions, then wasted by ending up in the environment rather the product due to unnecessary process, intensive drying, inefficient boilers and steam systems. Driven by the growing fuel prices and strong concerns on the global environment, process industries find it necessary to develop and employ heat recovery approaches to cut down the energy consumption and consequently contribute to the reduction of greenhouse gas emission and environmental improvement.

Because of their high reliability, noiseless operation, low maintenance and long life, thermoelectric generation are preferred to other energy conversion devices particularly in harsh environments, despite of their relatively low efficiency. The type of thermoelectric material used for industrial utilities is dependent on the operating temperature range of the applied areas. For example, the available temperature ranges from 325K to 1100K for processing plants of combustible solid waste [108], depending on the used materials of the generators for different operating temperature ranges. In steel plant, the furnace provides a steady source of convenient piped water which can be readily converted by thermoelectric generators into electricity when large amounts of cooling water were discharged at around 90°C. Bismuth telluride thermoelectric material was employed to produce a total electrical power of 8MW in major components of a modern steel plant [109].

The possibility of employing thermoelectric technology to generate electrical power from low temperature heat source on off-shore oil platforms was discussed in 1992 [110]. The oil reservoir located at a depth of around 3km and the temperature at the working depth is in the range of 80-100K. It was concluded that it was technically feasible to use thermoelectric power generation in this circumstance but the cost of transmitting dc power from the platforms to the adjacent mainland was considered to be uneconomic. If the electrical power can be stored by being converted to other type of energy like hydrogen, the high cost for the dc power transmission could have been avoided.

Applications in both small scale and large scale for recovering heat from combustible solid waste have been conducted [111, 112]. An estimated conversion efficiency of 4.36% was achieved in a small-scale on-site experiment using a 60W thermoelectric module installed near the boiler section of an incinerator plant [113]. It was estimated that an output of 426 kW could be obtained according to an analysis of a conceptual large scale system burning 100 ton of waste during a 16-hour-working day. The possibility of utilizing the waste heat from incinerated municipal solid waste has also been considered and an on-site experiment using 60W thermoelectric module was conducted. The module was installed near the boiler section of an incinerator plant where the waste gas temperature varied between 823K and 973 K. An estimated conversion efficiency of about 4.4% has been achieved. Thermoelectric generators operating on natural gas, propane or diesel have been developed with different thermoelectric alloys with the maximum hot side temperature ranging from 525K up to 875K [114]. These devices have been used in various industrial applications for data acquisition and telecommunications.

#### **2.2.2.4. Thin film application**

Thin films have attracted considerable attention because of their potential application in the micro-fabrication of integrated thermoelectric devices and its flexibility in installations. Due to the small thickness, thin film applications allows exceptionally high heat fluxes and low thermal resistances which delivers much higher power densities compared with conventional modules. However, the challenge of thin film applications lies in the growth process. Current, there are quite a few advanced methods that have been developed to fabricate the thin film structure. Different from the commonly-used fabrication methods which include flash evaporation [115], hot wall epitaxy [116], sputtering[117], metal organic chemical-vapour deposition [118] and molecular beam epitaxy [119], co-evaporation [120] was claimed to require less

preparation time, lower fabrication cost and be compatible with microelectronic processing. In the work, high-purity (99.999%) bismuth and telluride were used as evaporants which were evaporated from molybdenum boat and a tantalum crucible, respectively. The films were deposited by the co-evaporation of bismuth and telluride onto a heated, clean glass substrate. The best quality of thin films obtained using co-evaporation technology has  $\alpha=81\mu V/K$ ,  $\rho=0.32\times 10^{-3}\Omega$  for p-type and  $\alpha=-228\mu V/K$ ,  $\rho=1.30\times 10^{-3}\Omega$  for n-type, respectively.

#### **2.2.2.5. Other application areas**

The earliest thermoelectric application example was using the heat from kerosene lamp to power a wireless set [121]. Certain amounts of electrical power could be also provided to remote regions like Northern Sweden using thermoelectric generators to ease the local electricity scarcity [122]. Additionally, marine vessels like ships and submarines can be the primary targets for thermoelectric generation which can harvest waste heat from the propulsion engine.

Insight [123] has also been shed onto the heat recovery from long wave infrared radiation leaving the surface of the earth. Thin film thermoelectric device is applied for power generation in high altitude, long duration communications platform.

### **2.3 Summary**

In order to make the thermoelectric application more economically feasible, increasing efforts have been made to discover and develop advanced thermoelectric materials with high figure-of-merit. Fabrication methods such as superlattice, plasma treatment, segmented element, nanocomposite and nanostructure have been introduced to improve ZT value of thermoelectric materials. These methods have shown positive results by changing the material properties and improving module shape and structure, such as reducing thermal conductivity, enhancing electrical conductivity and adopting novel module shape and structure, such as ring-shape and thin film.

With continuous efforts being made, the difficulty in making a breakthrough in material research and development in terms of fabrication, construction and commercialisation is still one of the major factors that have limited thermoelectric application to only specialised areas. Due to the advantages of no moving parts, long lifespan and quiet operation, thermoelectric modules have been used in many areas such as automobile, aerospace, industries and domestic sector. They have not been used as widely and intensively as expected due to lack of economical feasibility. The energy efficiency of conventional thermoelectric applications is far too less to compensate the system cost due to low conversion efficiency, and only suitable for some specialised areas.

## Chapter 3 Domestic building energy analysis

This chapter takes the UK as an example to introduce the energy profile of domestic sector in the regions/countries with temperate climate which the domestic boiler plays the major role of supplying space and water heating in residential houses. The proportion of the energy used for space/water heating in the overall energy consumption of a residential house has been introduced together with the role of domestic boiler in space and water heating to show the importance and necessity of improving the thermal efficiency of domestic boiler. The use of thermoelectric applications in domestic sector has been reviewed to show the necessity of developing a system concept that gives a more economically viable performance. The thermoelectric material that is suitable to be used in domestic environment is introduced according to the available heat sources in residential house. The availability of solar energy and waste heat from domestic boiler has been discussed in different scenarios for a case study conducted in chapter 7.

### 3.1. Energy consumption analysis

In domestic sector in the UK, the energy consumption consists of space heating, water heating, lighting, appliances and cooking. The majority of energy consumption is for space heating. Reference [124] has demonstrated the results of an investigation on the energy consumption in domestic sector in the UK conducted by the Department of Trade and Industry. It shows the energy consumed by space heating in domestic sector. For example, in 1970 and 2000, it accounted for 58% of all the consumed energy. It increased up to 61% in 2009, taking the dominant position.

Figure 3-1 shows the energy saving due to better house insulation and heating efficiency between 1970 and 2006. The energy consumed by space heating would have been twice of current consumption if there was no improvement in house insulation and heating efficiency. However, the energy consumption for space heating still shows a steady rising trend, as indicated by the blue part, caused by the increasing demand for heating requirements.

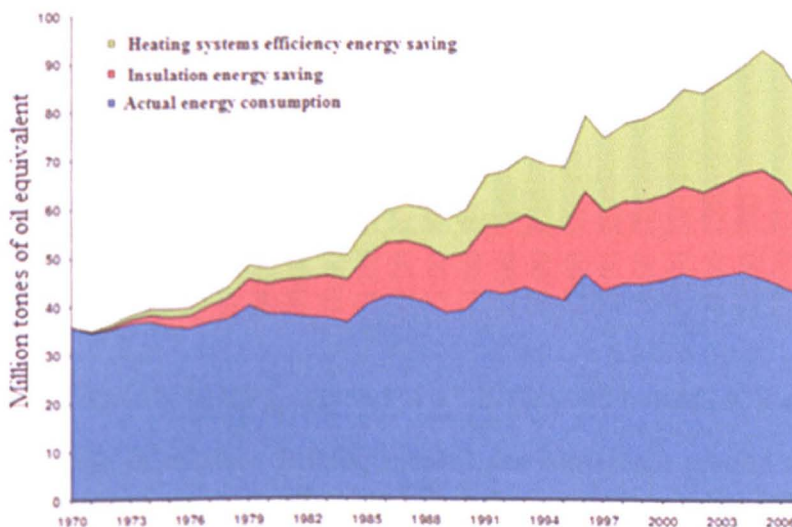


Figure 3-1 Saving in space heating due to better insulation and heating efficiency in the UK between 1970 and 2007



In any year, space heating is largely dependent on outside temperatures which explain the year-to-year fluctuations. Taking the period between 1970 and 2000 as an example, despite the increased use of house insulation, the growth in central heating has contributed to the increases over the period.

In 1970, about 10% of households in the UK were centrally heated by gas and 9% used solid fuels. Whilst in 2000, 71% used gas for central heating and 3% used solid fuels. For electrical storage heating, it accounted for 6% of the total in 1970 and 9% in 2000. The central heating has risen from less than one third of all house stock in 1970 to 89% in 2000.

The gas consumption accounted for 24% of total domestic energy consumption in 1997 and for 67% in 2001, respectively. Meanwhile, coal accounted for 39% and 45% in 1970 and 2001, respectively. Electricity consumption has increased by 50% over the period of 1970 to 2001, due to the increased use of electricity for lighting and appliances in the home.

Temperature is the important factor that affects the energy demand of the house. For example when the temperature is very low in winter, much energy needs to be used for space heating. This energy demand has risen when we have been approaching from 1970 to 2000 as the demand for the indoor temperature has been raised by the occupants' demand although the outside temperature has increased from 5.8° C in 1970 to 7.2° C in 2000.

Figure 3-2 shows the daily heating demand of a two-bed bungalow house in the UK around a year. This data, provided by Cooling Planet Ltd, shows the hourly heating demand in a day of four seasons. Although the heating is supplied by using an air source heat pump, the usage profile should show the pattern of dynamic heating demand of this house which would reflect the operational pattern if the heating was supplied by a boiler.

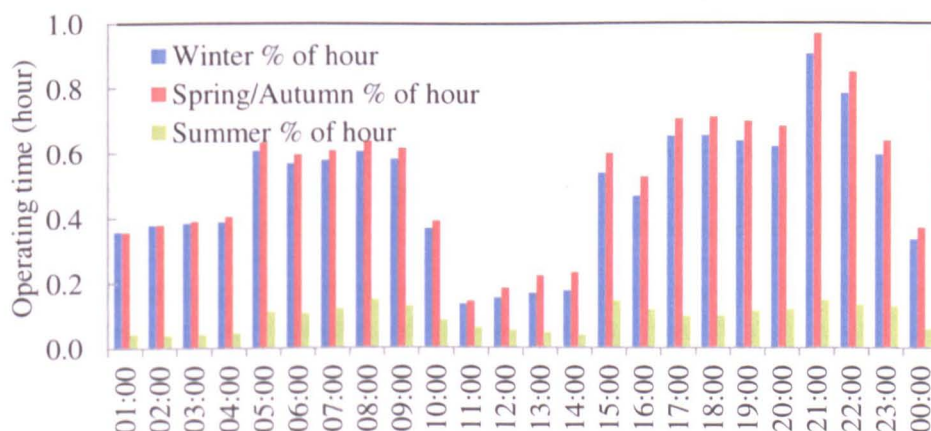


Figure 3-2 Hourly heating demand of a UK two-bed bungalow in a year

Playing a vital role in modern Britain, natural gas represents around two fifths of final energy consumed and dominates the UK domestic sector. In the last forty years, the gas consumption in the domestic sector has grown dramatically to the current over six times of the level in 1970. The major factors that drive the rapid growth of

gas demand in domestic sector include population increase, larger numbers of households and higher standards living.

In order to gain a general idea of the gas consumption of domestic sector in the UK, a report of gas consumption in the UK by British Gas is cited [125]. British Gas commissioned the Centre for Economics and Business Research ('Cebr') to assess the factors that have reduced domestic natural gas consumption over the last five years. The focus of this part is to determine the key drivers of natural gas consumption by utilising a British Gas analysis of domestic energy consumption based on 40 million meter readings from four million customers between 2006 and 2009.

Taking 2009 as an example, the total primary gas consumption was 44.3 million tonnes of oil equivalent, representing 65.2% of the UK's total energy consumption in domestic sector. It is mainly used for space heating, water heating and cooking. Overall, the gas consumption in 2009 is over six times higher than that in 1970 on a primary energy equivalent basis, which is equivalent to a compound annual growth rate of 4.9%. A number of factors are attributed to the rapid increase of natural gas consumption. Households, population and household disposable income are the major three direct factors that drive the gas consumption in domestic sector. Energy intensity (energy consumption per household, person and disposable income) shows different trend between 1971 and 2009. Energy intensity by household and by disposable income shows a fall by 12.6% and 55.3%, respectively. Meanwhile, energy intensity by population shows a 10.6% increase. According to the Office for National Statistics' latest population projections, the UK's population shows an annual growth at 0.6% forwards to 2033, 0.9% increase for household. That means more energy is expected to be consumed.

### **3.2. Profile of heating demand**

The heating demand for a typical UK house varies with the season. In each season, the demand also varies with the time of the day. The boiler is a common device for domestic heating. Usually, it operates according to the required room temperature level set in thermostat. Therefore, the boiler runs only when the room temperature is below the set level without having to run all the time. Due to the same control regime, this operating pattern can be reflected by that of air source heat pump provided it is used for the same house, the pattern can be referred in Figure 3-2.

It shows the heating demand of two-bed bungalow in the UK and the average daily heating hours in four seasons of a year, among which spring and autumn are considered together due to the similar temperature level. The heating demand in winter takes the largest proportion whilst the sum of heating demand in spring and autumn is slightly less than that of winter; the heat demand in summer is minor.

### **3.3. Heating methods**

#### **3.3.1 Solar power**

In order to fully understand the availability of solar power, a comprehensive study on the solar energy arriving at the surface of the earth has been conducted by the Institute for Environment and Sustainability of European Commission [126]. The relevant results are cited to show the solar availability in different regions and

countries. The amount of available solar energy depends on the geographical variability, weather conditions and time dynamics. The geographical analysis of the availability helps us understand the contribution that TCS could make to the improvement of domestic power conditions. Taking the UK as an example, supposing the modules are mounted at the optimum angle, the yearly sum of generated electricity per area in the UK is 820kWh/kW<sub>p</sub>. For a 1/kW<sub>p</sub> peak power, the required area of solar PV is 6.7m<sup>2</sup> on the assumption of 150W/m<sup>2</sup> power density. Hence, the equivalent yearly sum of absorbed direct solar radiation is approximately 122.4kWh/m<sup>2</sup>.

### 3.3.2 Boiler

For residual spaces, apart from the solar radiation which is generally utilised in most circumstances with the presence of sunshine, one of the main available heat sources in domestic environment is the waste heat from domestic boiler. It is a very common heating device which has been widely used in the UK. Good understanding of the availabilities of these heat resources is necessary to unveil the potential and benefit of applying thermoelectric co-generation system in residential houses.

The temperature of boiler flue gas used to be very high which contains a big amount of heat loss in the form of latent and sensible heat. Modifications have been done to improve the performance and efficiency by reclaiming the latent and sensible heat. For example, the condensing boiler is able to recover the latent heat by using the second heat exchanger which reclaims the heat escaped from the first heat exchanger. However, the temperature of flue gas from the conventional new boilers still lies in the range of 150-200°C [127] which contains considerable amount of energy when exhausted to the environment. This represents a great opportunity of establishing a domestic power generation device/system by recovering the heat and converting it to electrical power. Domestic power consumption in the United Kingdom between 1970-2000 has been studied and given by the department of trade and industry of National Statistics in the UK [128]. It shows that energy consumed on space heating and water heating represents 82% of the overall energy consumption in households.

Table 3-1 Yearly sum of gas consumption per consumer in the UK [1]

Year	2001	2002	2003	2004	2005
Qty of Consumer (thousands)	20490	20587	20683	20791	21595
Sales per Consumer(kWh)	19942	20118	20111	20496	19020
Year	2006	2007	2008	2009	
Qty of Consumer (thousands)	21884	22224	22327	22568	
Sales per Consumer(kWh)	18241	17614	16906	15384	
Gas per user means the gas consumption per each boiler in the form of thermal energy.					

Although improvements have been done to use the domestic energy more efficiently, there are still large amount that is wasted by escaping to the outside through waste heat exhausting. This part of heat, if recovered, would play an important role both in cutting down the domestic energy consumption and improving the energy utilisation efficiency. Generally, the amount of waste heat exhausted from conventional domestic boilers depends on the boiler efficiency which varies with the manufacturers, specifications and used period. The efficiency normally lies below

80%. Here a boiler with efficiency of 80% is taken as an example to estimate the total waste heat exhausted by one domestic boiler annually in the UK. The annual waste heat per boiler is.  $Q_w = 30768kWh$ .

One of the major reasons of using the TCS concept is to enhance the energy efficiency of domestic appliance by recovering the waste heat in the domestic sector and partially meeting the energy demand rather than replacing the current power and heating supply. The amount of power and heating that it supplies largely relies on the amount of available heat.

### 3.3.3 Wood burning/biomass stove

In developing countries, wood burning or biomass domestic stoves are commonly used especially in rural areas where the winters are relatively cold and there is no reliable electric power supply. This type of domestic stove is commonly used for cooking and space heating in some occasions. Biomass combustion meets basic energy needs for cooking and heating in rural households. The energy accounts for about 90% of the total rural supplies. Biomass stove is a CO<sub>2</sub>-neutral renewable source of energy. It is usually used as open fire stove which has low efficiency and emits harmful air pollutants [129]. Generally, a cooking stove consumes biomass energy at a rate of 10kW with 2kW available for thermoelectric power generation [130].

### 3.3.4 Furnaces

For remote communities far from the grid and the connection to the grid is not cost effective, the use of thermoelectric power generation could ease the need for electricity. Qiu [131] demonstrates a thermoelectric application with a power generation capacity of 550W which is thermally fed by a purposely-built fuel-powered furnace, intended for domestic central heating. The power output was adequate to power all electrical components for a residential central heating system without using any externally generated electricity.



Figure 3-3 Purposefully designed fuel-powered furnace for central heating system integrated with thermoelectric generation [131]



It has the heat conducting fins on the internal wall of combustion space to enhance the heat absorption by the internal wall from the gaseous combustion, shown in Figure 3-3. A 552°C temperature difference was achieved between the hot and cold walls. Table 3-2 shows more details of the experimental parameters.

Table 3-2 Furnace combustion performance

Fuel input (kW)	Excess air (°C)	Combustion load <sup>a</sup> (W cm <sup>-2</sup> )	Burner surface temperature (°C)	Temperature of combustion products (°C)
15.6	5	31.3	993	1120
15.5	12	31.3	929	1035
17.5	5	35.1	1050	1186
17.5	12	35.1	964	1092

<sup>a</sup> Combustion load refers to the burner surface area.

3.4. Previous research

Insight has been shed into improving the energy performance in domestic dwellings by recovering the heat from drain water using drain water heat recovery (DHR) system [132]. It pre-heats the fresh supply water of the dwelling with the heat of warm drain water of the shower. Liu [133] has also looked into recovering heat from the public shower facilities. It integrates the drain water system with an electric heat pump which recycles the exhaust heat from the collected warm drain water to heat the shower’s tap water. Similar [134, 135] studies have also been conducted. The common thing about them is that they recovery the heat at a low temperature level (around 30°C).

For the thermoelectric technology, the energy efficiency of domestic dwelling is improved by using thermoelectric technology for power generation, mentioned in previous studies [16, 17, 18, 19]. However, not many have looked into its application in building services. Unlike PV technology, thermoelectric technology doesn’t rely on solar radiation. It is useable on almost all types of heat sources, especially beneficial to utilise the rewarding waste heat.

The thermoelectric generator generates electricity by converting heat (temperature gradient) directly into electrical power, using Seebeck effect shown in semiconductor materials such as bismuth telluride, alloys of lead telluride and silicon germanium. Due to the energy conversion characteristic of thermoelectric technology, almost any heat resources existing in domestic environments are eligible for energy conversion. For example, the houses where wood/diesel/biomass burning stove or other available heating facilities are regularly used have the great potential to generate electrical power by using thermoelectric generator [136]. In this situation, the efficiency could be improved by producing extra electrical power with wasted heat. Daniel has developed a concept of self powered domestic boilers in two separate studies in [137] and [138] at different development stage, both of which were intended to adopt thermoelectric power generation to power all the components in the central heating system. Creveling [137] used a boiler with the nominal capacity at 15kW, generating up to 109W of power, rejecting heat to a water loop at near ambient temperatures (27°C). It indicated the merit of further development of self-powered heating devices. Similar applications were introduced in other studies [139]. The TE

generator converts about 5% of heat output from the gas/oil burner into electrical power before the heat output reaches the central heating hot water exchanger and the remained 95% heat output is transferred to the hot water exchanger for space heating in the house. It was concluded that the circulating pump was powered by the generated 50W with two PbTe modules when operated at hot and cold side temperatures of 550°C and 50°C. Fitting with thermoelectric generators, biomass boilers and heat pumps can be operated self-sufficiently and independently without extra power supply. Thermoelectric power generation in applications where solar radiation or waste heat is used can be defined as a green technology as the cost for heat input is free. In this situation, the system's power output outweighs the conversion efficiency in determining the system's economic viability.

Due to the low conversion efficiency, most of the conventional thermoelectric applications only convert small amount of absorbed thermal energy to electrical power. The rest, which represents over 95%, is wasted to the environment. The research aims to introduce a system concept which attempts to overcome the issue of low energy utilisation efficiency by developing a thermoelectric cogeneration system for domestic use and pointing a potential direction of improving the energy utilisation efficiency in residential houses.

### 3.5. Material selection

According to operating temperature, thermoelectric materials are classified into three categories: low temperature, intermediate temperature and high temperature. The low temperature type including alloys based on bismuth in combinations with antimony, tellurium or selenium utilises general waste heat or heat from warm/hot water, while the latter two which include lead alloys and silicon germanium alloys are oriented for incineration/steel plants and automobile exhaust, respectively. The application of high temperature type means more cost. Suitable application of thermoelectric material is generally referred to large electrical power factor, good cost effectiveness and being environmentally friendly. For example, when the utilised heat is free, the cost-per-watt is mainly determined by the power-per-unit area and the operating period [ 140 ]. For high operating temperature, modules with segmented thermoelectric elements have larger average figure of merit over a large temperature drop compared to those using same alloy in the element. The thermoelectric efficiency reached as high as 20% operating between 300K and 975K [ 141 ]. However, for the domestic power environment (under 473K),  $Bi_2Te_3$ , one of the commercialized thermoelectric materials whose good ZT (0.98) lies in the range of 353-413K, shows a better performance and lower cost due to a good figure-of-merit in operating temperature range in domestic applications.

### 3.6. Availability

Figure 3-4 shows the thermal cycle of thermoelectric cogeneration system. The heat source (or multiple heat sources) provides the hot side heat exchanger thermal energy, denoted as  $Q$ . The hot side heat exchanger absorbs the heat from the flue gas and uses the harnessed heat for thermoelectric cogeneration. The harnessed heat is used as the heat input of the system, denoted as  $Q_{input}$ ,  $Q_{loss}$  and  $\eta_{hx}$  for the heat loss and the effectiveness of hot side heat exchanger. The converted heat is used to

produce electrical power, denoted as power output  $P$ . The unconverted part is dissipated into the cooling water for preheating purpose, denoted as  $Q_{output}$ .  $\eta_{hx}$  and  $\eta_m$  are the effectiveness of heat exchanger and conversion efficiency of the module. For a given heat source, the available amount of the heat supplied from heat source is known. Then the heat input can be calculated by Eq.(3-1):

$$Q_{input} = \eta_{hx} Q \quad (3-1)$$

The system thermal efficiency  $\eta_{co}$  is defined by ratio of the sum of heat output and power output to the total amount of available heat supplied by the heat source.

$$\eta_{co} = (P + Q_{output}) / Q_{input} \quad (3-2)$$

The TCS concept is used in a domestic environment where the heat source includes boiler waste heat and solar energy. The amount of heat that heat exchanger can absorb relies on the amount of available heat source. The presence of both heat sources are separately determined by different factors. The boiler waste heat is decided by the boiler efficiency, the running period which is determined by the outdoor temperature, the set level of thermostat and the house insulation. Meanwhile, the solar radiation is determined by geographical location, weather condition and time variation during the day.

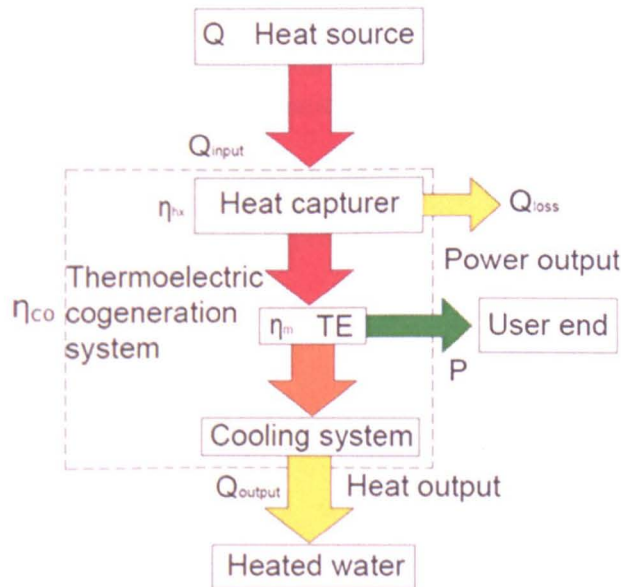


Figure 3-4 Thermal cycle of thermoelectric cogeneration system

The boiler operates according to the settings of time schedule and the thermostat installed in the house. Denoting the time of each continuous operation of the boiler as  $t_{op}$ . When the oil tank is heated with the presence of both the solar power and the boiler waste heat, the achievable oil temperature  $T_o$  could go up higher. The oil temperature are analysed under three circumstances: 1, boiler waste heat; 2, solar power; 3. Boiler waste heat plus solar power.

## 1. Boiler waste

The boiler waste heat is present when the boiler is running. Assuming the yearly sum of gas consumption by the boiler is  $Q$  and the boiler efficiency is  $\eta$ , then the waste heat from the exhaust  $Q_w$  can be approximately expressed by

$$Q_w = (1 - \eta)Q \quad (3-3)$$

The waste heat from the exhaust is captured by the flue heat exchanger integrated into the flue pipe. The amount of captured heat  $Q_{cp}$  is determined by the effectiveness of flue heat exchanger  $\eta_c$ , namely  $Q_{cp} = \eta_c Q_w$ . Then this captured heat  $Q_{cp}$  is used to heat the oil. To heat the oil to temperature  $T_o$ , the heating time can be calculated by Eq.(3-4)

$$t = \frac{c_o \rho_o v_o (T_o - T_a)}{Q_{cp}} \quad (3-4)$$

Where  $C_o = 2500J/kgC$ ,  $\rho_o = 0.888g/ml$ ,  $T_a$  is the ambient temperature,  $t$  represents the response time of reaching the designed operating condition.

## 2. Solar power

To calculate the available solar power, the required parameters include the area of solar concentrator  $A_{con}$  and the solar radiation  $I$ .

For the solar collector with solar concentration measure, the amount of available solar power  $Q_{solar}$  can be calculated by Eq.(3-5)

$$Q_{solar} = A_{con} I \quad (3-5)$$

Provided the efficiency of solar collector is  $\eta_s$ , then the absorbed solar power can be calculated by

$$Q_{as} = \eta_s Q_{solar} \quad (3-6)$$

If heat transfer medium is applied (heat transfer oil is used in this study), it has a maximum operating temperature, the oil temperature must be no higher than this temperature for the safety sake. The oil volume  $v_o$  can be fixed according to the thermal condition given by the boiler waste. Hence, the time of heating the oil tank to the maximum operating temperature can be calculated by using Eq.(3-4). Due to the high intensity of solar radiation achieved by solar concentration, the oil temperature could heat the oil to the maximum operating temperature. In order to ensure the safety and reliability of the system, certain measure must be taken to make sure the oil temperature goes down to the level beneath the maximum operating temperature. The cooling system must be switched on with the presence of either boiler waste or

solar power. When the cooling system is integrated into the water feed system, the cooling system would not work if the boiler is not working. In this situation, the pump water must be circulated in accordance with the oil temperature level or the presence of solar power. Therefore, the operation of cooling system needs to be based on the temperature of heat source, or the hot side temperature.

### 3. Boiler waste and solar power

When both the boiler waste and solar power are available, the amount of heat is the sum of boiler waste and solar power. The days with the presence of both sources will be fixed by the days with the heating demand and the average sunny day in the region during this period. The overlapped days are the time when the boiler waste and the solar power are both available.

Together with solar radiation, the temperature of the exhaust decides the level of oil temperature in the tank. If the flue gas temperature is  $T_f$ , assuming the temperature decreases from flue gas to the hot side of thermoelectric generators is  $\Delta T_{fh}$ , the hot side temperature of TE generator can be calculated by  $T_h = T_f - \Delta T_{fh}$ .

Table 3-1 shows the yearly sum of gas consumption per boiler. Due to the introduction of wall insulation, loft insulation and double glazing to the house, the gas consumption shows a declining trend. Here taking 2009 as an example, the yearly sum of gas consumption is 15384kWh. More details are introduced in section 7.1.2.

### 3.7. Summary

The energy consumption of residential house in the UK in the last few decades shows a steady rise and a rising trend is projected as we are heading forward. Despite the increased use of house insulation, the energy used for space/water heating takes up about 80% of overall energy consumption and is still climbing up as the living standard improves and the number of household increases.

Available heat sources such as solar power, boiler, stove and furnace are typical heating appliances for supplying space/water heating in the UK. Among which domestic gas boiler plays the major role (up to 65.2%) in providing space/water heating in the UK. A typical boiler with seasonable efficiency at 80% gives waste heat at approximately  $Q_w = 30768kWh$  per year.

Comparing to different thermoelectric materials, the one that is suitable for domestic application is identified to be  $Bi_2Te_3$  according to the analysis of temperature level of available heat sources in the UK residential houses. This chapter comes to the conclusion that a more economically feasible system concept is needed to overcome the issues presented in conventional thermoelectric power generation applications.

## Chapter 4 Heat sourcing

This chapter introduces the system concept and breaks down the issues that are confronted by this research and need to be solved to improve the domestic energy efficiency by employing the domestic thermoelectric cogeneration system. The hot side heat exchangers including the solar heat exchanger and boiler flue heat exchanger have been discussed. For the boiler flue heat exchanger, harvesting the waste heat in boiler exhaust pipe by installing arrays of heat pipe heat exchangers has been proposed as an attempt of efficient and suitable method in this research due to the advanced heat transfer characteristic shown in heat pipe heat exchangers. A series of numerical simulations have been carried out to investigate four parameters that affect the performance to identify the suitable design of boiler flue heat exchanger using heat pipe.

### 4.1 Background

The factors that significantly influence the thermal efficiency of thermoelectric application include the boundary conditions of hot and cold side, thermodynamic cycle and thermoelectric materials. Among which, the thermal boundary conditions of hot and cold side are involved with the available ways of extracting the heat from heat sources and dissipating the unconverted heat from the cold side which significantly influences the efficiency. This leads to the technical aspects of heat exchange design. The heat sourcing and heat dissipation determines the system's thermal resistance, which takes us to the consideration of thermodynamic cycle design.

According to the style of heat sourcing and heat dissipation, the heat exchange can be classified into the following four categories.

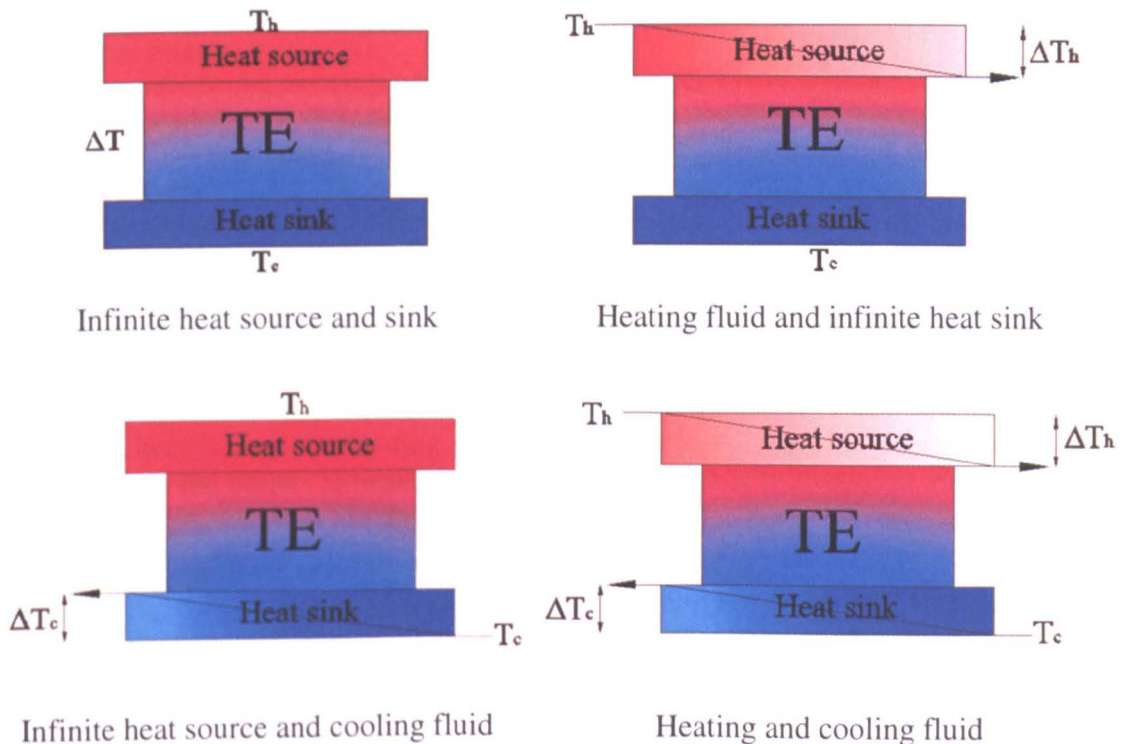


Figure 4-1 Heat exchange types in thermoelectric applications



As shown in Figure 4-1, four main categories of thermal boundary conditions exist in thermoelectric applications. The most commonly investigated boundary condition (Figure 4-1-a) assume that both the hot and cold sides are isotropic at temperatures  $T_h$  and  $T_c$ , respectively. This condition is used in most studies, but has been rarely achieved in practical applications. However, the configurations (Figure 4-1- b, c, d) that replace one or both of the isotropic boundaries with convective media as sources or sinks for thermal power are more common in today's applications. Assuming the thermal energy  $Q_h$  passes through the hot side of the module at temperature  $T_h$  and unconverted heat is dissipated at temperature  $T_c$  on the cold side. As described by Seebeck effect, this temperature difference  $T_h - T_c$  induces a conductive thermal flux which consequently generates electricity. The amount of power output  $P$  is determined by temperature difference  $T_h - T_c$  and the properties of thermoelectric materials ( $S$ ), explained by  $P = (S(T_h - T_c))^2 / R_L$ , where  $S$  is the seebeck coefficient determined by material,  $R_L$  is the external load.

## 4.2 System description

The thermoelectric cogeneration system concept, capturing the boiler waste heat and solar energy to generate electricity and produce preheated water for home use, has been put into experimental investigations [142] and the feasibility of enhancing the energy use efficiency in the residential house by integrating this approach into the existing domestic boiler has been proven with positive results. This system reuses up to 80% of the recovered waste heat, in which up to 5% is converted into electrical power and the rest is dissipated to boiler feed water for preheating. The results proved that this approach, capable of cutting down CO<sub>2</sub> emission by producing electrical power and hot water using free energy input simultaneously, leads us to a direction of environmentally friendly and sustainable energy generation method for residential houses.

In this concept shown in Figure 4-2, one primary heat source is waste heat from the boiler exhaust. A cooling fluid is circulated in a purposely-designed heat exchanger on the cold side of the TE generator to convert boiler waste heat to electricity and provide thermal energy for the onsite heat feeding devices or facilities. The system is also capable of using solar energy absorbed by a solar collector mounted on the roof of a building whereby solar energy is absorbed and supplied to the thermoelectric module hot side. This can be achieved by direct utilisation or indirect utilisation of solar energy, depending on the heat exchanger design. The heat absorbed from the two aforementioned heat sources can be used to generate "free" electricity and attendant heat is used for heating purposes, increasing the overall energy utilisation efficiency of the boiler. However one of the challenges is to overcome limitations of heat transfer to and from the thermoelectric module.

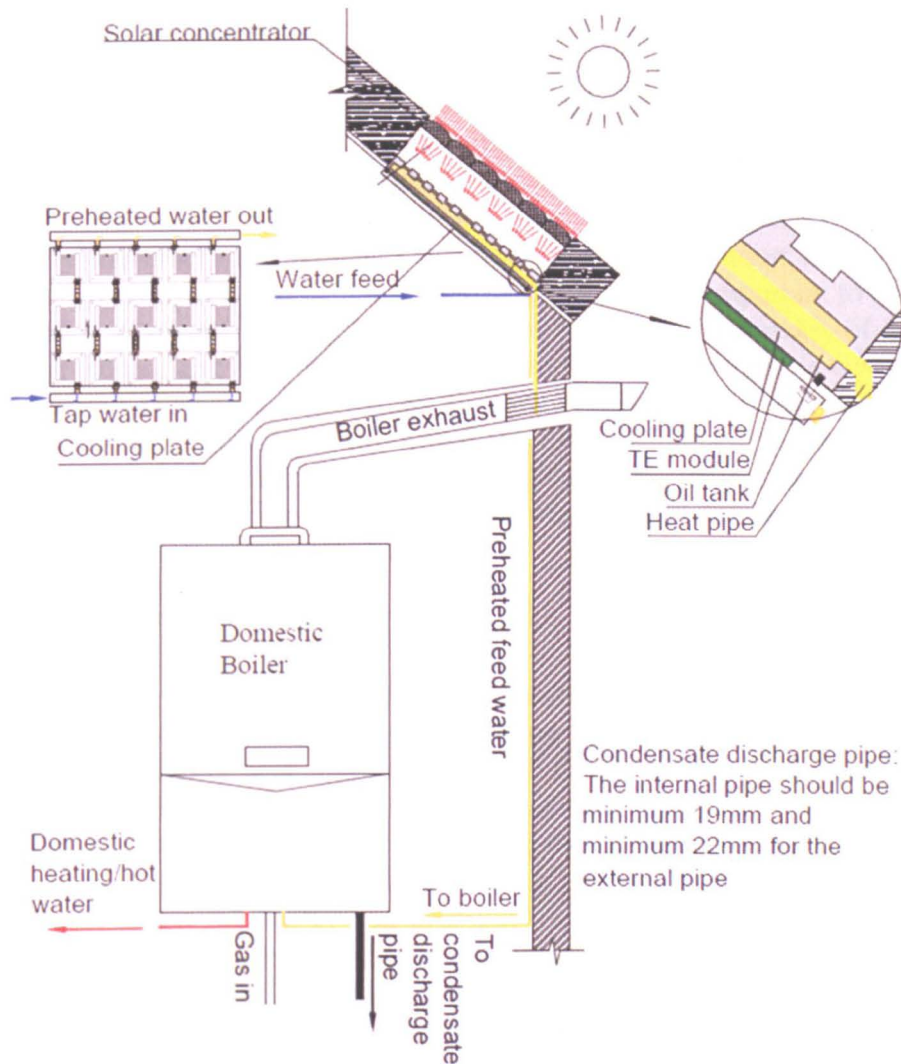


Figure 4-2 Concept diagram of domestic thermoelectric cogeneration system

Figure 4-2 shows the concept of domestic thermoelectric cogeneration system which absorbs heat from exhaust waste of domestic combustion appliance and solar energy. The heat rejected from the cold side of thermoelectric modules is taken away by the cooling plate which is connected to the boiler to provide the preheated water for domestic use, such as feed water for the boiler or under floor heating. In order to achieve this purpose, the following challenges need to be tackled:

#### a. Heat sourcing

Capturing heat from the available heat sources in residential house is one of the primary issues that need to be tackled. It decides the amount of heat that can be used by the thermoelectric system. Specifically designed for recovering the waste heat existing in the boiler exhaust, the flue heat exchanger plays two important roles in the system, including heat recovering and heat transportation. More details based on CFD are given in Section 4.3. The heat captured from the heat sources is directed to the TE modules which converts part of the heat flux into electricity and leaves the rest, unconverted heat flux, to be dissipated into the cold side heat exchanger for other purposes, such as water preheating. It provides heat for the modules, which are mounted between heat exchangers. More details about mechanical assembly are introduced in Section 6.5.



## **b. System performance**

Only when the system characteristic is well understood can the energy products can be efficiently used. This includes the system performance under different thermal conditions and system structures. It includes conversion, utilisation and management of converted heat and unconverted heat. DC electricity is produced from the heat converted by thermoelectric module. The parameter identification that affects the maximum power output under different thermal conditions is important to the design of the external electrical circuit for the sake of the maximal harvest of electrical power and good use and management of generated power in domestic environment. The unconverted heat, which is wasted to environment in conventional heat sink design, is re-used to heat the feed water for existing combustion appliances in residential house. The challenge lies in mitigating the increased pressure drop without significantly affecting the heat transfer performance between the feed water and thermoelectric cogeneration system.

## **c. Heat dissipation**

Cold side heat exchanger shoulders the responsibility of dissipating the unconverted heat. The design of heat dissipation, including the dissipating destination and consumed energy during heat dissipation, is the threshold for good overall energy utilisation efficiency. Conventional fan assisted heat dissipation only gives the energy utilisation efficiency of less than 5% because the unconverted heat is wasted by escaping to the environment without being used. Moreover, the use of fan represents extra electrical energy consumption. Heat dissipation by adopting fluid-based heat exchanger makes it more practical to utilise the unconverted heat in managing-friendly way due to compactness and effective characteristic. However, the transportation of thermal fluid involves the use of electrically-powered pump. The capacity of the pump is determined by hydraulic characteristic of heat exchanger. The design of a suitable heat dissipation method and the exploration of suitable operating regime, which determines the amount of net energy harvest, are introduced by conducting experimental and numerical studies. The development of the model that suits the system is one of major aims of this study.

## **d. System integration**

System integration determines how well the thermoelectric applications can be suitably fitted into the host facilities: It includes the design, construction and integration of thermoelectric cogeneration system to the residential environment without degrading the boiler performance. It includes two major tasks: thermoelectric system construction and domestic integration. The former one determines how well the thermoelectric system can perform with the given thermoelectric generators. The latter one decides the way that thermoelectric cogeneration system can serve the host house in an efficient way. More details are given in chapter 6.

## **4.3 Solar heat exchanger**

The hot side heat exchanger is specifically designed for absorbing the heat from boiler waste and solar energy. Two concepts of hot side heat exchanger are shown in Figure 4-3. Figure 4-3 (A) shows the indirect use in which heat transfer oil absorbs

the heat from boiler waste and solar energy. The oil is heated up by the absorbed energy and flows through the TE module to proceed with the energy conversion and water preheating. Figure 4-3 (B) shows the direct use where the solar energy and boiler waste heat is used directly to heat the TE hot side. The selection can be made according to characteristics of heat sources and requirements on the system response time. Solar concentration measures can also be taken to promote the temperature level at the heat source side.

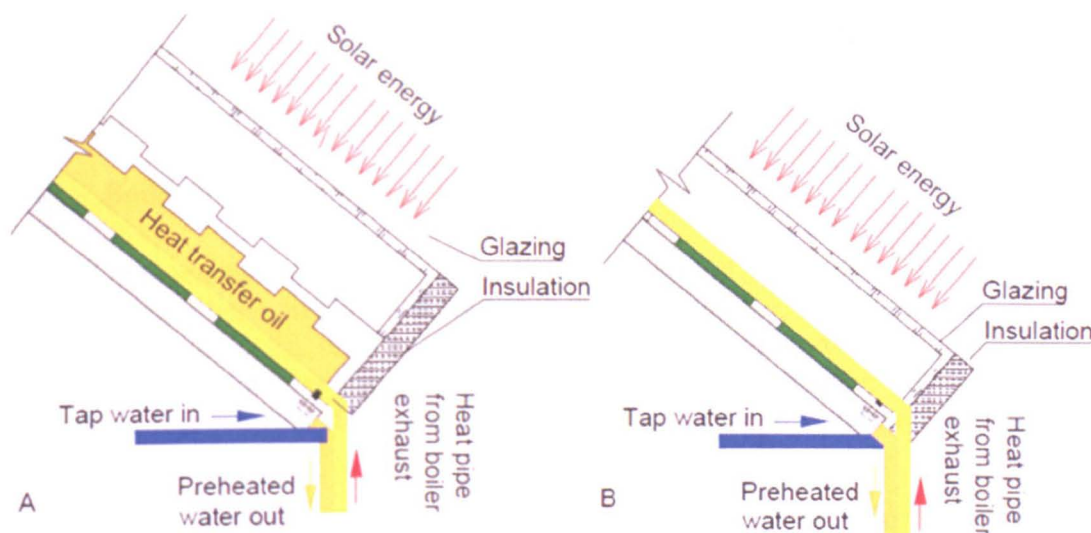


Figure 4-3 Schematic diagram of hot side heat exchanger

In the design of heat sourcing, the major attention of this research is focused on the study of flue heat exchanging part which aims to recover the waste heat from boiler flue gas. Considering the existing mature technology of absorbing the solar energy, the part of absorbing solar energy is briefly discussed and described based on the results of previous researches.

In this thermoelectric cogeneration system, the solar heat exchanging part of hot side heat exchanger can use the flat-plate solar collector. It consists of the following components:

- **Glazing.** One or more sheets of glass or other radiation-transmitting material allows the solar radiation to go through and prevents the absorbed solar energy to escape to the environment.
- **Absorber plates.** Flat, corrugated, or grooved plates, to which the thermoelectric generators are attached (with thermal energy storage) or liquid heat exchanger is attached (without thermal energy storage).
- **Insulation.** To eliminate or reduce the heat loss to the environment by increasing the thermal resistance at the back and sides of the system and make sure most of the thermal energy flow through thermoelectric generators;
- **Container or casing.** To surround the other components and protect them from dust, moisture, etc.
- **Thermal expansion tank.** In case of using thermal storage, a thermal expansion tank is required to accommodate the increased pressure caused by the expansion of heat transfer fluid at high operating temperature.
- **Heat transfer fluid.** In the system designed with thermal energy storage, heat transfer fluid is used to store the absorbed energy from solar radiation and

boiler waste and instantly spread the heat in the whole storage space to obtain even temperature distribution.

- **Solar concentrator.** Different from the conventional flat solar collector, a high temperature is favourable for thermoelectric generation which shows higher conversion efficiency at bigger operating temperature difference. Heat transfer fluid, capable of operating at high temperature such as heat transfer oil up to 260°C, is used to enable the system to achieve high temperature difference across the thermoelectric generators. This in turn helps enhance the conversion efficiency. Therefore, some of the detailed designs of conventional flat solar collector need to be modified according to the need of system operation to meet the onsite thermal conditions.

#### **4.4 Boiler flue heat exchanger**

Mature mathematical model that are able to describe the similar heat transfer style in this study have been discussed in previous studies. However, the models are based on the constant pipe cross section, whereas the model in this study has a cross section change at the joint between the pipe and flue heat exchanger. Just that minor difference changes the downstream flow pattern which disqualifies the previous mathematical model.

Therefore, the parameter that straightforwardly shows the performance is used to evaluate the design in this study. The parameter is the net energy gain by adopting the flue heat exchanger in the boiler exhaust pipe. More details about the study are introduced further in this section together with previous mathematical models. This part of study based on numerical simulation is a CFD based research exercise. The further experimental study has yet to be carried out to validate the results.

##### **4.4.1 Design and investigation plan**

Capturing waste heat from the boiler flue pipe is a technical challenge, because it adds another heat exchanger to the flue pipe. Either the boiler performance would be affected by the increased back pressure in the flue pipe or the effectiveness of flue heat exchanging would be compromised if a low pressure drop design is favoured in the design.

The flue heat exchanger reclaims the heat from the boiler flue gas. The design determines the rate at which the heat can be absorbed from the boiler flue gas, namely the effectiveness. The absorbed thermal energy is used by the system to convert into electrical power and thermal energy. The design of hot side heat exchanger needs to be compatible with capturing the heat from both of them. This section introduces the design and investigation of flue heat exchanger.

Boilers have gone through a strong evolution over the last few decades, improving the physical design, performance and efficiency. Taking condensing boiler as an example, its seasonal efficiency is up to 90%. It uses the secondary heat exchanger to recover the unabsorbed heat from the first heat exchanger, which would have been wasted by escaping to the environment. According to the estimates by the Heating and Hot Water Industry Council, there are still around 4 million old, highly inefficient boilers used in homes around the country. For new conventional boilers, the efficiency is usually about 78% [143] which gives the corresponding temperature

of flue gas at approximately 180°C. This leaves us the space of imagination for the amount of wasted heat and the grade at which it is wasted by the old inefficient boilers. The boiler rating is given by SEDBUK according to the seasonal efficiency.



Figure 4-4 Rating chart of domestic boiler by SEDBUK

The boiler flue pipe is where the boiler waste is exhausted to the environment. Its construction usually consists of two parts, inner pipe and outer pipe, which is made of the galvanised steel and plastic. The typical structure is shown in Figure 4-5.

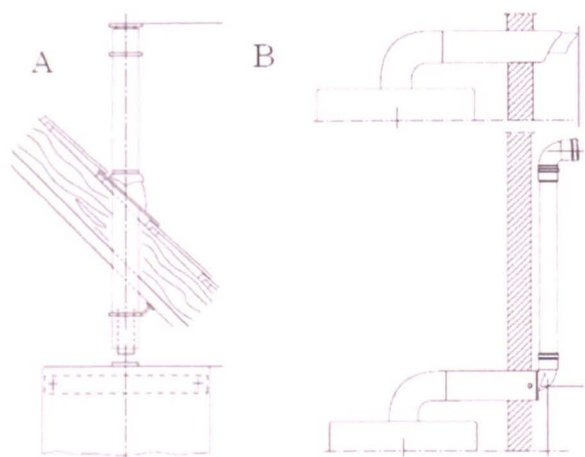


Figure 4-5 Roof installation and wall installation of boiler flue pipe (A. Roof installation; B. Wall installation.)

Figure 4-6 shows the photo of a typical boiler flue pipe. The dimension of flue pipe is usually given by standard concentric system at Ø60/100. The dimension of Ø80/100 is an optional choice, depending on the boiler type and capacity.



Figure 4-6 Typical boiler flue pipe

In order to recover the heat from the boiler flue pipe, heat exchanger needs to be used to extract heat out of flue gas. Typical heat exchangers, such as air-air or air-water

heat exchanger, can't meet the requirements due to the large size and extra energy consumption of fan/pump for heat transportation.

Heat pipe heat exchanger is suited for this application due to the following advantages:

- ☐ High effective thermal conductivity (5000-200,000 W/mK);
- ☐ No moving parts and no requirement of external power;
- ☐ An integral design minimising the adverse effects of metal expansion and it is maintenance free due to no moving parts and no cross contamination;
- ☐ Compact size and flexible usage;

Due to the high effective thermal conductivity, heat pipe can operate almost near isothermal mode with a small temperature drop (less than 4°C). It does not consume external power to transfer and transport heat. The only issue that needs to be taken into account is the increase of boiler back pressure by adding a heat exchanger in the exhaust pipe. Therefore, in the development of a suitable design, the heat pipe heat exchanger needs to effectively recover the heat from the flue gas but without significantly decreasing the boiler performance.

In order to tackle the technical issues described above, a passive heat recovery method for capturing domestic waste heat using heat pipe is introduced, in which a heat pipe heat exchanger is installed in the middle of flue pipe. The flue heat exchanger consists of an array of heat pipes which are vertically inserted into the flue heat exchanger from the top of flue pipe, the other ends are connected to the hot side surface of thermoelectric generators. On the surface of the enclosed part of heat pipes, the fins could be considered as a method of enhancing the heat transfer between the heat pipe and flue gas.

Numerical simulations using CFD is adopted in this part to study the relationship between the layout of heat pipe heat exchangers and the performance by investigating the performance of flue heat exchanger under different heat pipe heat exchanger design.

Due to the complex mechanism of heat transfer in heat pipe heat exchanger, it is technically impractical to take all the mechanisms into account in developing the model of the flue heat exchanger using numerical simulations. The heat pipe is simplified into a flow pipe with a fluid flowing inside at steady flow rate. The boundary conditions stay constant with only varying the physical geometries of heat exchanger. Apparently, this simplification cannot show the results in real applications, but it reflects which parametrical design is better in the progressive designs by providing the results in comparison.

To explore the model of flue heat exchanger, four variables, including heat pipe layout style, cross sectional area, pitch and joint style, are chosen to conduct the numerical studies and identify the best structure of flue heat exchanger. The numerical investigations are conducted in three steps which inspect this issue at different angle and in different depth. The first step is mainly focused on the identification of the suitable model structure of flue heat exchanger by looking into the models built on the basis of different variables. The second step aims at



narrowing the variables which are investigated in the first step down to a smaller number and identifying the optimal model structure of flue heat exchanger. The final step aims at detailing the identified model by investigating the models with sub-arrangements with different parameters.

The top view of each model is shown in Figure 4-7. 3D domains of all models have been established in Gambit. It consists of three parts, enclosure part, heat pipes and fins. The condensing end of heat pipe is connected to the hot side of TE generators directly or indirectly, which is shown in Figure 4-8. The recovered heat is rejected to the oil or the hot side of TE generators. Meanwhile, the solar power is absorbed by solar collector which is integrated to the oil tank or the hot side of TE modules, more details are shown in section 6.3.

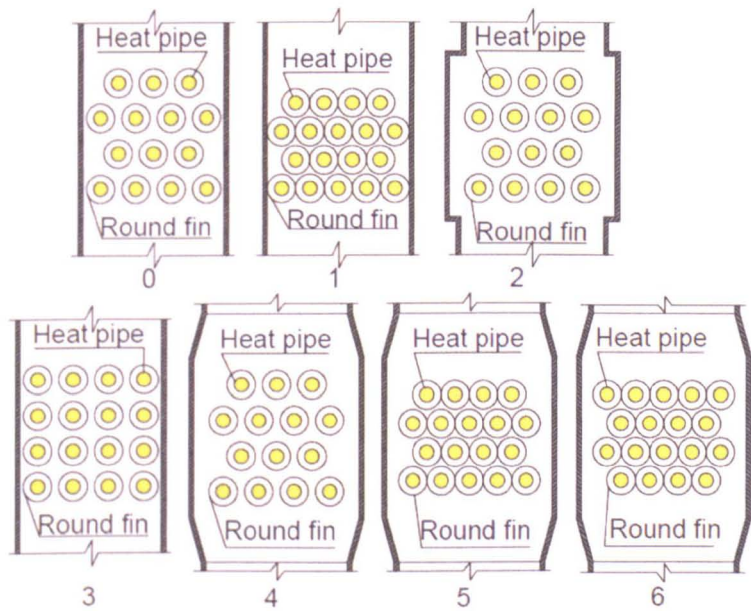


Figure 4-7 Investigated models of flue heat exchanger

Model 0: staggered layout ( $S_1=2.5d$ ,  $S_2=2.5d$ ); Model 1: staggered layout ( $S_1=2d$ ,  $S_2=2d$ ); Model 2: stagger layout with increased cross sectional area ( $S_1=2.5d$ ,  $S_2=2.5d$ , 0.14increment). Model 3: inline layout ( $S_1=2.5d$ ,  $S_2=2.5d$ ); Model 4: staggered layout with gradual joints ( $S_1=2.5d$ ,  $S_2=2.5d$ ); Model 5: staggered layout with gradual joints ( $S_1=2.0d$ ,  $S_2=2.0d$ ); Model 6 Staggered layout with gradual joints with mirrored layout of heat pipes of model 5.

Figure 4-8 shows the concept of domestic thermoelectric cogeneration system in residential house installed with domestic boiler. The flue heat exchanger for harnessing heat from the boiler exhaust is integrated in the exhaust pipe. The exact installing position of flue heat exchanger needs to consider the on-site situation, such as the position marked green.



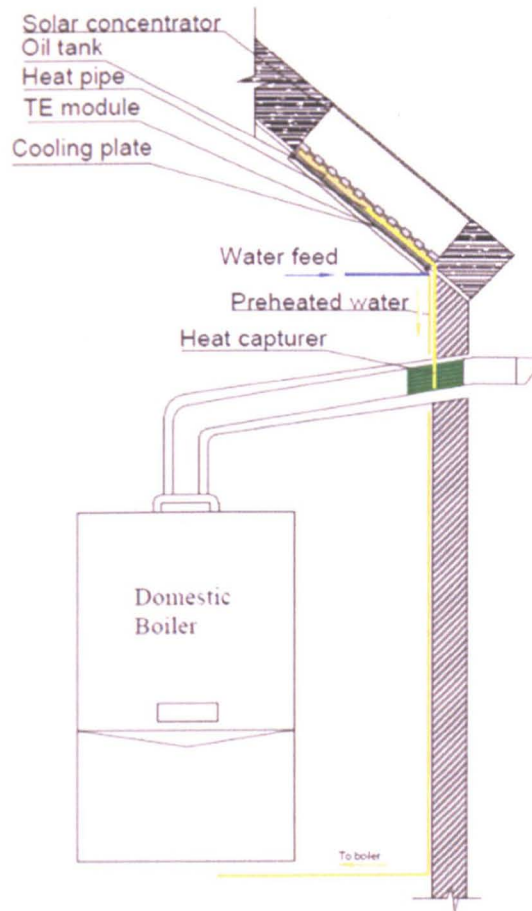


Figure 4-8 Concept of thermoelectric cogeneration system for domestic use

The heat exchanging of flue heat exchanger can be disassembled into heat transfer on tube-side and that on gas-side. Considering the fact that the gas-side heat transfer coefficient is typically much smaller than the tube-side value, it is important to increase the heat transfer coefficient on the gas-side. A plain surface geometry will do it by increasing the surface area for heat transferring. The use of enhanced fin surface geometries provides higher heat transfer coefficients than a plain surface [144]. To maintain a reasonable friction power with low-density gases, the gas velocity is usually less than 5m/s, which is obtained by considering the maximum flow velocity of flue gas in the boiler flue pipe (or full load operation). The data has been concluded from the nominal operating conditions given by a few major boiler manufacturers (Worcester Bosch, Baxi, Ferroli, Vaillant).

There are two types of heat pipe layout for the heat pipe heat exchangers, staggered geometry and inline geometry, shown in Figure 4-9. The layout is characterized by three parameters, the transverse pitch ( $S1$ ), longitudinal pitch ( $S2$ ) and the diameter of heat pipe is denoted by  $d$ .

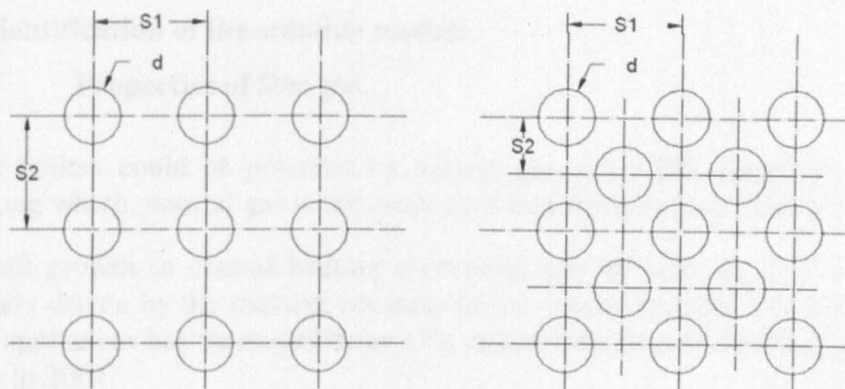


Figure 4-9 Inline layout and staggered layout

In previous studies, inline layout is seldom used because it provides substantially lower performance than the staggered layout [145]. For the inline bank, the heat transfer coefficient decreases with the rows whilst the opposite trend is shown in the staggered bank. The reason lies in a good mixing caused by the staggered layout. This conclusion has found the proof in the study conducted by Rabas and Huber [146] which has shown that the heat transfer coefficient of deep inline tube bank ( $N \geq 8$ ) may be as small as 60% of the staggered tube value at low  $Re_d$  ( $Re_d < 1000$ ), it increases when the  $Re_d$  increases. For instance, the ratio of inline to staggered increases up to 0.8 at  $Re_d = 50,000$ . Reported in Brauer's argument [145], the bypass effect in the inline arrangement are responsible for poor performance in inline layout. The flow pattern of staggered and inline layout is shown in Figure 4-10.

The Figure 4-10 (a) and Figure 4-10 (b) show the flow pattern in staggered and inline layout. The shading area from both of the figures can be seen, they represents the dead zones where not much flow is going through, namely a poor heat transfer performance. Averagely, a single pipe of inline layout has bigger area of dead zones than that of staggered layout. Therefore, the heat transfer coefficient of staggered layout is bigger than that of inline layout, and it is recommended to be used to enhance the heat transfer by the previous studies. The numerical study identifying the suitability of inline layout and staggered layout for this application is included in this research.

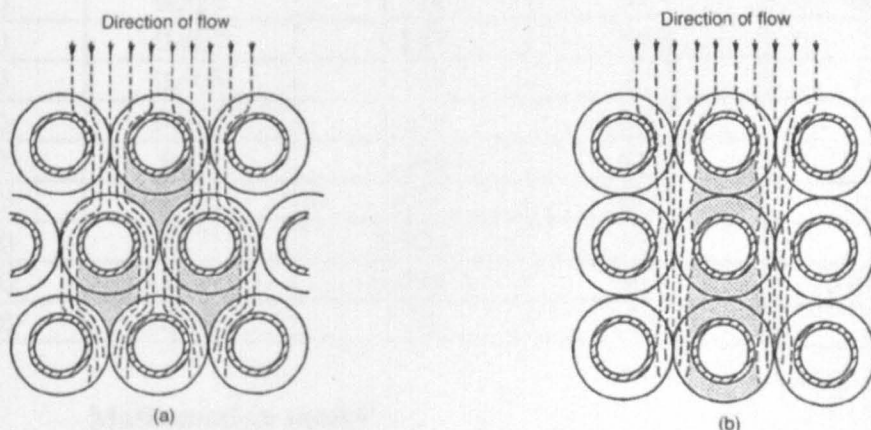


Figure 4-10 Flow patterns observed by Brauer [145] for (a) staggered and (b) inline finned tube banks

4.4.2 Identification of the suitable models

4.4.2.1. Properties of flue gas

Domestic boilers could be powered by natural gas, oil, LPG, electricity and solid fuel. Among which, natural gas is the most used fuel for domestic heating [147].

The overall growth in central heating ownership can be referred in [147] to have been largely driven by the massive increase in gas central heating. The ownership of gas-fired appliances has increased from 33% of centrally heated dwellings in 1970 to over 80% in 2001.

Considering the predominant market taken by the natural gas, this study is mainly based on the flue gas produced by gas-fuelled boiler. The principles can be applied to the boilers fired by other types of fuels, because the differences lie in the temperature level of flue gas and the chemical properties of flue gas due to the different type of fuels and combustion condition. Natural gas is combusted with air which contains about volumetric 79% of non-combustible nitrogen. Therefore, the largest part of composition in flue gas is nitrogen (N<sub>2</sub>). The second largest part is carbon dioxide (CO<sub>2</sub>), which lies in the range of 10-25 volume percentage, followed by about 11 volume percentage water vapour (H<sub>2</sub>O) produced by the combustion of hydrogen in the fuel with oxygen [148]. It also contains little amount of oxygen (O<sub>2</sub>), carbon monoxide (CO) and nitrogen oxides (NO<sub>x</sub>) in some operational situations such as imperfect combustion. The physical properties of flue gas can be referred in Table 4-1. The properties of flue gas are significantly affected by the temperature level.

Table 4-1 Physical properties of flue gas

(<http://www.pipeflowcalculations.com/tables/flue-gas.php>)

t (°C)	ρ (kg/m <sup>3</sup> )	c <sub>p</sub> (kJ / kgK)	μ×10 <sup>6</sup> (Pa · s)	ν×10 <sup>6</sup> (m <sup>2</sup> /s)
0	1.295	1.042	15.8	12.2
100	0.95	1.068	20.4	21.54
200	0.748	1.097	24.5	32.8
300	0.617	1.122	28.2	45.81
400	0.525	1.151	31.7	60.38
500	0.457	1.185	34.8	76.3
600	0.405	1.214	37.9	93.61
700	0.363	1.239	40.7	112.1
800	0.33	1.264	43.4	131.8
900	0.301	1.29	45.9	152.5
1000	0.275	1.306	48.4	174.3
1100	0.257	1.323	50.7	197.1
1200	0.24	1.34	53	221

4.4.2.2. Mathematical model

The mathematical model has been established to theoretically evaluate and understand the mechanism and performance of flue heat exchanger. The heat

exchanger absorbs heat from the mainstream of flue gas and transport the absorbed heat to the TE hot side for energy conversion. This process can be analyzed from two aspects: heat transfer and flow dynamics.

For a given operating condition of domestic boiler, the flow rate of flue gas should be in a certain range which depends on the boiler specification. The design of boiler waste flue heat exchanger needs to comply with the nominal conditions which were originally designed by the boiler manufacturer.

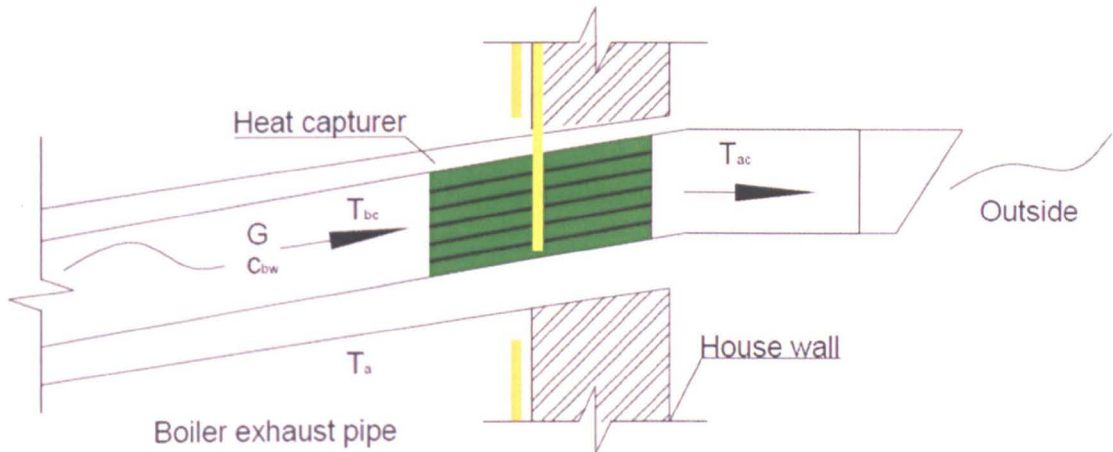


Figure 4-11 Schematic of flue heat exchanger integrated in boiler exhaust pipe

Figure 4-11 shows a horizontally-mounted flue pipe titled upwards slightly in a residential home. A flue heat exchanger, the part marked by green, is installed in the flue gas pipe. Denoting  $Q_{bw}$  as the amount of heat content contained in flue gas, it consists of three parts, absorbed by flue heat exchanger, lost to the environment via pipe wall and exhausted to the environment. Assuming the pipe insulation is good enough, the heat loss through the pipe wall is not significant and neglected. Therefore,  $Q_{bw}$  consists of the heat absorbed by flue heat exchanger and the heat exhausted to the environment.  $Q_{bw}$  can be described by Eq.(4-1):

$$Q_{bw} = c_p^{bw} G_{bw} (T_{bc} - T_a) \quad (4-1)$$

Where,  $c_p^{bw}$ ,  $G_{bw}$ ,  $T_{bc}$  and  $T_a$  are the specific heat capacity, the mass flow rate of flue gas, the temperature of flue gas before passes through the flue heat exchanger and the ambient, respectively.

The heat absorbed by flue heat exchanger is expressed by

$$Q_a = c_p^{bw} G_{bw} (T_{bc} - T_{ac}) \quad (4-2)$$

Where,  $T_{ac}$  is the temperature of flue gas after flue heat exchanger.

The heat exhausted to the environment is expressed by

$$Q_e = c_p^{bw} G_{bw} (T_{ac} - T_a) \quad (4-3)$$

It also equals to the heat transferred from the surface area of flue heat exchanger:

$$Q_{conv} = h_{fx} A_{fx} (T_{bw} - T_f) \quad (4-4)$$

Where  $h_{fx}$ ,  $A_{fx}$ ,  $T_f$  and  $T_{bw}$  are the heat transfer coefficient between the pipe surface and the mainstream of flue gas, the heat transfer surface area, the temperature of the pipe surface and boiler flue gas, respectively.

The effectiveness of flue heat exchanger, denoted by  $\eta_a$ , can be described by

$$\eta_a = Q_a / Q_{bw} \quad (4-5)$$

The effectiveness characterizes the performance of flue heat exchanger in recovering the heat from the boiler flue gas.

According to Eq.(4-4), the heat transfer coefficient  $h_{fx}$  can be calculated by

$$h_{fx} = Q_{conv} / A_{fx} (T_{bw} - T_f) \quad (4-6)$$

The flow between the mainstream of flue gas and the pipe flow replacing heat pipe is cross-flow.  $T_f$  can be taken as the average value of inlet temperature and outlet temperature.

The pressure drop caused by installing flue heat exchanger in flue pipe is the other parameter that needs to be considered in the design and evaluation of flue heat exchanger. It represents the amount of energy input for thermal medium transportation. A good thermal performance normally involves sophisticated structure with a large friction area, which consequently leads to a large value of pressure drop because of the contribution of frictional flow resistance.

Usually, the heat transfer capacity is used to characterize the performance of heat exchanger. But the increase of pressure drop caused by adopting enhanced heat transfer design needs to be considered because it also affects the system performance by increasing the back pressure, which is manifested in the requirement of extra driving force, equivalent fan power  $W$ .

Therefore, in this research the net energy gain is used to characterize the performance of flue heat exchanger, which is defined by the net energy output or gain  $E_n$ , given by Eq.(4-7).

$$E_n = Q_a - W \quad (4-7)$$

Where,  $Q_a$  and  $W$  is the absorbed heat from the flue gas and the increased fan power to offset the increased back pressure due to the use of flue heat exchanger.

Despite the different quantity of heat pipes used by the models, the overall performance of flue heat exchanger models can be compared because the analysis is based on the combination of thermal performance and hydraulic performance of flue heat exchanger.

The thermal performance of heat exchanger must be weighed against the energy required to operate the system, which would be the fan power if the increased



pressure drop needs to be offset by electric fan to make sure the boiler performance is not significantly affected. The required fan power due to the increased pressure loss caused by the use of flue heat exchanger can be calculated by Eq.(4-8):

$$W = \Delta P Q / \eta_f \quad (4-8)$$

Where,  $\Delta P$  is the pressure drop across the flue heat exchanger,  $Q$  is the volumetric flow rate of the fluid passing through the heat exchanger,  $\eta_f$  is the overall fan efficiency, assuming the fan operates at the peak efficiency (75% as an example). It varies with the category and manufacturer.

The performance of the flue heat exchanger is determined by the amount of heat input and output, characterized by the net energy gain which is given by Eq.(4-7).

#### 4.4.2.3. Numerical investigations

##### 1. Physical model

The numerical studies investigate the thermal and hydraulic characteristics of flue heat exchanger based on the four major variables that possess the potential of affecting the performance significantly. They include heat pipe layout, cross sectional area of flue heat exchanger, heat pipe pitch and heat exchanger joint style. The intention is to understand how the parameters affect the performance of flue heat exchanger.

In this part, designs are introduced on the basis of the numerical simulations progressively at three stages. The performance of the presented designs is to be compared with each other using the hydraulic performance, thermal performance and the value of net energy gain. The physical model of flue heat exchanger for numerical simulation is simplified to the one shown in Figure 4-12. The fins are not considered in the simulation due to much larger computer memory need that would be required by taking the fins into account.

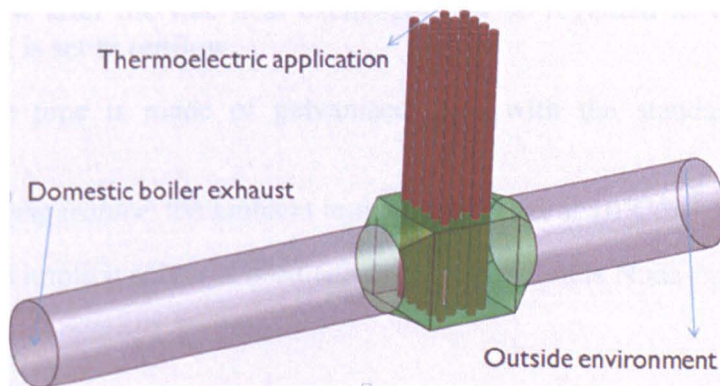


Figure 4-12 Computational domain of flue heat exchanger

Figure 4-12 shows the computational domain of flue heat exchanger installed in the boiler exhaust pipe. The unused heat from the boiler combustion chamber flows into the flue pipe and passes through the flue heat exchanger. The heat content in flue gas is absorbed by the flue heat exchanger and transferred to TE hot side by the heat pipe heat exchanger. The meshing details of the computational domain are shown in Figure 4-13.



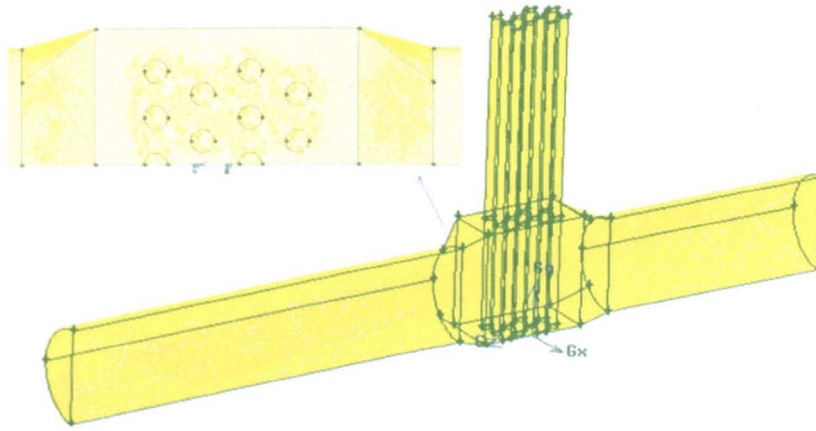


Figure 4-13 Mesh details of flue heat exchanger

A combination of structured and unstructured mesh has been used in meshing the regular and irregular shape parts of the domain. The regions near the heat pipes and the joints between flue pipe and flue heat exchanger are the areas which need accurate results. Therefore, finer meshing was adopted in those positions.

## 2. Boundary conditions

**Flue gas:** carbon dioxide (13%), water vapour (11%) and nitrogen (76%), more details can be referred in section 4.3.2.1;

**Inlet:** the velocity of flue gas in a typical domestic boiler is less than 5m/s, depending on the operating load. The investigated velocities is 1m/s, 2m/s, 3m/s, 4m/s and 5 m/s;

**Heat pipe:** due to the complex mechanism of heat pipe, it is simplified to a pipe flow, the pipe material is copper and flue gas enters the pipe driven by 10Pa pressure differential at the temperature 10°C;

**Outlet:** the flow after the flue heat exchanger can be regarded as fully developed flow, the outlet is set as outflow;

**Flue pipe:** the pipe is made of galvanised steel with the standard diameter of Ø60mm;

**Environment temperature:** the ambient temperature is set at 10°C;

The segregated implicit solver is used and the computation is Node-based for a better accuracy.

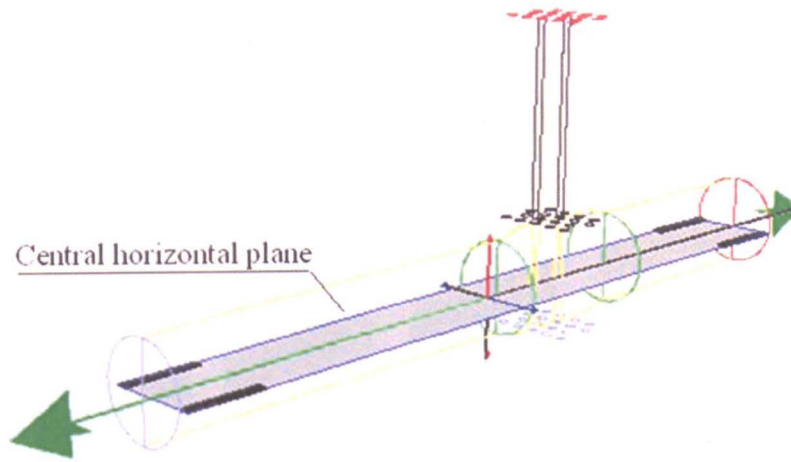


Figure 4-14 Velocity contour in the flow direction of flue heat exchanger

#### 4.4.2.4. Results

##### 1. Heat pipe layout

The design of heat pipe layout is based on the results of previous studies which have compared the heat transfer performance of inline layout and staggered layout, the fundamental concept is used in the design of flue heat exchanger in this study, shown in Figure 4-15.

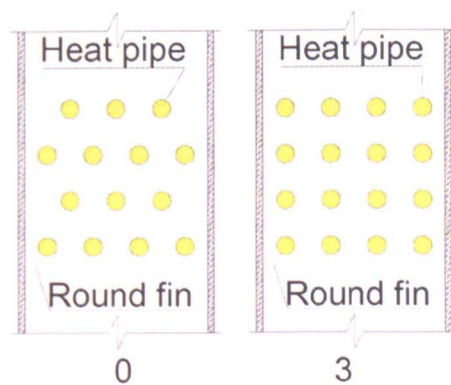


Figure 4-15 Staggered layout (0) and Inline layout (3) ( $S=2.5d$ )

It only shows the top view of the section which encloses the heat pipe heat exchanger. It consists of an array of heat pipes in certain type of layout and fins which are mounted on the surface of heat pipes. In the numerical simulation, the fins are omitted to simplify the model at this stage of study. The simplification can increase the computing speed of each case by eliminating the slow computation process due to no-need of high-standard processor and memory. This simplification does not affect the primary purpose of this study because the numerical simulations are based on changing one variable each time. The simplification also applies to other simulation cases.

Figure 4-16 shows the velocity contour of central horizontal plane, defined in Figure 4-14, when flue gas is exhausted to the flue pipe at the velocity of 1m/s, 2m/s, 3m/s, 4m/s and 5m/s, respectively.

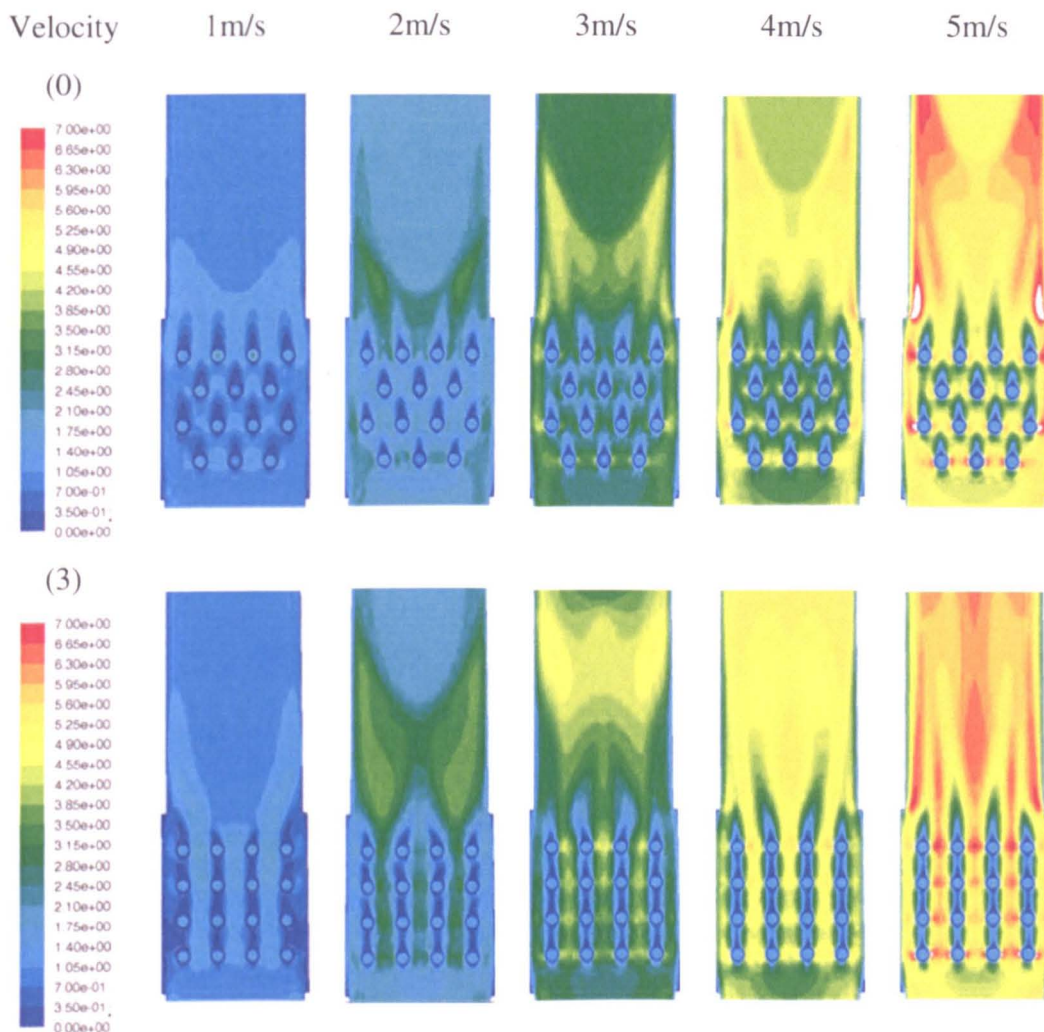


Figure 4-16 Velocity contour of central horizontal plane at different flue gas velocity

From the figure, the “bypass effect”, found out in the previous study described in Figure 4-10, can also be seen in the central two columns when the flue gas velocity is 1m/s and all four columns when the flue gas velocity is 3m/s, 4m/s and 5m/s. However, for the side columns when the flue gas velocity is 1m/s and all four columns when the velocity is 2m/s, the “bypass effect” is not visually obvious.

Figure 4-17 shows the temperature distribution on central horizontal plane when the flue gas velocity is at 1m/s, 2m/s, 3m/s, 4m/s and 5m/s, respectively. The obvious result that the inline layout gives a lower temperature than that of staggered layout can be seen when the velocity is 1m/s, 2m/s and 3m/s. More statistical details are shown in Figure 4-18, in which the inline layout gives a lower outlet temperature than that given by the staggered layout in the investigated range of flue gas velocity. It means the heat transfer performance of inline layout is better than the staggered layout, which is different from the conclusion that previous researches have drawn, discussed in section 4.3.1. However, this does not conflict with the missing “bypass effect” in central horizontal plane around the edge columns at 1m/s and all columns at 2m/s.



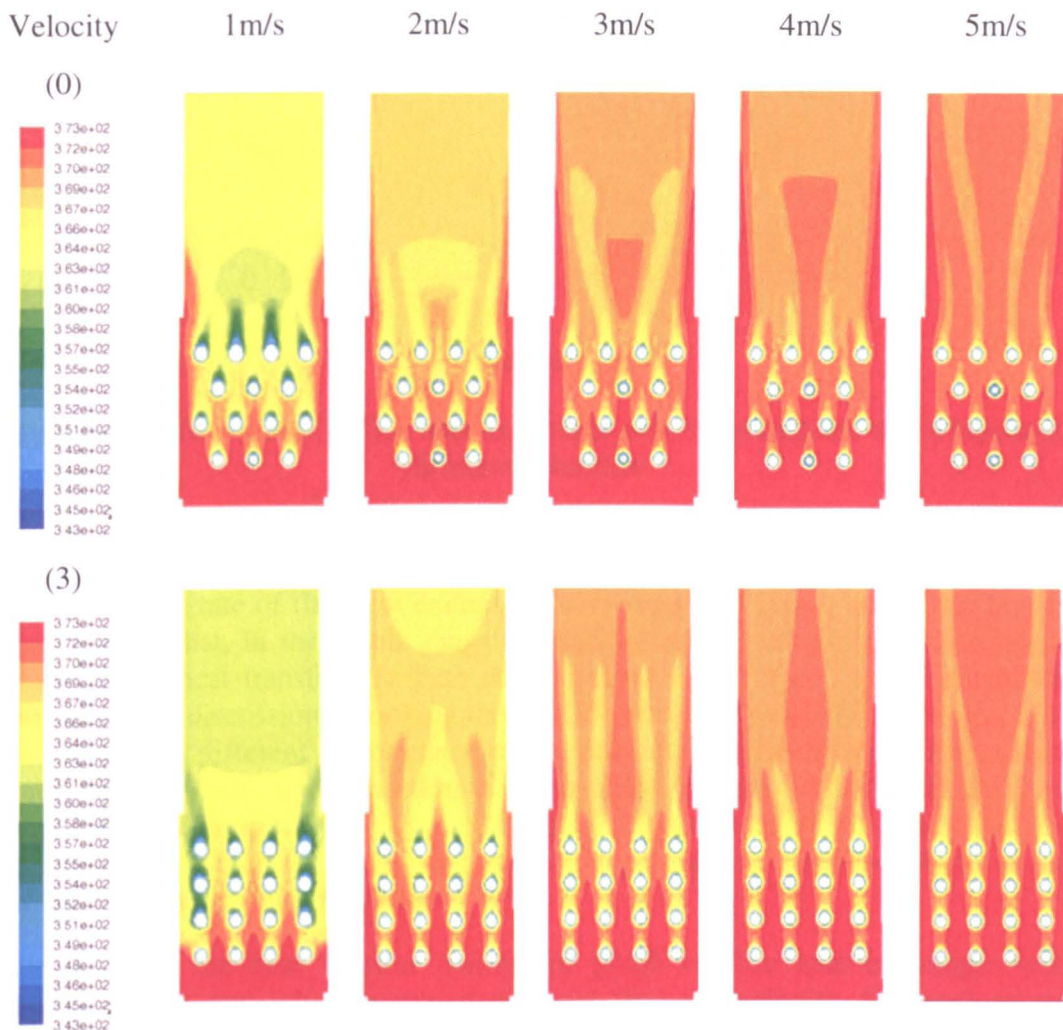


Figure 4-17 Temperature contour of central horizontal plane at different flue gas velocity

The central horizontal plane was chosen as a reference to visualise the performance, unable to represent the whole length. The effectiveness that characterizes the thermal performance of flue heat exchanger is shown in Figure 4-19, which does not represent the effectiveness in practical applications but is able to show the effectiveness of inline layout is bigger than that of staggered layout.

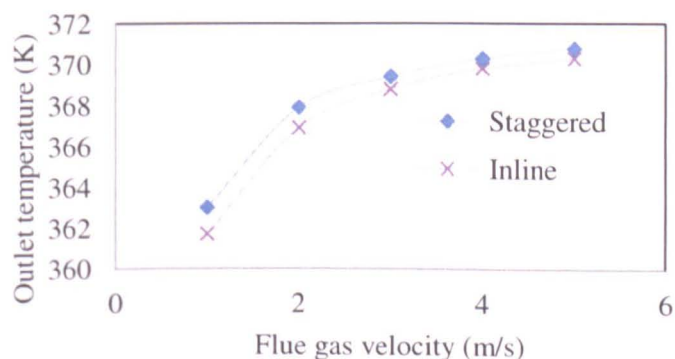


Figure 4-18 Outlet temperature when the flue gas is exhausted at different velocities

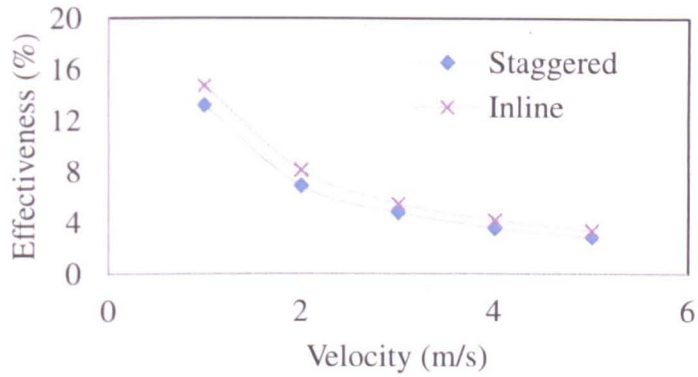


Figure 4-19 Effectiveness of flue heat exchanger with staggered and inline layout at different velocities

The conclusion that the staggered layout gives a better thermal performance than inline layout is not agreed by the result of this numerical study. Figure 4-21 shows the heat transfer rate of flue heat exchanger with staggered layout and inline layout, which tells us that, in the whole range of investigated velocities, the inline layout gives a higher heat transfer rate than the staggered layout does. This confirms the aforementioned discussions. Looking through the results of velocity and temperature distribution, this different performance can be attributed to the different flow pattern in previous study which was based on a uniform flow pattern. In this study, the flow pattern has been altered when it goes through the junction of the flue pipe and flue heat exchanger, which in consequence does not produce the “bypass effect” in the flow among the array of heat pipes.

Figure 4-20 is the heat transfer coefficient graph of flue heat exchanger with staggered layout and inline layout at different flue gas velocity. For both of the layout in the whole range of flue gas velocity, the heat transfer coefficient increases along with the flue gas velocity. But the inline layout gives a higher heat transfer coefficient than the staggered layout does. When the velocity is approaching to 5m/s, the coefficient of the two layouts reaches the same level. However, the heat transfer rate of inline layout is higher than that of staggered layout.

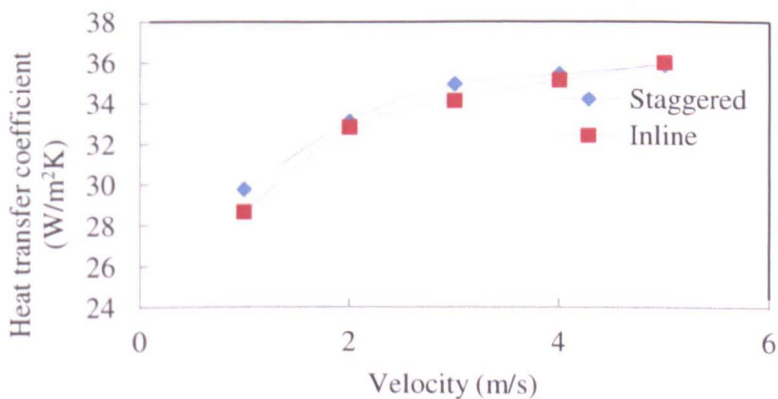


Figure 4-20 Heat transfer coefficient of flue heat exchanger with staggered layout and inline layout

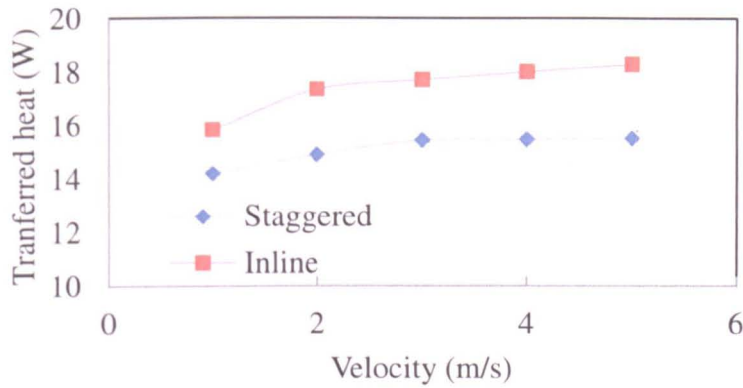


Figure 4-21 Transferred heat of staggered layout and inline layout at different flue gas velocity

Figure 4-22 shows the pressure drop caused by the flue heat exchanger when the flue gas is exhausted from the boiler at different velocities. Inline layout shows a smaller pressure drop than the staggered layout does.

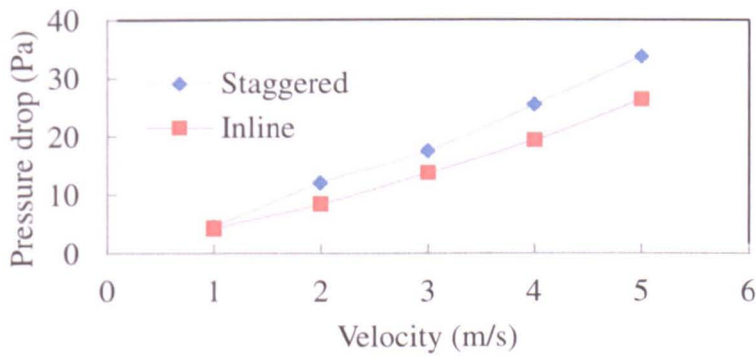


Figure 4-22 Pressure drop of staggered layout and inline layout at different flue gas velocity

Figure 4-23 shows the equivalent fan power for offsetting the increased pressure drop due to the use of flue heat exchanger. The one with staggered layout requires more fan power than that with inline layout does, especially when the flue gas velocity increases from 1m/s, the higher the velocity, the bigger the difference is.

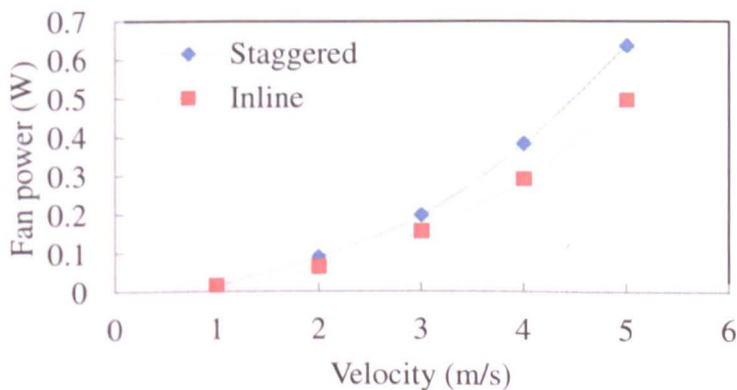


Figure 4-23 Fan power of staggered layout and inline layout under different flue gas velocity

The net energy gain under different flue gas velocity is shown in Figure 4-24. An obvious trend that model 3 gives a bigger value of net energy gain under the whole



velocity range. The advantage of using inline layout is slightly more obvious than that of staggered layout at high flue gas velocity in this configuration.

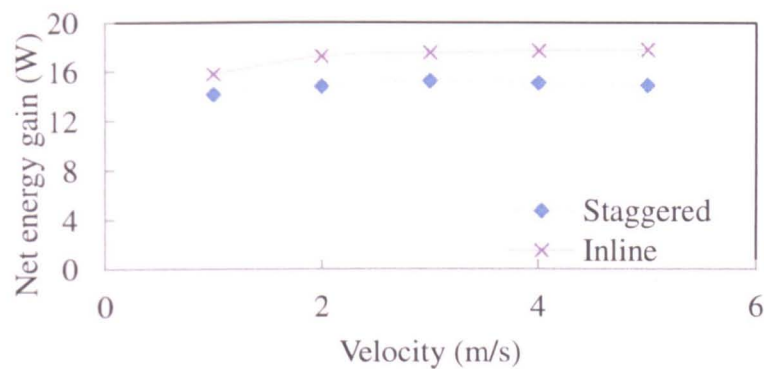


Figure 4-24 Net energy gain under different flow velocity

## 2. Cross section of flue heat exchanger

The reason of looking into the impact of the cross sectional area to the performance is due to the consideration of flow velocity around the surface of heat pipes in flue heat exchanger, which affects the heat transfer performance between the gas and the heat pipe surface. The cross sectional area affects the surface area for heat transfer. In order to obtain a large heat transfer surface area and technically feasible fabrication, the original circular cross section of boiler exhaust pipe is transited to rectangular cross section in flue heat exchanger. Two different cross sectional area of flue heat exchanger have been studied to initially investigate the impact of cross sectional area. The corresponding models with inline layout and staggered layout are model 2 and model 0 in Figure 4-7. It is also shown in Figure 4-25.  $A_0$  in Figure 4-25 (A) and  $A_2$  in Figure 4-25 (B) represent the minimum cross sectional area of model 0 and model 2, and  $A_0=0.91A$ ,  $A_2=1.19A$ ,  $A$  is the cross sectional area of boiler flue pipe.

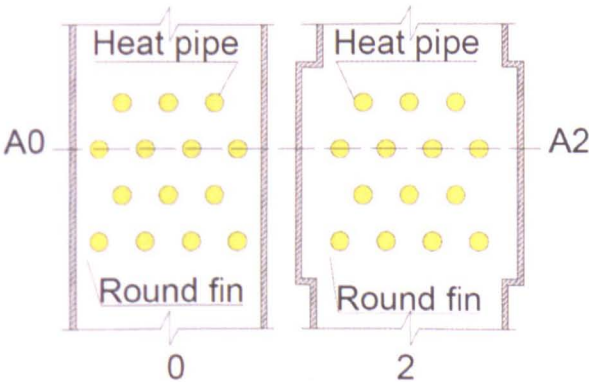


Figure 4-25 Cross sectional area ( $A_0=0.91A$ ,  $A_2=1.19A$ ,  $S=2.5d$ )

Figure 4-27 shows the velocity distribution on central horizontal plane of two models at different flue gas velocity. The obvious difference in velocity distribution between the two models is that the flow in flue heat exchanger section of model 2 is more dispersed towards the wall side compared to the model 0. This makes the flow in model 2 better mixed in the heat exchanger and the velocity distribution is more even, which means a better heat transfer is achieved in model 2. The visualised comparison results can be seen in Figure 4-30. The statistic result is shown in Figure

4-29, which tells the model 2 with bigger cross section area has a higher value of effectiveness than the model 0 does.

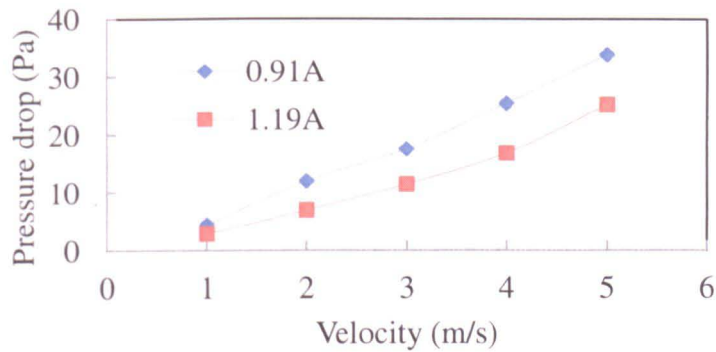


Figure 4-26 Pressure drop of models with cross section at 0.91A and 1.19A at different flue gas velocity

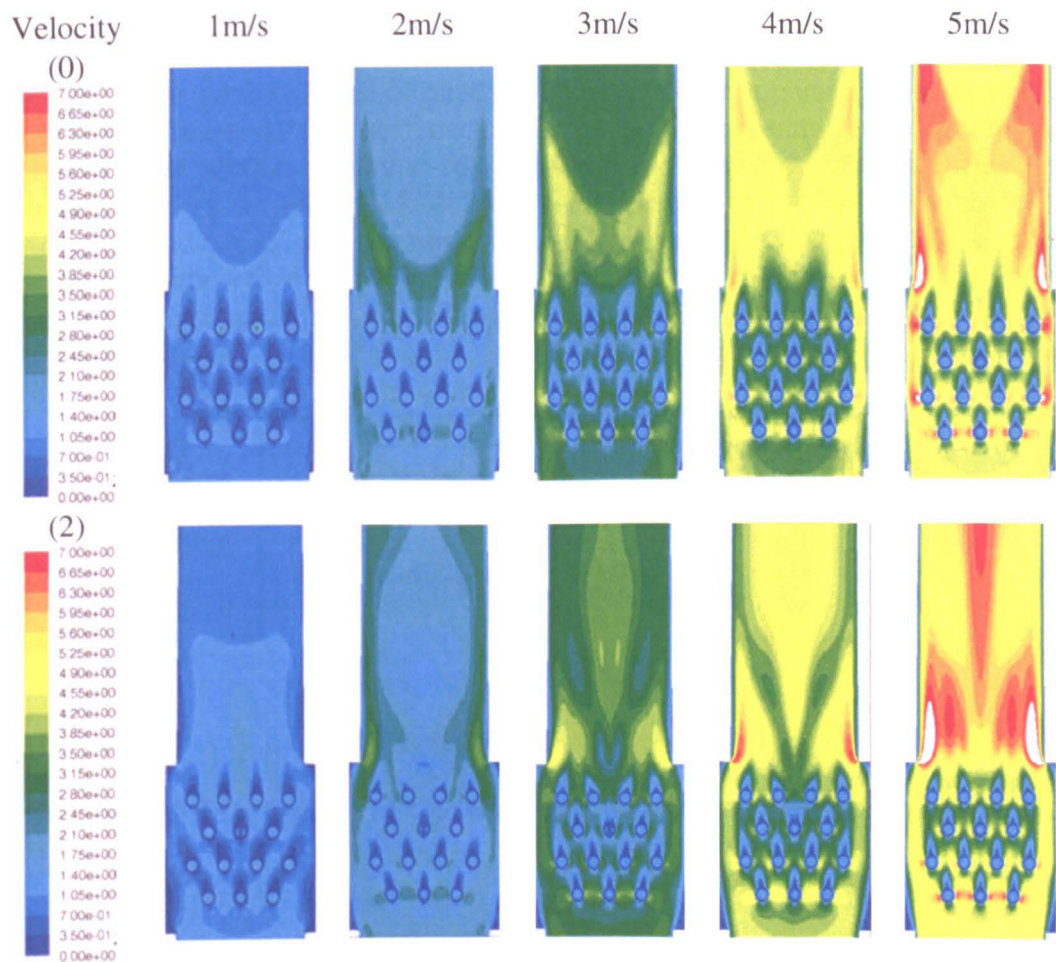


Figure 4-27 Velocity contour of central horizontal plane at different flue gas velocity

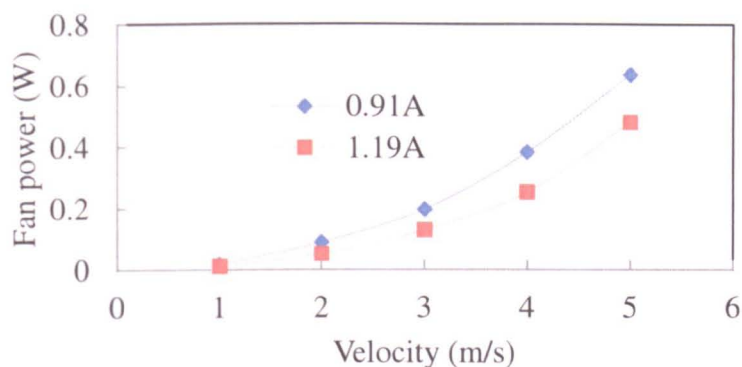


Figure 4-28 Fan power of the models with cross section at 0.91A and 1.19A at different flue gas velocity

However, compared to model 0, a higher speed region can be seen at the edge of flue heat exchanger outlet of model 2. This shows the opportunity to modify the inner structure to further reduce the pressure drop.

When the cross sectional area is increased, low velocity regions appears at the top and bottom corners of flue heat exchanger on both the central cross section and minimum cross section. Figure 4-26 shows the pressure drop when the flue heat exchanger's cross section is 0.91A and 1.19A, respectively. The one with 0.91A shows higher value of pressure drop than that with 1.19A, which becomes more apparent when the velocity increases. Therefore, more fan power is required to offset the increased pressure drop caused by the use of flue heat exchanger, shown in Figure 4-28.

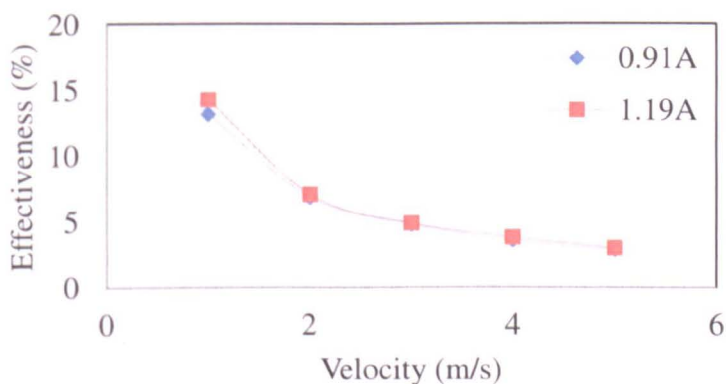


Figure 4-29 Effectiveness of flue heat exchanger with different cross sections



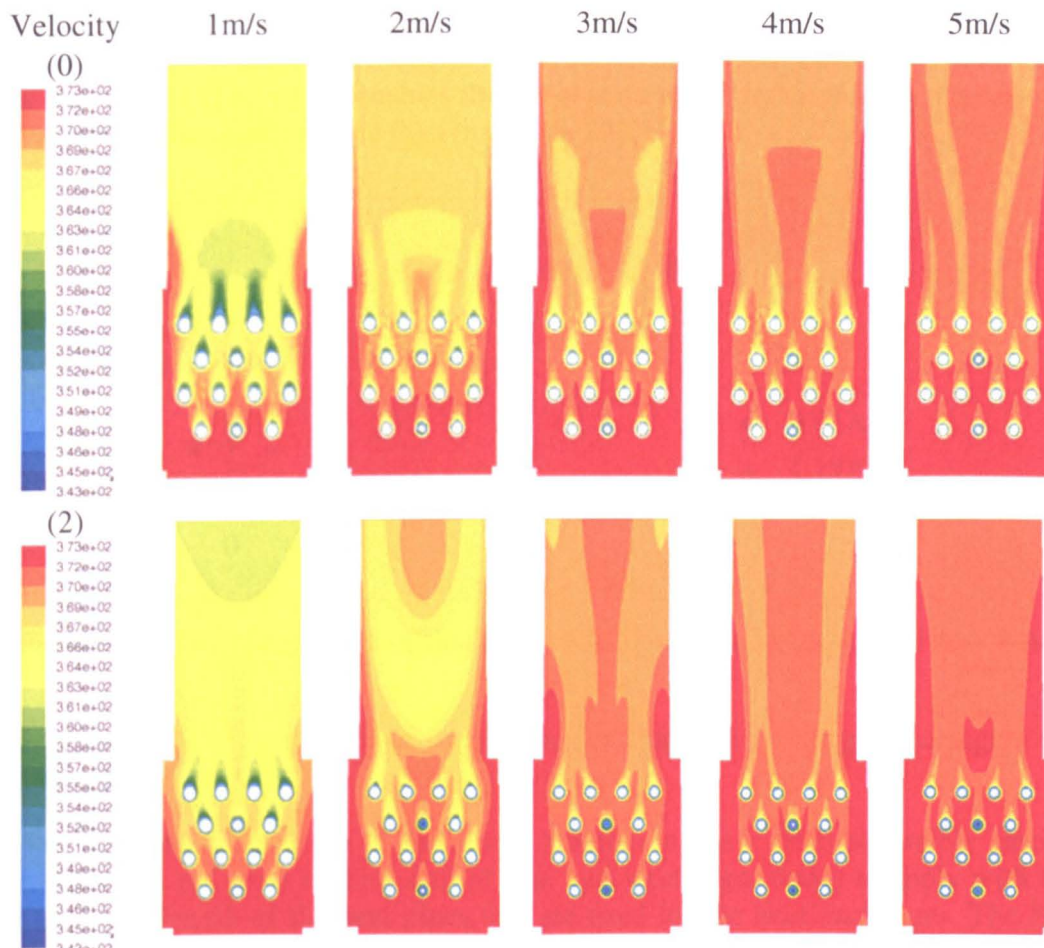


Figure 4-30 Temperature contour of central horizontal plane at different flue gas velocity

Figure 4-32 shows the net energy gain of flue heat exchanger with 0.91A and 1.19A cross section. As the flue gas velocity increases, it shows a gentle increase. However, the net energy gain of the model with 1.19A cross section area is 2.2%-8.5% bigger than that with 0.91A. The heat transfer rate of flue heat exchanger with 0.91A and 1.19A cross section is shown in Figure 4-31. The heat transfer rate of the one with 1.19A cross section is slightly higher than that of 0.91A cross section. Therefore, the model with 1.19A cross sectional area gives a better performance than that with 0.91A cross section does.

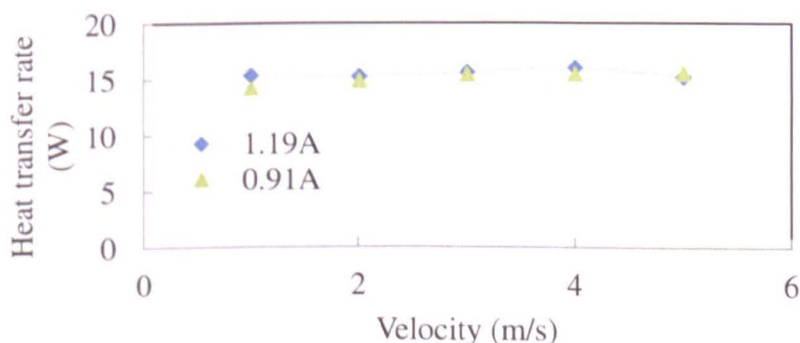


Figure 4-31 Heat transfer rate of flue heat exchanger with 0.91A and 1.19A cross section

The net energy gain of the models with 0.91A cross section and 1.19A cross section is shown in Figure 4-32. The model with 1.19A cross section gains more net energy than that with 0.91A, which enables the conclusion to be drawn that the model with 1.19A has a better performance than that with 0.91A.

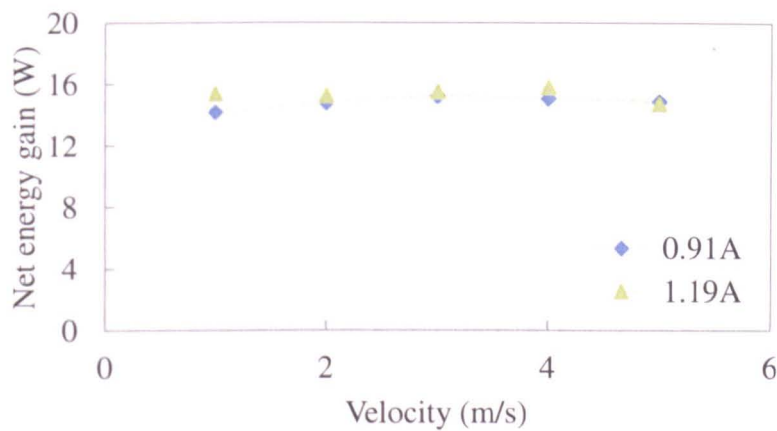


Figure 4-32 Net energy gain of flue heat exchanger with 0.91A and 1.19A cross section

Does it mean the bigger the cross section area of flue heat exchanger, the higher the net energy gain is?

In order to find it out, a set of numerical simulations have been separately carried out. However, the cross section area of flue heat exchanger needs to apply with the condensation length of the heat pipes that are used in flue heat exchanger. The flue heat exchangers with cross section area 0.91A, 1.02A, 1.13A, 1.25A and 1.36A have been investigated under the flue flow velocity of 1m/s, 2m/s, 3m/s, 4m/s and 5m/s, respectively.

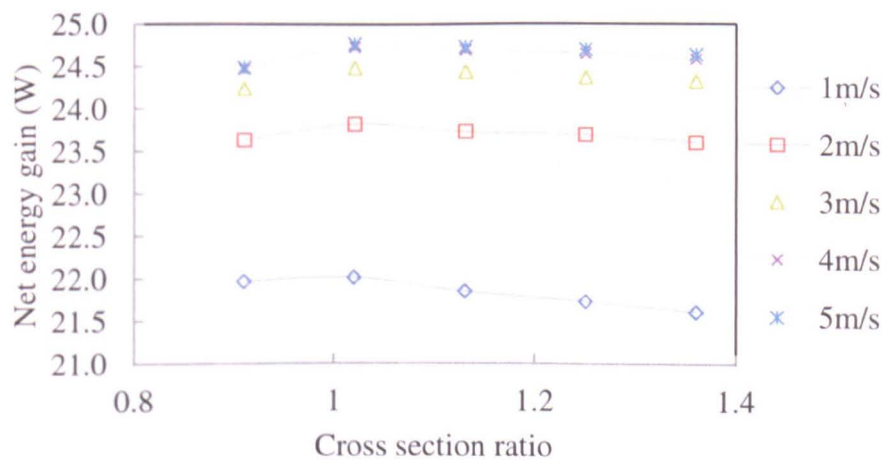


Figure 4-33 Net energy gain of flue heat exchanger with different cross section area

The result in Figure 4-33 shows that the net energy gain increased when the cross section area of flue heat exchanger increased from 0.91A to 1.02A. However, the net energy gain decreased along with the increase of the cross section area from 1.02A to 1.36A. Hereby, the flue heat exchanger with 1.02A cross section area shows the best performance of them all. Namely, a cross section area close to the original flue gas pipe cross section area is a good choice as it gives the best overall performance in the

investigated five heat exchangers. In the design of cross section of flue heat exchanger, this factor needs to be considered.

### 3. Heat pipe pitch

The distance between the heat pipes, called pitch, is one of the factors that influence the performance of flue heat exchanger. Figure 4-35 shows two flue heat exchangers with different pitch, the layout is staggered. The heat pipes are equilaterally arrayed in flue heat exchanger. The transverse pitch  $S_1$  and longitudinal pitch  $S_2$  in Figure 4-35 (A) and Figure 4-35 (B) is  $S_1=S_2=2.5d$  and  $S_1=S_2=2d$ ,  $d$  is the diameter of heat pipe.

Figure 4-34 and Figure 4-36 show the velocity contour and temperature contour of central horizontal plane of the models with  $2.5d$  pitch and  $2d$  pitch, respectively. Averagely, the velocity in flue heat exchanger and downstream area with  $2.0d$  pitch is higher than that with  $2.5d$  pitch at all the investigated velocities.

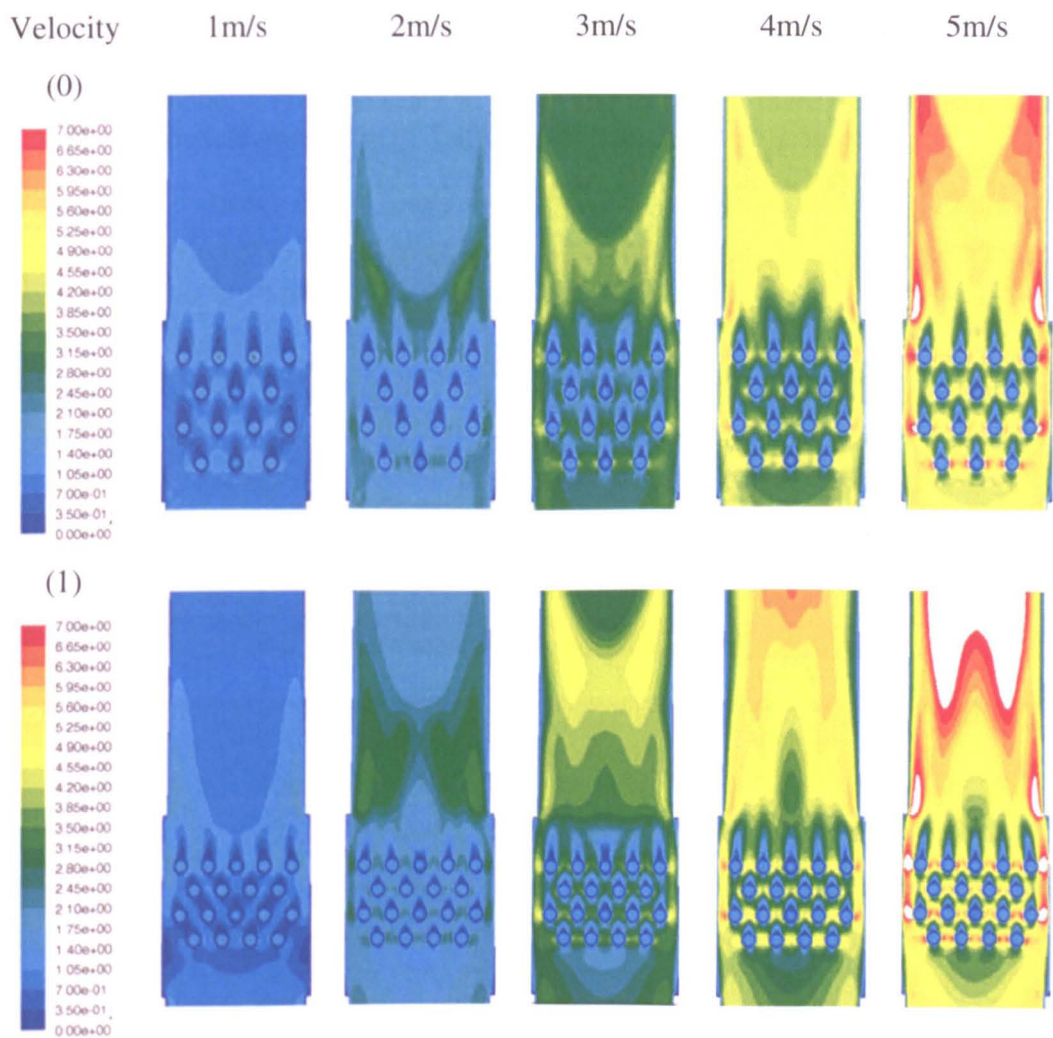


Figure 4-34 Velocity contour of central horizontal plane at different flue gas velocity



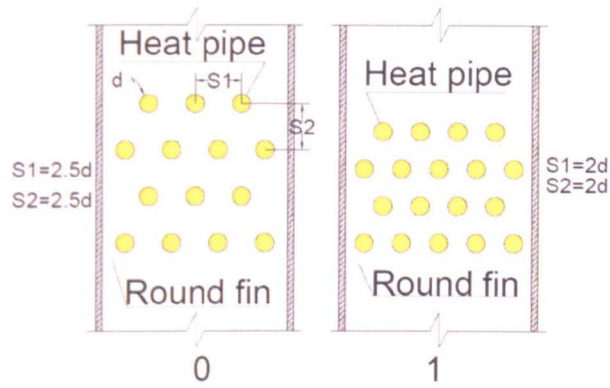


Figure 4-35 Staggered layout with different pitch (A:  $S1=S2=2.5d$ ; B:  $S1=S2=2d$ )

The flue temperature in the downstream of the model with  $2d$  pitch is lower than that of  $2.5d$ , as shown in Figure 4-36, which implies the thermal performance of  $2d$  model is better than that of  $2.5d$  model. Figure 4-37 shows the pressure drop of model with the pitch at  $2.5d$  (model 0) and  $2.0d$  (model 1), which indicates that apart from a gentle increase in the pressure when the flue gas velocity is at  $5\text{m/s}$ , the value of pressure drop stays almost the same level. Correspondingly, the required fan power of the model with  $2.0d$  pitch to offset the increased pressure drop due to the use of flue heat exchanger is up to  $7.4\%$  bigger than that with  $2.5d$  pitch.

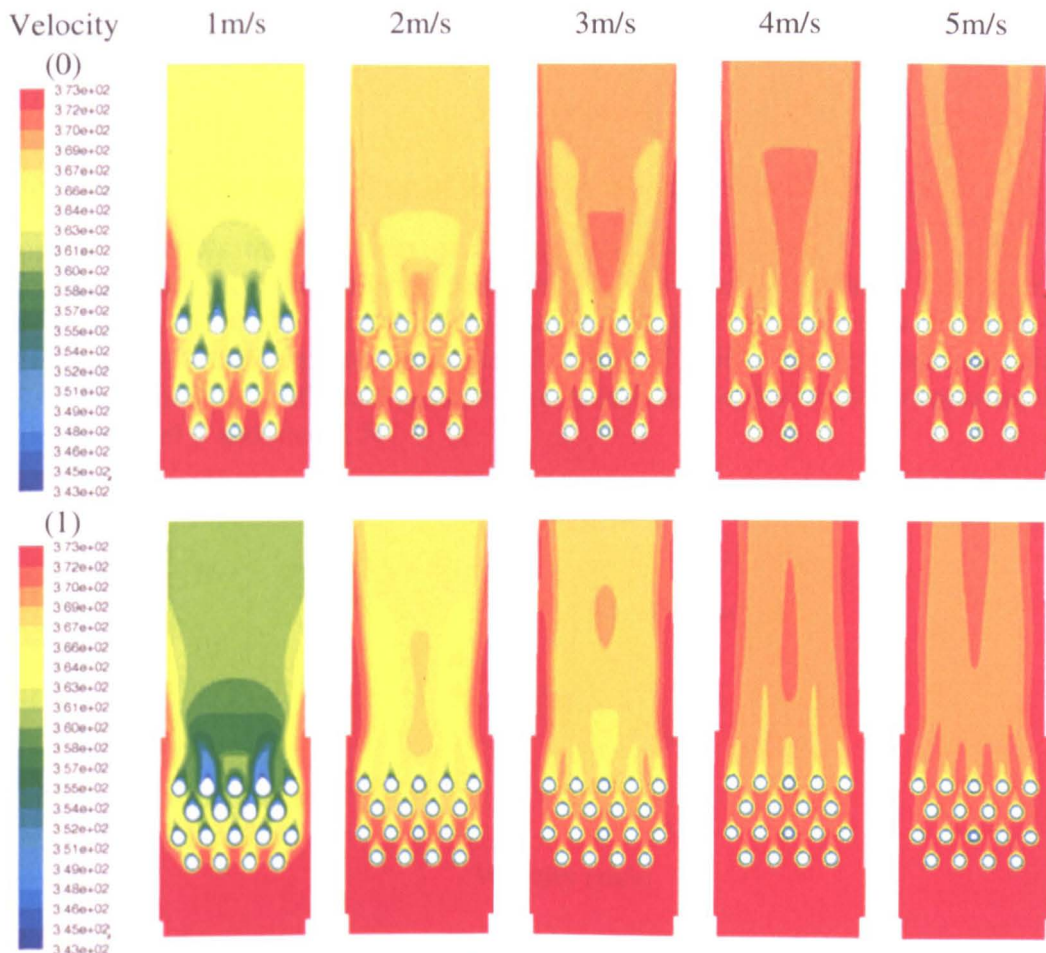


Figure 4-36 Temperature contour of central horizontal plane at different flue gas velocity

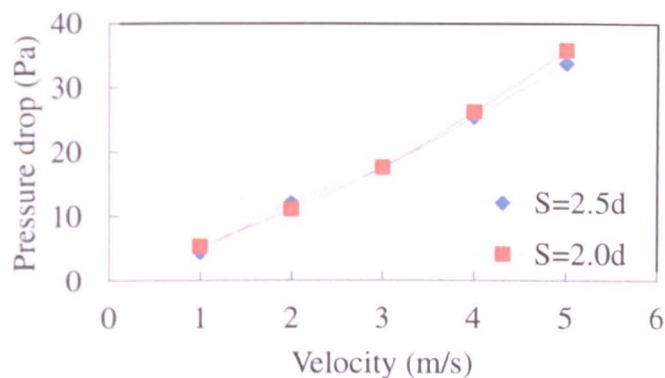


Figure 4-37 Pressure drop of flue heat exchanger with different pitch

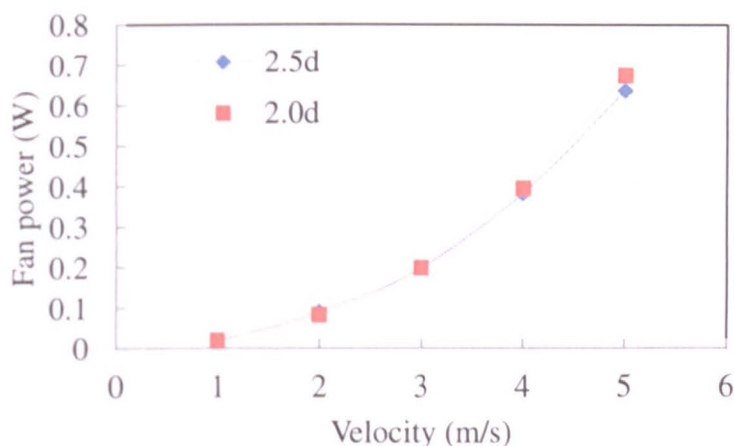


Figure 4-38 Pressure drop of flue heat exchanger with different pitch

Figure 4-39 shows the flue heat exchanger with 2d pitch has a bigger value of effectiveness at all the investigated velocities. Both of the heat transfer rate and net energy gain of 2d model is higher than those of 2.5d model, shown in Figure 4-40 and Figure 4-41. Therefore, the model with 2d pitch shows better overall performance than that with 2.5d pitch, which is also further proved by comparing the results of model 4 and model 5.

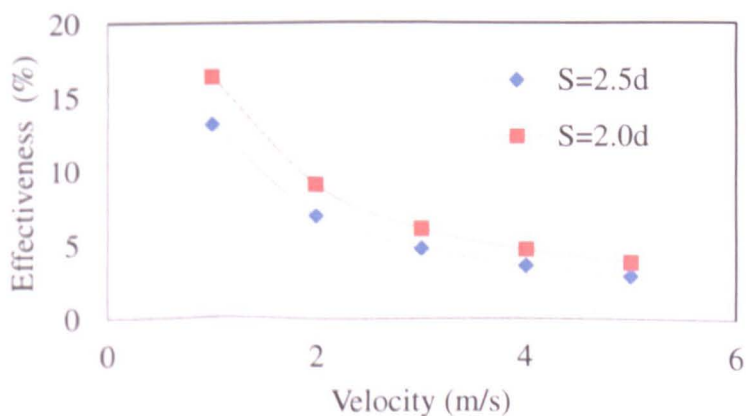


Figure 4-39 Effectiveness of flue heat exchanger with different pitch

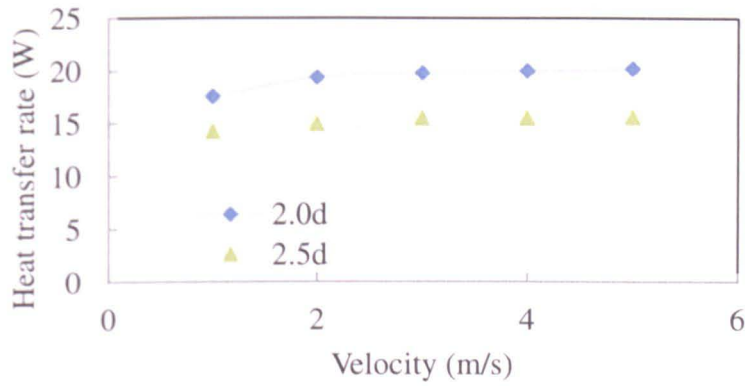


Figure 4-40 Heat transfer rate of pitch 2.0d and 2.5d

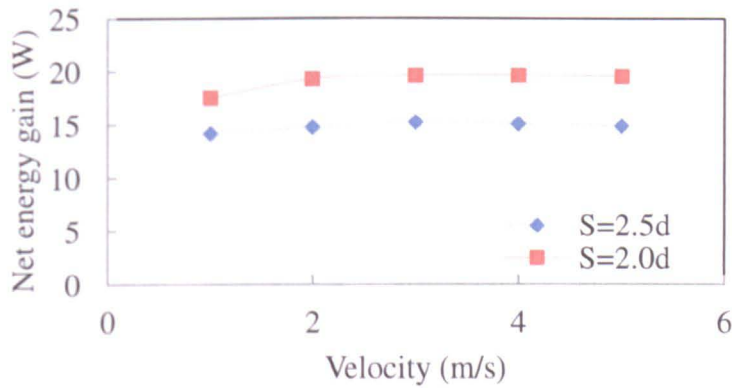


Figure 4-41 Net energy gain of flue heat exchanger with different pitch

#### 4. Joint style of flue heat exchanger

The cross section of flue heat exchanger and flue pipe are square and circular, which need to be connected. The connecting manner determines the flow field in the heat exchanger space. As shown in Figure 4-27, the velocity at the edge of flue heat exchanger outlet is higher than other areas, which contributes significant to the pressure drop. Hence, the sudden constriction and sudden expansion in model 2 is streamlined with gradual constriction and gradual expansion. The models are shown in Figure 4-42. Figure 4-42 (A) and Figure 4-42 (B) are the sudden junction and gradual junction respectively. The following numerical simulations compare them in terms of thermal and hydraulic performance at 1m/s, 2m/s, 3m/s, 4m/s and 5m/s.

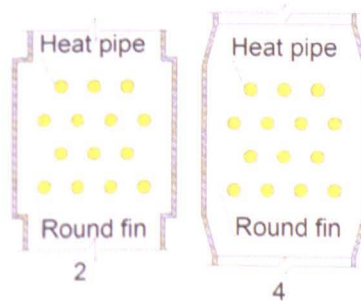


Figure 4-42 Sudden junction (A) and gradual junction (B)

Figure 4-43 shows the velocity contour of central horizontal plane of the two models. In the one with gradual junction (model 4), we can see a high velocity region is



formed near the wall. Meanwhile, this phenomenon is not obvious in the model with sudden junction (model 2) at 1m/s and 2m/s. Compared to model 2, obvious improvements can be spotted at the inlet and outlet where the high velocity zone and low velocity zone are not present in model 4. This means a flow improvement has been achieved by streamlining the junction. However, due to the change to the inlet, most of flue gas is induced to flow in the near-wall regions. A corresponding decrease is achieved in pressure drop shown in Figure 4-44, which becomes more apparent when the velocity increases.

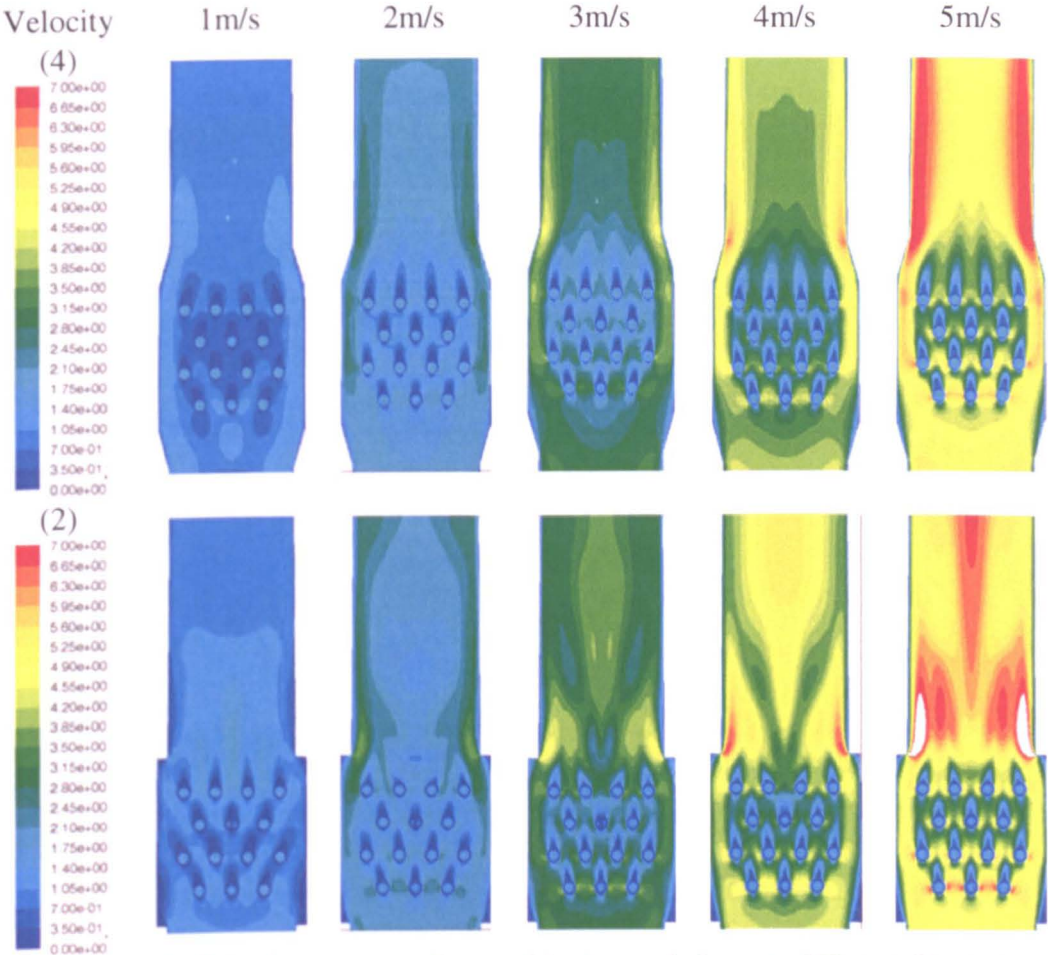


Figure 4-43 Velocity contour of central horizontal plane at different flue gas velocity

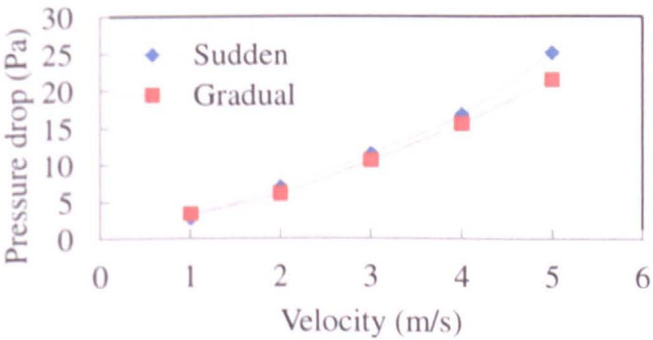


Figure 4-44 Pressure drop of models with sudden and gradual junction at different flue gas velocity

Figure 4-45 shows the temperature distribution of the two models at 1m/s, 2m/s, 3m/s, 4m/s and 5m/s. When the velocity is 1m/s, the flue heat exchanger with sudden junction has higher effectiveness and heat transfer rate, which is shown in Figure 4-46. This can be explained by the velocity distribution in Figure 4-43 where most of flue gas passes through the near-wall area in model 4 which directs the flue gas to the outlet without mixing with the heat pipes for heat transferring, implying a possible direction of further improvement by keeping the sudden junction at the inlet junction. For the rest four velocities, the effectiveness does not show much difference. However, the heat transfer rate of the gradual model is slightly higher than that of sudden junction at 2m/s, 3m/s, 4m/s and 5m/s.

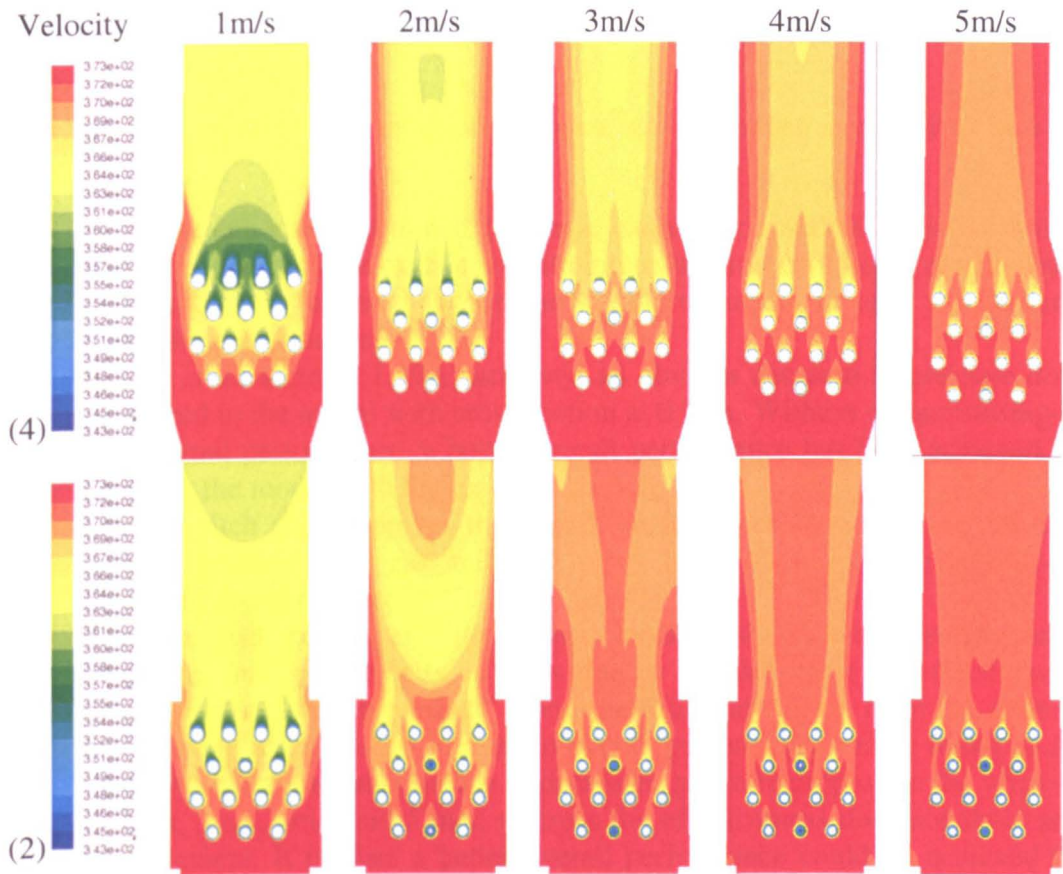


Figure 4-45 Temperature contour of central horizontal plane at different flue gas velocity

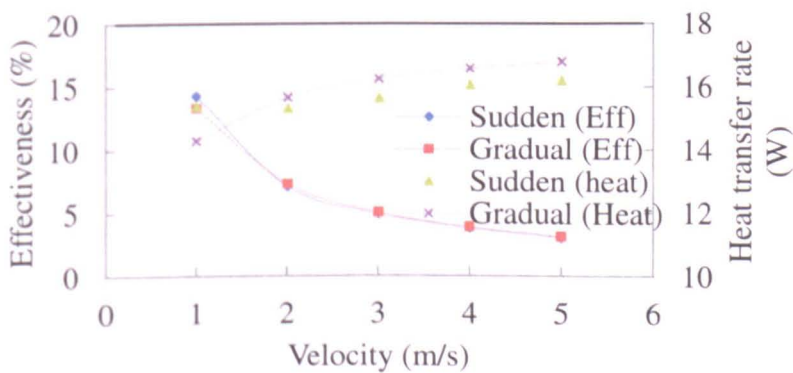


Figure 4-46 Effectiveness and heat transfer rate of flue heat exchanger with sudden junction and gradual junction at different flue gas velocity



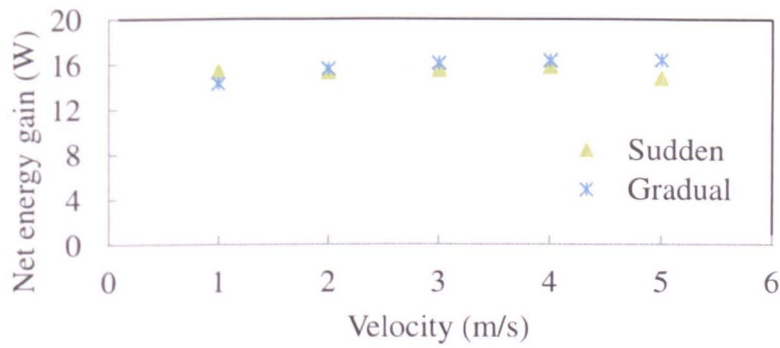


Figure 4-47 Net energy gain of flue heat exchanger with sudden junction and gradual junction

From the four comparisons introduced above, the following conclusions can be made:

1. In the square-cross sectioned flue heat exchanger installed amid the boiler flue pipe, the flue heat exchanger with inline layout shows better performance than that with staggered layout due to improvements in both thermal and hydraulic performance;
2. Bigger cross section (1.19A) achieved an obvious decrease in pressure drop compared to the model with cross section at 0.91A. Without compromising to the thermal performance, a better overall performance has been achieved by adopting the model with bigger cross section;
3. Smaller pitch (2d) improves the overall performance by enhancing the heat transfer between flue gas and heat pipes but without causing significant change in pressure drop;
4. The flue heat exchanger with gradual junction shows worse performance when the flue gas velocity is 1m/s due to smaller value of effectiveness caused by the “inducing effect” along the near-wall region from the gradual constriction, a slight improvement in overall performance can be found in the model with gradual junction due to decreased pressure drop when the velocity is 2m/s, 3m/s, 4m/s and 5 m/s; whereas the effectiveness does not show any improvement. It implies a better overall performance could be achieved by adopting sudden junction and gradual junction at inlet and outlet junction respectively.

These conclusions drawn at phase 1 provide guidelines for designing and improving the flue heat exchanger model in the phase 2 numerical simulation.

Figure 4-48 shows the fan power need corresponding to the increased pressure drop due to the use of flue heat exchanger. The model 4 needs the lowest fan power, closely followed by M4 (M4 is the model studied in the phase 2, which can be referred in 4.3.3). Looking at the net energy gain of all the investigated models shown in Figure 4-49, it demonstrates the model 5 and M4 gives the highest net energy gain. When the velocity of flue gas lies between 3.5m/s and 5m/s, M4 has the higher net energy gain than the model 5, whilst in the range of 1m/s-3.5m/s, the higher net energy gain goes to model 5. Hence, model 5 is suitable for part load operation whilst the M4 is suitable for full load operation among the models investigated in phase 1.

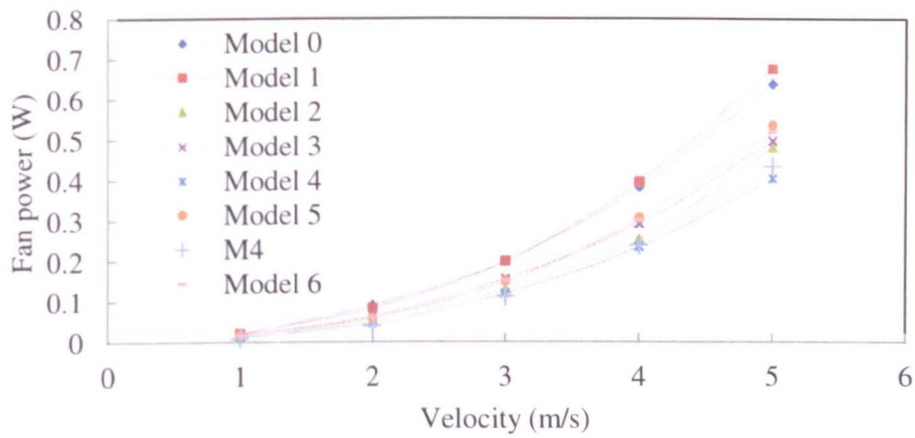


Figure 4-48 Fan power need of all the investigated models of flue heat exchanger

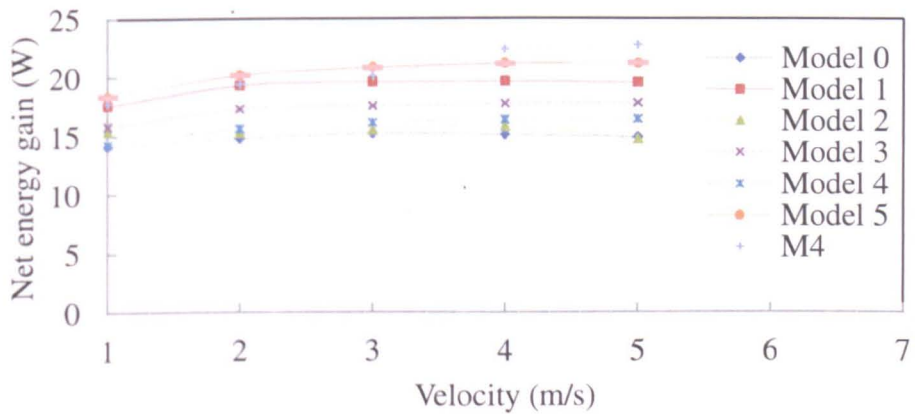


Figure 4-49 Net energy gain of all the investigated models of flue heat exchanger

#### 4.4.3 Identification of the modified models

Based on the results of phase 1 numerical simulation introduced in section 4.3.2, five modified models are built to identify the suitable model for flue heat exchanger. They are shown in Figure 4-50. In phase 1 numerical study, it was found out that the model with sudden constriction and gradual expansion has the potential to give a better overall performance. Therefore, in these models, sudden constriction and gradual expansion is used to connect flue gas pipe and flue heat exchanger. In case of the influence from the change of joint style, the staggered layout (2.5d), the inline layout (2.5d) and staggered layout (2d) are repeated here again to further confirm the results of the phase 1 study.

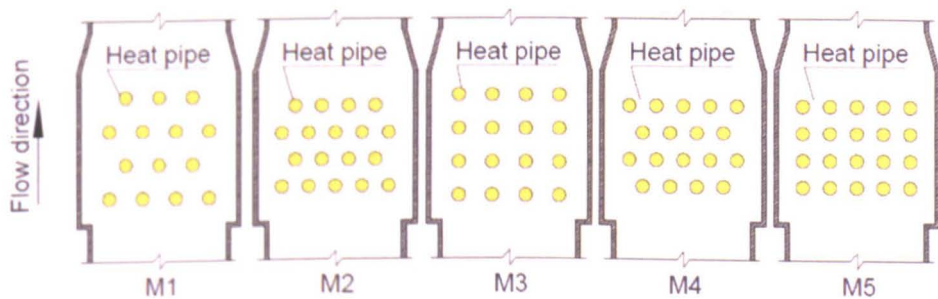


Figure 4-50 Modified models based on the previous numerical results

The boundary conditions, the mathematical modelling are the same with the ones introduced in the section 4.3.2 and hence not repeated here.

Figure 4-51 shows the velocity contour on central horizontal plane when the flue gas is exhausted at 1m/s, 2m/s and 3m/s.

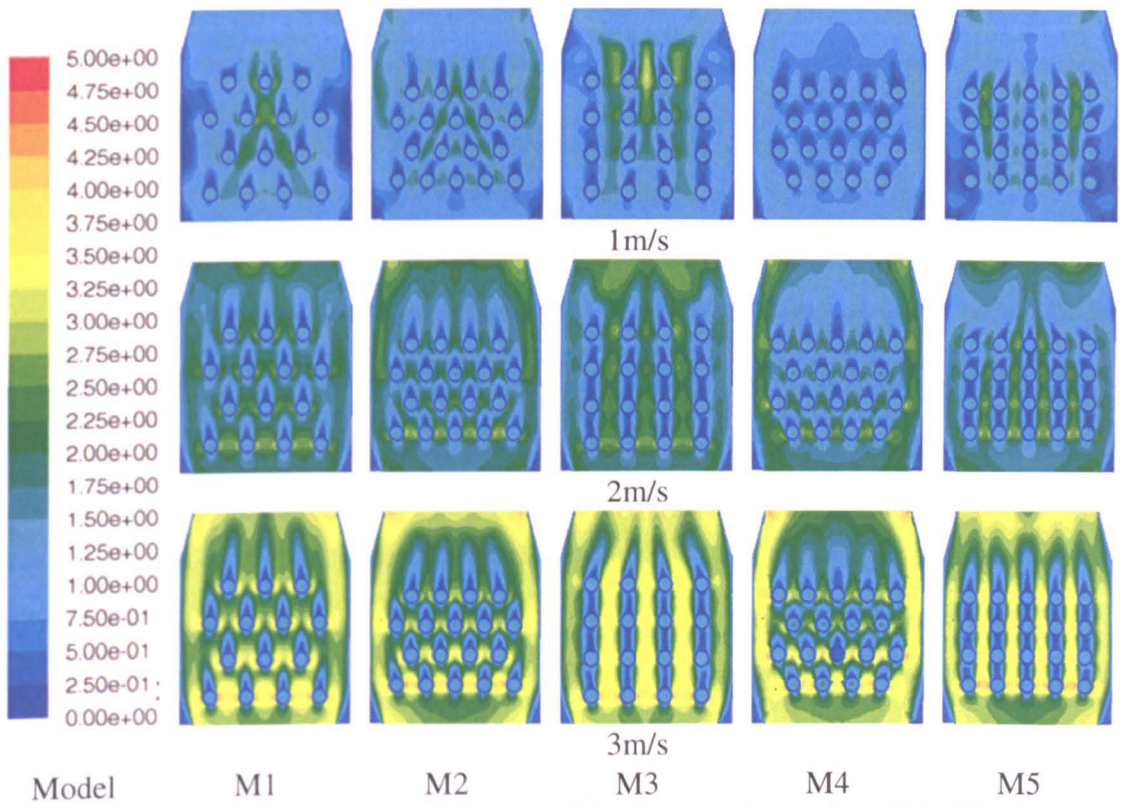


Figure 4-51 Velocity contour on the central horizontal plane of modified flue heat exchanger

Figure 4-52 shows the temperature contour on central horizontal plane of modified models of flue heat exchangers at 1m/s, 2m/s and 3m/s. The temperature contours don't represent the performance of real applications, but provide us the comparing results to decide which design shows better performance.



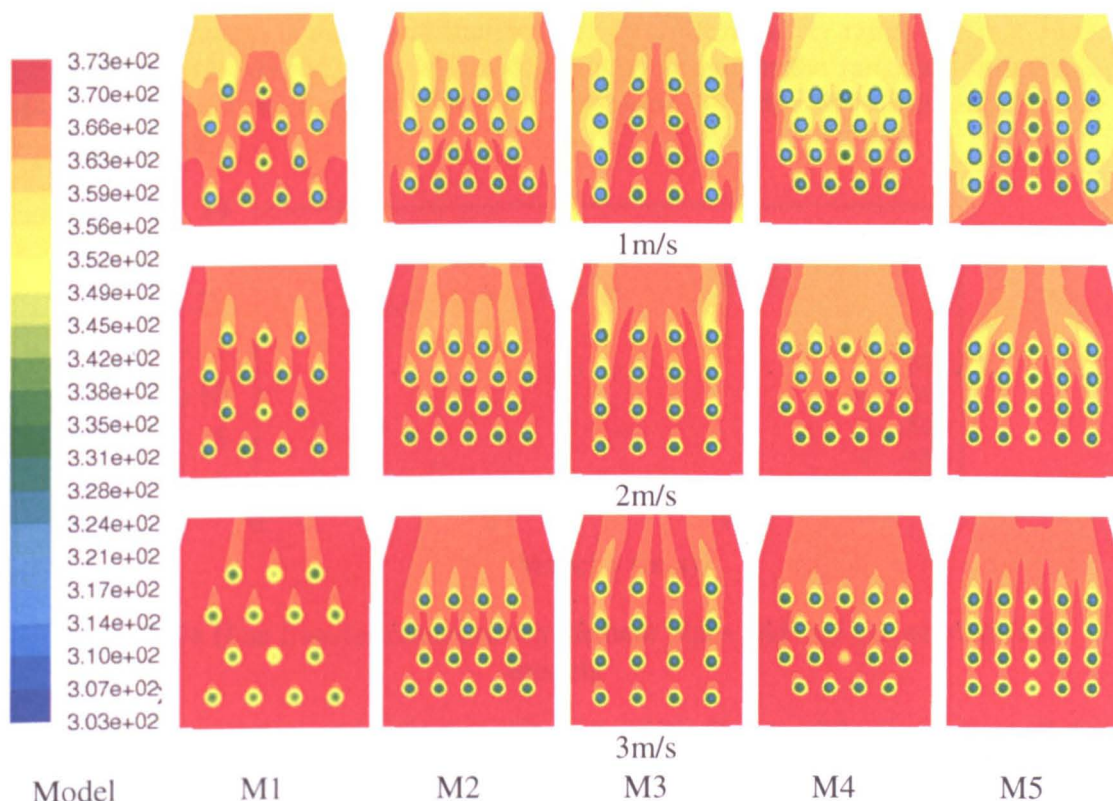


Figure 4-52 Temperature contour on the central horizontal plane of modified cooling plates

Figure 4-53 shows the heat transfer coefficient at the interface between the pipe wall and flue gas in boiler flue pipe in five modified models. When flue gas is exhausted at 1m/s, 2m/s, 3m/s, 4m/s and 5m/s, M2 shows the biggest value of heat transfer coefficient followed by M4, M1, M3 and M5, respectively. The heat transfer coefficient of M4 increases rapidly and takes over the top position when flue gas velocity lies between 3m/s and 5m/s. Hence, M2 shows the highest transfer coefficient in the range of 1m/s-3m/s, whilst M4 the highest in the range of 3m/s-5m/s.

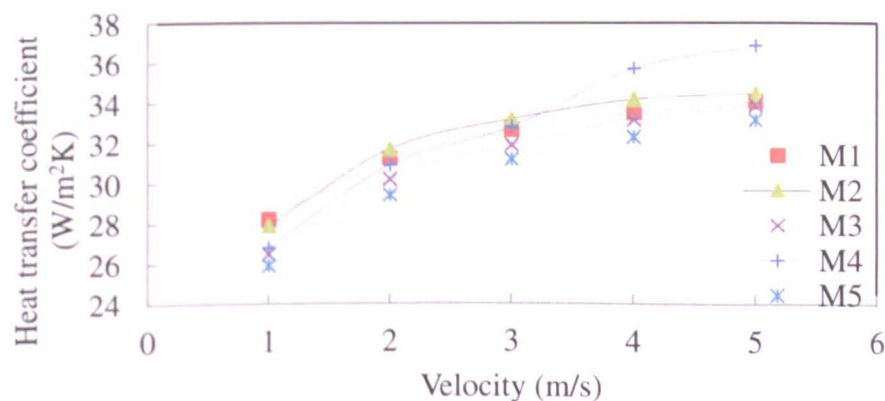


Figure 4-53 Heat transfer coefficient between the heat pipes and flue gas of modified models

As shown in Figure 4-54, the increase of the heat transfer capacity of each flue heat exchanger lies between 13% and 30% when the flue gas velocity increases from 1m/s

to 5m/s. M5 has the highest heat transfer rate over the velocity range of 1m/s-3m/s, followed by M2, M4, M3 and M1 in descending order. In the range of 3m/s-5m/s, M4 has the highest heat transfer rate, followed by M2, M1, M3 and M5 in descending order.

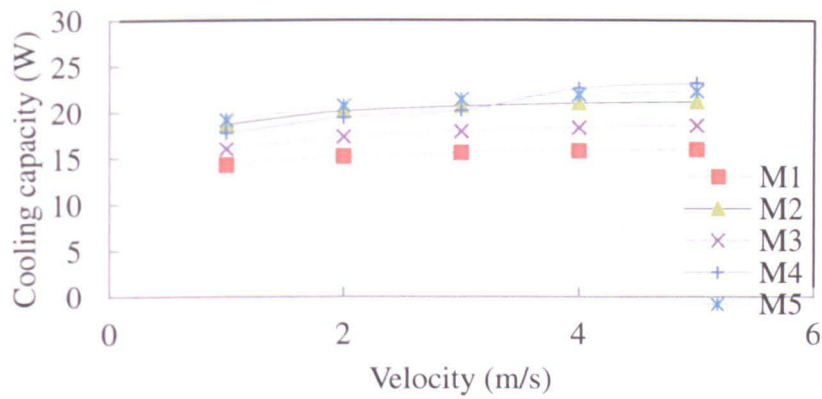


Figure 4-54 Heat transfer rate between the heat pipes and flue gas of modified models

Figure 4-55 shows the value of net energy gain of the five modified models at all the investigated velocities. For all the five modified models, the value shows a steady increasing trend when the velocity increases, which means that the increase of inlet velocity gains slightly more net energy. However, the value of M4 and M5 shows the dominant advantage over other modified models in the whole range of velocity. It means the modified model M5 can transfer the most heat per unit pressure drop, although M4 shows slightly higher value of net energy gain than M5 at 4m/s and 5m/s.

Based on the discussions above, M4 is selected to be the model of flue heat exchanger for further detailed design and investigations.

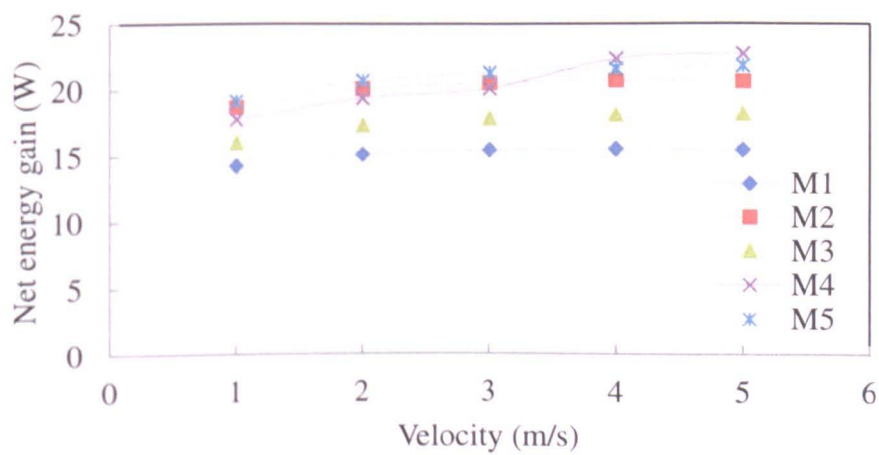


Figure 4-55 Net energy gain of the five modified models

#### 4.4.4 Detailed modification

The detailed modification is based on the result from the section 4.3.3 where the optimal model structure has been identified as M4. This section is the final step of



the numerical simulation which looks into the detailed structure and component arrangement, which all together finalises the eventual design of the flue heat exchanger.

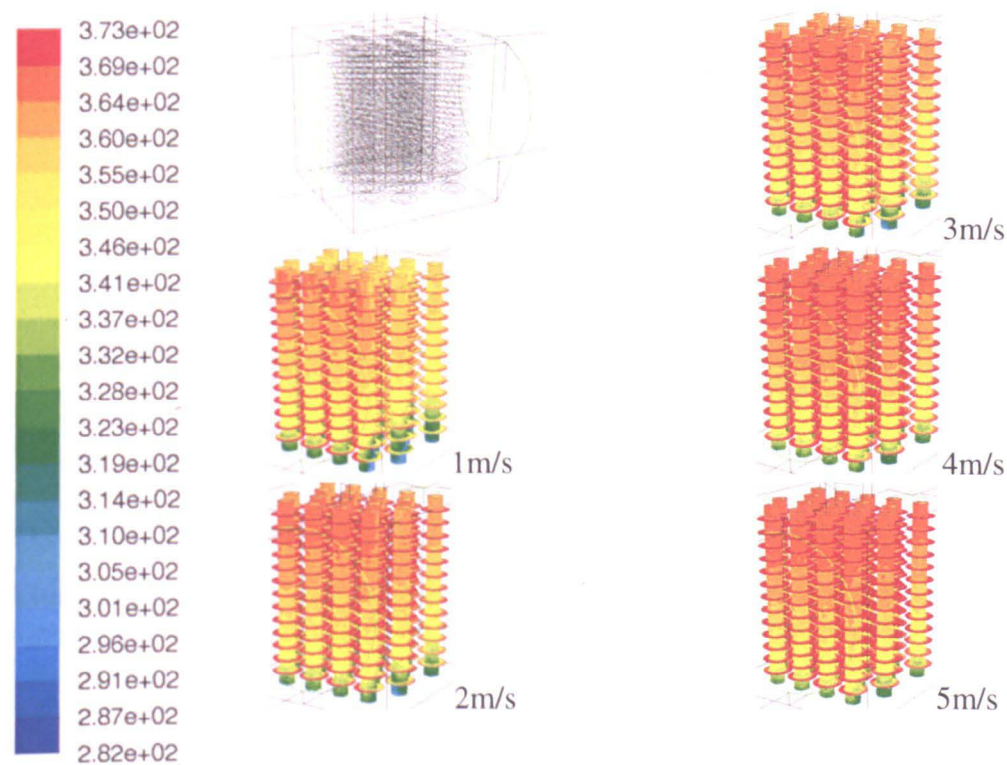


Figure 4-56 Temperature distribution on the exterior surface of fins and pipes

Figure 4-56 shows the temperature distribution on the exterior surface of fins and heat pipes under different inlet velocity, where we can see that the temperature at the bottom section is lower than that of middle and upper section. This can be attributed to lower temperature of the flow at the beginning section. The buoyancy effect caused by the temperature difference directs most of the gas to the upper section of the heat pipe. Hence, in order to enhance the heat transfer, the lower section of heat pipe can be decreased and the upper section of heat pipe can be increased.

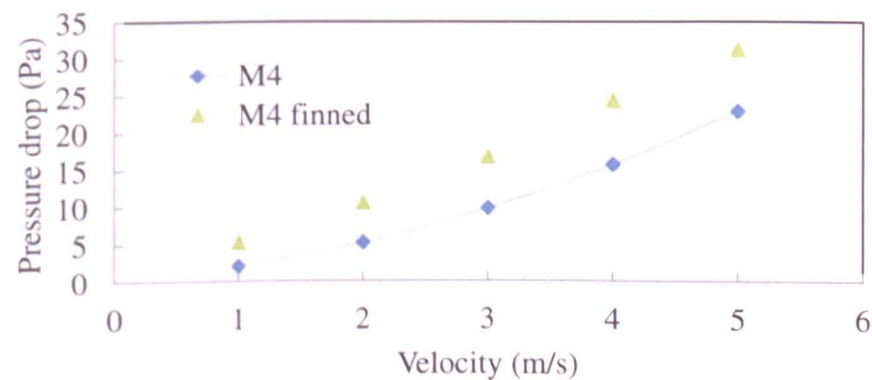


Figure 4-57 Pressure drop of M4 model before and after finned under different flow velocity

Figure 4-57 shows the pressure drop of M4 model before finned and after finned. The fins are installed at the density of 200fins/m. The pressure drop of finned M4

increases to 5.27Pa from 2.15Pa at 1m/s flow velocity, to 31.23Pa from 22.99Pa at 5m/s.

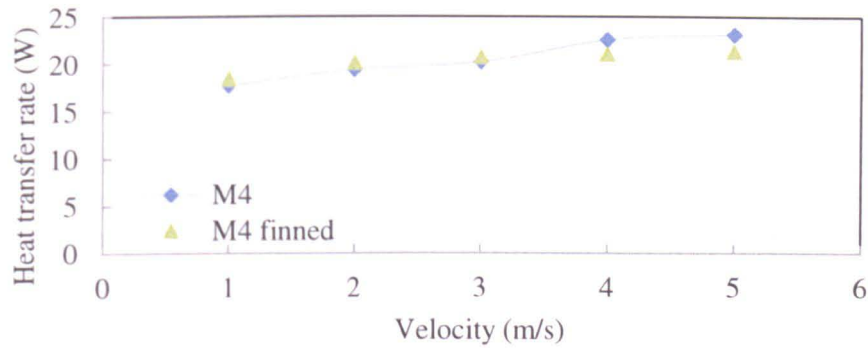


Figure 4-58 Cooling capacity of M4 before finned and after under different flow velocity

The heat transfer capacity of finned M4 shows its enhanced heat transfer in the range of 1m/s-3m/s, whilst in the range of 3m/s-5m/s, the heat transfer capacity of bare M4 is better than finned M4.

With the use of heat transfer enhancement design-fins, the thermal performance is improved at 1m/s, 2m/s and 3m/s (the enhancement in heat transfer rate is 3.9%, 3.8% and 2.7%), shown in Figure 4-58. For the velocity at 4m/s and 5m/s, no enhancement has been shown. Meanwhile, the pressure drop has been increased by using the heat enhancement method at 1m/s, 2m/s, 3m/s, 4m/s and 5m/s, the corresponding pressure drop increase is 145%, 102%, 69.7%, 54.3% and 42%, respectively.

In the numerical simulations, the working mechanism of heat pipes has been simplified into the pipe flow. The results of heat transfer result can't be used to represent the thermal performance of heat pipe heat exchanger in real applications. Therefore, it is improper to make the final decision whether the installation of fins on the heat pipes is beneficial to the overall system performance. Future effort needs to be made to investigate the real impact of fin designs to the flue heat exchanger based on experimental studies and numerical simulations that accommodates the real mechanisms of heat pipe.

#### 4.4.5 Other considerations

Due to the chemical properties of flue gas and the temperature level at which the flue gas is exhausted to the environment. A few considerations need to be taken into account in the design process of flue heat exchanger.

##### 4.3.5.1. Corrosion

Usually, the selection of heat pipe heat exchanger is dependent on the chemical properties of flue gas. For different applications, different materials are used to fabricate the container of heat pipe heat exchanger. A heat pipe heat exchanger made of copper and using water as working fluid has been highly recommended in reclaiming waste heat from domestic waste heat such as furnace flue gas, waste hot water and the fireplace [149]. The temperature of flue gas in domestic furnace for

space heating is about 260°C, which is about 12% of the energy available from the fuel [150].

#### **4.3.5.2. Condensate draining**

With the use of flue heat exchanger, the temperature of flue gas drops down to the level lower than the dew point of water vapour, which condenses on the inner surface of flue heat exchanger. Therefore, condensate drainage measure needs to be taken to make sure it does not flow back to the boiler and corrode the components. All external condensate pipe work should be piped in a diameter of at least 32mm. External condensate pipe work should be lagged/insulated. The pipe must be smaller than 3 metres in length and should keep horizontal runs to a minimum. When extension pipes are used the flue system must be designed to have a continuous fall to the boiler of at least 3° to allow condensate to run out via the drain.

A plastic drain pipe should be fitted to allow discharge of condensate to a drain. If possible, condensate should be discharged into the internal household draining system. If this is not practical due to on-site condition, discharge can be made externally to the household drainage system or a purpose designed soakaway.

The extremely cold weather could result in freezing drainage pipe, causing temporary boiler shut down. The reason is mainly attributed to the part of drainage pipe that is exposed to outside. In order to minimise the risk of freezing, the following recommendations for routing condensate drainage pipe should be followed:

1. Wherever possible, the condensate drainage pipe should be terminated at a suitable internal foul water discharge point such as an internal soil and vent stack, internal kitchen or bathroom waste pipe, washing machine waste pipe-ensuring that condensate drains away from the boiler under gravity. The possibility of drainage pipes freezing downstream of the internal connection should also be considered in determining a suitable connection point;
2. Where internal termination under gravity flow is not practical, the installer should ensure that the customer is made aware of the freezing risk of external pipe work under extreme conditions and the corresponding consequences;

#### **4.5 Summary**

Bypass effect shown in inline layout is not present in this study due to interference of changed flow pattern by the junction between exhaust pipe and flue heat exchanger. The model with cross section ratio of 1.02 gives the best overall performance of five models with the cross section area at 0.91A, 1.02A, 1.13A, 1.25A and 1.36A. The heat pipe pitch 2.0d gives the better performance than that with 2.5d.

The model with sudden expansion and gradual constriction has been identified gives the most suitable structure of flue gas heat exchanger. M4 and M5 show better overall performance than other models. M4 shows better performance than in the velocity range of 3.6m/s-5m/s, whilst M5 shows better performance between 0-3.6m/s. Other considerations such as corrosion and condensate draining have been discussed when this application is in residential environment.



## Chapter 5 Heat dissipation

In general, the heat dissipation is used to cool down the cold side of thermoelectric generator in order to create a low temperature. Additionally, it also shoulders the responsibility of managing the unconverted heat which is usually wasted in conventional design. The cold side heat exchanger plays the role of heat dissipation and keeps the cold side of TE module at a low temperature by extracting the heat and dissipating it to environment or managing it for other useful purposes. Hence, it must be very efficient in dissipating the heat from the cold side so as to keep the cold side temperature at a low level and efficiently use the unconverted heat at the same time. However, when the heat exchanger is designed, the cooling capacity needs to match with the rest of the components in the system.

This chapter reviews the heat dissipation methods that are used in the previous researches and applications. In comparisons with the disadvantages shown in the conventional heat dissipation, an oriented cooling method for the domestic TCS has been proposed on the basis of experimental study and numerical study. In this research, the cooling plates are supposed to be integrated between the main water supply and boiler. The water is preheated in the cooling plates before goes to the boiler. The goal of adopting this cooling plate is to cool down the thermoelectric generator cold side effectively with minimum penalty in pumping power.

### 5.1. Design

In the field of heat dissipation, the main emphasis has been traditionally placed on the thermal performance, although there are other issues that influence its economic and technical viability. One of these is the pressure drop, which affects the power required by the pump. It also affects the weight and size of the device.

In thermoelectric applications, the design of heat dissipation has found the important position in creating oriented thermal conditions for a good thermoelectric performance. It shoulders the responsibility of cooling the cold side surface of thermoelectric module and decides where and at what rate the heat output is dissipated into the environment or managed for other purposes such as preheating water for home heating devices. The cooling methods that have been used as heat sink in thermoelectric power generations normally include fan cooling, heat pipe and water cooling. They can be categorized into active cooling (mechanical air/water cooling) and passive cooling (heat pipe). In previous research, the fan cooling is the most used method that dissipates heat to the environment in [151], [152], [153]. The typical installation is shown in Figure 5-1.

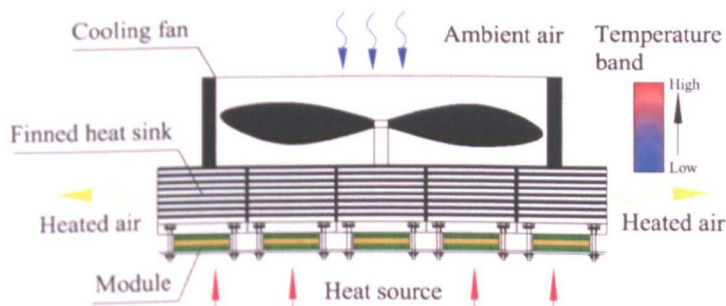


Figure 5-1 Typical fan cooling for thermoelectric power generation



This fan cooling method is effective due to its forced convection. The disadvantage lies in extra electricity consumption, limited lifespan, existence of moving parts which possibly causes noisy operation and the waste of unconverted heat. Some method such as heat pipe combined large heat sink keeps cold side temperature at a low level by extracting the heat from module cold side surface and dissipating it into the environment in a passive way. This method uses the phase change process to transfer heat passively using heat pipe which does not need extra energy input. Two typical examples are shown in Figure 5-2 [154].

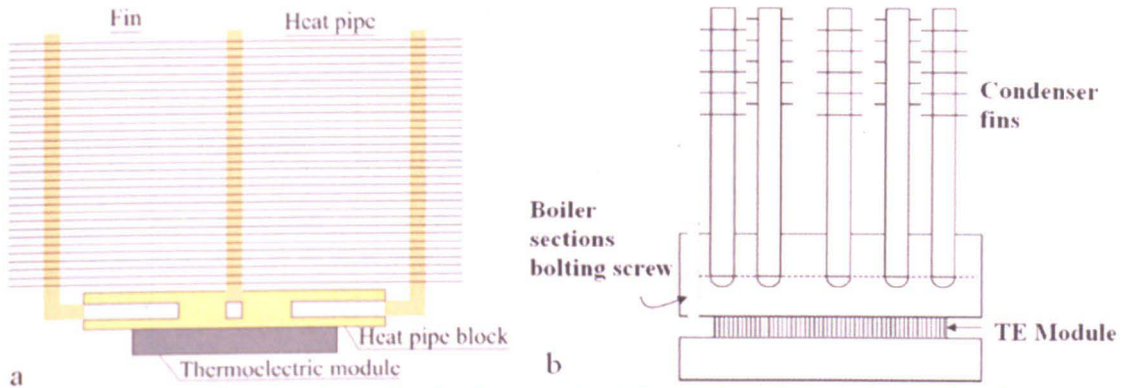


Figure 5-2 Passive heat dissipating method- heat pipe sink (a. heat pipe; b. thermosyphonic heat sink)

The advantages of this method is energy saving and quiet due to its zero energy consumption and none moving parts compared to other methods that are related to the use of electric fan. However, both of them dissipate the unconverted heat into local environment, which optimistically helps improve the local thermal condition if heat is required by the local environment such as in winter, or it deteriorates the indoor thermal condition if the heat is not required such as in summer. Consequently it delivers low thermal efficiency (which is one of the major factors that limit its wide application), takes up a large space and increases the system weight, not practical for the applications where compact systems are needed.

An oriented cooling method involves the optimum match of hydraulic characteristic and heat exchange capacity of the cold side heat exchanger. The hydraulic characteristic represents the hydraulic performance of heat exchanger. The pressure drop caused by utilising heat exchanger is directly related to the hydraulic characteristic. The capacity of a heat exchanger needs to match with the system. If it is smaller than that required by the system, the conversion efficiency would be decreased because of the lowered temperature difference across the generators. If it is bigger, it would consume extra unnecessary energy. Hence, an oriented cooling design for the thermoelectric cogeneration needs to take these two factors into consideration. Conventionally, the thermal performance is taken as the major task in the design or development of heat sink. The pressure drop is not the primary factor to be considered due to the characteristic of applied areas, such as the heat sink used in electronic engineering areas where the effective heat dissipation and compact size is the key requirement. In this research, the thermoelectric cogeneration system aims to achieve the possible maximum net energy output. This goal leads to the needs of maximum recovery of boiler waste heat and efficient use of solar energy as well as the minimum need of extra power input such as pump power. Hence, it is essential to

see pressure drop as the other major factor that significantly affects the overall system performance and should be considered.

Based on the aforementioned reviews of thermoelectric applications, there are two ways of assembling thermoelectric modules, including individual assembly and whole assembly. In practical applications, when the system uses multiple modules, the typical assembly method is sandwiching all the modules together between the surfaces of two heat exchangers. This assembling method is called whole assembly, shown in Figure 5-3 (b).

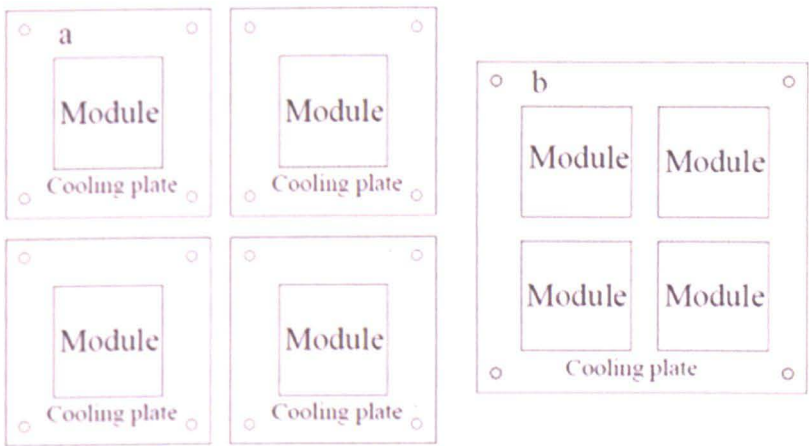


Figure 5-3 Schematic diagram of individual assembly (a) and whole assembly (b)

In the whole assembly, the pressure is loaded on each module ceramic substrate from the same surface. Uneven pressure load could be caused by module thickness difference. The module thickness difference makes each module take the pressure at different level. The more different the thickness of each module is, the more uneven the pressure on each module will be loaded. Consequently, the system performance is deviated from the optimum performance because the pressure load is an important factor that determines the system performance by affecting the heat transfer. It can even damage the modules due to the concentrated pressure load at the corner or edge of ceramic substrate and the semiconductor element sandwiched between two ceramic substrates, examples are shown in Figure 5-4, taken in the experiment. Uneven pressure load can concentrate the pressure on the edge which is delicate to support excessive pressure load. Therefore, the edge collapsed and the thermoelectric element is destroyed. In this circumstance, the module can't operate as normal due to the increased electrical resistance in the cracks which weakens or even cuts off the electric circuit.

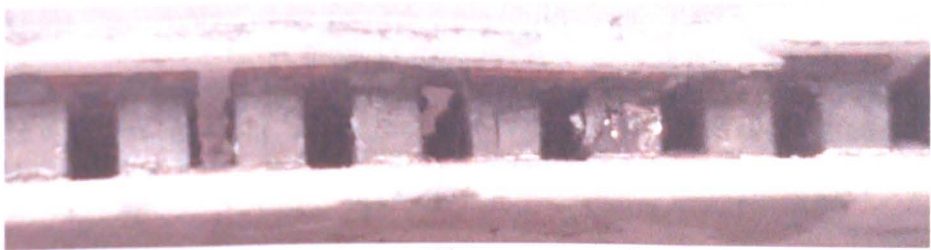


Figure 5-4 Module damages caused by uneven and excessive pressure load

Figure 5-5 shows the results of measuring the thickness of 20 thermoelectric modules which are randomly chosen from newly produced modules. They have been



measured using a digitronic calliper. It lies in the range of 3.84mm-3.96mm with 0.12mm maximum thickness difference.

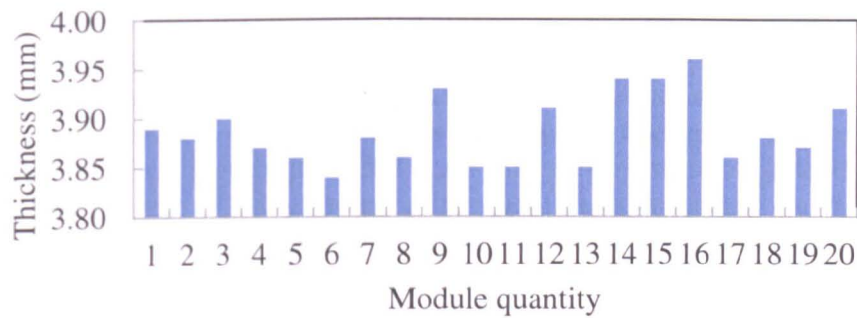


Figure 5-5 Thickness of 20 random thermoelectric modules

This creates a difference in the pressure load on each module. The impact of the different pressure load to the performance of thermoelectric generation is investigated by conducting two sets of tests. In the tests, individual assembly and whole assembly are used to install the thermoelectric modules. Same pressure is loaded on each test; the result is shown in Figure 5-6.

The results of the two sets of experiments show that the individual assembly outweighs the performance of whole assembly by delivering more power output in the whole range of temperature difference. The bigger the temperature difference is, the more obvious of the advantage the individual assembly shows. At temperature difference 130K, the power output of individual assembly is 54% more than the average power output of single module in whole assembly.

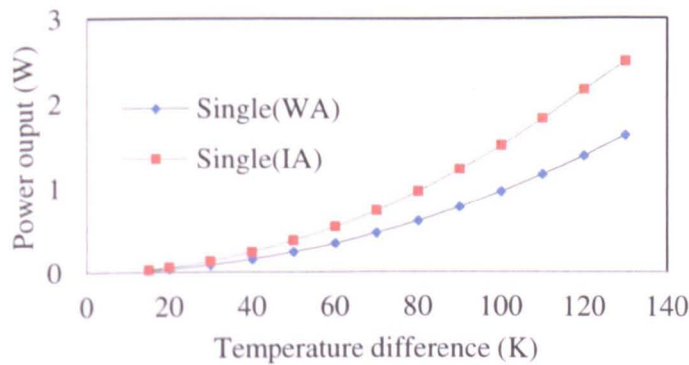


Figure 5-6 Single module performance in whole assembly (WA) and individual assembly (IA)

The whole assembly, despite the possibility of degrading thermoelectric performance, shows a large module density, which is defined by the quantity of accommodated thermoelectric modules in a given surface area. It is suitable for the facilities with limited space. However, restrictions on the thickness difference of the used TE modules must be adopted in selecting the modules to make sure the thickness difference is not in the performance-degrading range, which needs to be found out in future study.

Individual assembly means each thermoelectric module is individually assembled with a set of assembling configurations, shown in Figure 5-3 (a). Due to being

sandwiched between different pair of surfaces, the pressure load on each module can be individually set at the optimum level which has been experimentally verified.

A cooling plate oriented for domestic thermoelectric cogeneration is presented. The plate structure with multiple-channel is shown in Figure 5-7, which is looped together by two common main channels. It is made of an aluminium block through which fluid channels are machined across the plate to emerge at both ends into a common header. The adoption of such a fluid flow looped structure enables the flow to “sweep” the whole plate with good temperature distribution on the surface, eliminating heat build-up and hot spots. This design also is characterised by lower pressure drop than the traditional designs with embedded coiled tube. The channel sizes are designed to comply with the required flow rate of feed water for nominal boiler operation. In the real application, the cooling plates are integrated in the existing domestic hydraulic system between the feed water and boiler. The tap water is preheated in the cooling plates before fed to the boiler.

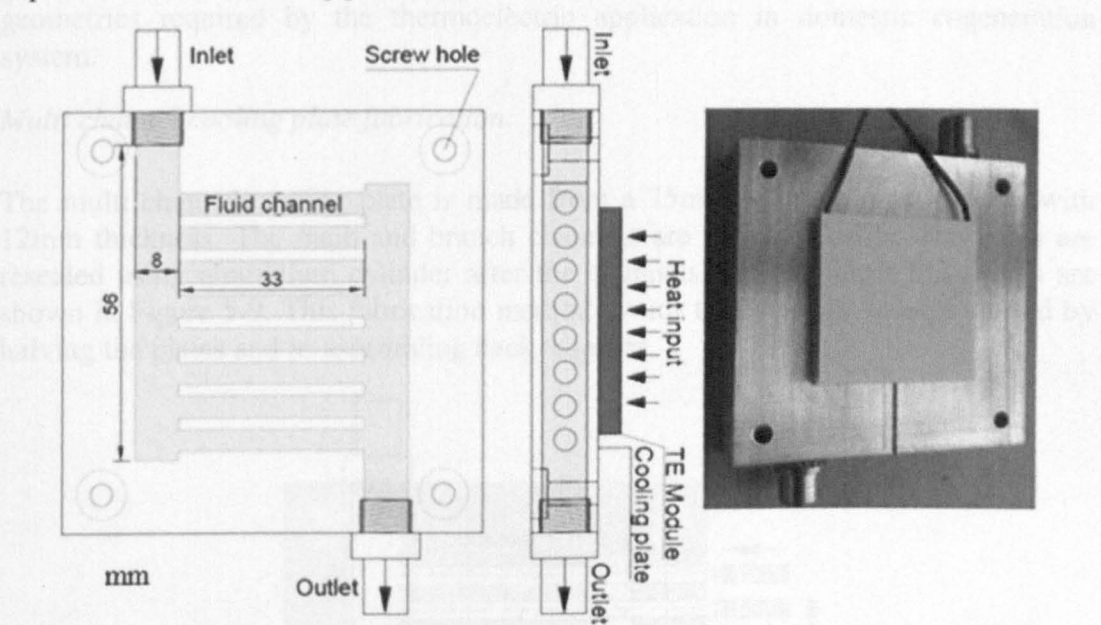


Figure 5-7 Cooling plate for thermoelectric cogeneration [155]

Figure 5-8 shows the photo of an assembled single thermoelectric cogeneration block. It consists of a cooling plate, an oil tank and a thermoelectric generator. The thermoelectric module is sandwiched between the cooling plate and hot side heat exchanger by four stainless steel screws. A flat metal washer, a crinkle washer and a fibre washer are placed between each screw and the cooling plate, shown in Figure 5-8. The crinkle washer and the fibre washer play the roles of accommodating thermal expansion and thermally insulating, respectively. A groove has been made on the cooling plate and hot side heat exchanger to hold thermocouple for measuring the temperatures at the module hot side and cold side.

The cooling plate is designed to overcome the uneven pressure load shown in whole assembly by individually enclosing each module with the cooling plate. Afterwards, all the cooling plates are softly-connected without imposing any mechanical force against each other. Hence, the pressure load on each module is individually defined by adopting the experimentally proven assembling method.



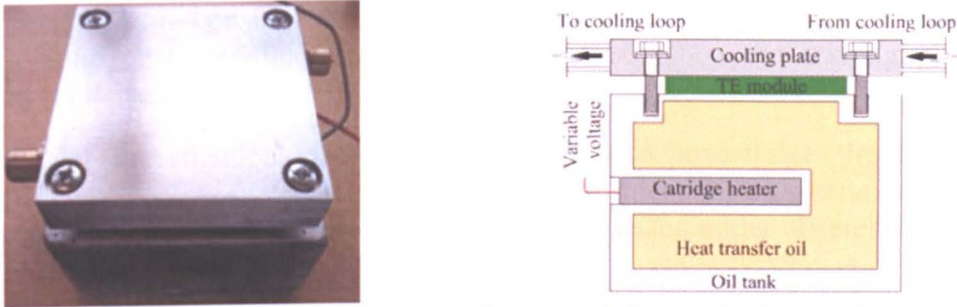


Figure 5-8 The photo and schematic diagram of the single thermoelectric cogeneration block

It is important to take into account of heat transfer and pressure drop when practical engineering applications are foresighted [156]. In this research, the combined performance of heat transfer and pressure drop is assessed based on the physical geometries required by the thermoelectric application in domestic cogeneration system.

#### *Multi channel cooling plate fabrication:*

The multi channel cooling plate is made from a 75mm square aluminium bar with 12mm thickness. The main and branch channels are made by drills. The holes are resealed using aluminium cylinder after the channels are machined; the details are shown in Figure 5-9. This fabrication method avoids the possible leakage caused by halving the plates and re-assembling back together.

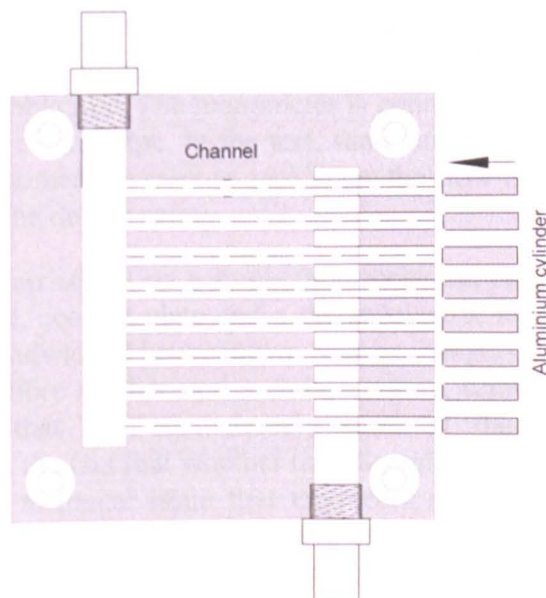


Figure 5-9 Fabrication schematic diagram of multi channel cooking plate

## **5.2. Experiment methodology**

It must be understood that the integration of cooling plate changes the hydraulic characteristic of the original boiler water feeding system. The overall pressure drop is increased; the increased part represents extra energy consumption which is manifested in the use of more pump power. It needs to be maintained at possibly the

lowest level so as to consume the minimum electrical power. Therefore, the thermal and hydraulic characteristic needs to be understood when the cooling plate is designed for domestic TCS.

Experimental investigations have been conducted to investigate the hydraulic performance of cooling plate and the performance of micro TE cogeneration system. The hydraulic performance of cooling plate has been tested under different flow rate using a manometer, shown in Figure 5-10.

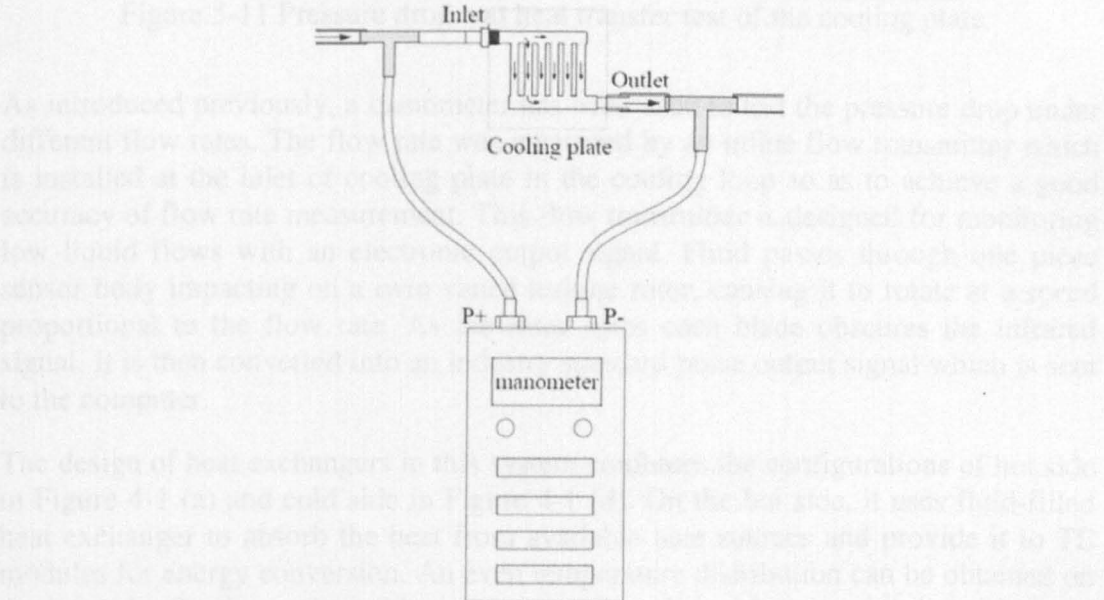


Figure 5-10 Pressure drop test of cooling plates at different inlet velocity

Both ends of cooling plate are connected to straight water pipes. Water flows through cooling plate at adjustable rate. The manometer is connected to the inlet and outlet of cooling plate through plastic pipe. In the test, same amount of air is kept in the two plastic pipes. The manometer is reset to zero when the flow is at static state to ensure the test accuracy and the device safety.

The system test was carried out on a single thermoelectric cogeneration block which consists of an oil tank, cooling plate and a thermoelectric module, shown in Figure 5-8. The module is sandwiched between two heat exchangers using a crinkle washer, a flat metal washer, fibre washer and a stainless steel screw. This is the common assembling method that has been widely used in thermoelectric application assembling. However, the fact that whether this assembling method is suitable for the system or not is the technical issue that engineers and manufacturers are highly concerned for. This issue is discussed in Chapter 6 which introduces the impact of mechanical assembly on the performance of thermoelectric applications.

The thermal performance has been investigated on the single thermoelectric block test rig. The real time cooling capacity has been tested under different inlet water velocity together with the pressure drop; the test rig is shown in Figure 5-11.



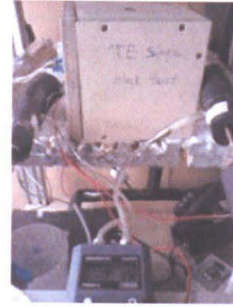
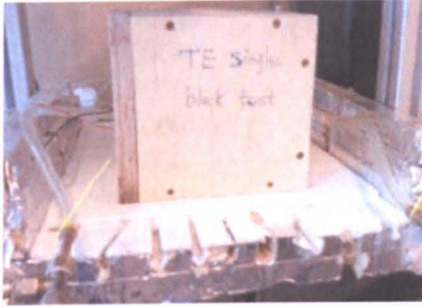


Figure 5-11 Pressure drop and heat transfer test of the cooling plate

As introduced previously, a manometer has been used to test the pressure drop under different flow rates. The flow rate was measured by an inline flow transmitter which is installed at the inlet of cooling plate in the cooling loop so as to achieve a good accuracy of flow rate measurement. This flow transmitter is designed for monitoring low liquid flows with an electronic output signal. Fluid passes through one piece sensor body impacting on a twin vaned turbine rotor, causing it to rotate at a speed proportional to the flow rate. As the rotor spins each blade obscures the infrared signal. It is then converted into an industry standard pulse output signal which is sent to the computer.

The design of heat exchangers in this system combines the configurations of hot side in Figure 4-1 (a) and cold side in Figure 4-1 (d). On the hot side, it uses fluid-filled heat exchanger to absorb the heat from available heat sources and provide it to TE modules for energy conversion. An even temperature distribution can be obtained on the hot side. On the cooling side, water is used as the coolant to cool down the cold side of thermoelectric module. A relatively even temperature distribution can be achieved due to the multi-channel design in the cooling plate.

Experimental investigations have been conducted on cooling plates with three different branch channel dimensions, 3mm, 4mm and 5mm. The hydraulic characteristics and the system performance were studied in two separate tests.

### 5.3. Hydraulic performance

The hydraulic characteristic is investigated by a manometer. It measures the pressure drop of cooling plate at different water velocity, shown in Figure 5-10. The cooling plate is assembled with each module using an experimentally verified assembling method to ensure both sides are attached with the surface of hot side heat exchanger and cooling plate at the optimum pressure load. Figure 5-12 shows the pressure drop at different inlet velocities. The tested velocity range in the main channel is between 0.39-1.92m/s (3898-19208 of Reynolds number in the main channel,) lying in the range of transition flow and turbulent flow. In the branch channel, the velocity ranges from 0.35-1.71m/s (Reynolds number: 1299-6402). Therefore, the pressure drop at lower range can be predicted by extending the curve of pressure drop-velocity to the laminar flow zone with smaller velocity. The dotted curve represents the pressure drop at the lower velocity range.

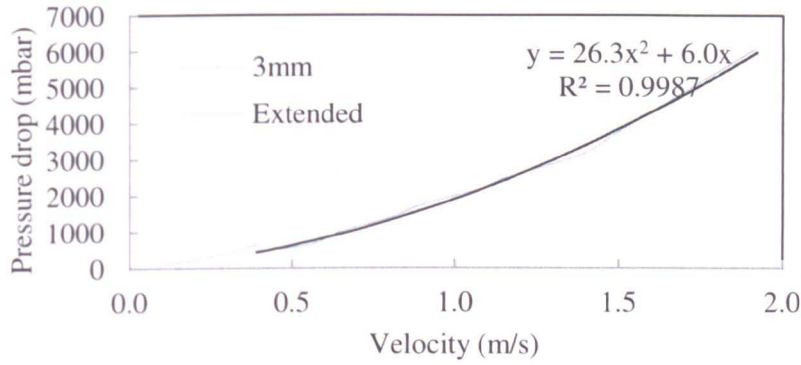


Figure 5-12 Hydraulic performance of the cooling plate

For the cooling plate, the correlation between pressure drop and the inlet velocity is unknown and here is described by Eq.(5-1).

$$\Delta P_{cp} = av^2 + bv \quad (5-1)$$

According to the hydraulic test which investigates the pressure drop at different inlet velocity, the value of a, b and c can be obtained and the correlation is expressed by Eq.(5-2).

$$\Delta P_{cp} = 26.3v^2 + 6.0v \quad (R^2=0.9987) \quad (5-2)$$

Pressure drop represents the required energy by the water pump to supply driving force for the flow in the cooling plate. Heat exchangers oriented for enhancing the heat transfer normally have a sophisticated flow channel structure which has the possible best heat transfer capacity due to the largest heat transfer area with the liquid flow. For these types of heat exchangers, the pressure drop normally lies at a relatively high level. Taking the panel heat exchanger and the coiled tube-plate heat exchanger as an example, in the design of cooling plate for the TCS, considerations must be given to investigating the balance point of cooling capacity and the pressure drop. The cooling plate discussed in this paper is designed on purpose for this application to deliver the required capacity by causing as little pressure drop as possible.

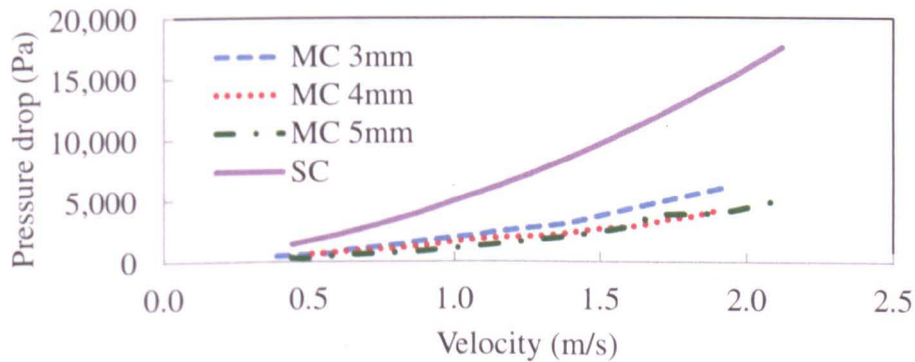


Figure 5-13 Pressure drop comparison of single channel (SC) and multi-channel (MC) cooling plates

Figure 5-13 shows the pressure drop of single channel cooling plate and multi-channel cooling plates with 3mm, 4mm and 5mm branch channel. Under the same



flow rate, the 3mm MC cooling plate shows a lower pressure drop compared to the coiled tube cold plate. The pressure drop difference becomes bigger when the velocity increases. 5mm plate shows the smallest pressure drop, with 4mm plates in the second place followed by 3mm plate. As mentioned earlier, pressure drop is not the only primary factor that evaluates the performance of cooling plate. It also needs the thermal performance to make the final conclusion. The system performance, which includes the thermal performance of cooling plate, is introduced in the following section on the basis of experimental results.

#### 5.4. System performance

The experimental rig is shown in Figure 5-14. The heat source is given by stable heat input from cartridge heaters. On the heat sink side, the heat is taken away by cooling water which dissipates the heat in the condenser. Part of the collected heat is converted into electricity and the rest could be used to preheat water for other facilities like the domestic boiler and under-floor heating. The pump can be replaced by the existing pump in the heating system. The condenser cools down the circulated water, passively or actively, for the test by dissipating the heat to the environment; the temperature could be adjusted using fan controller. This avoids wasting large amount of tap water by circulating the water in the system although some electricity is consumed when the active cooling is required.

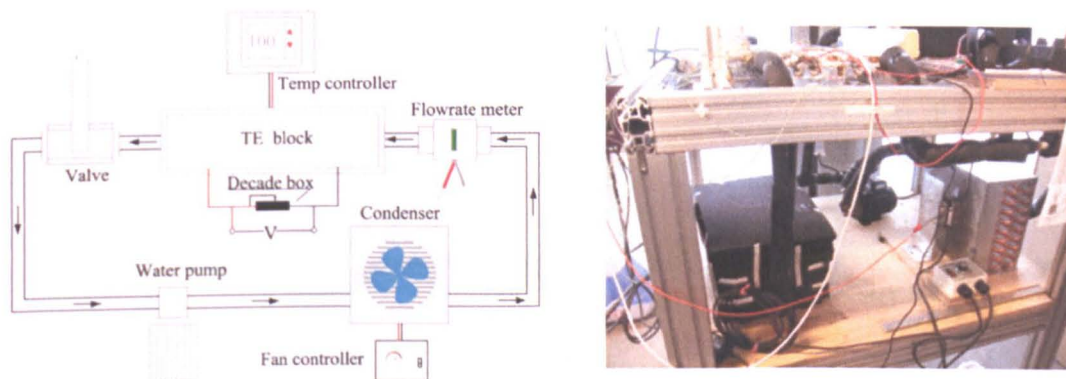


Figure 5-14 Schematic diagram of test rig

The conventional thermoelectric generation system only converts less than 5% of absorbed energy into electricity in most cases. The unconverted part, which represents over 95% of the absorbed heat, is dissipated to the environment through the heat sink without being used. This conventional thermoelectric application, showing extremely low thermal efficiency, makes the thermoelectric technologies lose its appeal in wide range of applications. The thermoelectric cogeneration system introduced in this research is designed to harvest the absorbed energy to the maximum by utilising both the converted and unconverted energy.

This goal has been achieved by using the multi-channel cooling plate designed especially for the thermoelectric cogeneration system, enabling the system to use up to 80% of absorbed energy by converting it to electrical power and recovering the unconverted energy for other purposes. The system performance has been investigated with the integration of 3mm, 4mm and 5mm cooling plates, respectively. The temperature of water that enters the cooling plates in the whole test

period is shown in Figure 5-15, which shows the water enters the cooling plates around 25°C with minor difference.

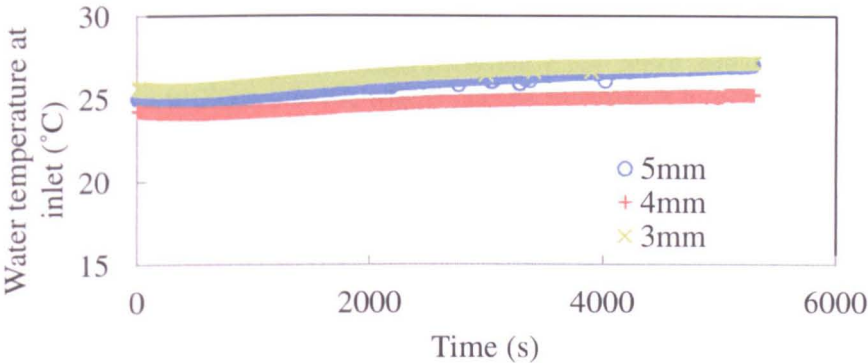


Figure 5-15 Water temperature at the inlet of three cooling plates

Figure 5-17 shows the thermal efficiency when the heat input of the system is 47W and 93W, respectively. Two cartridge heaters, rating at 100W each, are used to heat the oil in the tank at varying input. It takes a certain period of time for the system to reach a stable performance. An initial test has been carried out to measure the time that the system needs to stabilize from the beginning. As shown in Figure 5-16, the time is approximately 4800 seconds. In the experiments, each set is tested for 5400 seconds (1.5 hours) to guarantee the data accuracy.

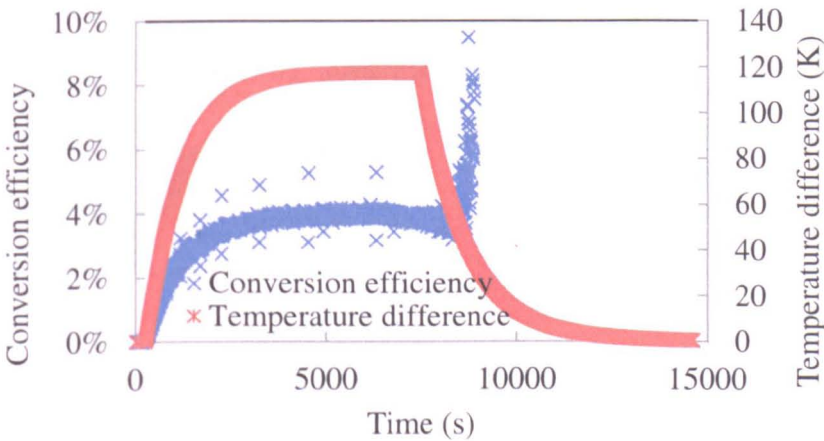


Figure 5-16 Measurement of the system stabilizing time

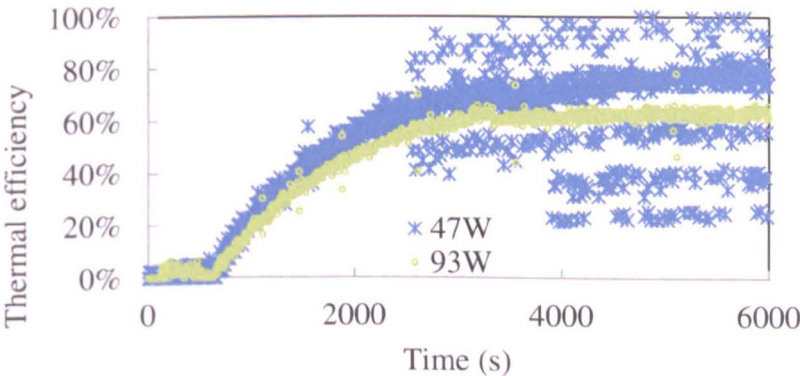


Figure 5-17 Thermal efficiency with the heat inputs at 47W and 93W vs. time

The system performances integrated with cooling plate with branch channel at 3mm, 4mm and 5mm have been tested under 93W heat input. Figure 5-18 shows the power output of cooling plates with 3mm, 4mm and 5 mm branch channel. The system cooled by the 5mm plate shows the biggest power output, with 3mm in the second place followed by 4mm. The conversion efficiency for 3mm and 5mm is almost at the same level shown in Figure 5-19, which can be explained by the slightly less heat output of 3mm plate shown in Figure 5-20. Figure 5-21 shows the 5mm plate produces the most heat output, with 4mm plate in the second place followed by 3mm plate. However, the difference in heat output of three plates is minor.

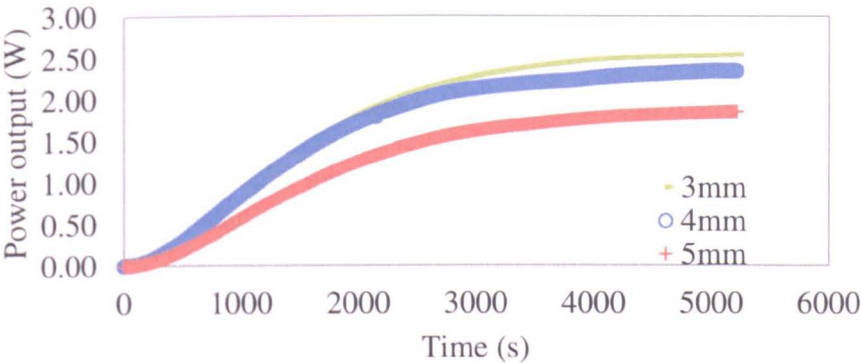


Figure 5-18 Power output of three cooling plates vs. time

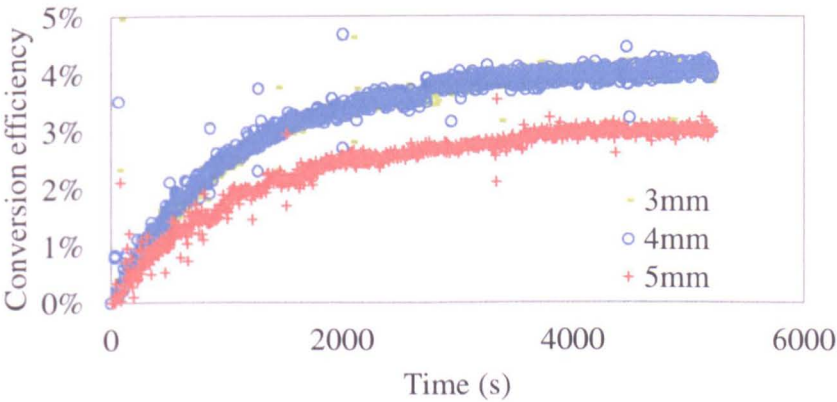


Figure 5-19 Conversion efficiency of three cooling plates vs. time

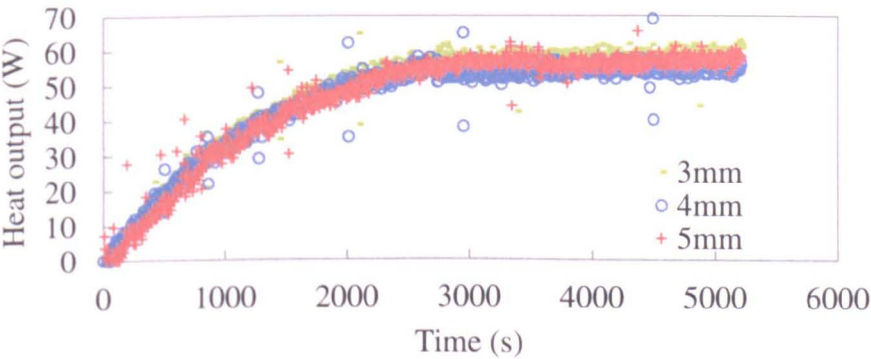


Figure 5-20 Heat output of three cooling plates vs. time



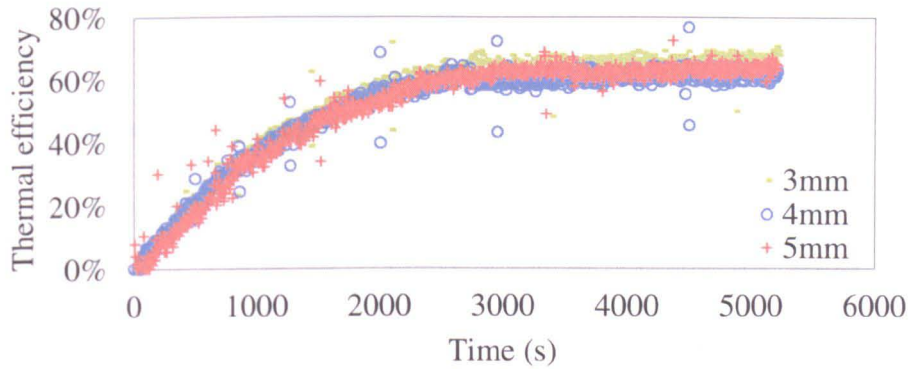


Figure 5-21 Thermal efficiency of three cooling plates vs. time

The system voltage output has been tested when the external resistance is loaded at  $1\Omega$ ,  $2\Omega$ ,  $3\Omega$ ,  $4\Omega$ ,  $5\Omega$ ,  $6\Omega$ ,  $7\Omega$ ,  $8\Omega$ ,  $9\Omega$ ,  $10\Omega$ ,  $15\Omega$ ,  $20\Omega$ ,  $25\Omega$ ,  $30\Omega$ ,  $35\Omega$  and  $40\Omega$  using decade box, respectively. Figure 5-22 shows the voltage output of the system loaded with different resistance value. This has been tested with the integration of 3mm, 4mm and 5mm cooling plate. The result of the cooling plate with 5mm branch channel shows the maximum voltage output followed by the 3mm cooling plate with 4mm cooling plate showing the smallest voltage output. This is according to the result shown in Figure 5-18. Therefore, the cooling plate with 5mm branch channel gives the best performance because it has the highest conversion efficiency and thermal efficiency but causing the least pressure drop among the three investigated cooling plates.

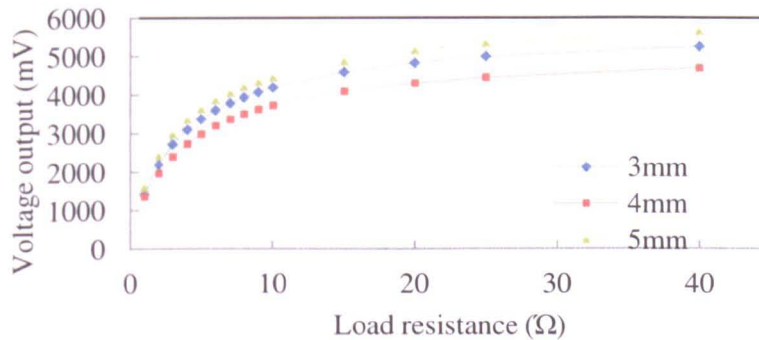


Figure 5-22 Voltage output at different load resistance of the system integrated with 3mm, 4mm and 5mm cooling plate

#### 5.4.1 Effect of coolant flow velocity

The cooling capacity needs to be investigated under different flow rate to understand the system performance in different conditions. The test has been done at different inlet flow velocity. For each velocity change, the test is run until its output stabilizes, which takes between 1-2 minutes counting from the beginning. In order to obtain accurate results, the time length for each velocity range is set at 10 minutes. The power output, heat output, conversion efficiency and thermal efficiency are shown in Figure 5-23, Figure 5-26, Figure 5-27, and Figure 5-29, respectively. An average value was calculated from the test results in each time length to represent the cooling capacity of cooling plate, the result is shown in Figure 5-26. The accuracy of the results shown below has been further proved by another set of experiment which delivers the same system performance.



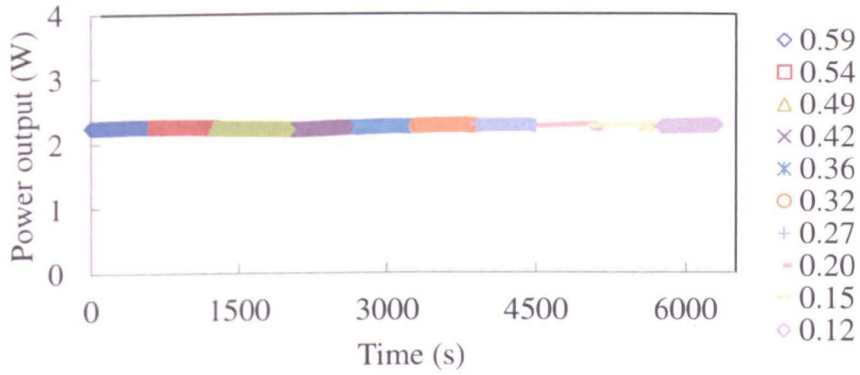


Figure 5-23 Power output at different inlet velocity (m/s)

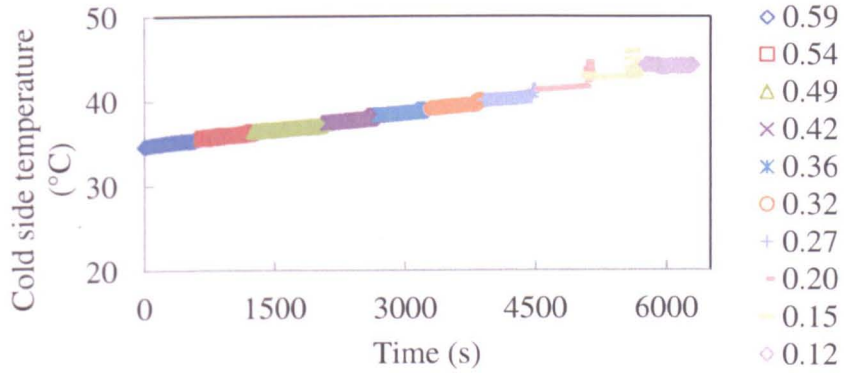


Figure 5-24 Cold side temperature at different inlet velocity (m/s)

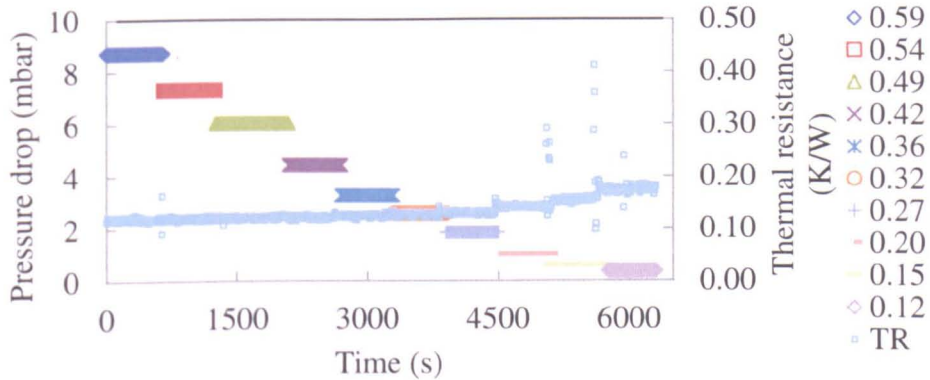


Figure 5-25 Pressure drop and thermal resistance (TR) at different inlet velocity (m/s)

Figure 5-23 shows that the system power output has hardly changed when the flow velocity at the inlet of cooling plate changes in the range of 0.12m/s-0.59m/s. The inlet velocity starts to be altered after the system stabilizes. In the experiments, the cold side temperature rises up when the inlet velocity decreases, as shown in Figure 5-24. The decreased inlet velocity increases its thermal resistance, shown in Figure 5-25. The temperature rise at the cold side of thermoelectric module leads to an increase of heat output, namely the cooling capacity, which is shown in Figure 5-26. For the cooling plate, the heat transfer model can be described by:

$$\Delta T_{cp} = R_{cp} Q_{output} \quad (5-3)$$

Where,  $\Delta T_{cp}$  is the temperature difference between cooling water and the module cold side;  $R_{cp}$  is the thermal resistance of the cooling plate on the module side;  $Q_{output}$  is the cooling capacity.

As shown in Figure 5-25,  $R_{cp}$  stays at a stable level when the inlet velocity decreases until it reaches 0.32m/s at which point  $R_{cp}$  starts rising up. According to Eq.(5-3), the temperature difference  $\Delta T_{cp}$  increases when the inlet water velocity slows down. This explains the temperature rise shown in Figure 5-24 when the velocity decreases because the temperature of inlet water is constant.

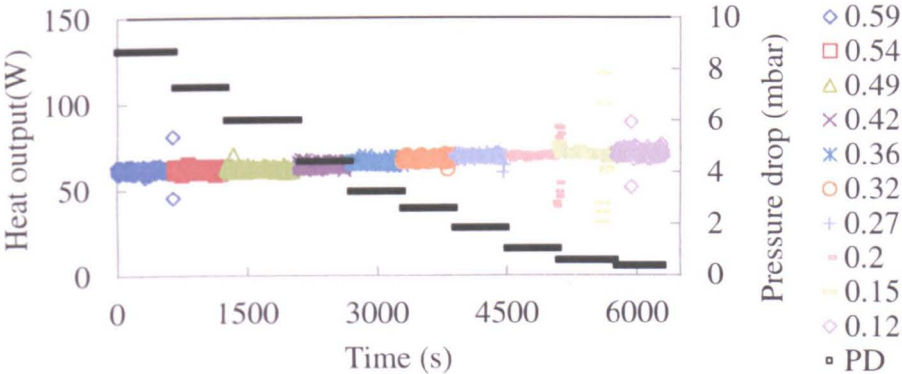


Figure 5-26 Heat output and pressure drop vs. Inlet velocity (m/s) (PD represents pressure drop)

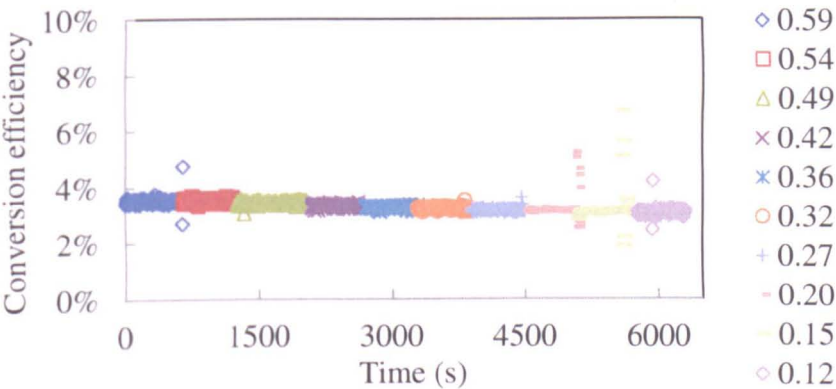


Figure 5-27 Conversion efficiency at different inlet velocity (m/s)

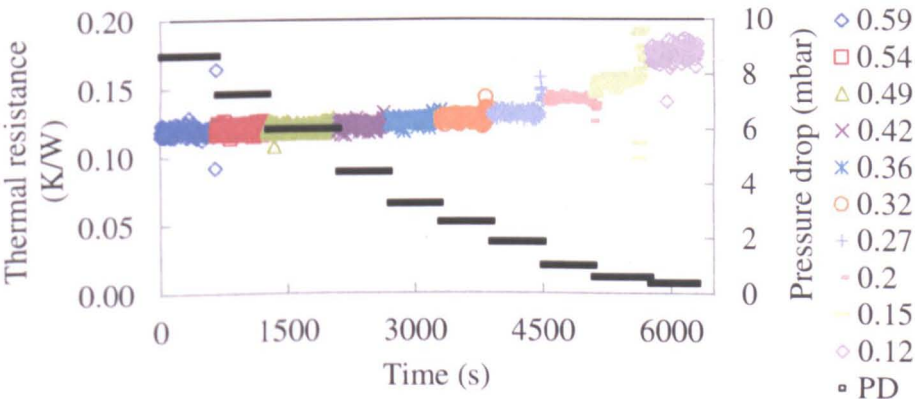


Figure 5-28 Thermal resistance at different water velocity (m/s)

The thermal efficiency defined as the ratio of the sum of power output and heat output to the energy absorbed by hot side heat exchanger, increases with the decreasing inlet velocity, shown in Figure 5-29. However, the conversion efficiency, defined as the ratio of power output to the sum of power output and heat output, shows the opposite trend in a slight way, shown in Figure 5-27.

Therefore, we can come to two conclusions according to the experimental results provided the system heat input stays constant. First, the inlet velocity doesn't significantly impact the system power output. However, the conversion efficiency slightly goes down when inlet water velocity decreases.

Second, the system heat output is increased by the decrease of the inlet velocity. This change can be explained by Eq.(5-4):

$$Q_{output} = cAv(T_{outlet} - T_{inlet}) \quad (5-4)$$

Where  $c$  is the specific heat capacity of water,  $A$  is the cross section area of cooling plate inlet,  $v$  is the inlet velocity,  $T_{outlet}$  and  $T_{inlet}$  are the inlet and outlet water temperature, respectively. When  $v$  decreases,  $T_{outlet}$  increases. However, as shown in Figure 5-26, the heat output increases due to the influence from temperature rise ( $T_{outlet} - T_{inlet}$ ) which is bigger than that caused by the velocity decrease, with a consequence of increased thermal efficiency.

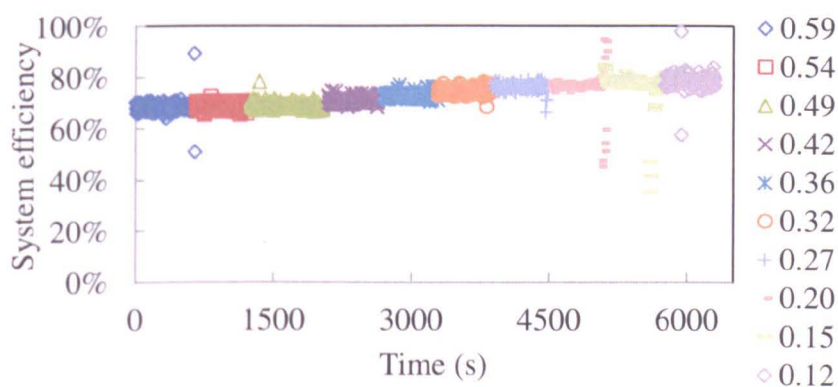


Figure 5-29 Thermal efficiency at different inlet velocity

Figure 5-29 shows that the thermal efficiency goes up more significantly when it operates at the inlet velocity range of 0.12-0.27m/s, in which the pressure drop lies in the range of 0-2.9mbar. Based on the discussion, the economic operating zone lies in 0.12-0.27m/s where the system gives higher thermal efficiency whilst the power output stays at the same level within the higher range of flow rate. However, the optimum inlet velocity is eventually determined by the combination of the system architecture and the hydraulic conditions in real applications. Considerations must be taken on identifying the flow rate in the hydraulic system which the thermoelectric application is integrated in. Taking the domestic boiler as an example, the boiler needs a nominal flow rate of water feed when it supplies hot water to the heating system and hot water user ends. In this situation, the designed cooling block needs to be oriented for the required flow rate to make sure the normal operation of the boiler while delivering the designed performance. It leads to the demand of a suitable design of cooling block for the thermoelectric application, which is going to be introduced in the part of flexible design of cooling system.



5.4.2 Effect of cooling temperature

As shown in the previous analysis, the cooling capacity of cooling plate stays at a fairly stable level except a slight fluctuation when the flow rate changes. Hence, the change of inlet water temperature has the potential of affecting the system performance by varying the temperature of cold side surface of thermoelectric module. The test has been carried out to understand the exact impact.

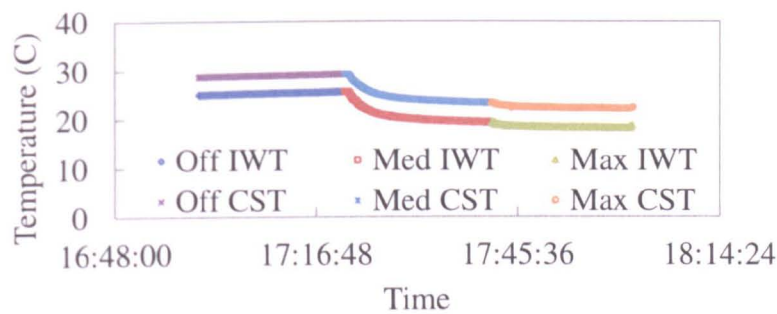


Figure 5-30 Temperature of inlet water (IWT) and TE cold side (CST) against fan operation

Where , “Off”, “Med” and “Max” means the conditions of “fan off”, “Medium fan speed” and “Maximum fan speed”, respectively. This applies to Figure 5-32 and Figure 5-33.

The inlet water temperature is adjusted by changing the fan speed of a condenser which dissipates the heat into the ambient air. Three cooling levels were investigated by adjusting the fan speed to achieve different inlet water temperature while the system is operating with a 47W heat input. The temperature of inlet water and the module cold side surface were measured under three different condenser operating conditions: fan off, medium fan speed and maximum fan speed. The result is shown in Figure 5-30.

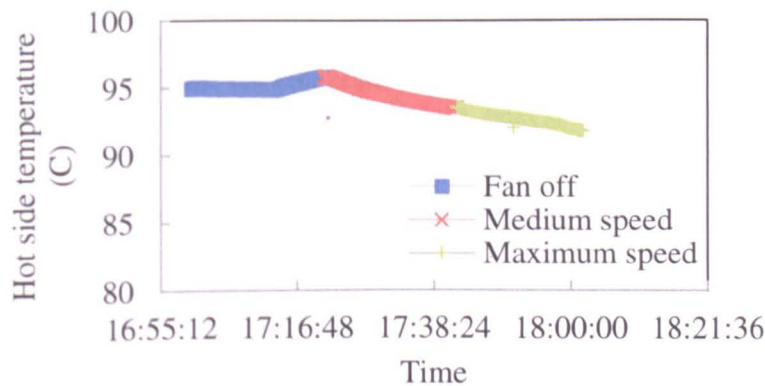


Figure 5-31 Temperature of TE hot side under different cooling conditions

The inlet water temperature decreases when the fan speed increases, which also leads to a decrease in the temperature of cold side surface. Meanwhile, the temperature of hot side surface doesn't show an obvious influence from the cooling condition despite a slight downward tilt, shown in Figure 5-31. These results obtain a positive impact on power output which, different from the opposite influence caused by the temperature rise, increases when water enters the cooling plate at a lower temperature. However, the conversion efficiency doesn't show a rising trend when



the inlet water temperature decreases. The reason can be explained by the increased heat output caused by the temperature drop of inlet water.

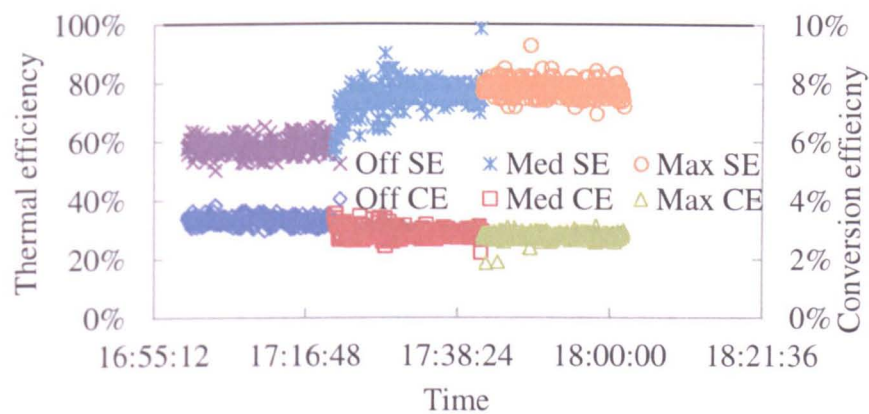


Figure 5-32 Thermal efficiency (SE) and conversion efficiency (CE) vs. Fan operation

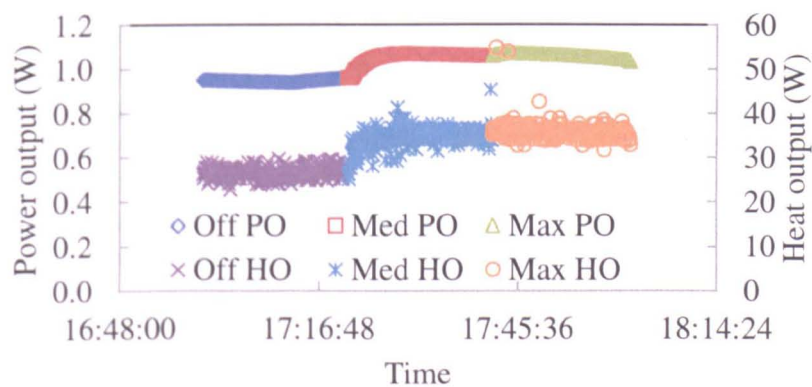


Figure 5-33 Power output (PO) and heat output (HO) vs. Fan condition

In conclusion, the temperature decline of inlet water enhances the thermal efficiency by enlarging the system heat output. The power output is slightly increased. The reason why the conversion efficiency showed a decrease is because the increase of heat output enlarges the base for calculating conversion efficiency. However, it can be concluded that a lower cooling temperature gets a better system performance when other conditions stay the same.

5.4.3 Dynamic thermal response of the system

The use of a heat transfer fluid to recover heat from a waste heat source and channel it to the thermoelectric hot plate introduces further design challenges in minimising the thermal inertia of the system. The time required to heat the fluid (heat transfer oil) in the TE module hot plate heat exchanger to the designed temperature can be determined by Eq.(3-4).

The temperature of heat transfer oil was measured for a heat exchanger storage capacity of 144ml and at the design condition of a 100W heat input, the dynamic response of the system is shown in Figure 5-34.

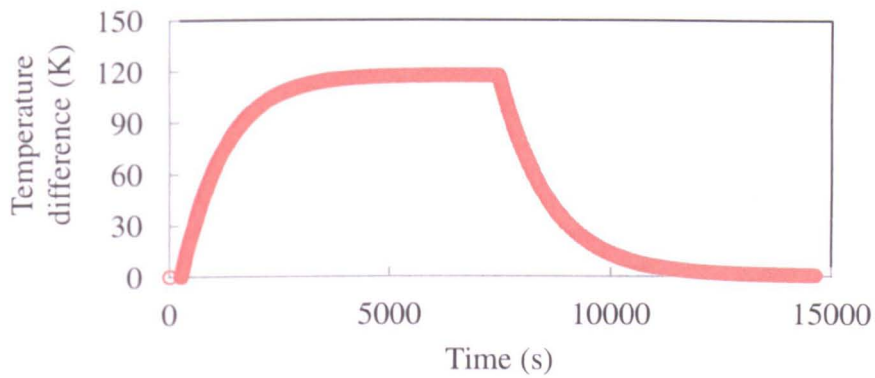


Figure 5-34 Dynamic thermal response of the system

Figure 5-34 shows that when the oil is heated from ambient temperature it takes approximately 3000s to reach steady state temperature of 120°C. This represents a time constant of the system to reach the steady state thermal condition; it is desirable to have a fast response system. However, in applications for exploitation of renewable energy sources, energy storages capability could present a potential advantage. The thermal response of the system after the removal of the heat source is shown in Figure 5-35. It can be seen that during the cooling down of the stored oil the system still works, though the power output would be limited by the voltage output level. Removing the effect of voltage level, the total power output generated during the cooling phase amounts to 1.7Wh and is given by the sum of shaded area of green and red. The total heat output produced during the cooling phase amounts to 10.2Wh and is given by the shaded area of red colour.

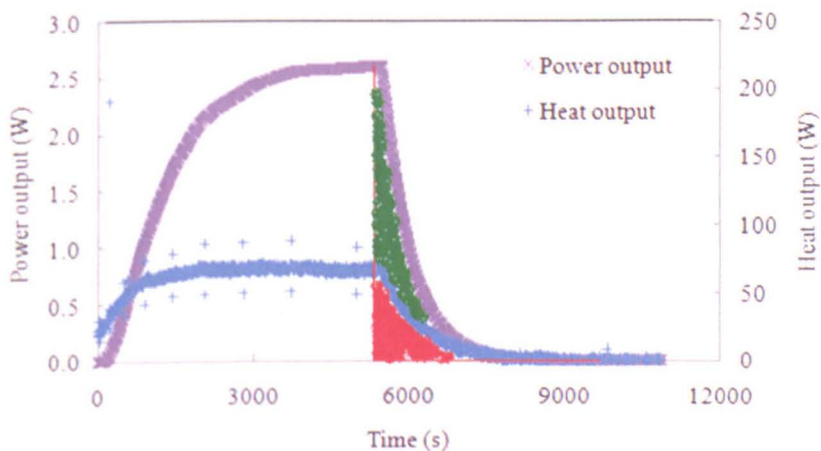


Figure 5-35 Power output and heat output in a test cycle

This system, with 144ml heat transfer oil storage, is able to generate electricity for 2700s (0.75hour) when the heat input (100W) is cut off. This test has been repeated with the input at 53W, 80W, 100W and 133W to understand the relation between storing time and intensity of heat input.

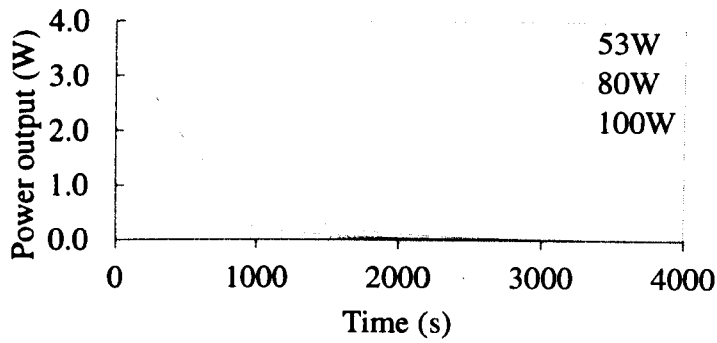


Figure 5-36 Storing performance at 53W, 80W, 100W and 133W heat input

Results are shown in Figure 5-36. The length of working time after the heat input is cut off is not significantly affected by the strength of heat input. The declining rate of power output after the heat input is cut off is proportional to the original heat input. More details are shown in Table 5-1.

Table 5-1 Power output after heat input is cut off from 53W, 80W, 100W and 133W

Heat input (W)	Power output	R <sup>2</sup>
53	$P=0.7674\omega e^{-0.002t}$	0.9995
80	$P=1.3984\omega e^{-0.002t}$	0.9995
100	$P=2.6018\omega e^{-0.002t}$	0.9993
133	$P=4.2006\omega e^{-0.002t}$	0.9993

The correlation between power output and the operating time can be described by Eq.(5-5):

$$P=\omega \times e^{-0.002 t} \quad (5-5)$$

Where P is the power output, t is the time counted from when the heat input is off, and S is the heat storing factor which describes the energy level stored in the system. It can be expressed by Eq.(5-6):

$$\omega=\frac{P}{e^{-0.002 t}} \quad (5-6)$$

According to the experimental results, the relation between heat storing factor and heat input can be shown by Figure 5-37. It shows that the storing coefficient S is determined by the original heat input. The stronger the heat input, the larger value S has, which also means more power output is given by the system after the heat input is cut off.

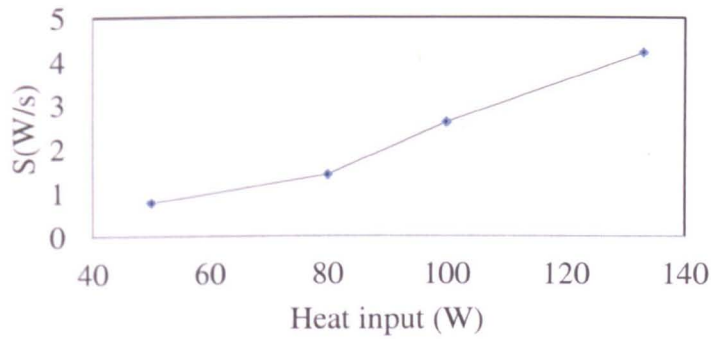


Figure 5-37 Correlation between heat input and heat storing coefficient

## 5.5. Further modifications based on CFD

### 5.5.1 Individual assembly

#### 5.5.1.1 Mathematical model

The mathematical model comprises of two parts: heat transfer and fluid dynamics. The heat transfer occurs from the cold side surface of the module, through solid part of cooling plate and the interface of cooling plate and finally to the fluid flow in the cooling plate (here water is used). The cooling plate, made of aluminium, is assumed to have isotropic thermal conductivity. The cooling water is assumed to be incompressible Newtonian flow due to the small change in pressure. The simulations have been conducted on the basis of overlapped area of module surface and cooling plate. The problem schematic is shown in Figure 5-38.

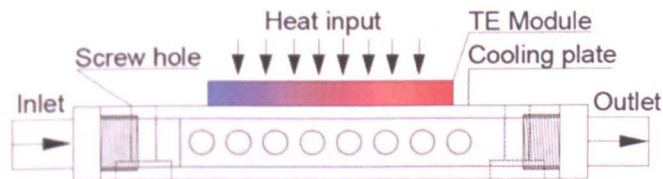


Figure 5-38 Problem schematic of cooling plate on the module cold side

In the numerical investigations, considering the compatibility with thermoelectric applications, the single channelled cooling plate, which is one of the common heat exchanger structures on market, is chosen as the reference for analyzing and evaluating the oriented cooling design by comparing the thermal and hydraulic performance using numerical investigations. The thermoelectric cogeneration block consists of three parts, a cooling plate, an oil tank and a thermoelectric generator. As previously mentioned, the thermoelectric module is sandwiched between the cooling plate and the oil tank by four stainless screws. A flat metal washer, a crinkle washer and a fibre washer are placed between the screw and the cooling plate. The crinkle washer and the fibre washer play the roles of accommodating thermal expansion and thermally insulating the unintended heat conducting path, respectively. A groove has been made on the cooling plate and oil tank for the installation of thermocouple to measure the temperatures at the hot side and cold side of thermoelectric module.

### Governing equations

For the solid part, the model of heat transfer addresses heat conduction, the governing equation is described by Eq.(5-7):



$$k_{Al} \nabla^2 T = 0 \quad (5-7)$$

Where  $k_{Al}$  is the thermal conductivity of aluminium;  $T$  is the temperature.

In the flow channel, considerations are given to water flow and convective heat transfer. The conservation of mass, momentum and energy are given by Eq.(5-8), Eq.(5-9) and Eq.(5-10), respectively.

$$\nabla(\rho v) = 0 \quad (5-8)$$

$$\nabla(\rho v \otimes v) = -\nabla p + \nabla \cdot [\mu_w (\nabla v + (\nabla v)^T)] \quad (5-9)$$

$$\rho c_{p,w} v \nabla T = k_w \nabla^2 T \quad (5-10)$$

Where  $\rho$  is the water density,  $u$  is the flow velocity,  $p$  is the pressure,  $\mu_w$ ,  $c_{p,w}$  and  $k_w$  is the dynamic viscosity, specific heat and thermal conductivity of water, respectively.

### Boundary conditions

Inlet: the mass flow rate and temperature of inlet were given according to the experimental result.

$$T = T_{inlet}, \quad v = v_{in} \quad (5-11)$$

Outlet: The outlet is described as outflow which is obeyed in fully-developed flows where the diffusion flux for all flow variables in the exit direction are zero;

Heated surface: the hot side surface of thermoelectric module has been given the temperature value,  $T_1 = 166.9^\circ C$ , and the thermal conductivity  $\lambda_{TE} = 1.0 W / mK$ , which were both derived from the experimental results.

Flow channel/cooling plate interface: The thermal conditions for the interface is set as “coupled” for conjugate heat transfer.

$$v = 0 \quad (5-12)$$

Conventionally, the heat transfer coefficient is used as the key guiding parameter to characterize the performance of heat exchanger. This is suitable for the applications where the heat exchanger capacity is essential to the performance of the whole system, such as computer processors and electrical chipsets that dissipate large amount of heat and their normal operations rely on effective cooling. Therefore, effective heat transfer is taken as the primary consideration, whilst the pressure drop is not used as the major parameter that describes the system performance.

However, in this research study, apart from thermal performance, the hydraulic performance also needs to be taken into account in the evaluation of overall performance of heat exchanger. The reason lies in the need of considering the power consumption caused by the pressure drop.

The thermal performance of heat exchanger must be weighed against the energy required to operate the system, which would be the pumping power if the increased pressure drop needs to be offset by the water pump. The required pumping power due to the increased pressure loss caused by the use of the cooling plate can be calculated by Eq.(5-13):

$$W_{cp} = \Delta P_{cp} G / \eta_p \quad (5-13)$$

Where,  $\Delta P_{cp}$  is the pressure drop across the cooling plat,  $G$  is the volumetric flow rate of the fluid passing through the heat exchanger,  $\eta_p$  is the overall pump efficiency. Generally, the pump efficiency varies with the flow rate. The water pump is assumed to operate at a steady flow rate with overall efficiency at 60%.

To comprehensively evaluate the performance of a heat exchanger, the Colburn factor ( $j$ ) is used against the Reynolds number ( $Re$ ) [157]. The Colburn  $j$  factor characterizes the heat transfer performance based on the measured convection coefficient and the necessary velocity of the coolant in order to achieve the corresponding convection coefficient. It has become one of the standard methods for reporting the performance of heat exchangers. It is described by Eq.(5-14).

$$j = \frac{h_{cp}}{\rho c v} \left( \frac{v}{\alpha} \right)^{2/3} \quad (5-14)$$

Where,  $h_{cp}$ ,  $\rho$ ,  $c$ ,  $v$ ,  $\nu$  and  $\alpha$  are the heat transfer coefficient of cooling plate, density, specific heat capacity, velocity, kinematic viscosity and thermal diffusivity of water.

### Local resistance coefficient

Due to the irregular structure of flow channel in the cooling plates, it is difficult to characterize the hydraulic characteristics of cooling plate by Fanning friction factor. Instead, the cooling plate is treated as a “black block” that causes local resistance loss. The local resistance coefficient  $\zeta$  is used to characterize the hydraulic characteristics of the cooling plate. It can be described by

$$\zeta = \frac{2\Delta P_{cp}}{\rho v^2} \quad (5-15)$$

Where  $\Delta P_{cp}$  is the pressure drop when the fluid passes through the cooling plate at velocity  $v$ ;  $\rho$  is the water density;

#### 5.5.1.2 Physical model

The initial concept of cooling plate for thermoelectric cogeneration has been developed and the performance has been verified in showing its advantage over the

cooling plates with the traditional design. In order to fully modify the current concept, the modification job includes the following three major tasks:

1. For a fixed amount of branch channels, finding out the relation between  $r_{cp}$  (the ratio of cross section area of branch channel to that of main channel) and the performance of the cooling plate in this thermoelectric cogeneration system.
2. For a fixed branch channel dimension, finding out the relation between the quantity of branch channel and the performance of the cooling plates.
3. When the diameter and quantity of branch channel is fixed, finding out how the angle of branch channel with the main channel affects the performance.

The physical models of investigated models are shown in Figure 5-39.

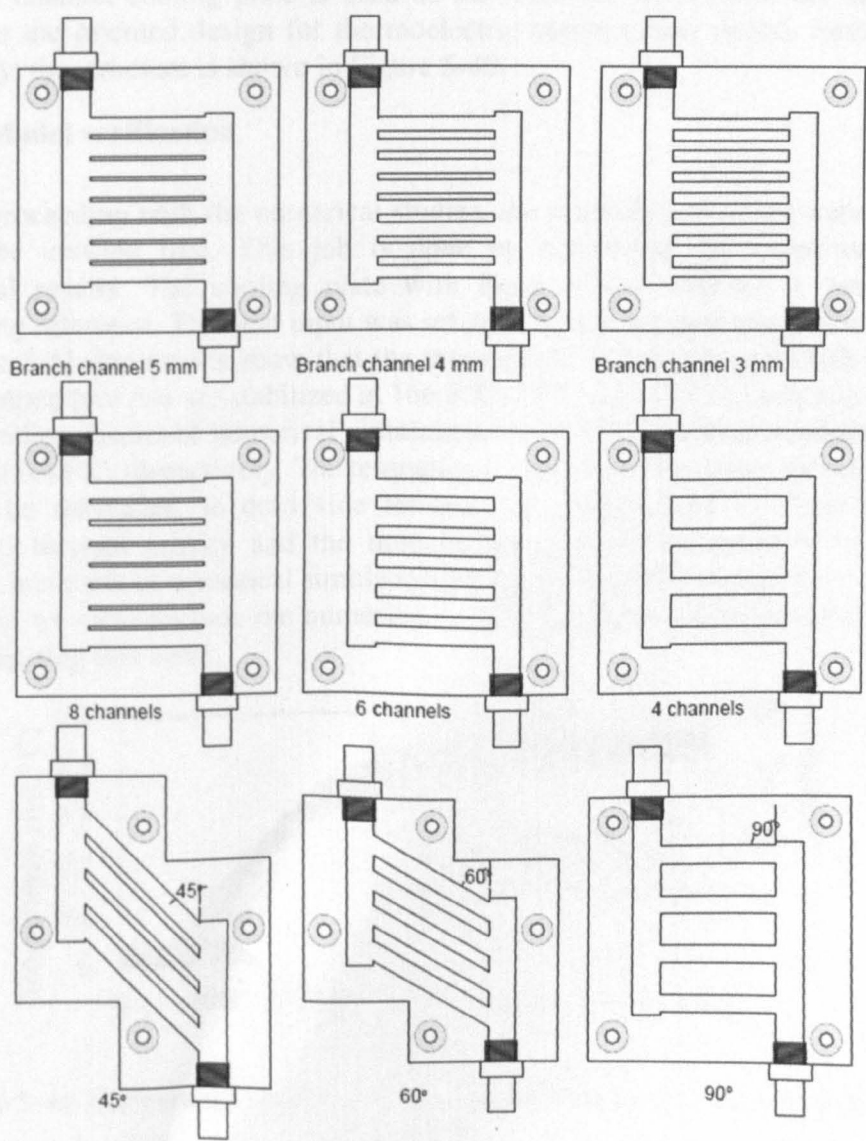


Figure 5-39 Physical models of investigated multi-channel cooling plates

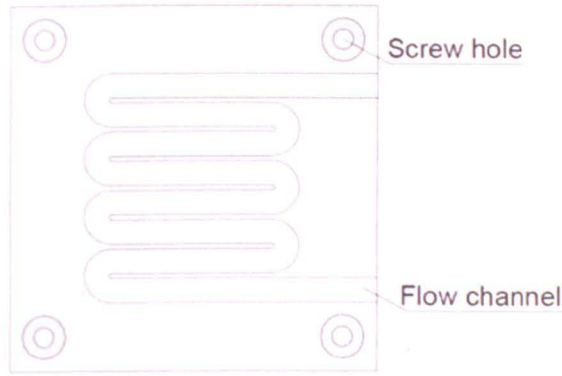


Figure 5-40 Single channel cooling plate

A single channel cooling plate is used as the reference to evaluate the advantages shown in the oriented design for thermoelectric cogeneration system introduced in this study; the structure is shown in Figure 5-40.

### 5.5.1.3 Model verification

Before proceeding with the numerical studies, the reliability of mathematical model should be verified first. This job is done by comparing the experimental and numerical results. The cooling plate with 5mm branch channel is used as the comparing reference. The heat input was set at 93W and the performance was tested. In Figure 5-41, the results show that the temperature of hot side, cold side and inlet water temperature rise are stabilized at 166.8°C, 34°C and 0.435°C, respectively. The corresponding results of numerical simulations show the according results at 165°C, 38°C and 0.44°C, respectively. The temperature rise in cooling water shows the same result. The derivation in cold side temperature is estimated to come from the converted thermal energy and the non-consideration of the effect from thermal interface materials in numerical simulations, which is used in the experimental study. Therefore, we can conclude the numerical simulation shows the reasonable accuracy in investigating this issue.

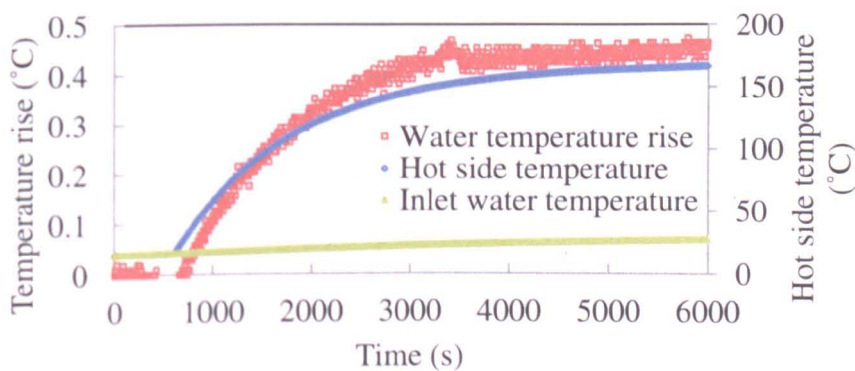
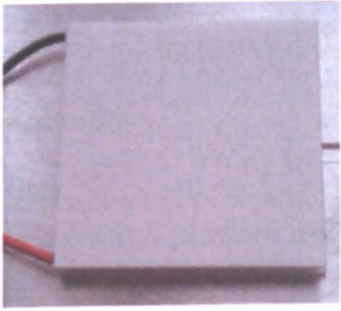


Figure 5-41 Temperature result of multi-channel cooling plate attached with the module

The specifications of the module used in the test can be referred in Table 5-2.



Table 5-2 Specifications of the thermoelectric generators

	Specifications
	Material: Bismuth telluride
	Dimensions: $l \times w \times t = 40\text{mm} \times 40\text{mm} \times 4\text{mm}$
	Couple pairs: 127
	Maximum operating temperature : $250^{\circ}\text{C}$

Here the parameters  $l$  and  $k$  are given by Table 5-2. The thermal resistance  $R_m$  can be calculated by the experimental data using Eq.(5-16).

$$R_m = (T_1 - T_2) / Q_{output} \tag{5-16}$$

In the experiment, the cold side temperature  $T_c$  and hot side temperature  $T_h$  have been measured by two separate thermocouples which are installed in the slots carved in the hot side and cold side heat exchangers to make sure the module surfaces are well contacted with heat exchangers, shown in Figure 5-42.



Figure 5-42 Slots on the heat exchangers for the thermocouples (left to right: hot side, cold side)

In the corresponding numerical simulation, the value of thermal conductivity of TE module is set the same with the result obtained from the test, shown in Figure 5-43. The average value of thermal conductivity is  $1.0\text{W/mK}$ . The hot side temperature is initialised by inputting the same value as experimental result,  $166.9^{\circ}\text{C}$ .

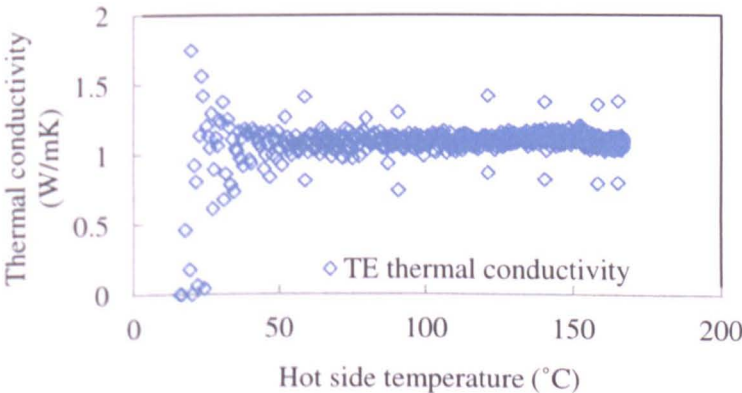


Figure 5-43 The experimental result of TE module thermal conductivity

The deviation of temperature rise between the simulation result and experiment result is acceptable in this study. Hence, using CFD to study the hydraulic and thermal performance of the cooling plate and modify the physical models is a feasible approach for conducting many scenarios in a cost-saving and efficient way.

5.5.1.4 Results

The results of numerical simulation of the single channel cooling plate, including the cooling capacity, pressure drop, outlet temperature, TE cold side temperature and surface heat transfer coefficient of flow channel wall, are shown in Figure 5-44 and Figure 5-45.

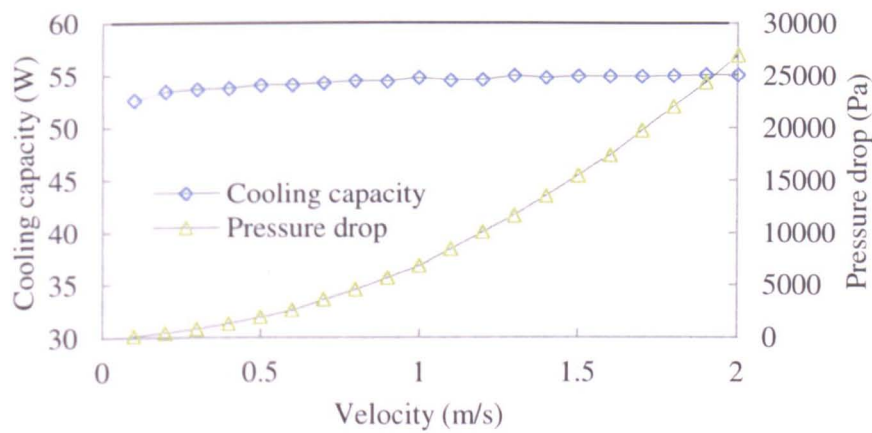


Figure 5-44 Cooling capacity and pressure drop of single channel cooling plate

Figure 5-44 shows the pressure drop increases rapidly alongside the increase of flow velocity whilst the cooling capacity generally shows a steady state. It means that the cooling capacity is not significantly influenced by the flow rate in the cooling plate, whilst the level of pressure drop is affected significantly. Hence, the optimal operating condition is suited for the small flow rate whilst meeting the need of feed water volume by the domestic boiler.

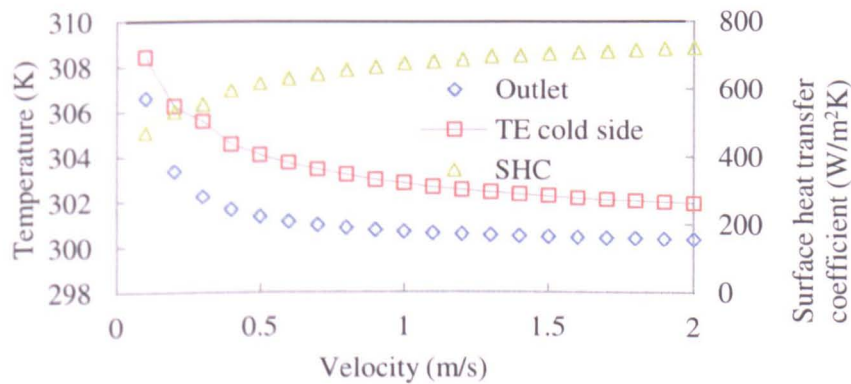


Figure 5-45 Surface heat transfer coefficient (SHC) of flow channel, temperature at outlet and TE cold side surface

Figure 5-45 shows the surface heat transfer coefficient increases when the flow velocity increases in the range of 0.1m/s-2.0m/s. It shows more rapid increase between 0.1m/s-0.5m/s (Re: 615-3076), compared to the range of 0.5m/s-2.0m/s (Re:

3076-12307). The velocity increase in laminar and transient flow enhances the heat transfer more than in turbulent flow.

The outlet water temperature, TE cold side surface temperature and pressure drop are shown in Figure 5-45 under different water flow velocity (0.1m/s-2.0m/s). When the flow velocity increases, the temperature of outlet water and TE cold side surface goes through an abrupt decline between 0.1m/s-0.5m/s (Re: 615-3076) and then gradually comes to a comparatively steady state 0.5m/s-2.0m/s (Re: 3076-12307), whereas the pressure drop increases rapidly in the whole range.

### Branch channel diameter

The cooling plates with three different branch channel dimensions are shown in Figure 5-39, with 3mm, 4mm, and 5mm circular branch channel, which were chosen according to the ratio of the cross section area of main channel to the sum of cross section area of the branch channels. The starting dimension of 3mm is fixed by summing the cross section area of the branch channels equal to that of main channel. In this circumstance, theoretically the water flow from the main channel can all be bypassed into branch channels without detention. With the same amount of branch channel, cooling plates with the diameter at 4mm and 5mm are chosen to be fabricated to thermally and hydraulically compare with 3mm considering the necessity of bigger heat exchange area for a better thermal performance. Smaller dimensions are not studied because of smaller surface area of flow channel and bigger local pressure loss.

For the cooling plate, the flow resistance coefficient is determined by the ratio  $r_{cp}$  of cross section area of branch channels to that of main channel. Assuming the diameter of main channel and branch channel are denoted as  $d_m$  and  $d_b$ , respectively. The ratio  $r_{cp}$  can be described by Eq.(5-17):

$$r_{cp} = \frac{nd_b^2}{d_m^2} \quad (5-17)$$

Where, 3mm:  $r_{cp} = 1.12$  ; 4mm:  $r_{cp} = 2$  ; 5mm:  $r_{cp} = 3.13$  ;  $n$  is the quantity of branch channel.

The correlation between  $r_{cp}$  and the flow resistance of the cooling plates with three different branch channel dimensions is investigated using CFD. Domain and corresponding meshing of cooling plate with 3mm branch channel is shown in Figure 5-46. It applies to cooling plates with 4mm and 5mm branch channel. Individual meshing has been adopted in each parts of the domain. Finer meshing has been used in the junctions to obtain accurate results.



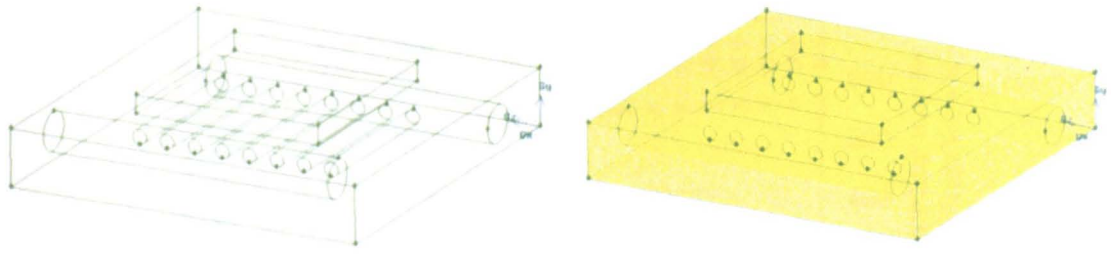


Figure 5-46 Schematic diagram of computing domain and meshing of cooling plate

According to the current design, the results from the experimental tests and numerical simulations show a good performance from this oriented-design for the domestic application. The modification of cooling plate is based on the change of the branch channel size which determines the hydraulic performance and consequently the thermal performance when used as a cooling plate to extract heat from the cold side of TE module.

Figure 5-47 shows the pressure drop of cooling plate with 3mm branch channel at different flow rate in comparison with the aforementioned single channel cooling plate. The pressure drop of multi-channel cooling plate is lower than single channel cooling plate in the whole range of investigated velocity (0-2m/s). At 2m/s, the pressure drop caused by multi-channel cooling plate is only 21% of that caused by the single channel cooling plate.

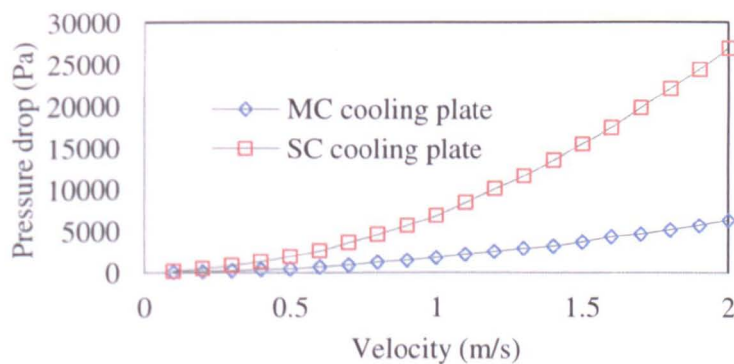


Figure 5-47 Pressure drop against velocity of cooling water of single channel cooling plate

The surface heat transfer coefficient of multi-channel cooling plate is bigger (15%-45%) than that of single channel cooling plate, shown in Figure 5-48. The cooling capacity of multi-channel cooling plate is 8%-10% bigger than single channel cooling plate.

The results above tell us that achieving the similar level of heat transfer rate, the single channel cooling plate loses much more pressure than the multi-channel cooling plate does. The conclusion can be made that the multi-channel cooling design shows a much better performance by giving bigger value of heat transfer coefficient and delivering bigger cooling capacity while consuming much less pressure head.



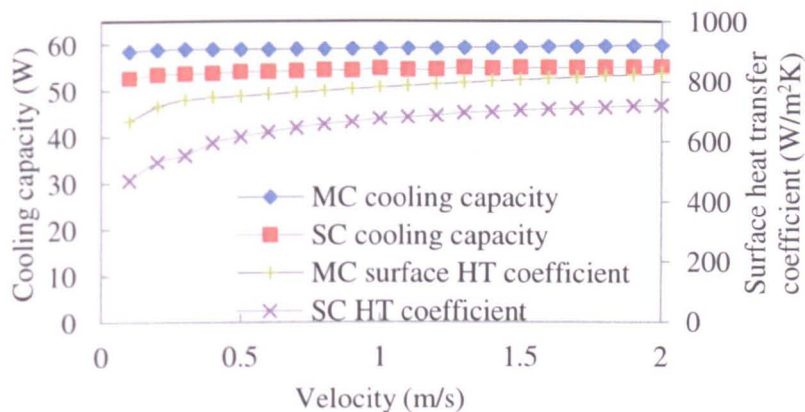


Figure 5-48 Cooling capacity and Surface heat transfer coefficient against velocity of cooling water (SC vs. MC)

Figure 5-49 shows the velocity distribution in flow channel of cooling plates with 3mm, 4mm and 5mm branch channels. It demonstrates that the flow rate of 3mm cooling plate is the most evenly distributed in each branch channel, although the water flow tends to flow into the ports near the inlet. This is more obvious in 4mm and the most obvious in 5mm cooling plate. The water in the branch channels near to the outlet stays for longer than that in branch channels near to the inlet of cooling plate. We can thus conclude that the smaller value of  $r_{cp}$  gives a more even distribution of water flow in each branch channel.

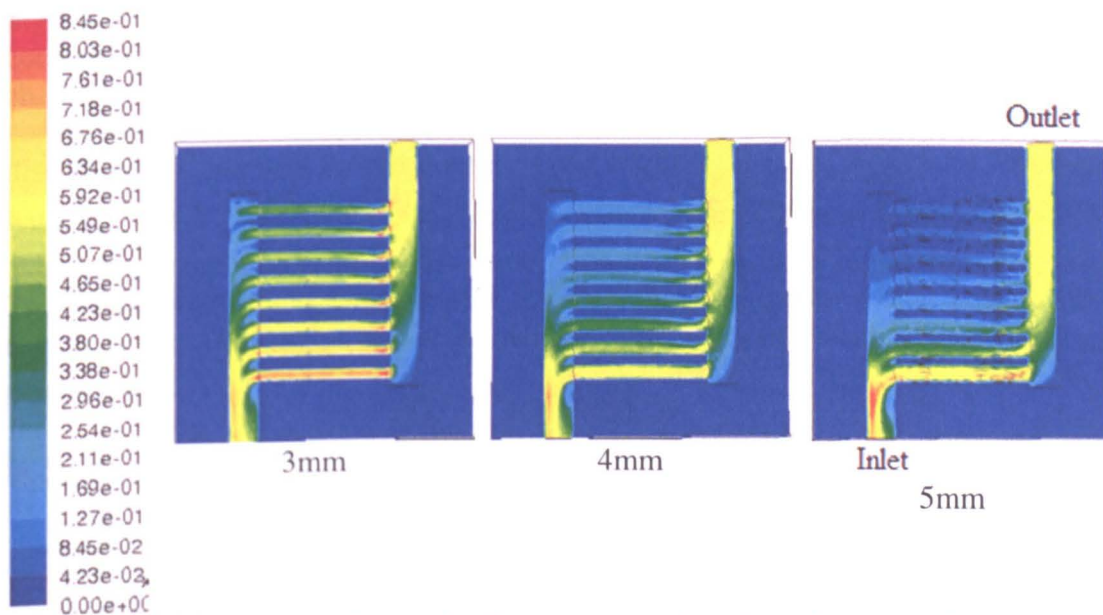


Figure 5-49 Velocity distribution in flow channel of cooling plates with 5mm, 4mm and 3mm branch channel

Figure 5-50 shows the pressure drop of each cooling plate under different flow velocity in comparison with the experimental results. The cooling plate with 3mm branch channel has the largest pressure drop of them all, followed by the cooling plates with 4mm and 5mm branch channel (3mm:  $r_{cp} = 1.12$  ; 4mm:  $r_{cp} = 2.0$  ; 5mm:  $r_{cp} = 3.13$  ).

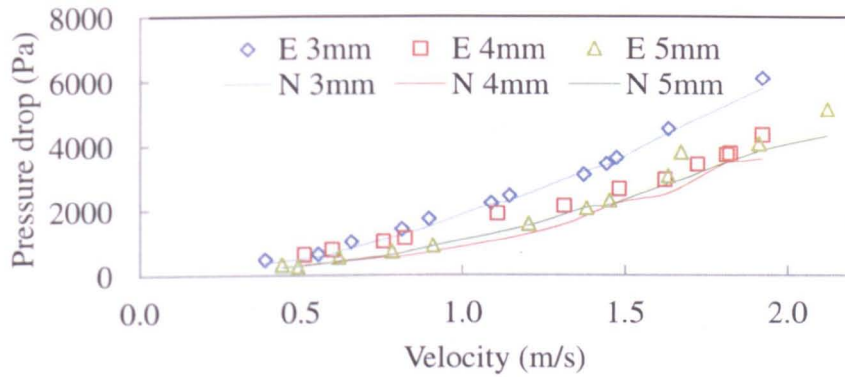


Figure 5-50 Pressure drop of cooling plates with different branch channel dimensions in comparison with experimental result

A consistence is shown in the pressure drop value of experimental result and numerical result, although some discrepancy is shown for the one with 4mm branch channel at 1.2m/s. (E and N represent experimental and numerical data, respectively)

Figure 5-51 and Figure 5-52 show the temperature at the cold side surface of TE generator and central horizontal cross section of cooling plate, respectively. It can be seen that the 5mm cooling plate gives the highest temperature at the cold side of TE generator, followed by 3mm and 4mm, whose temperature level are at the similar level indicated by the temperature band. For the temperature distribution at the central horizontal cross section of cooling plate, the 5mm cooling plate has the highest value of temperature with the temperature built up at the top left corner of cooling plate. This is caused by the uneven flow rate distribution among each branch channel. The cooling plates with 3mm and 4 mm branch channels have comparatively better temperature distribution due to the aforementioned even flow distribution. Compared to the cooling plates with  $r_{cp} = 2$  and  $r_{cp} = 3.13$ , the one with  $r_{cp} = 1.12$  gives more even flow distribution among branch channel which avoids the thermal built up in the corner. However, it shows a bigger pressure loss. The influence of uneven temperature distribution to the power output needs to be further investigated so as to decide which  $r_{cp}$  gives cooling plate a better overall performance.

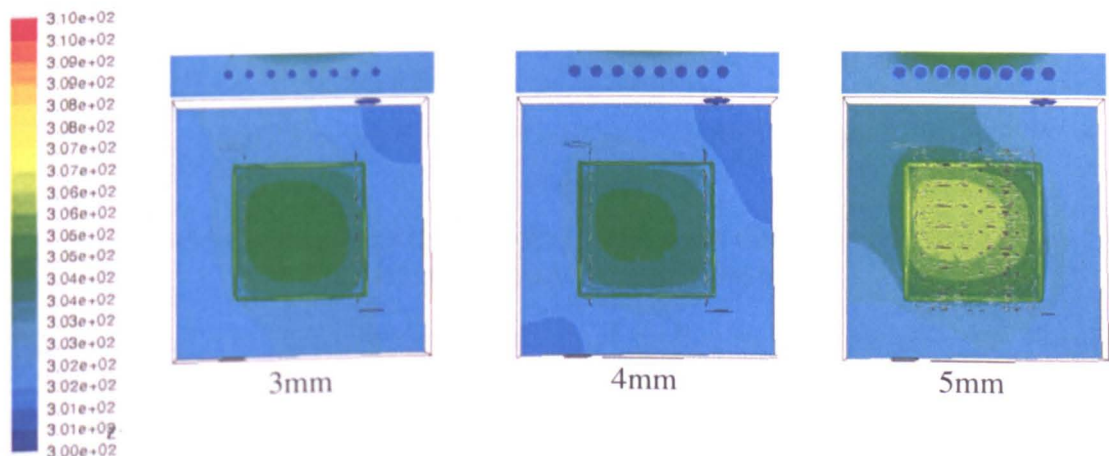


Figure 5-51 Temperature distribution on cold side surface of TE module attached with 5mm, 4mm and 3mm cooling plates



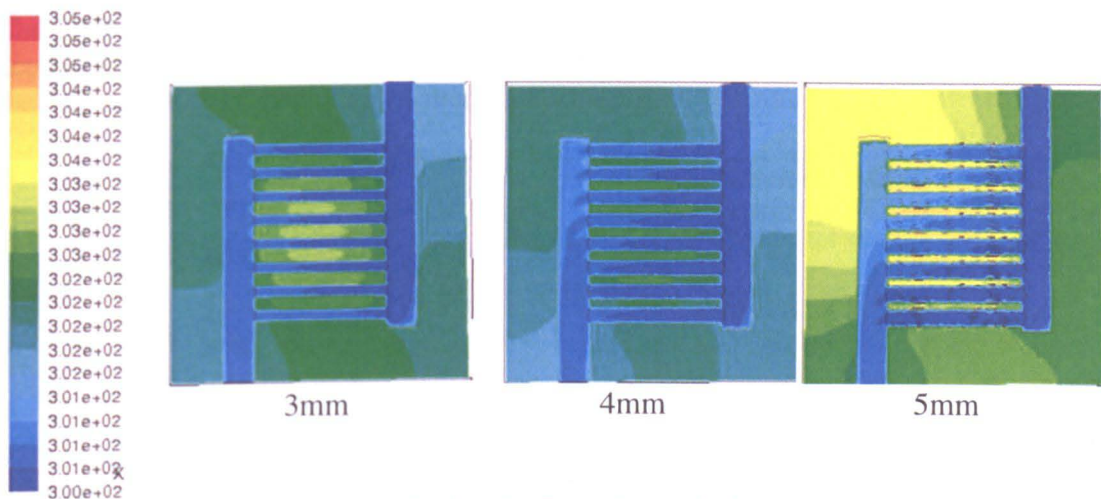


Figure 5-52 Temperature distribution in flow channel of cooling plates with 5mm, 4mm and 3mm branch channel

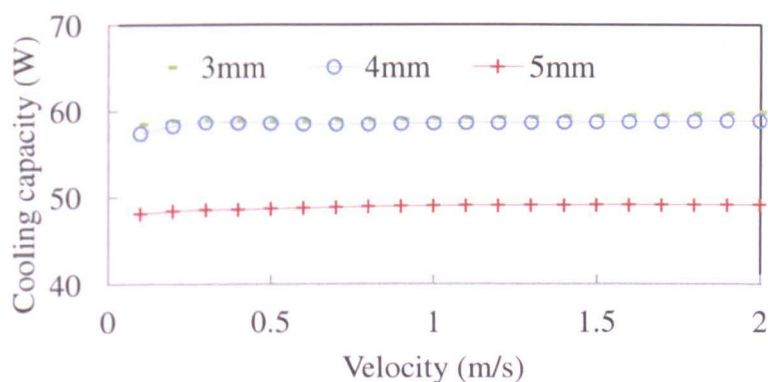


Figure 5-53 Cooling capacity of cooling plates with different branch channel dimension by numerical simulations

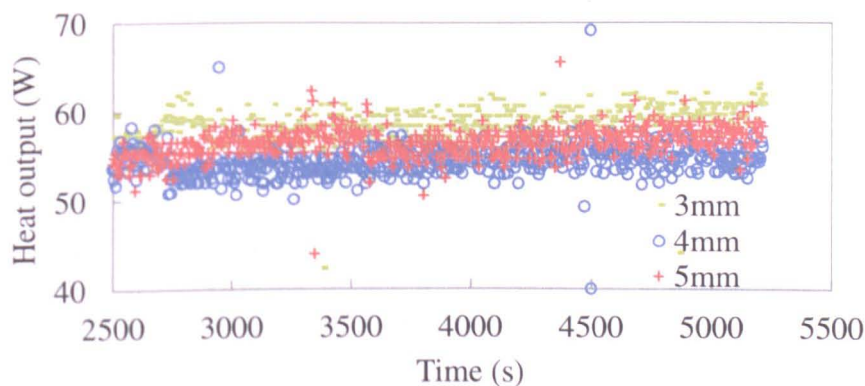


Figure 5-54 Cooling capacity of cooling plates with different branch channel dimension measured in experiment

The numerical result and experimental result of cooling capacity are shown in Figure 5-53 and Figure 5-54, respectively. Comparing the results, less than 5% discrepancy is shown in the cooling capacity of the cooling plates with 3mm and 4mm branch channels. For the one with 5mm branch channel, a 10% discrepancy is shown between the numerical and experimental results. This could be caused by the difference in the fabrication process, which alters the structure of real model.

The hydraulic characteristic curve of three cooling plates is shown in Figure 5-50. In accordance to the predicted trend, the curves show a decrease in pressure drop when the dimension of branch channel increases from 3mm to 5mm.

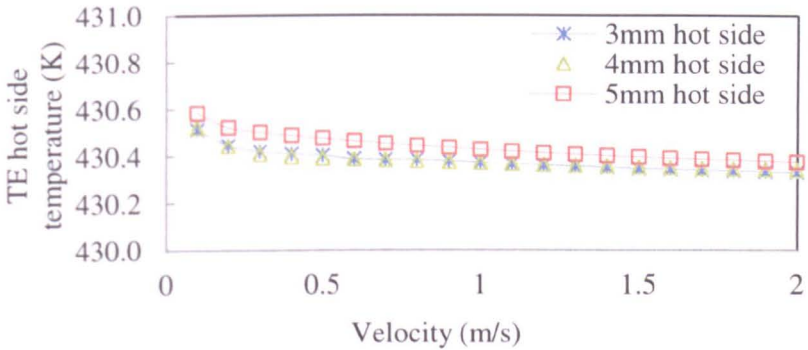


Figure 5-55 TE hot side temperature using cooling plate with 3mm, 4mm and 5mm branch channel

As shown in Figure 5-56, the temperature at cold side surface of each plate is different. The plate with 5mm branch channel has the highest temperature at the cold side, followed by 3mm and 4mm, respectively. For the 5mm cooling plate, the reason lies in the longest period that the water stays in the branch channel due to the lowest replacing rate by the new water. This is because the summed area of cross section of branch channel is much larger than the cross section area of main channel contributing to the build-up of hot spot in the regions where the flow is weak.

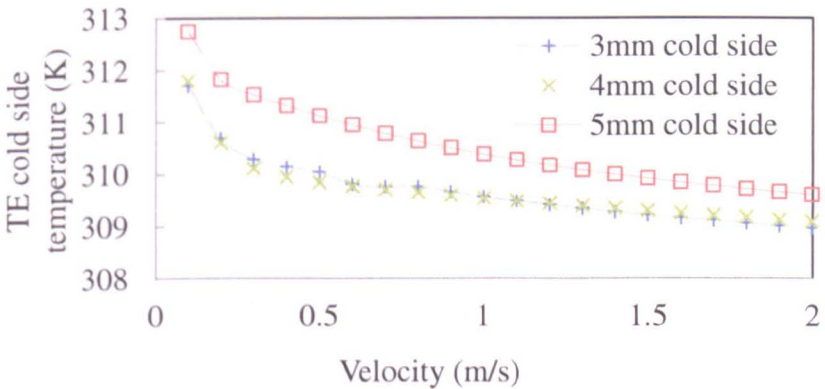


Figure 5-56 TE cold side temperature using cooling plate with 3mm, 4mm and 5mm branch channel

The pressure drop is reflected in the pumping power that is used to offset the pressure loss associated with using the cooling plate. The required pumping power of the three cooling plates under different flow rate is shown in Figure 5-57. It shows that the plates with 4mm and 5mm branch channel need a lower pumping power than the one with 3mm branch channel. When the flow rate is 5727ml/min, the pumping power of the 4mm plate and 5mm plate is 67% and 58% of that of the 3mm plate, respectively.



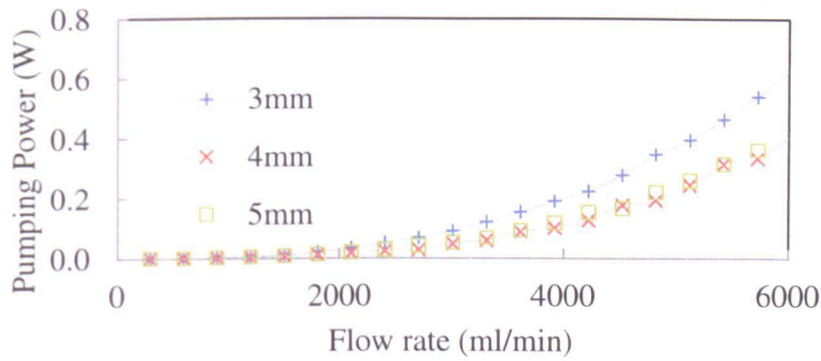


Figure 5-57 Pumping power of the cooling plates with 3mm, 4mm and 5mm branch channel

Taking both the cooling capacity and pressure drop into account to evaluate the overall performance of the cooling plates, the net energy gain is used. Figure 5-58 shows the net energy gain of the three cooling plates. The net energy gain by the 3mm and 4mm plate is 21% and 20% higher than that of 5mm plate, while the 3mm and 4mm plate have the similar net energy gain with a slightly higher value in 3mm plate.

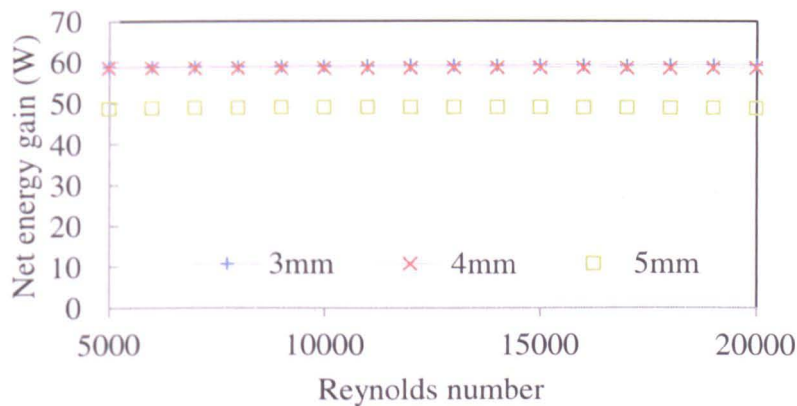


Figure 5-58 Net energy gain of the cooling plates with 3mm, 4mm and 5mm branch channel

Figure 5-59 shows the surface heat transfer coefficient (SHTC) under different flow velocity. It tells us that the cooling plate with 3mm branch channel has the highest surface heat transfer coefficient, which can be explained by the aforementioned flow distribution.

In the 3mm cooling plate, the flow distribution is the most even which leads to strong turbulence intensity in the flow, consequently enhancing the heat transfer between the flow and the wall of flow channel. The 4mm cooling plate takes the second place which is according to the situation of flow distribution, followed by the 5mm cooling plate. Considering the discussions above, it is acceptable to make the conclusion that the 3mm and 4mm plate are more suitable for this application than the 5mm plate.

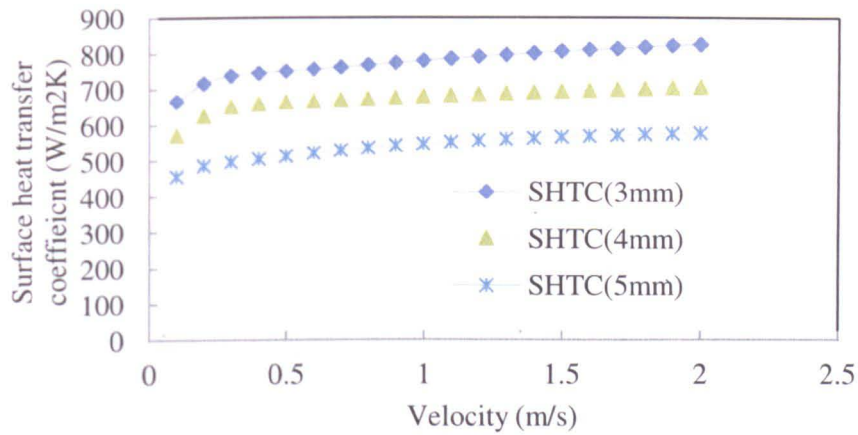


Figure 5-59 Surface heat transfer coefficient and HPPD of cooling plate with 3mm, 4mm and 5mm branch channel

### Channel quantity

The channel quantity not only determines the heat transfer area but also the hydraulic characteristic of cooling plate by varying the cross sectional area of branch channels. Therefore, the correlation between channel quantity and the performance is investigated. Numerical simulations have been made to the cooling plates with 4, 6 and 8 branch channels (the diameter of branch channel is 5mm). The structure of them is shown in Figure 5-60.

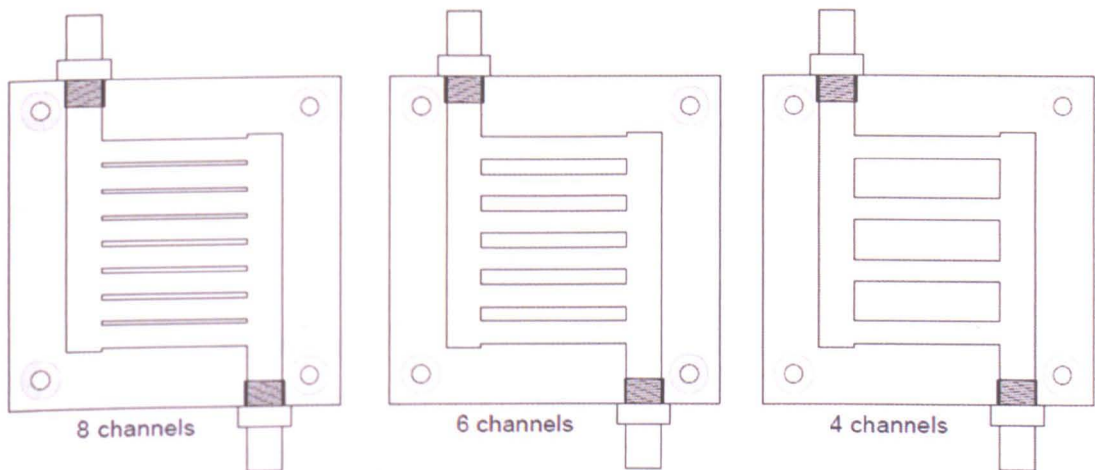


Figure 5-60 Cooling plates with 4, 6 and 8 branch channels

### Hydraulic performance:

Figure 5-61 and Figure 5-62 show the contour of velocity and turbulence intensity of flow in the channel, from which we can tell that the high speed flow is shown in the region near to first branch channel in the flow direction, rendered by red colour. For all the three cooling plates, the distribution of flow rate in branch channels varies with the channel quantity. The one with 4 channels has the most even flow distribution among the branch channels. For the one with 6 channels, as indicated by the rendering, the farther the branch channel from the inlet, the less flow passes through. This is more obvious in the cooling plate with 8 channels, where most of the flow passes through the branch channels near inlet, establishing uneven flow

distribution. This, in turn, creates a thermal hotspot at the top-left corner rendered by the yellowish colour in Figure 5-64.

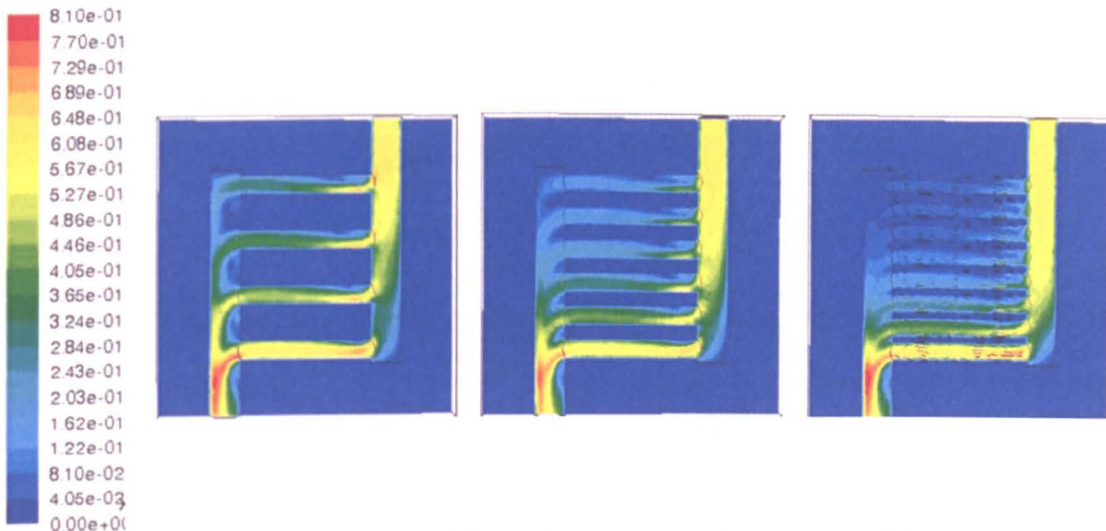


Figure 5-61 Velocity contour of flow channel in cooling plates with 4, 6 and 8 branch channels (5mm)

The pressure drop of each plate under different flow velocity shown in Figure 5-63 lies in the same level in the range of 0.1-1m/s. In the range of 1m/s-2m/s, the one with 6 channels has the lowest pressure drop followed by the 8 channels and 4 channels in ascending order. Nevertheless, a small difference is shown in the pressure drop of each cooling plate. Therefore, it can be concluded that the channel quantity does not affect the pressure drop significantly when the diameter of branch channel is constant.

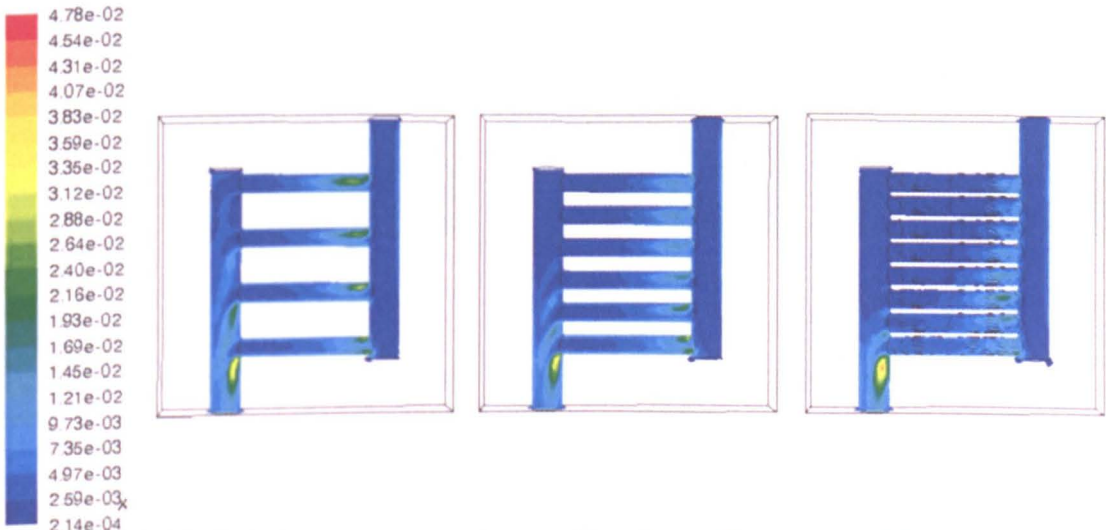


Figure 5-62 Turbulence contour of water flow in cooling plates with 4, 6 and 8 branch channels (5mm)



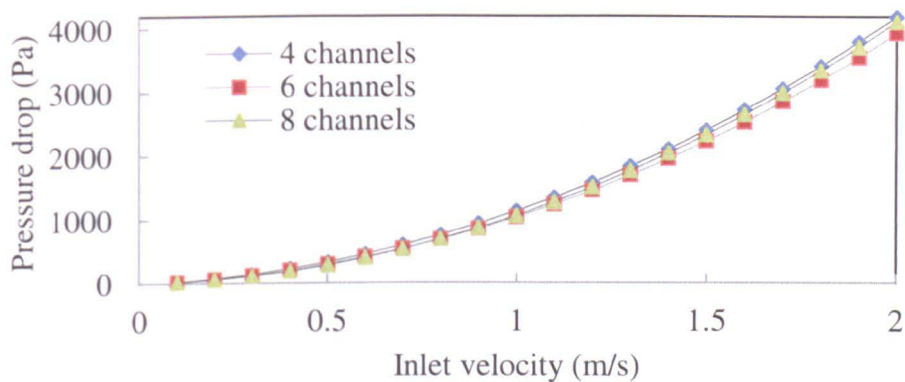


Figure 5-63 Pressure drop of cooling plates with 4, 6 and 8 branch channels

### Thermal performance

Figure 5-64 shows the temperature distribution on the central horizontal plane of cooling plate. It tells us that the cooling plate with 6 channels has the lowest temperature of them all. The temperature distribution on the TE cold side surface is shown in Figure 5-65, from which we can see that the temperature distribution on the ones with 4 and 6 channels is more uniform than that with 8 channels. Among them, the one with 6 channels give the lowest temperature value and most even temperature distribution which is technically beneficial for establishing a good thermal condition for thermoelectric application.

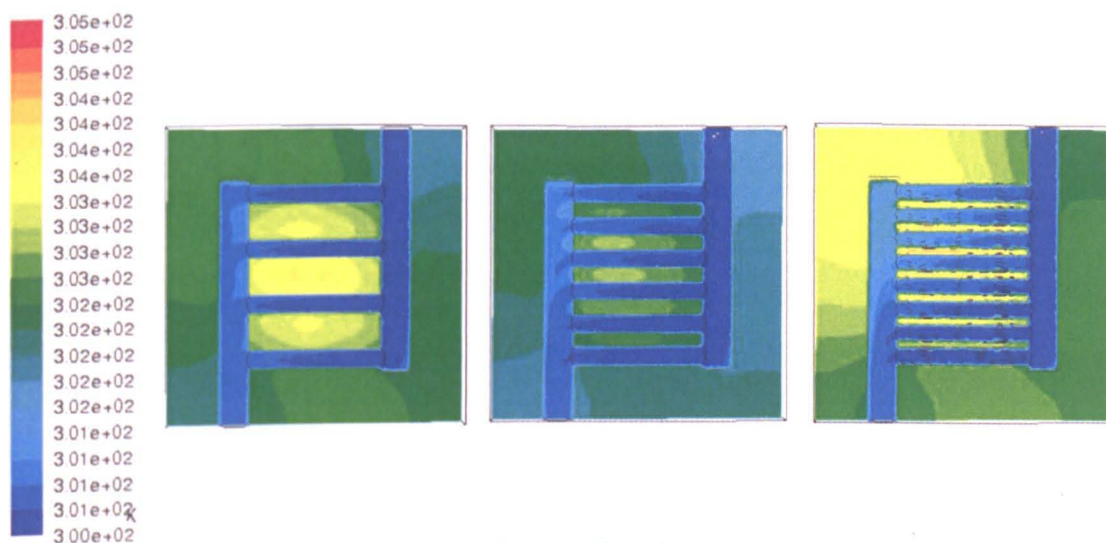


Figure 5-64 Temperature contour of water flow in cooling plates with 4, 6 and 8 branch channels (5mm)



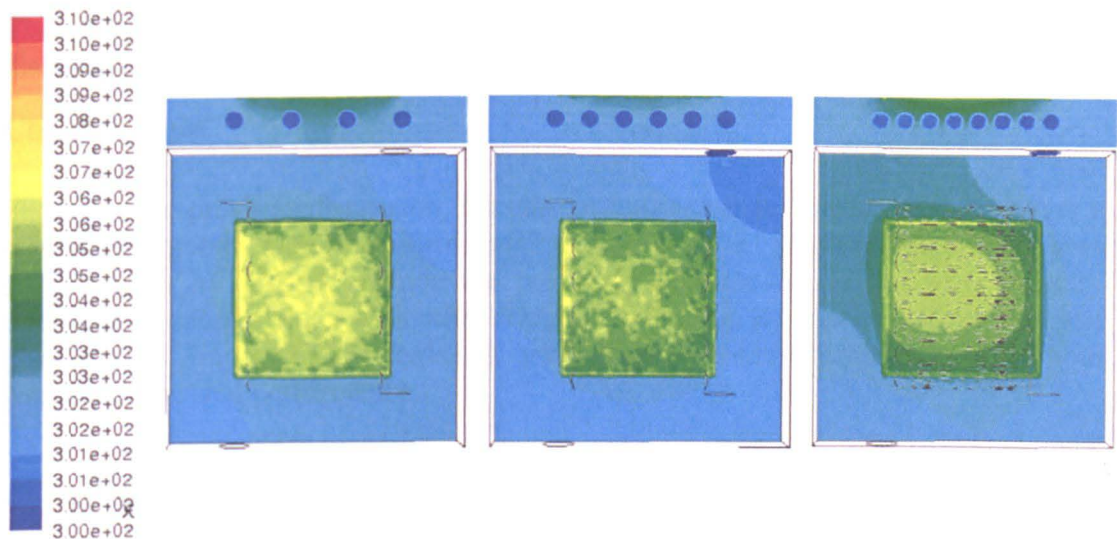


Figure 5-65 Temperature contour of water flow in cooling plates with 4, 6 and 8 branch channels (5mm)

Figure 5-66 shows the cooling capacity of each cooling plate. The one with 4 branch channel has the highest cooling capacity in the whole range of flow velocity, closely followed by the one with 6 channels. The cooling capacity of the one with 8 channels is approximately 20% smaller than the ones with 4 and 6 channels. The  $r_{cp}$  of the cooling plates with 4 channels, 6 channels and 8 channels is 1.56, 2.33 and 3.13, respectively.

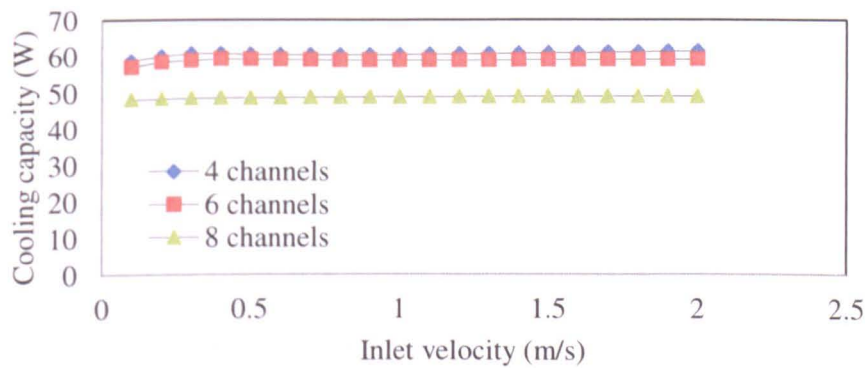


Figure 5-66 Cooling capacity of cooling plate with 4, 6 and 8 branch channels

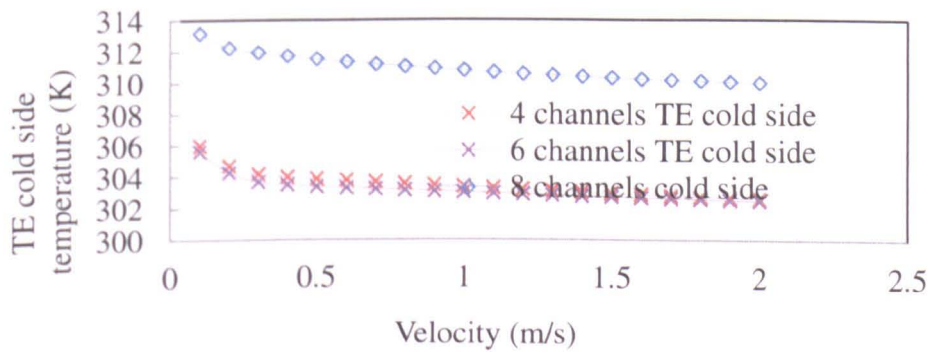


Figure 5-67 TE cold side temperature when using cooling plate with 4, 6 and 8 channels

The pumping power and net energy gain of these three plates are analyzed and discussed in 5.5.1.5.

### Channel angle

Shown in the previous discussion, the current multi-channel cooling plate delivers a reasonably good overall performance. However, the pressure drop increases significantly. In order to reduce the pressure drop caused by the high velocity operation in cooling plates with other designs, further job is carried out to explore the possibility of improving the hydraulic performance on the precondition of without worsening thermal performance.

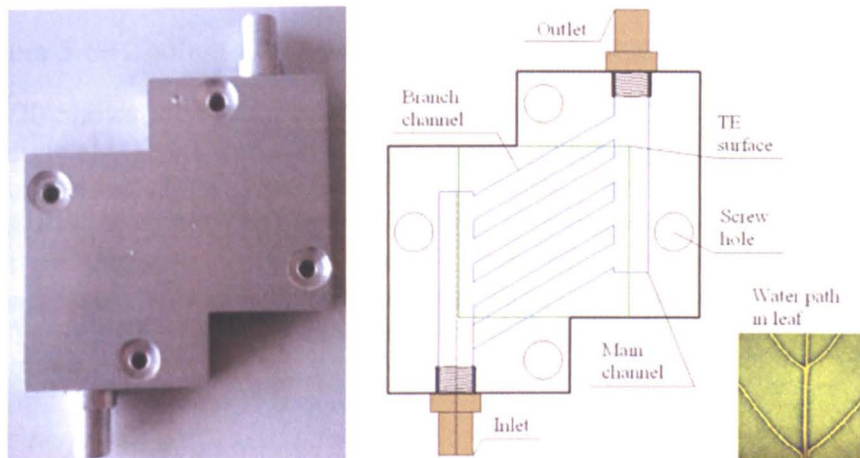


Figure 5-68 Advanced modification of the cooling plate

Figure 5-68 shows the modification design of the cooling plate, which is inspired by the water channel in plant's leaf. Tree has a massive water transportation mission due to the complex system comprised of the trunk, branches and leaves hierarchically. The water is transported from the root to every part of the massive tree body to keep the whole system alive and thriving. This massive water transportation task is managed by the tree silently and efficiently. One of the secrets lies in the special structure of selective and complying water channels [158] which has been naturally developed in the evolution process. The structure can be claimed to be perfect for the remarkable capability of transporting the water. Therefore, in this study, the concept of water channel from plants will be used to modify the flow channel of cooling plate. It is an attempt of mimicking the channel structure in plants to reduce the pressure drop of cooling plate without compromising to the thermal performance. The inspiration is crystallised on adjusting the angle between the main channel and branch channel. Other factors such as capillary effect are not considered.

The angel of branch channel with main channel is investigated at  $90^\circ$ ,  $60^\circ$  and  $45^\circ$  using numerical simulations. The structure is shown in Figure 5-69.

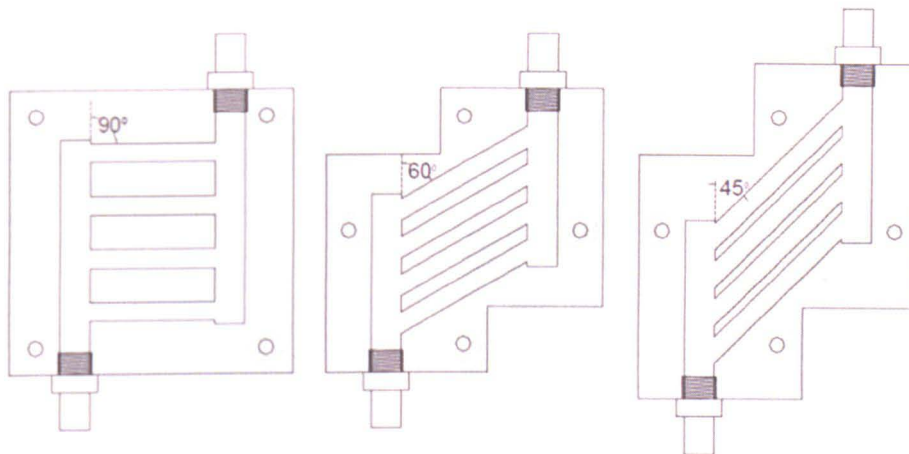


Figure 5-69 Cooling plates with branch channels at angle 90°, 60° and 45°

Figure 5-70 shows the flow pattern in flow channel of cooling plates with branch channel angle at 90°, 60° and 45°. The 90° cooling plate has a high velocity and more intense turbulence at the first branch channel indicated by the red colour. This represents a large contingent of pressure drop of the whole cooling plates, whereas the velocity at the same position in the 60° cooling plate is smaller, followed by the 45° cooling plate, both of which show more even velocity distribution in the flow channel. This can be proved by the turbulence intensity of the three cooling plates shown in Figure 5-71.

#### Hydraulic performance

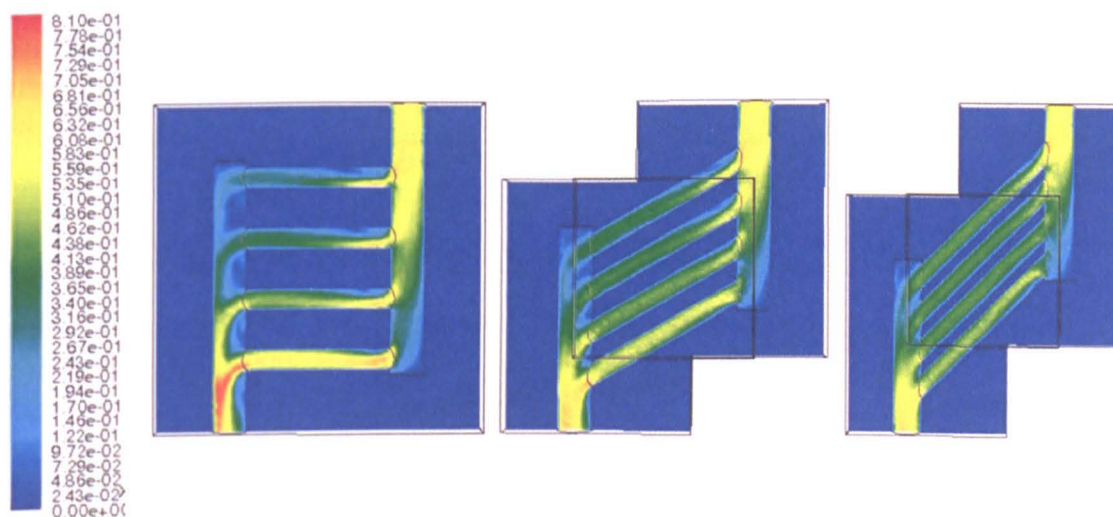


Figure 5-70 Velocity contour of flow channel in cooling plates with branch channel (5mm) angle at 45°, 60° and 90°



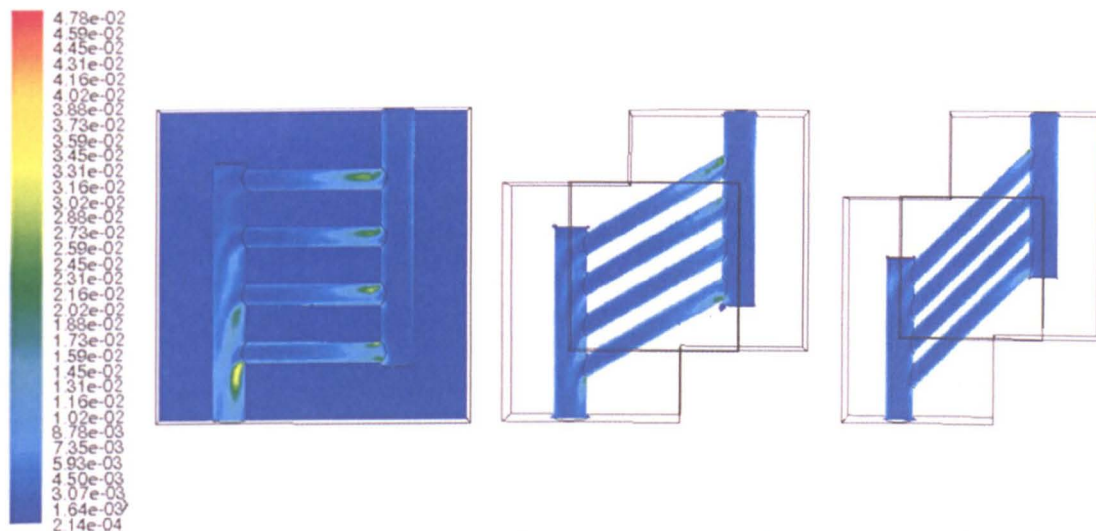


Figure 5-71 Turbulence contour of flow channel in cooling plates with branch channel (5mm) angle at 45°, 60° and 90°

Therefore, as shown in Figure 5-72, the pressure drop of the 90° cooling plate increases when the flow velocity increases, the increasing trend gets more obvious when the velocity lies in the higher speed zone (1m/s-2m/s). The 60° cooling plate shows a lower pressure drop than the 90° one, which becomes more obvious in the range of 1m/s-2m/s. This is followed by the 45° cooling plate. At 2m/s, the pressure drop of the 60° cooling plate is 52% of pressure drop of the 90° cooling plate, whilst it is 37% for the 45° one. This tackles the original goal of reducing the pressure drop. The following part will investigate how the thermal performance is affected by the angle change.

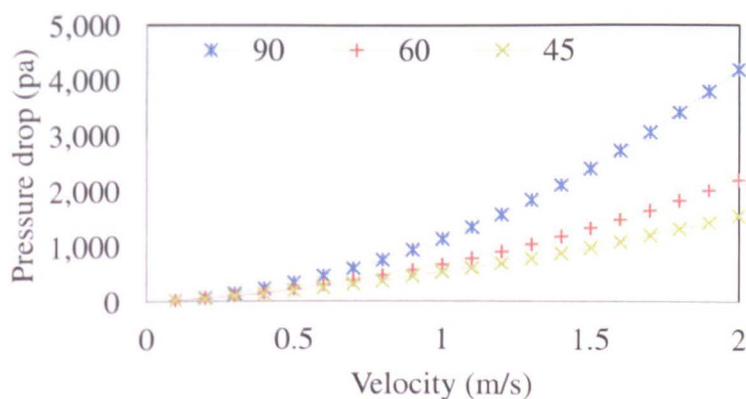


Figure 5-72 Pressure drop of cooling plates (5mm) with branch channel angle at 45°, 60° and 90°

### Thermal performance

Figure 5-73 shows the temperature contour of TE cold side when cooled by the cooling plate with branch channel at 45°, 60° and 90°. In the 45° and 60° cooling plates, minor temperature hotspots can be seen at the top-left corner and right-bottom corner. This can be attributed to the layout of flow channels that do not cover the whole area attached with thermoelectric module. The hotspot is not seen on the TE cold side installed with the 90° cooling plate. The similar phenomenon can be seen



from temperature contour of central horizontal cross section plane of cooling plate, shown in Figure 5-74.

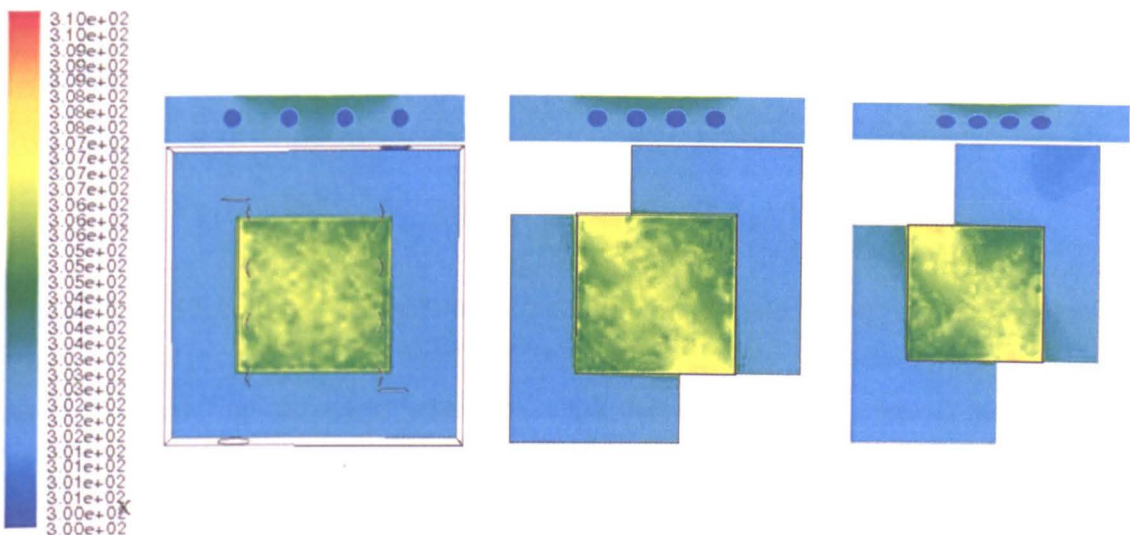


Figure 5-73 TE cold side temperature contour using cooling plates with branch channel (5mm) angle at 45°, 60° and 90°

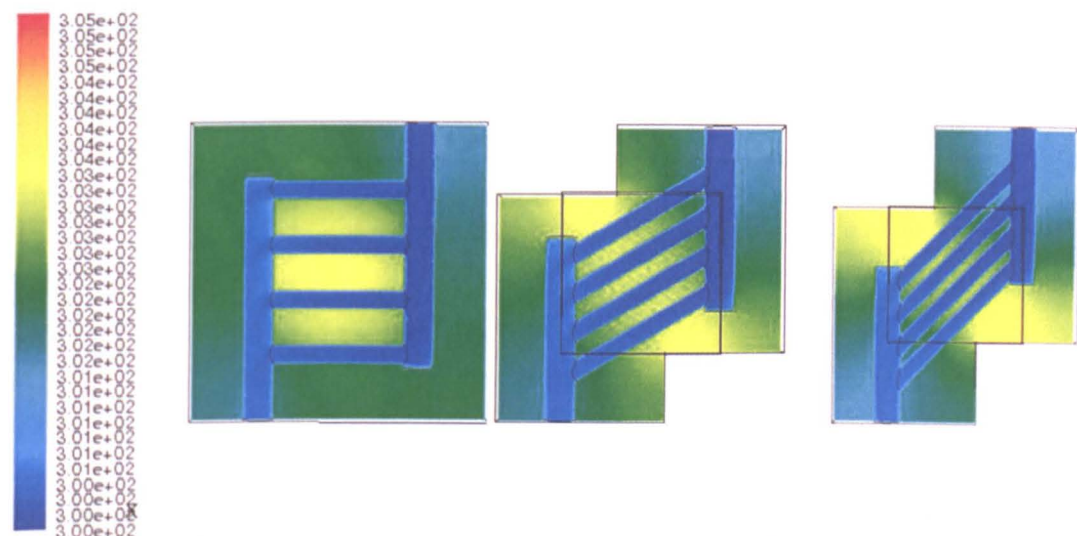


Figure 5-74 Temperature contour of flow channel in cooling plates with branch channel (5mm) angle at 45°, 60° and 90°

However, the average TE cold side temperature of the 45°, 60° and 90° cooling plates stays almost at the same level when the flow velocity lies in the range of 0.1m/s-1m/s. The difference only comes into sight when the flow velocity increases further from 1m/s. In the range of 1m/s-2m/s, the TE cold side temperature of the 90° cooling plate is slightly lower than 60°, followed by 45°, shown in Figure 5-75.

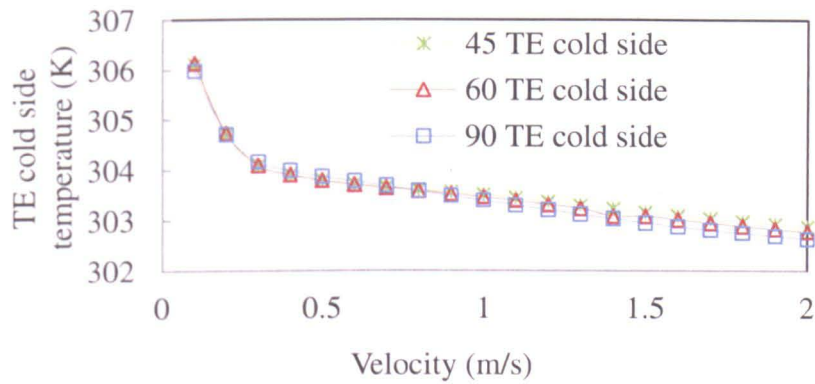


Figure 5-75 TE cold side temperature for cooling plates with branch channel (5mm) angle at 45°, 60° and 90°

As for the cooling capacity, when the angle between branch channel and main channel decreases down from 90° to 60° and 45°, the cooling capacity goes down for 6.2% and 7.8%, respectively, which is shown in Figure 5-76.

Therefore, by reducing the angle between the main channel and branch channel, the pressure drop reduces significantly as mentioned earlier, which means the required pumping power to offset the pressure drop is decreased. However, the heating capacity decreases at the same time when the angle gets smaller. The overall benefit needs to be evaluated and the net energy gain is used to compare. The result is shown in section 5.6.1.5.

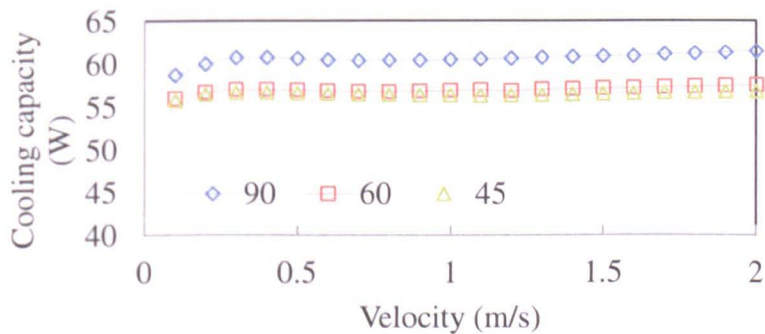


Figure 5-76 Cooling capacity of cooling plates (5mm) with branch channel angle at 45°, 60° and 90°

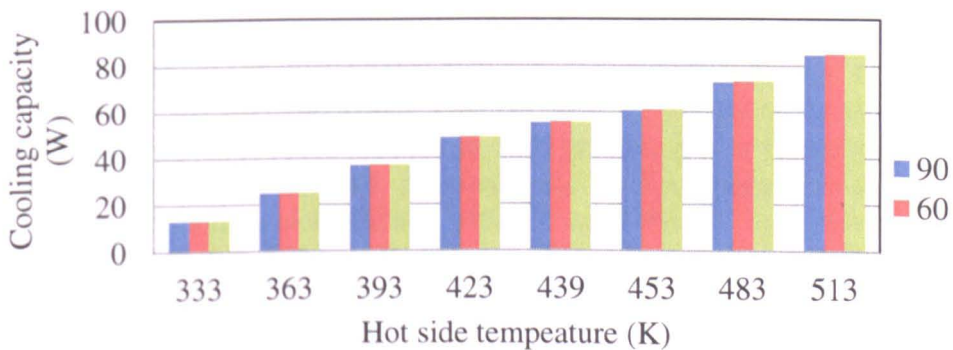


Figure 5-77 Cooling capacity vs. TE hot side temperature

Figure 5-77 shows the cooling capacity of these three plates under different TE hot side temperature. It gives us an idea how much unconverted heat can be absorbed by the cooling plates under different temperature level.

5.5.1.5 Comparisons

The cooling capacity of the cooling plates is shown in Figure 5-78. The one with eight 5mm branch channels lies at the lowest level, followed by the single channel cooling plate.

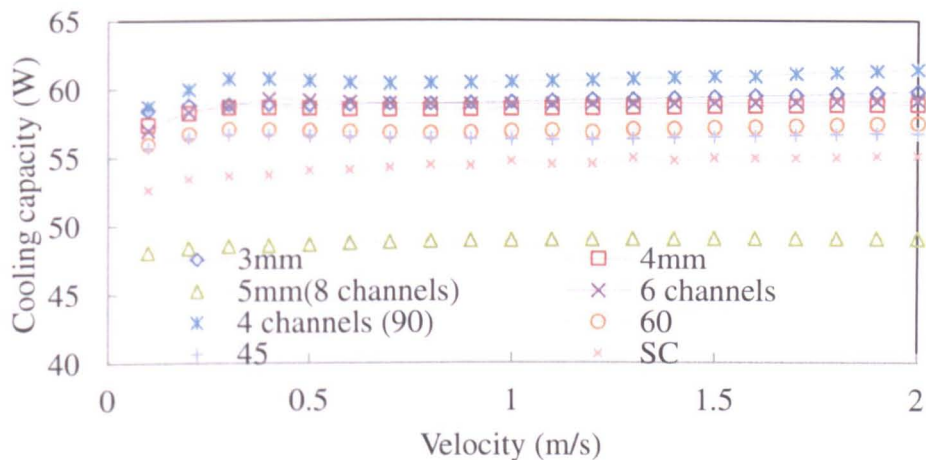


Figure 5-78 Cooling capacity of the cooling plates

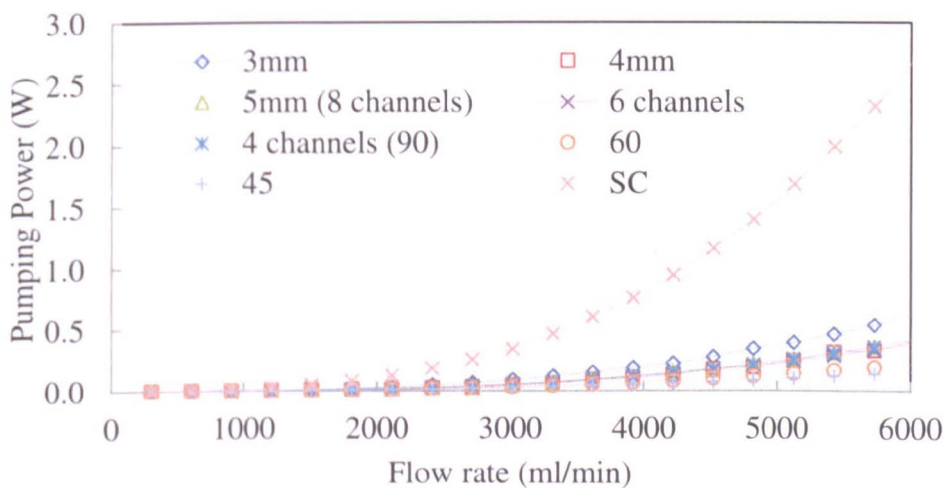


Figure 5-79 Pumping power of the cooling plates vs. Flow rate

Figure 5-79 shows the pumping power required by different heat exchangers under different coolant flow velocity. All the data is based on heat exchanger for single TE module. We can see that the single channel heat exchanger consumes the most pumping power, which is more obvious at high velocity range. Comparing with the single channel cooling plate, all multi-channel cooling plates need much less pumping power. Among which, the one with 45° consumes the least pumping power, followed by the one with 60° branch channel. The ones with 4mm and 5mm branch channel, 6 channels and 4 channels share the similar level of pumping power. A big improvement in hydraulic performance can be seen by reducing the angle between main channel and branch channel. Comparing the one with 60° and 45°, the one with 45° needs the smaller pumping power, which possibly draws the conclusion that smaller angle achieves better hydraulic performance.



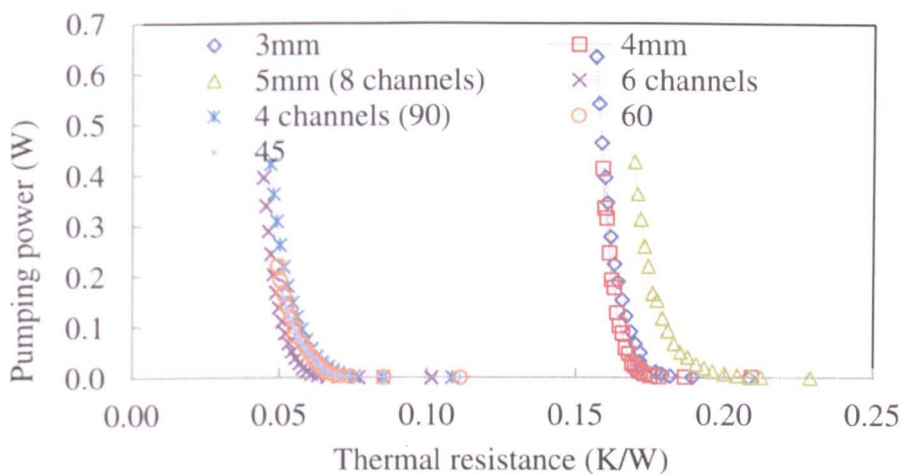


Figure 5-80 Pumping power plotted against thermal resistance

Figure 5-80 shows the pumping power required for the operation against thermal resistance of different cooling plates between liquid and TE cold side surface. It shows the larger the pumping power, the smaller the thermal resistance is. This also reflects the correlation between the flow velocity and thermal resistance that the larger the flow velocity, the smaller the thermal resistance is. The cooling plates are located in two groups. The ones with 3mm, 4mm and 5mm branch channels are in the high thermal resistance region, whilst the rest locate in the low thermal resistance region. In the higher thermal resistance region, for the same pumping power, the cooling plate with 4mm branch channel has the lowest thermal resistance with the 3mm one taking the second place and the 5mm one showing the largest thermal resistance. In the lower thermal resistance region, for the same pumping power, the cooling plate with 6 branch channels shows the lowest thermal resistance, followed by the one with 45° angle, 60° angle and 90° angle. However, the one with 45° angle has the lowest pumping power in the whole velocity range.

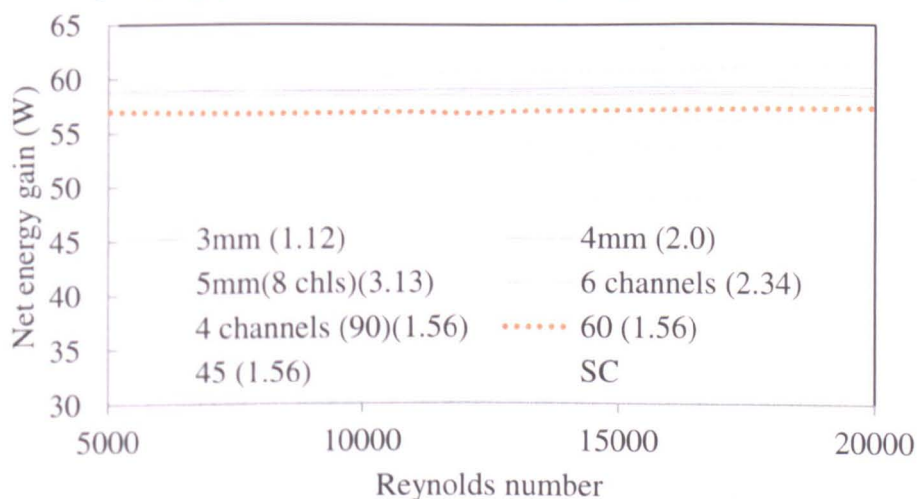


Figure 5-81 Net energy gain of the cooling plates against Reynolds number

Figure 5-81 shows the net energy gain of cooling plates under different Reynolds number (Re is calculated according to the main channel). The cooling plates that deliver the net energy gain in ascending order are single channel cooling plate (SC), the plate with 5mm branch channel or 8 branch channels, the plate with 45° channel



angle, the plate with 60° channel angle, the plate with 4mm branch channel, the plate with 6 branch channels, the plate with 3mm branch channel and the plate with 4 branch channels, respectively.

	$r_{cp}$	Type
High	1.56	4 channels (90)
	1.12	3mm
	2.34	6 channels
	2.00	4mm
	1.56	60
Low	1.56	45
	3.13	5mm (8 channels)

Figure 5-82 Net energy gain level of the plates with different configuration

Figure 5-82 shows the net energy gain level of the plates with different configuration, low level at the bottom to high level at the top. Either comparing the branch channel size or quantity, we can find that the closer of  $r_{cp}$  to 1, the higher the net energy gain level is. This applies to the plates in the same comparison. For instance, the plate with 4 channels with  $r_{cp}$  at 1.56 has a higher level of net energy gain than that of 3mm branch channel with  $r_{cp}$  at 1.12. The highest net energy gain goes to the one that has four 5mm channels and 90° branch channel and main channel angle, which outweighs the effect of  $r_{cp}$ .

Colburn j factor is the accurate analogy to characterize the heat exchanger performance. It gives a heat transfer performance comparing the convection coefficient to the required flow rate of a heat exchanger. It is based on the measured convection coefficient (  $h$  ), the necessary velocity of the coolant to achieve the corresponding convection coefficient. Figure 5-83 shows the Colburn j factor at different flow velocity. The cooling plate with 60° has the highest j factor of them all.

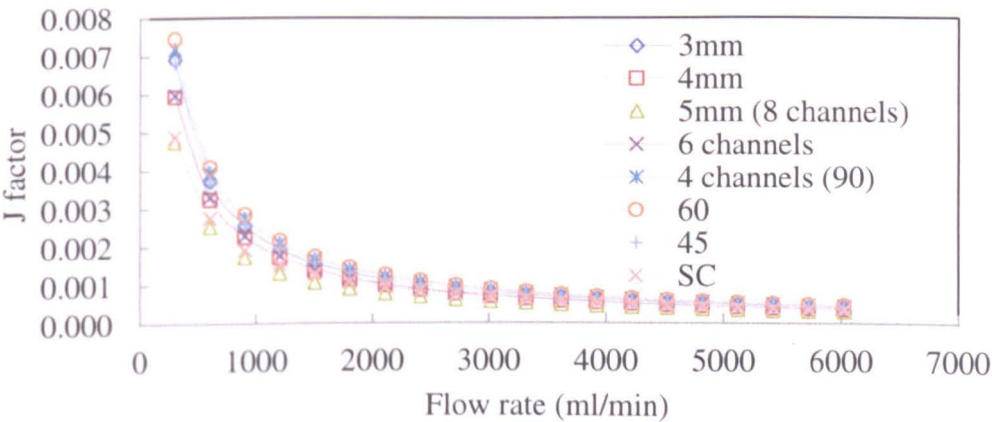


Figure 5-83 The Colburn j factor plotted against Reynolds number (Re is calculated according to the main channel)

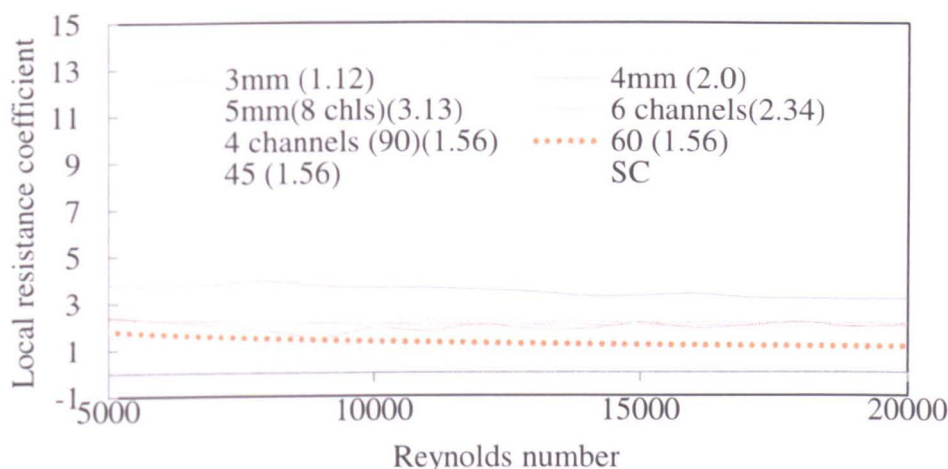


Figure 5-84 The local resistance coefficient plotted against Reynolds number

The cooling plate can be treated as a component that causes local pressure drop when the fluid passes through. The local resistance coefficient  $\zeta$  is used to characterize the hydraulic property of cooling plates with different designs. The result is shown in Figure 5-84, which reveals the value of local resistance coefficient calculated at different velocity and it tends to reach a stable level as the velocity increases.

#### 5.5.1.6 Discussion

In this multi-channel cooling plate, an even flow distribution among the branch channels is essential to establishing even temperature distribution on the module cold side and maintaining a temperature on the module cold side at a low level. From the results of numerical simulations, it can be concluded that an even flow distribution among the branch channels is closely related to  $r_{cp}$  (the ratio of the summed cross sectional area of branch channels to that of main channel). In general, it is beneficial to have the value of  $r_{cp}$  located around 1 which gives a more temperature distribution. However, the value of  $r_{cp}$  needs to be controlled by the consideration of the pump power that is needed to offset the pressure drop.

Talking about the multi-channel cooling plates investigated by alternating the key parameters, the question that why the current commercialised heat exchanger can't be used as the heat dissipation in this thermoelectric cogeneration system should be raised and discussed.

The major reason is given by the need of high flow rate required by the boiler water feed system. Most of the compact or micro heat exchangers deliver a big heat exchanging capacity due to the need of high thermal flux required by special applications such as high power LED lamps, super CPU and electronic devices that dissipate heat at high thermal flux and need efficient cooling to enable a satisfactory performance. In this case, a good cooling capacity is the primary goal to achieve in the design of heat exchanger. The pressure drop, which reflects the amount of pumping power, takes the secondary priority in the considerations. For example, Yang [159] introduces micro heat exchangers for laptop processor cooling and compared three different channel structures. The flow rate lies in the range of 50



ml/min-250ml/min, suitable for cooling the application that gives high heat flux with limited space, but not for the boiler water feeding flow rate.

### 5.5.2 Whole assembly

The individual assembly is the assembling method for solving the uneven pressure load caused by relatively noticeable thickness difference shown in the modules used in the whole assembly. This uneven pressure load degrades the performance of thermoelectric applications because the thermoelectric performance is dependent on the pressure load in the system construction. Despite the advantage of individual assembly in obtaining a better performance, it has to be admitted that individual assembly, compared to the whole assembly, has more procedures due to joints between each neighbored cooling plates. However, the individual assembly is not the only method to solve the degraded performance due to uneven pressure load. In the whole assembly, restrictions on the thickness difference can be adopted in choosing the modules to make sure the thickness difference is not in the performance-degrading range. The corresponding cooling plate for the whole assembly can still use this multi-channel structure. An example is shown in Figure 5-85. The liquid channel can be fabricated on two plates and then assembled as a whole cold side heat exchanger. The modules with the restricted thickness are sandwiched between hot side and cold side heat exchangers by screws and washers. The optimum pressure, verified by experimental investigations, can be loaded evenly using a torque wrench.

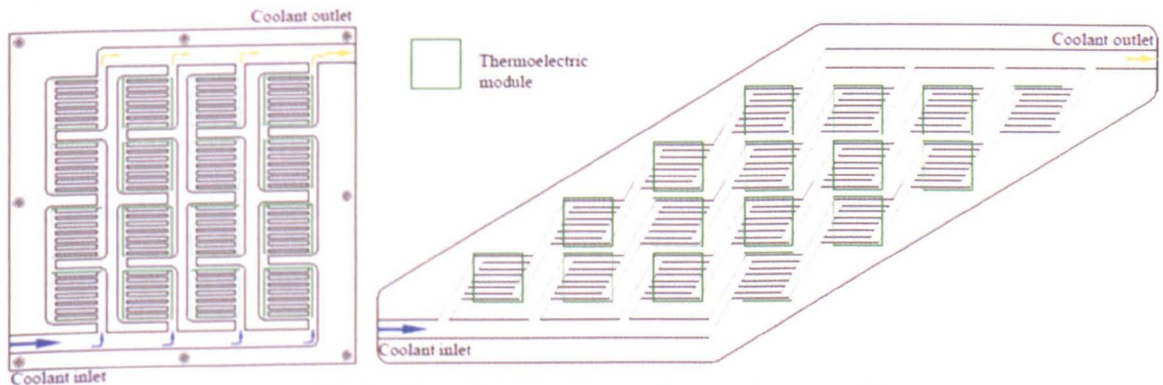


Figure 5-85 Cooling plate concepts for whole assembly

#### 5.5.2.1. Physical model

Figure 5-85 shows the schematic diagram of cooling plate for whole assembly. It consists of 16 sub-cooling regions, which lay out in four rows and four columns. Each row or column consists of four areas for installing thermoelectric modules.

Figure 5-86 shows the schematic diagram of the inlet corner of whole assembly cooling plate. The angle between the main channel and the sub-main channel is 60°, same for the angle between the sub-main channel and branch channel. This angle value is obtained from the results of previous numerical simulation, introduced in section 5.6.1. All the channels are circular, with the diameters at 4mm, 8mm and 16mm for the branch channel, sub-main channel and main channel, respectively.

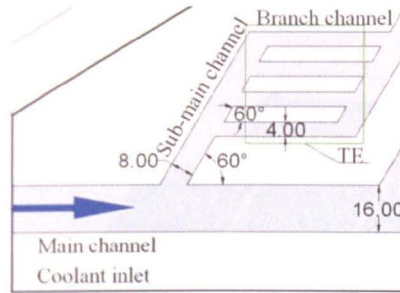


Figure 5-86 Schematic diagram of channel structure and dimension at the inlet corner

### 5.5.2.2. Boundary conditions

**Inlet:** the inlet velocity of cooling plate is calculated according to the nominal flow rate of boiler feed water. The performance will be investigated in the range of 0-2m/s with a 0.1m./s interval;

**Outlet:** Considering the flow at the outlet is fully developed, it is set as outflow;

**TE hot side surface:** To enable the comparison with the results obtained from the numerical study of cooling plate for individual assembly, the temperature of TE hot side surface is set at 166°C according to the experimental result;

**Thermoelectric module:** the thermal conductivity is set at 1W/mK, which is obtained from the previous test;

**Cooling plate:** cooling plate is made of aluminium;

### 5.5.2.3. Results

The modules and channels are numbered in Figure 5-87. The four sub channels are numbered as Sub A, Sub B, Sub C, and Sub D from the inlet. In the downstream direction of each sub-channel, the modules are numbered as 1, 2, 3 and 4, respectively. The results of numerical simulation are introduced using this numbering regime.

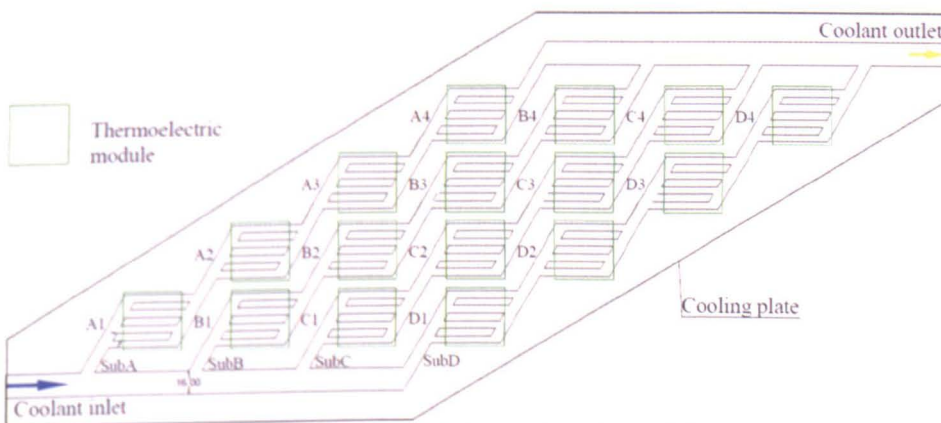


Figure 5-87 Numbering of channel and module positions

In numerical simulations, due to the meshing difficulty involved in small gap in the domain, the whole cooling plate has to be divided into 16 individual blocks. The domain and temperature contour on the module cold side is shown in Figure 5-88.



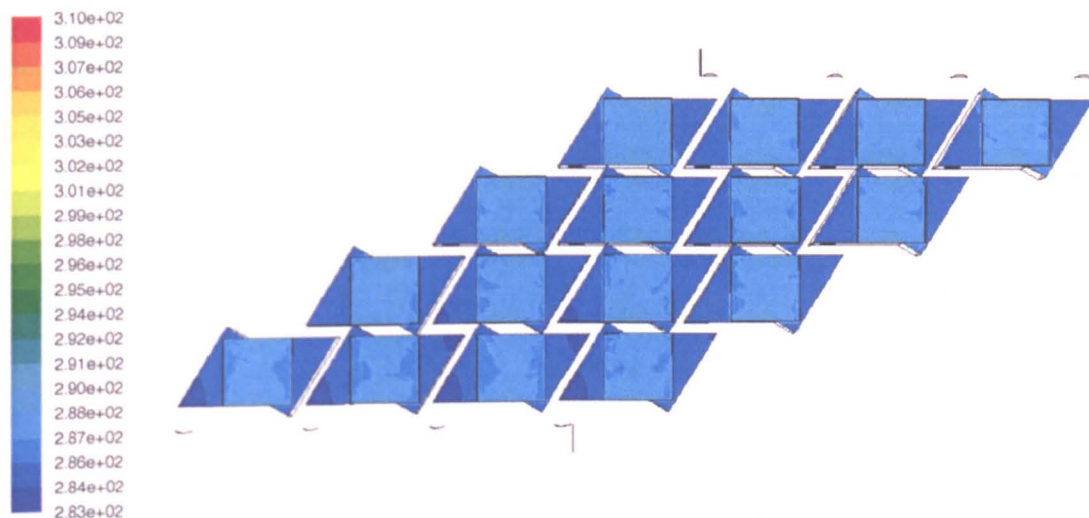


Figure 5-88 Domain and temperature distribution of the module cold side

The value of average temperature on each TE cold side is shown in Table 5-3.

Table 5-3 Average temperature of the module cold side (°C)

Model		1	2	3	4
Sub-channel	A	293.20	293.51	286.38	293.91
	B	285.77	285.98	286.17	293.63
	C	285.86	286.11	286.27	293.79
	D	285.97	286.18	286.38	286.60

The flow rate in each sub-channel is shown in Table 5-4. Standard deviation is used to describe the uniformity of flow rate among all the sub-channels. A low standard deviation indicates that the data points tend to be very close to the mean value of all, whereas high standard deviation indicates that the data points are spread out over a large range of values.

Table 5-4 Mass flow rate of each sub-channel (kg/s)

Sub-channel	A	B	C	D
Mass flow rate (0.9m/s)	0.0424	0.0480	0.0452	0.0432
Mass flow rate (1m/s)	0.0515	0.0531	0.0496	0.0446
Mass flow rate (1.1m/s)	0.0585	0.0563	0.0560	0.0478
Mass flow rate (1.2m/s)	0.0616	0.0616	0.0580	0.0573
Mass flow rate (1.3m/s)	0.0607	0.0736	0.0622	0.0618
Mass flow rate (1.4m/s)	0.0708	0.0746	0.0702	0.0627
Mass flow rate (1.5m/s)	0.0749	0.0828	0.0698	0.0707
Mass flow rate (1.6m/s)	0.0855	0.0819	0.0738	0.0769
Mass flow rate (1.7m/s)	0.0853	0.0894	0.0848	0.0783
Mass flow rate (1.8m/s)	0.0865	0.0962	0.0897	0.0854
Mass flow rate (1.9m/s)	0.0981	0.0999	0.0886	0.0910
Mass flow rate (2.0m/s)	0.1010	0.1062	0.0965	0.0938

Figure 5-89 shows the standard deviation of the cold side temperature of each module when the flow rate is in the practical range of feed water stream to the

domestic boiler. It shows a good uniformity of the temperature distribution among the 16 modules on the cooling plate for whole assembly.

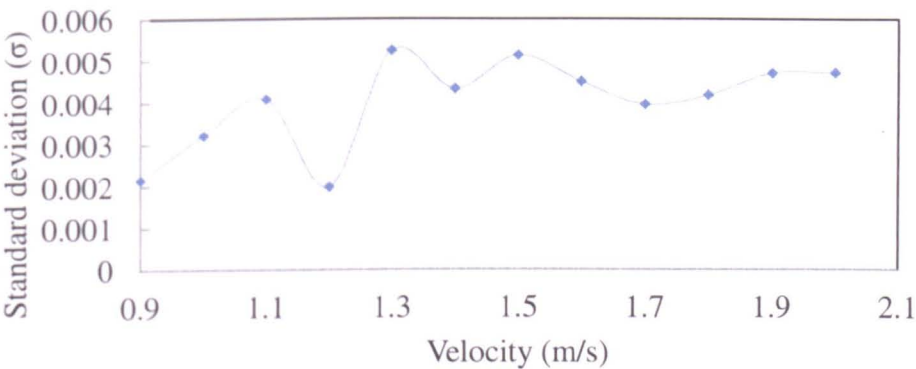


Figure 5-89 Standard deviation of the cold side temperature of each thermoelectric module

### 5.5.3 Integration

The flow rate of feed water varies with the capacity of boilers and also varies slightly with the manufacturer. Table 5-5 lists the samples of major boiler manufacturers in the UK:

Table 5-5 Minimum flow rate through boiler (L/min)

Capacity	1	2	3	4
Vaillant (Minimum)	10.8	12.9	20.3	27.2
Ferrol	10	13.1	15.4	
Worcester Bosch	9.8-11.4	10.2-12.3	11.1-17.2	20-25
Baxi (Maximum)	9.8	11.5	13.5	16

The dimension of heating fitting mainly includes two sizes, 22mm and 15mm, varying with the boiler type and manufacture. Usually, the dimension of 22mm is used in condensing boiler. The size 15mm is usually used in conventional boilers.

Considering the thermoelectric cogeneration system is designed to recover the waste heat from the conventional boiler which has lower boiler efficiency compared to the condensing boiler, the size 15mm is regarded as the reference for designing the cooling plate.

According to the flow rate range in Table 5-5, the velocity of feed water to the boiler installed with 15mm inlet of cooling block approximately lies in the range of 0.9m/s-2.0m/s, varying with the working load.

### 5.6. Summary

A series of numerical studies have been conducted to modify the design for this system concept by looking into three structural parameters and two assembling methods.

Flow distribution among the branch channels is closely related to  $r_{cp}$  (the ratio of the summed cross sectional area of branch channels to that of main channel), which

essentially determines the temperature distribution on the surface of cooling plate attached to the module. In general, it is beneficial to have the value of  $r_{cp}$  located around 1 which gives more even temperature distribution. The channel quantity does not affect the pressure drop significantly when the diameter of branch channel and main channel is constant, but deteriorates the thermal performance when it increases. Bigger quantity of branch channel diverts the flow to limited area of cooling plate and leads to uneven temperature distribution. The angle between branch channel and main channel affects the hydraulic characteristic. The pressure drop of the cooling plate can be reduced significantly by decreasing the angle between the branch channel and main channel. However, the heat transfer coefficient is decreased at the same time.

The cooling plate with four  $\varnothing 5\text{mm}$  branch channels angled at  $90^\circ$  against the main channel delivers the best overall performance out of 9 cooling plates built according to three variables.

## Chapter 6 Experimental investigations

This chapter introduces the experimental investigations of one-stage thermoelectric cogeneration system and two-stage cogeneration system based on the use of a simulated heat source and purpose-designed heat dissipation-multi channel cooling plate. Insight is also shed on the investigation to the performance of one-stage cogeneration system and the parametric factors that influence the system performance.

### 6.1. Theoretical analysis

#### 6.1.1 One-stage TCS

The energy conservative equation is

$$Q_{input} = P + Q_{output} + Q_{loss} \quad (6-1)$$

Where  $Q_{input}$  is the sum of absorbed thermal energy (which includes solar radiation, waste heat from boiler flue gas or other available heat sources),  $P$  is the total power output,  $Q_{loss}$  is the heat loss to the environment and  $Q_{output}$  is the heat output from heat sink. Assuming boiler waste heat and solar radiation are the heat sources, the heat input can be expressed by Eq.(6-2):

$$Q_{input} = Q_{solar} + Q_{bw} \quad (6-2)$$

In the real situation, the solar radiation varies with the weather condition and the time of the day. As shown in Eq.(6-1), the capacity of heat source which is also the heat input equals to the sum of power output, heat output and heat loss. Denoting the temperature of heat source, heat sink, TE hot side, TE cold side and ambient environment are  $T_h$ ,  $T_c$ ,  $T_1$ ,  $T_2$  and  $T_a$ , respectively. The coolant temperatures at the inlet and outlet of heat sink and coolant flow rate are  $T_{outlet}$ ,  $T_{inlet}$  and  $G$ , respectively. Therefore, power output, heat output and heat loss can be calculated by Eq.(6-3), Eq(6-4) and Eq.(6-5).

$$P = \frac{S^2 (T_1 - T_2)^2}{4R_{ex}} \quad (6-3)$$

Where,  $P$  is the maximum power output taken out by the external load (when the internal load and external load are matched, the maximum power output is obtained),  $S$  is the Seebeck coefficient, its value varies with the hot side temperature, namely  $T_1$ .  $R_{ex}$  is the external load, it is determined by the module load  $R_m$

$$Q_{output} = c\rho G(T_{outlet} - T_{inlet}) \quad (6-4)$$

Where,  $c$  and  $\rho$  are the heat specific capacity and density of water.

$$Q_{loss} = h_{ins} A_{ins} (T_h - T_a) \quad (6-5)$$



Where,  $h_{ins}$  and  $A_{ins}$  are heat transfer coefficient and the exterior surface area of heat source.

Therefore, for this experimental study, the heat source capacity  $Q_{input}$  can be determined. In the experimental study, heat transfer oil is used as the heat medium, whilst electrical heater is used to simulate the heat source at the required temperature  $T_h$ . The tank size decides the required time period for heating the oil up to  $T_h$ .

For a single block, the tank size is designed as 60mm×60mm×40mm, shown in Figure 6-1. The oil volume is  $V_o = 144ml$ . The time length of heating the oil to  $T_h$  is calculated by Eq.(3-4):

The required heat amount to heat the oil from ambient temperature to 250°C is 70329 J. Hence, for a heat input at 1kW, it takes at least 70s for the oil to be heated up to 250°C. However, it takes less time for the system to produce electricity and hot water because the electrical power is generated with the presence of temperature gradient.

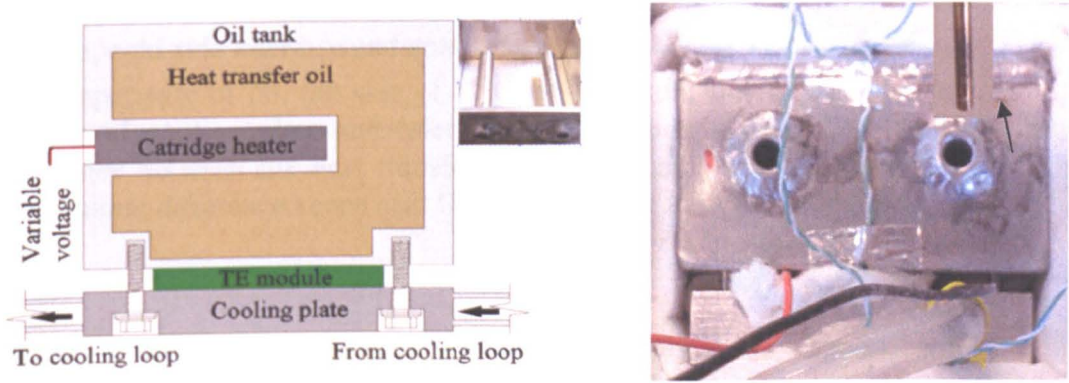


Figure 6-1 Schematic diagram and photo of TCS with single module

When the heat is supplied on the hot side, the total heat flux is split into two directions. One is flowing through thermoelectric module (part is for power generation and the rest is absorbed by heat sink), the other escapes into the ambient environment, shown in Figure 6-2. The distribution of heat flux is demonstrated by Eq.(6-6),

$$Q = Q_{loss} + Q_{sys} \quad (6-6)$$

In real application,  $Q_{loss}$  represents the heat flux that flows into environment, namely heat loss. It needs to be maintained at the possibly lowest level. That means a good thermal insulation is needed to prevent the heat to escape to the environment,  $R_{ins}$  is the thermal resistance of system thermal insulation.  $Q_{sys}$  represents the heat flux that flows into the system.

Assuming the temperature of inlet water into cooling plate is the same as the environment temperature, the thermal cycle of the whole system can be explained by Figure 6-2.

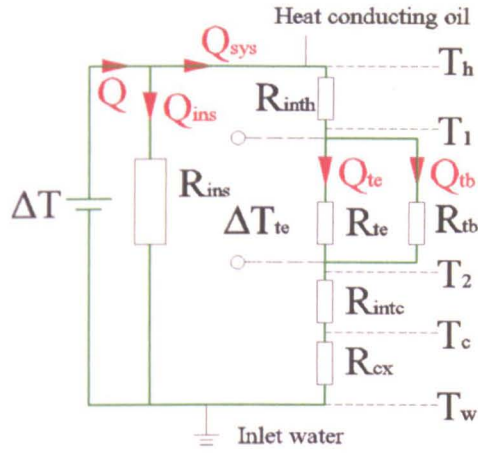


Figure 6-2 Schematic diagram of heat flux distribution in single-stage TCS

In Figure 6-2,  $Q$ ,  $Q_{ins}$  and  $Q_{sys}$  are the total thermal flux, thermal flux to the environment and thermal flux to the system, respectively.  $R_{ins}$ ,  $R_{inth}$ ,  $R_{te}$ ,  $R_{intc}$  and  $R_{cx}$  represent the thermal resistance of insulation, hot side interface, thermoelectric module, cold side interface and cold side heat exchanger;  $T_h$ ,  $T_1$ ,  $T_2$ ,  $T_c$  and  $T_{inlet}$  are the temperature of oil, hot side of TEG module, cold side of TEG module, cooling surface of cooling plate and inlet water of cooling plate,  $\Delta T$  is the temperature difference between the heat transfer oil and the inlet water to cooling plate. This temperature difference keeps heat flow in the whole system.

$$\Delta T = Q_{sys} R \quad (6-7)$$

Where,  $R$  is the system thermal resistance, it equals to the value of connecting the thermal resistance of the system and the insulation layer in parallel. Hence,  $R$  can be described by Eq.(6-8):

$$R = \frac{1}{1/R_{ins} + 1/R_{sys}} \quad (6-8)$$

Where,  $R_{sys}$  is the system thermal resistance.

As shown in Figure 6-2,  $\Delta T_{te}$  is the temperature difference established at the two sides of thermoelectric module. The larger  $\Delta T_{te}$ , the bigger the conversion efficiency is. So for a given  $\Delta T$ , the maximum  $\Delta T_{te}$  can be obtained by achieving the following four aspects:

First, the system needs to be well insulated to minimize the system heat loss. Second, the thermal resistance of hot side interface and cold side interface needs to be maintained at a low level to make sure the temperature drops  $\Delta(T_h - T_1)$ ,  $\Delta(T_2 - T_c)$  and  $\Delta(T_c - T_w)$ , as small as possible. Third, the thermal resistance of cold side heat exchanger needs to be maintained at possibly lowest level. Finally, the thermal bypass effect needs to be minimized, which means the thermal resistance of thermal bypass needs to be maintained at the possibly biggest level.

$$\Delta T_{te} = \Delta T R_t / (R_{int h} + R_t + R_{int c} + R_{cx}) \quad (6-9)$$

Where,  $R_t$  is the thermal resistance of TE module and thermal bypass which are connected in parallel, namely  $R_t = 1/(1/R_m + 1/R_{th})$ .

The power output can be obtained under given operating temperature difference as calculated by Eq.(6-10):

$$P = \eta_m Q_{input} \quad (6-10)$$

Where,  $\eta$  is the conversion efficiency of thermoelectric module,  $Q_{input}$  is the heat flux.

In order to obtain a maximum temperature difference between the two sides of TE module under a given temperature difference,  $R_t / (R_{int h} + R_t + R_{int c} + R_{cx})$  needs to be maintained at the maximum level. For given TE modules,  $R_t$  is constant. Hence,  $R_{int h}$ ,  $R_{int c}$  and  $R_{cx}$  are thermal resistance which needs to be maintained at the lowest level.  $R_{int h}$  and  $R_{int c}$  are determined by pressure load, thermal interface material and mechanical fabrication factor, whilst  $R_{cx}$  is determined by the heat transfer coefficient of cooling plate, which relies on the design of cooling plate.

In real applications, the optimum pressure should be evenly loaded to the surfaces of TE module (up to 200 psi). The optimum pressure load, which delivers the maximum thermal conductivity, makes sure the surfaces attached together with the maximum contact area without causing any damage to TE module. The corresponding mechanical assembling method for achieving this optimum pressure load is to be developed. In the fabricating process, the surfaces of TE module and heat exchangers need to be made with reasonably good flatness. However, no matter how mechanically flat they look in human eyes, the surfaces still have microscopic irregularities on the surface which together form gaps between two attached surfaces. These gaps deteriorate the heat transfer performance by increasing the thermal resistance. Thermal interface material is needed to fill this gap to mitigate this effect and ensure the heat conduction occurs on the maximum contact area. The achievable maximum contact area relies on the categories of thermal interface materials. The physical properties of thermal interface materials not only determine how well the gaps can be filled, but also the thermal conductivity of the interface. Thermal bypass does exist in the system during operation especially when the operating temperature is very high. Hence, the impact of thermal bypass to system performance and effective assembling methods for eliminating thermal bypass is investigated in this research, which is introduced in section 6.5.

As we know, if either the heat source or heat sink had a large thermal resistance, the heat flux that is supplied to the generator would be reduced. Heat exchangers used as sinks and sources are often characterized by a thermal resistance  $R$  which is defined as the temperature difference divided by the amount of heat flow ( $\Delta T = QR$ ). The temperature drop across the heat exchanger is proportional to the heat supplied.

In the practical experiment, it is difficult to accurately measure the temperature at the two ends of thermoelectric element. Instead, the hot side and cold side temperature is



measured from the surface of ceramic substrate. These temperatures are used to calculate the conversion efficiency of thermoelectric generators in the domestic TCS. The conversion efficiency calculated in this way is called module conversion efficiency rather than element conversion efficiency. This applies to all the data represented in this study.

### 6.1.2 Two-stage TCS

For single-stage TCS, there is a limit to the convertible energy since the unabsorbed energy, which represents a large contingent (over 95%), is expelled to environment or coolant. This is because of the low conversion efficiency given by the current commercially available thermoelectric generators. This fact brings about the idea of using the unconverted energy for the second conversion, which consequently strikes the author with the concept of two-stage TCS. It creates a new path for the unabsorbed heat to flow towards the low subsystem rather than escape to the environment. In this way, the coefficient-of-performance of the system might be increased by utilising overall heat input to the maximum level. Hence, two-stage TCS or multi-stage TCS is of some use in possibly improving the coefficient-of-performance when the operating temperature is high. However, this technical and economical viability of this system concept needs to be studied by measuring the overall conversion efficiency in comparison with that of one stage TCS. It is highly necessary to investigate this cogeneration system in two-stage, which is able to provide the information for the future study.

The optimum design of a two-stage or multi-stage TCS is not a simple matter since the optimum figure-of-merit for one stage is different from some other stage at different mean temperature. Here, this general case for multistage TCS is going to be discussed.

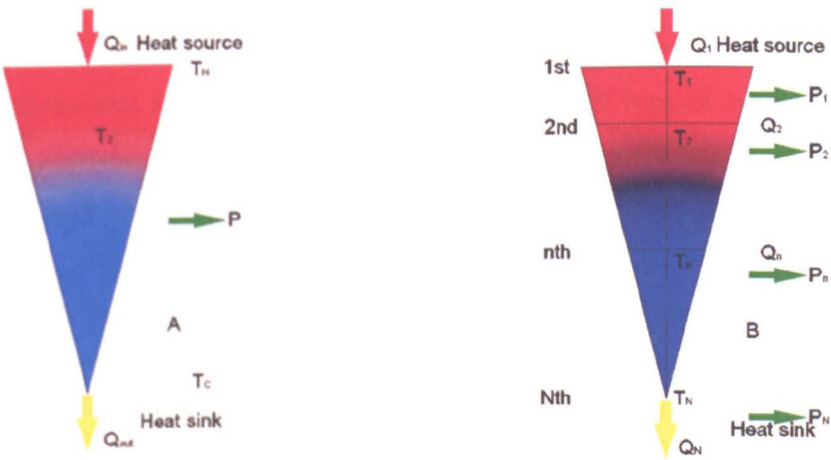


Figure 6-3 Schematic diagram of TCS working mechanism, A. Single-stage TCS; B. Multi-stage TCS

Let's suppose there is a N-stage TCS (shown in Figure 6-3), the Nth stage is bound to operate at the lowest temperature. Then the nth stage ( $n < N$ ) must have a thermal energy that is the sum of energy used at the (n+1)th, (n+2)th, ... Nth stage. The conversion efficiency of the nth stage is defined as  $\eta_n$  and the heat output at the nth stage is  $Q_n$ .



The power output at nth stage is  $P_n = \eta_n Q_n$ . The dissipated heat from nth stage is used as energy input for the (n+1)th stage,  $Q_{n+1} = Q_n(1 - \eta_n)$ . Therefore, theoretically the overall conversion efficiency of the system is

$$\eta = \eta_1 + \eta_2(1 - \eta_1) + \dots + \eta_n(1 - \eta_1)(1 - \eta_2) \dots (1 - \eta_{n-1}) \quad (6-11)$$

Where  $\eta_1, \eta_2 \dots \eta_N$  are the conversion efficiency of each stage, they can be calculated by Eq.(6-12)

$$\eta = \frac{T_1 - T_2}{T_2} \frac{\sqrt{1 + ZT} - 1}{\sqrt{1 + ZT} + T_c / T_h} \quad (6-12)$$

Where,  $Z = S^2 / \rho_T k_T$ ,  $\eta$  is the conversion efficiency,  $T_1$  is the absolute hot-junction temperature,  $T_2$  is the absolute cold-junction temperature,  $T$  is the mean absolute temperature,  $Z$  is the figure of merit,  $S$  is the Seebeck coefficient which is used to quantitatively describe the magnitude of generated thermoelectric voltage in response to the temperature difference,  $\rho_T$  is the specific electrical resistivity, and  $k_T$  is the specific thermal conductivity.

The total power output can be expressed by Eq.(6-13)

$$P = [\eta_1 + \eta_2(1 - \eta_1) + \dots + \eta_n(1 - \eta_1)(1 - \eta_2) \dots (1 - \eta_{n-1})] Q_1 \quad (6-13)$$

For the single-stage TCS, the conversion efficiency is denoted as  $\eta^1$ , the total power output of the single-stage TCS is calculated by Eq.(6-14)

$$P = \eta^1 Q_{input} \quad (6-14)$$

Without experimental study, it is difficult to decide which type of system has higher thermal efficiency. However, theoretically the multistage TCS has a larger capability of absorbing heat from heat sources and is more flexible with utilising the absorbed heat.

For the two-stage TCS in this research, solar radiation is also absorbed in the second stage to promote the temperature level of the hot side of the second stage. Denoting the input of solar energy in second stage is  $Q_2^*$ . Then the total power output is described by Eq.(6-15):

$$P^* = \eta_1 Q_1 + \eta_2^* (Q_2^* + Q_1 - \eta_1 Q_1) \quad (6-15)$$

Where,  $\eta_2^*$  is the conversion efficiency when there is solar input at 2<sup>nd</sup> stage.

For the case without heat input in the second stage, the total power output can be expressed by Eq.(6-16).

$$P = \eta_1 Q_1 + \eta_2(1 - \eta_1) Q_1 \quad (6-16)$$

So for two-stage TCS with heat input in second stage, the increased power output is given by Eq.(6-17).

$$\Delta P_{te} = \eta_2^* Q_2^* + (\eta_2^* - \eta_2)(1 - \eta_1) Q_1 \quad (6-17)$$

Therefore, extra power output might be obtained if heat could be inputted at other stages.

When we talk about the thermal efficiency of TCS which produces electrical power and hot water for residential houses, a different evaluation standard should be established. Conventional thermoelectric applications generally are designed for power generation only. The heat is normally expelled into the environment without being used for other purposes. The reasons lie in either the application areas where there is no suitable application that can use the dissipated heat or the temperature level is too low to be reused.

However, the TCS discussed here is designed for domestic use. With the presence of available heat sources, it can produce electrical power and hot water or preheated water for other purposes in domestic environment such as the boiler. Namely, this type of system has two outputs: power output and heat output. Therefore, it is insufficiently accurate to use the traditional performance standard to evaluate this TCS investigated in this research study. Considering this situation, a new evaluation model for domestic TCS is going to be established. This model applies to both single-stage TCS and multi-stage TCS.

The generated electrical power can either be used by the inhabited house or passed onto the grid. The expelled heat from the heat sink can either be used directly in the house or further heated by the domestic boiler before delivered to central heating system (The necessity of being further heated or not depends on the need of temperature level).

## 6.2. Experimental study for one stage TCS

### 6.2.1 System description

The domestic TCS in Figure 4-2 shows the concept of domestic thermoelectric cogeneration system which is designed to be integrated with the existing boiler system. One primary heat source is from a solar collector mounted on the roof of a building whereby solar energy is absorbed and supplied to the thermoelectric module hot side. This can be achieved by direct utilisation or indirect utilisation of solar energy, depending on the heat exchanger design. Two concepts of hot side heat exchanger are shown in Figure 6-4. Figure 6-4 (A) shows the indirect use in which heat transfer oil absorbs the heat from boiler waste and solar energy. The oil is heated up by the absorbed energy and flows through the TE module to proceed with the energy conversion and water preheating. Figure 6-4 (B) shows the direct use where the solar energy and boiler waste heat is used to heat the TE hot side skipping the use of heat transfer oil. The selection can be made according to characteristics of heat sources and requirements on the system reaction time. Solar concentration measures can also be taken to promote the temperature level at the heat source side. A cooling fluid is then circulated through a compact liquid heat exchanger on the cold side of the TE module to establish temperature difference for energy conversion and preheating. The other primary heat source is waste heat from the boiler exhaust.

It can be used to generate “free” electricity and attendant heat is used for heating purposes, increasing the overall energy utilisation efficiency of the boiler.

The heat rejected from the cold side of thermoelectric modules is taken away by the cooling plate which is connected to the boiler to provide the preheated water. The water goes into cooling plate to get preheated by absorbing the heat from the cold side of thermoelectric generators before enters the boiler for further heating. The generated electricity can either be used to power DC appliance like LED lights, or charge the battery for later use, more details are discussed in section 6.4. As a building block designed with a universal interface, it could be compatible with the presence of other available heat sources.

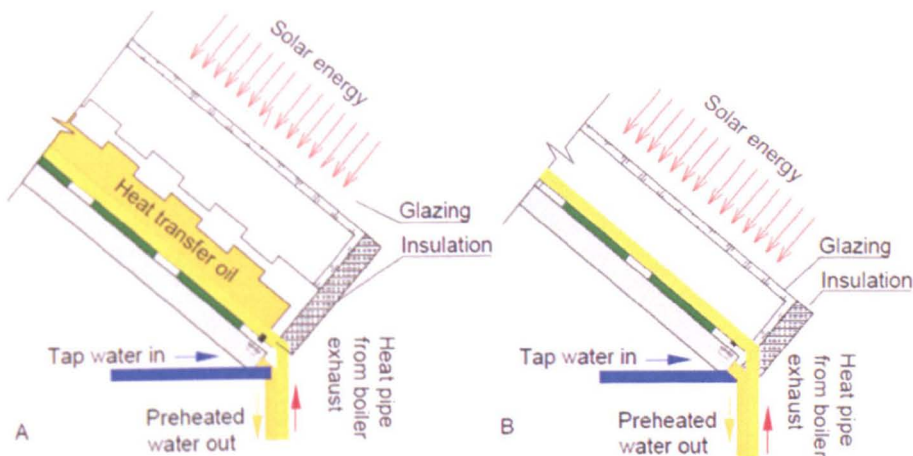


Figure 6-4 Schematic diagram of hot side heat exchanger

Experimental tests have been carried out on a bench-scale experimental prototype to investigate its performance as a building block producing electrical power and preheated/hot water. The prototype is classified according to the system assembling type into: whole assembly and individual assembly, shown in Figure 6-5.

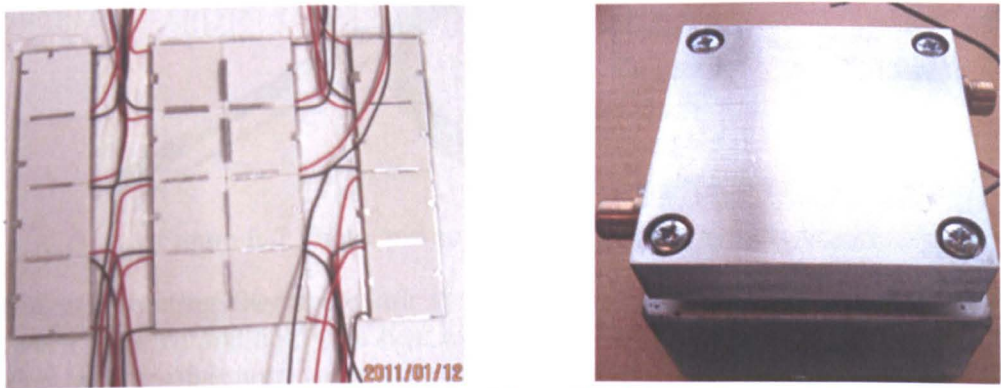


Figure 6-5 Whole assembly and individual assembly

In the whole assembly, shown in the thermoelectric block includes 16 modules, a cold side and hot side heat exchanger. Each module, made of  $\text{Bi}_2\text{Te}_3$ , has a dimension of  $40\text{mm} \times 40\text{mm} \times 3.8\text{mm}$  with 127 pairs of semiconductor elements. The following issues need to be addressed for a well-designed mounting system which should consider the importance of uniformly distributing the pressure load on the module surface to achieve optimum power performance and avoid damaging the module.



They are optimum pressure load, thermal expansion, thermal interface material and assembling configurations.

Heat exchangers are the devices that make sure the heat flux flow through the system effectively. In thermoelectric cogeneration system, heat exchangers include hot side heat exchanger and cold side heat exchanger. The hot side heat exchanger shoulders the responsibility of extracting energy from available heat sources and supplying the heat to the system for further operation. The cold side heat exchanger dissipates the heat away from the cold side of TE modules and expels it into coolant which is preheated before goes for further heating in the domestic boiler. In the experimental study, an oil tank with embedded cartridge heater has been designed as the heat source for thermoelectric module. Heat conducting oil is stored in the oil tank to obtain an even temperature distribution on the surface that the modules are attached to.

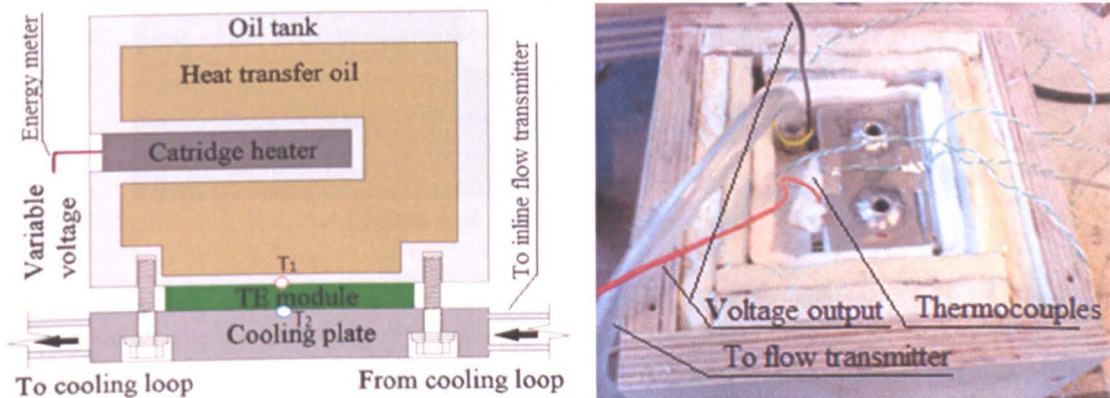


Figure 6-6 Schematic diagram and photo of the single TE block system

The heat source is simulated by two electric heaters rated at 100W which provide heat input to the system at adjustable voltage input, shown in Figure 6-7.



Figure 6-7 Photo and specifications of the electric heater

When constructing thermoelectric system, thermoelectric modules are sandwiched between hot side and cold side heat exchanger. The compression needs to be evenly loaded at the optimum value across the module surfaces to maximize the heat transfer between heat exchangers and thermoelectric module. The way that the module is being fixed between heat sink and heat source plays an important role in determining the efficiency of heat exchanging, thus the module performance. If the module was clamped to the heat source and the heat sink by simply bolting along the edges of the heat source and heat sink, bowing could occur, then large pressure would be loaded at the edge of module whilst a gap would form in the central area. A non-uniform temperature distribution (such as hotspot) across the module surface would be caused, poor performance from the module and even permanent damage to the module if the force at the perimeter is too large, like micro-cracking in



thermoelectric element and broken edges of ceramic substrates. The correct clamping method needs to achieve even load distribution across the module surface, accommodation of thermal expansion and small thermal bypass.

In assembling procedures, corresponding measures have been taken to eliminate or reduce the negative impacts caused by the aspects mentioned above. More details can be referred in section 6.5.

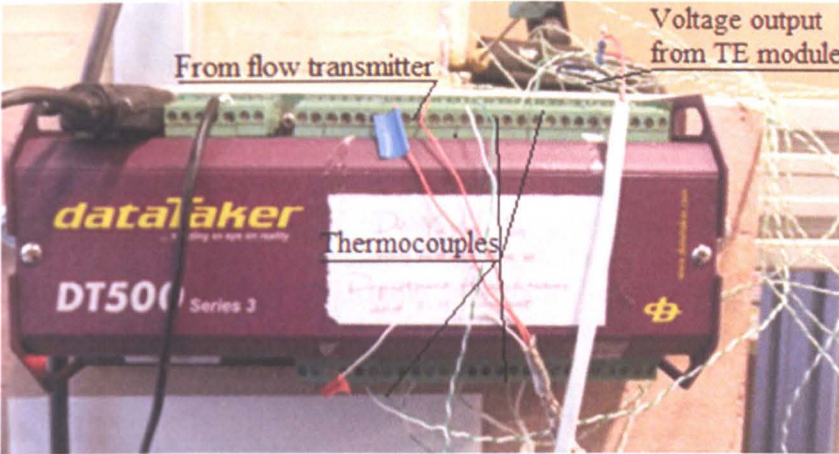
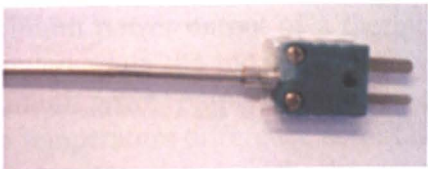


Figure 6-8 Acquisition data unit

The acquisition unit collects the temperatures (TE module hot side and cold side, cooling water inlet and outlet), flow rate of cooling water and voltage output of TE module, the wiring details are shown in Figure 6-8. The temperature are measured by k-type thermocouples, which are installed on the module surfaces, the positions are shown in Figure 5-42 and Figure 6-6 (indicated by  $T_1$  and  $T_2$  ). The water temperatures at the inlet and outlet of cooling plate are measured by two K type insulated thermocouple plugs; the photo and specifications are shown in Figure 6-9 (A). The temperatures at the module hot side surface and cold side surface are measured by K type thermocouple cable, shown in Figure 6-9(B).



Thermocouple Type	K
Max temperature sensed	+1100°C
Max temperature sensed	0°C
Probe Diameter	3mm
Probe Length	150mm

A



Thermocouple type	K
Max temperature sensed	250°C
Min temperature sensed	-50°C

B

Figure 6-9 Photos and specifications of thermocouples

The module is cooled down by water flow which is circulated in a cooling loop. The flow rate is measured by an inline flow transmitter, whose specifications can be referred in Figure 6-10 and the installing position is shown in Figure 6-11. A fan assisted condenser is used to dissipate the heat in water at different temperatures by

changing the fan speed.

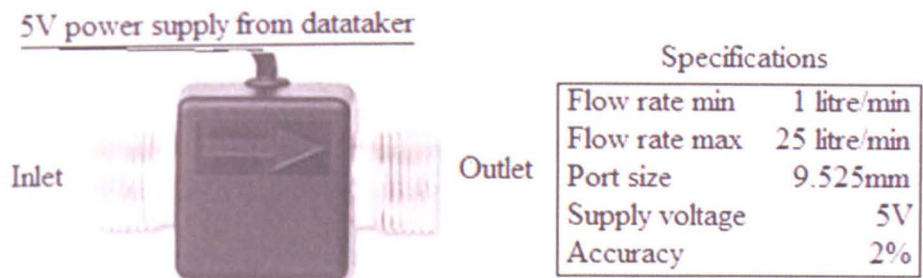


Figure 6-10 Photo and specifications of inline flow transmitter

Cooling loop consists of a water pump, a condenser, a cold plate, a water reservoir and a water tank, see Figure 6-11. It uses circulating water to dissipate the heat extracted from the cold side of thermoelectric modules to the circulated water. The condenser, whose fan speed is adjustable due to the use of fan speed controller, makes sure the temperature at the cold side of thermoelectric is controllable.

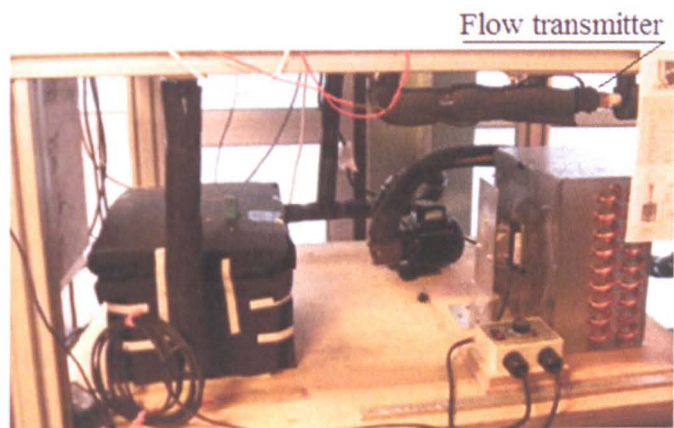


Figure 6-11 Cooling loop for single-stage TCS

6.2.2 Measurement

Maximum power output of a thermoelectric module is defined as the power output generated when the module resistance matches the load resistance. In principle, the maximum power output of a thermoelectric module can be measured readily when it has a temperature difference across it. However, a proper circuit which minimises the problems associated with the very low thermoelectric module resistance and fluctuations in signal measurements is needed to measure the power output accurately.

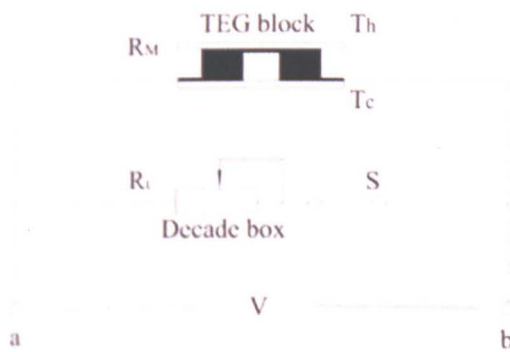


Figure 6-12 Circuit for measuring the maximum power output and internal resistance

In Figure 6-12, a circuit designed for accurately measuring the internal resistance and maximum power output overcomes these problems. When a temperature difference is established across the module, voltages  $V_1$  and  $V_2$  are measured at terminals a and b when the switch is open and closed, respectively. The maximum power output of the module can be calculated using Eq.(6-18)

$$P_{\max} = \frac{V_1^2}{4R_L(V_1/V_2 - 1)} \quad (6-18)$$

Where,  $R_L$  is the load resistance which includes contributions from all the wires and connections in the circuit. The electrical resistance of a module can be obtained from Eq.(6-19).

$$R_M = R_L(V_1/V_2 - 1) \quad (6-19)$$

In general, the optimum thermoelectric conversion efficiency depends on the device figure-of-merit and the temperature difference between the two ends of TEG. The conversion efficiency would be higher with a larger temperature difference and a greater value of figure-of-merit.

Power output and heat output have been measured to understand the system capacity and more importantly the performance characteristic under different operating conditions. The purpose of this study is to shed an insight to the potential application of thermoelectric cogeneration system in domestic environment and provide guidelines for the design and fabrication of thermoelectric building blocks. Maximum power output  $P_{\max}$  is defined as the power output generated when the load resistance is matched with the modules resistance. The load resistance  $R_L$  is matched with the modules resistance  $R_M$  by adjusting decade box.

The TE module is cooled by circulating water through the cold plate heat exchanger and rejecting it through a fan cooled condenser. The temperature at the heat source and heat sink is measured using K-type thermocouples and the flow rate of cooling water is measured by an inline flow transmitter. The thermocouples were located in slots machined on the surface of the heat exchangers to eliminate the bad contact by installing the thermocouples. The temperature, flow rate and voltage are recorded by a DT500 series 3 datataker, shown in Figure 6-8. A decade resistance box ranging from (1Ω-100kΩ) is connected to TE module to provide adjustable external load.

### 6.2.3 Electric performance

At steady state when a temperature difference is established across the TE module, the theoretical maximum power output from the module is given by Eq.(6-18).

A commercial TE module was tested with the heat input at 47W and 93W. The optimum external load electrical resistance was first determined corresponding to the maximum power output. This is achieved when the internal resistance of the module is equal to that of the external load.



Figure 6-13 shows the measured power output of the module as a function of the external load resistance. Maximum power output is achieved at an electrical resistance of  $3.61\Omega$  and  $3.82\Omega$  when the heat is supplied at 47W and 93W. The corresponding temperature of heat source and heat sink for the 47W and 93W is  $102^{\circ}\text{C}/31^{\circ}\text{C}$  and  $166^{\circ}\text{C}/34^{\circ}\text{C}$ , respectively. The maximum power output corresponds to a terminal voltage of 1.2V and load current 0.61A for the 47W and 2.73V and 0.91A for the 93W, respectively.

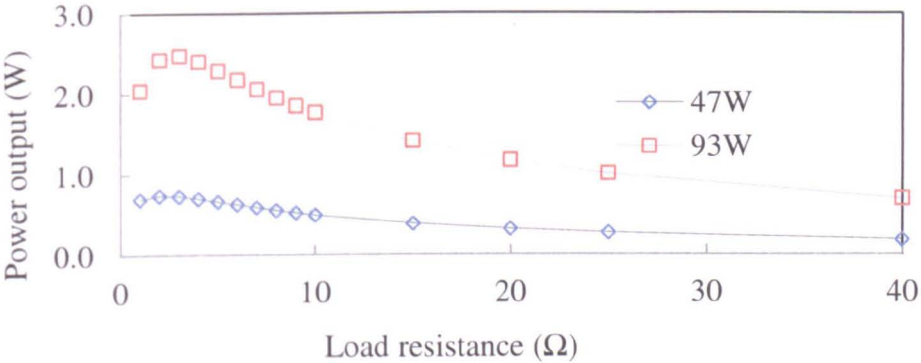


Figure 6-13 Maximum power output

Figure 6-14 shows the open voltage output and power output under different temperature difference. A linear correlation is shown between the temperature difference and open voltage which obeys this correlation:  $V = S\Delta T$ . Meanwhile, a parabola relationship is shown between temperature difference and maximum power output which also obeys the theory.

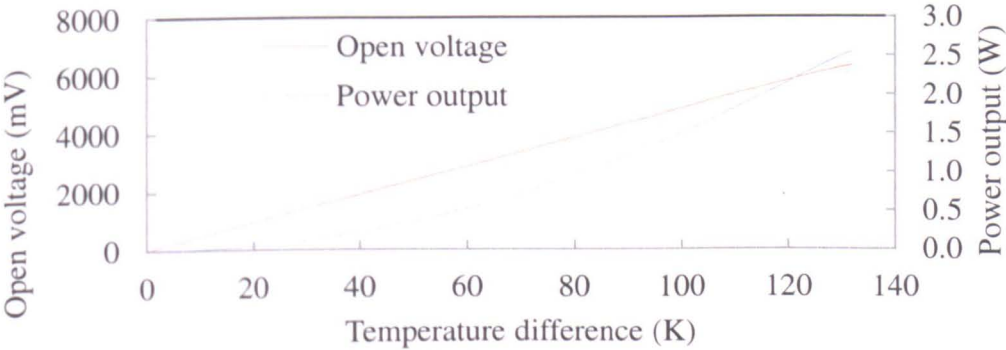


Figure 6-14 System open voltage output and power output at different temperature difference

The module electrical performance under different temperature gradients was determined by varying the heat source temperature while the heat sink temperature was constant. Figure 6-15 shows the maximum power output and conversion efficiency alongside the heat source temperature. The spots fluctuating around the main trend line can be omitted due to experimental errors. It shows that the conversion efficiency increases steadily when the temperature difference across the thermoelectric generator rises, whilst the power output increases more rapidly compared to conversion efficiency.



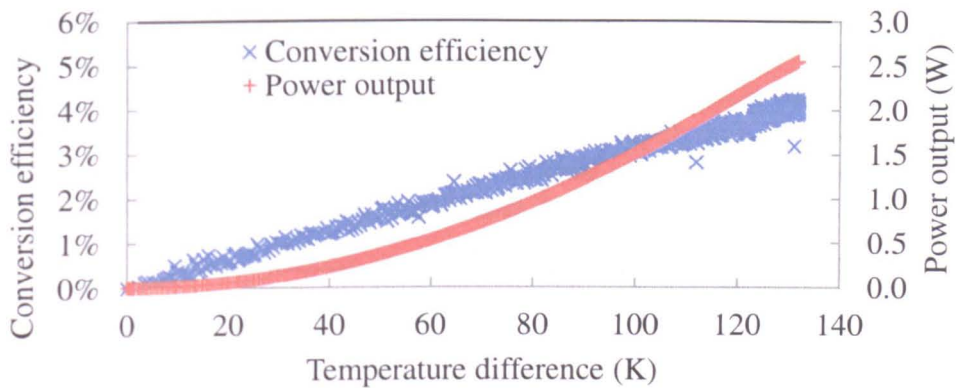


Figure 6-15 Maximum power output and conversion efficiency Vs. Heat source temperature

Understanding and measuring the maximum power output point is important in thermoelectric power generation application because it determines the design of external load which affects charging battery set or powering the electrical terminals.

The seebeck coefficient changes slightly with operating temperature. The values of seebeck coefficient of p-type element and n-type element, provided by the manufacturer, are given in Table 6-1.

Table 6-1 Seebeck coefficient of semiconductor elements of TE module

$T_1$ (°C)	30	40	50	60	70	80	90	100	110
$S_p$ (μV/K)	160	161	162	162.6	165.8	168.5	171	173.4	175.1
$S_n$ (μV/K)	184	185	186.4	188.1	189.5	190	191.9	192.7	193.2
$T_1$ (°C)	120	130	140	150	160	170	180	190	200
$S_p$ (μV/K)	178.4	179.2	180.9	182.1	183.6	184.3	184.4	184.1	183.6
$S_n$ (μV/K)	193.3	193.1	192.8	191.5	190.4	188.5	185.7	183.3	180

The relationship between the open voltage output and temperature difference is given by Eq.(6-20):

$$V_1 = N(S_p \Delta T_{te} + S_n \Delta T_{te}) \quad (6-20)$$

The maximum voltage output  $V_{\max}$  is achieved when the external load  $R_{ex}$  matches with the module resistance  $R_m$ , where  $V_{\max} = V_1 / 2$ . This is also when the maximum power output  $P_{\max}$  is obtained, it can be calculated by Eq.(6-21)

$$P_{\max} = V_{\max}^2 / R_m \quad (6-21)$$

The maximum voltage output and power output have been experimentally measured and calculated under different temperature differences up to 130°C, respectively. The theoretical results of voltage output and power output under different temperature differences (up to 200°C) have been calculated using Eq.(6-20), Eq.(6-21) and the data in Table 6-1, and compared with the experimental results, shown in Figure 6-16 and Figure 6-17. In Figure 6-16, a good consistency is shown between the experimental data and theoretical data of voltage output. In Figure 6-17, two theoretical data of power output is compared with the experimental data. In the

experiment, the module electrical resistance has been measured as  $3.82\Omega$ , whereas the data provided by the manufacturer is  $4.3\Omega$ . Hence, the theoretical data has been given based on two of them separately. If based on the module electrical resistance measured in the experiment, the theoretical power output shows a good consistency with the experimental data. If based on the module electrical resistance provided by the manufacturer, the theoretical power output drops slightly.

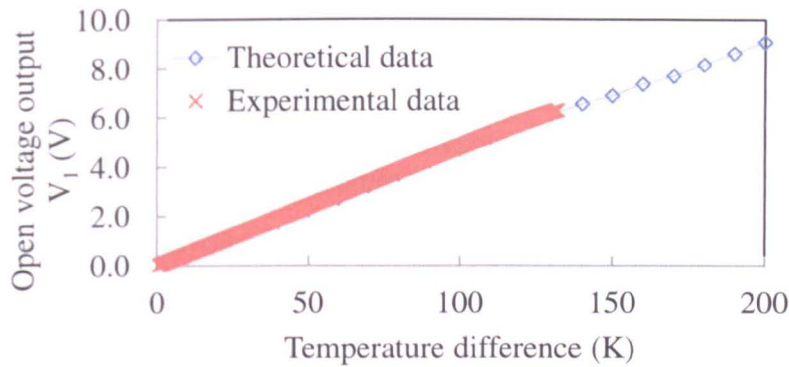


Figure 6-16 Experimental voltage output and theoretical voltage output under different temperature difference

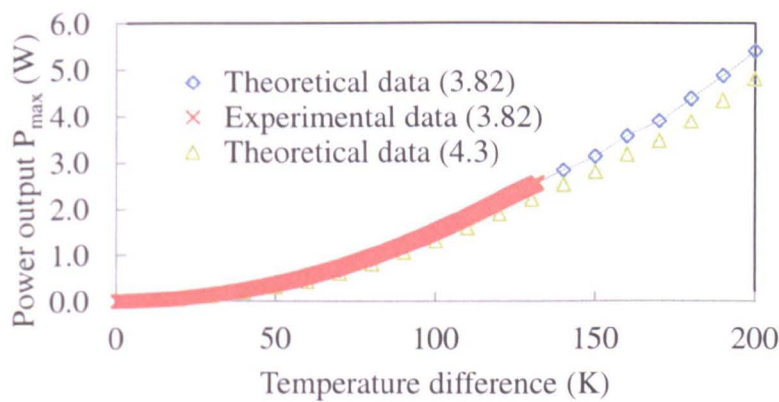


Figure 6-17 Experimental power output and theoretical power output under different temperature difference

#### 6.2.4 Thermal performance

At steady state The thermal performance of the TE co-generator was determined by measuring the heat recovered from different heat source temperatures when the heat sink temperature remains constant. Then the thermal efficiency is shown in Figure 6-18, which illustrates when the temperature difference across the modules increases, the conversion efficiency gives a rising trend, whilst the thermal efficiency shows a steady declining. The increase in conversion efficiency can be attributed to the rise of temperature difference across the TE module, which leads to the increase of power output.

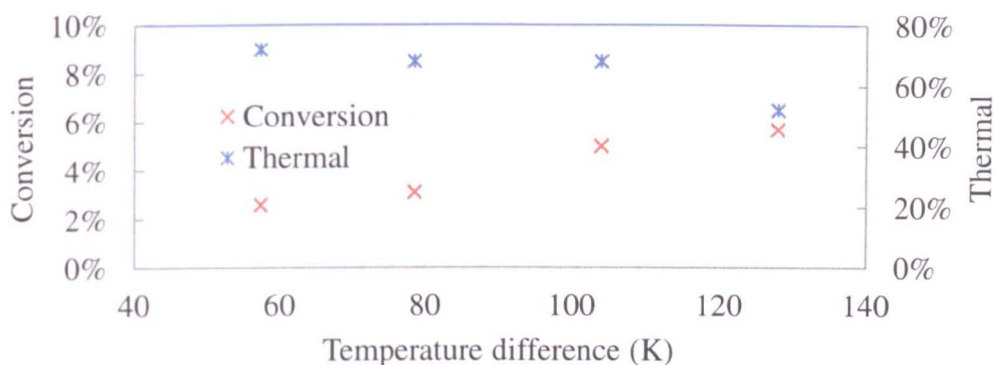


Figure 6-18 Thermal efficiency and conversion efficiency under different temperature differences

An average value of heat output was calculated from the test results in each time length, the result is shown in Figure 6-19. The accuracy of the results shown below has been further proved by another set of experiment which delivers the same system performance. The temperature rise of the coolant through the cooling plate increases along with the decrease of inlet flow velocity. The heat output goes up slightly along with the increase of the inlet flow velocity, as shown in Figure 6-19.

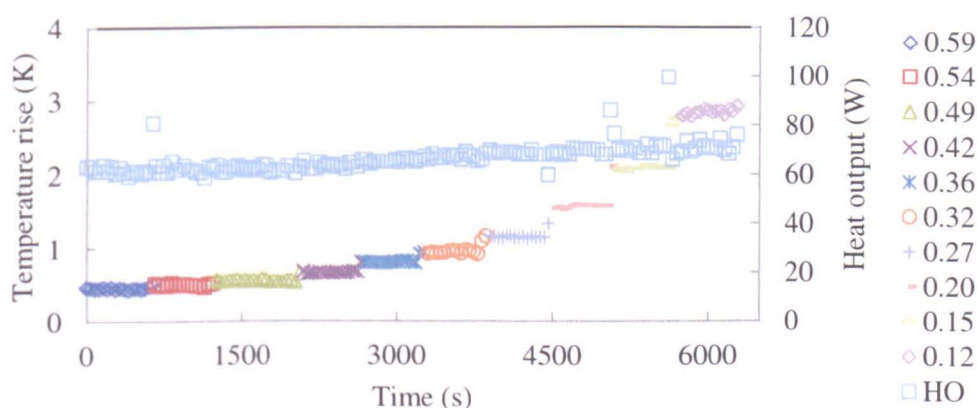


Figure 6-19 Heat output (HO) and corresponding temperature rise of coolant that flows through the cooling plate at different inlet coolant velocity

### 6.3. Experimental study of Two-stage TCS

#### 6.3.1 System introduction

The system, consisting of hot side heat exchanger, two heat pipe blocks, a heat pipe, a cold side heat exchanger and two thermoelectric modules, produces electrical power at two stages. The first stage is established by the hot side heat exchanger, a thermoelectric module and a heat pipe block. The thermoelectric module is sandwiched between the hot side heat exchanger and the heat pipe block. The second stage consists of a heat pipe block, a thermoelectric module and the cooling plate. Figure 6-20 and Figure 6-21 show the photo and schematic diagram of two-stage TCS, respectively.



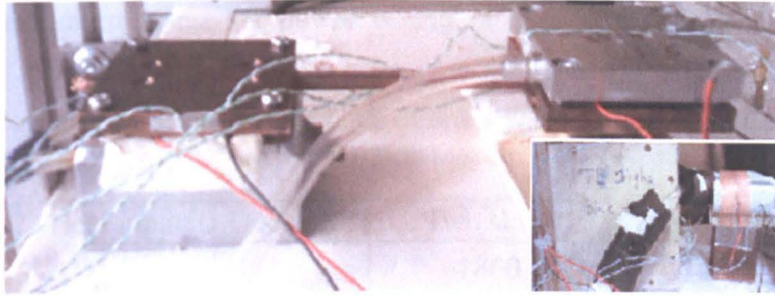


Figure 6-20 Test rig of two stage thermoelectric cogeneration system (the image at the right bottom corner shows the insulated two-stage TCS)

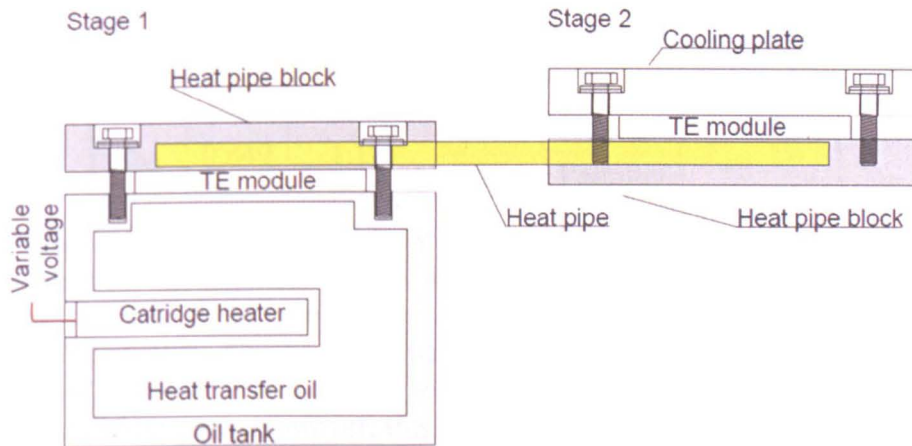


Figure 6-21 Schematic diagram of two stage thermoelectric cogeneration system

In the first stage, the hot side heat exchanger provides the high temperature by absorbing heat from available source. The heat is conducted from the hot side heat exchanger to the heat pipe block through the module. The heat on the heat pipe block on the evaporation end is taken away by the heat pipe and passed to the condensation end of the heat pipe.

In the second stage, the generation unit consists of the condensation heat pipe block, a thermoelectric module and the cooling plate. The heat passes from the heat pipe block, through the module and to the cooling plate where the water takes the heat away.

### 6.3.2 Performance

In order to understand the performance of two stage system, experimental studies have been conducted and compared with one stage performance under the same heat input. Due to the use of heat transfer oil in the hot side heat exchanger, it takes time for the system to reach the stable operating condition. Each set of the test takes about 1.5 hours to reach the stable level. The results are shown in Table 6-2.

$R_{2/1}$  is defined as the power output ratio of two-stage TCS to one-stage TCS under the same heat input. It characterizes the performance of two-stage TCS in comparison with one-stage TCS. Table 6-2 shows  $R_{2/1}$  at two different heat inputs. When the heat input is 47W, the power output ratio  $R_{2/1}$  is 0.584, whilst  $R_{2/1}$  rises up to 0.849 when the heat input is increased to 60W. In another way of saying, when the



operating temperature rises, the power output of two stage TCS shows the rising trend.

Table 6-2 Power generation performance of one stage and two stage thermoelectric cogeneration system

Heat input		One stage	Two stage		Result
47W		3475	1860		$V_{1st}$ (mv)
			1898		$V_{2nd}$ (mv)
$R_{2/1}$	0.584	0.873	0.510	Serial	$P_{\max}$ (W)
			0.510	Parrallel	
60W		4040	2279		$V_{1st}$ (mv)
			2943		$V_{2nd}$ (mv)
$R_{2/1}$	0.849	1.179	1.001	Serial	$P_{\max}$ (W)
			0.985	Parrallel	

Due to the limitation of maximum operating temperature of heat pipe, the experimental test has been carried out at three different heat inputs, 47W, 60W and 93W. The test has been successfully conducted under the first two heat inputs, namely 47W and 60W. However, the heat pipe doesn't work normally when the heat input is 93W because the operating temperature exceeds the maximum operating temperature of heat pipe. However, this trend leads us to speculate the possibility of approaching 1 could be achieved when this two-stage TCS operates at higher temperature. This can be initially proved by the temperature difference rising trend shown in Figure 6-22.

By using two-stage TCS, thermal energy can be converted at two stages. However, the temperature gradient is divided by the two stages as well. More heat loss occurs when the heat flux flows from the primary stage and secondary stage of the system. The main reason lies in the degradation of temperature level which leads to a lower conversion efficiency.

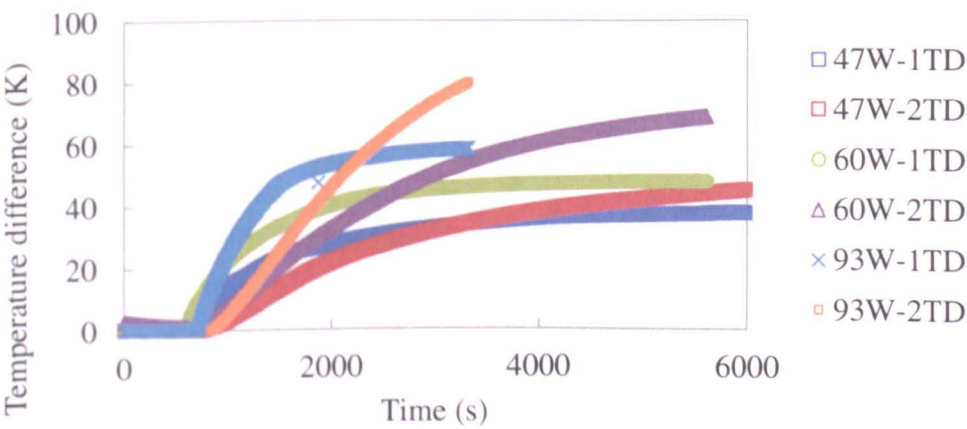


Figure 6-22 Temperature difference developing trend under 47W, 60W and 93W

Where, 1TD and 2TD stand for the temperature difference at the stage 1 and stage 2, respectively.

## 6.4. Energy management

### 6.4.1 Thermal energy

The concept of TCS is suitable for the areas where the waste heat is available and the thermal energy is needed. Taking the domestic environment as an example, heat output is one of the two energy products from thermoelectric cogeneration system. The heat output can be utilised for under floor heating or preheated feed water for domestic boiler. In this integration, a few aspects need to be considered in order to ensure the normal operation of the boiler and an effective use of thermal energy harvested from the cold side of TCS.

Waste heat is only available when the boiler is running. The availability of heat output and the operating condition of boiler needs to be discussed under a few circumstances. The existence of heat output is determined by the availability of heat source, which consists of boiler waste heat and solar power. There are three possibilities of the existence of the heat output as follow:

1. Solar power: Boiler is not running, only solar power is available;
2. Boiler waste heat: Boiler is operating but the solar power is not available;
3. Solar power plus boiler waste heat: The boiler is running with the presence of the solar power.

In case 2 and case 3, the presence of heat output can be matched with the boiler operation, because the heat output is produced when the boiler is running. Namely, the boiler needs feed water. Then the feed water can be pre-heated by the unconverted heat dissipated from the heat sink side of TCS before it is fed to the boiler for further heating. Therefore, the thermal energy can be readily used by the boiler without considering additional configuration.

In case 1, the boiler is not running. Hence the feed water is not required by the boiler. There is no cooling at the heat sink of TCS. In order to keep the normal operation of TCS, measures must be taken to dissipate the heat from the heat sink so as to keep the required temperature gradient for energy conversion.

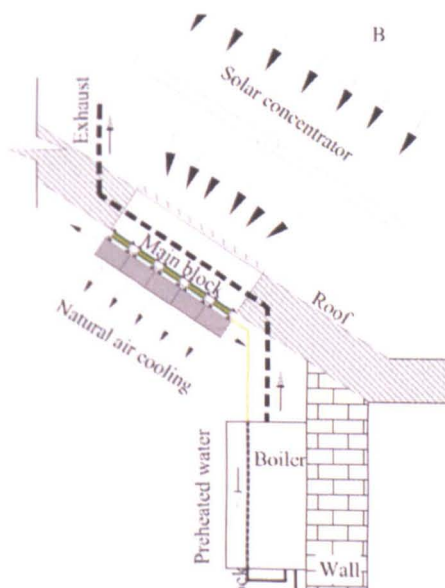


Figure 6-23 Natural air cooling for domestic TCS

Two measures can be taken to achieve this purpose, natural air cooling and water cooling. Figure 6-23 shows the concept of natural air cooling for the domestic TCS. In this concept, the heat sink is a heat exchanger with fins and water channel. It is capable of dissipating heat either through the water cooling or air cooling. When the feed water is required, the water cooling takes the major role of heat dissipation. When the feed water is not required, the heat can be dissipated through the fins via natural air convection or fan-assisted circulation. In this situation, the normal operation of the TCS and domestic boiler can be guaranteed by this heat sink design. However, one issue needs to be considered. The heat is dissipated into the room when the air cooling plays the major role of heat sink. In the case of summer time, the heat can lead to the temperature rise in the room where the heat is dissipated to. If the house in which this device is integrated locates in the region/countries where air conditioning is required in summer time, the heat dissipated into the room would impose a negative impact on the energy consumption of the house due to the increased power for air cooling from the extra heat load produced by TCS. This domestic TCS is designed for the countries with temperate climate, where normally the air conditioning is not required. Introducing fresh air by opening window could offset this dissipated heat. However, the impact, negative or not, needs to be verified by onsite experimental test. The concept is more suitable for the counties/ regions where the air conditioning is not required in summer time.

#### **6.4.2 Electrical power**

When the renewable such as solar PV and wind power provide electrical power, the process of balancing power supply and demand is always a complex issue. Energy storage can be an alternative method for managing the electrical power. Energy storage is accomplished by devices or physical media that store the power to perform useful operations at a later time.

Most renewable energy sources produce intermittent power which makes it difficult to match with the power demand. Energy storage becomes one option to ease this issue by storing the unused energy for later supply. There are three choices of charging battery using the generated electrical power: direct charging, charging by using a dc-dc converter and charging by using a dc-dc converted with MPPT (Maximum Power Point Tracking). The three methods deliver different charging performance due to varying condition of power output from thermoelectric generation. Eakburanawat [160] shows that the maximum chargeable power out of 8.4W power output using the three charging methods is 6.35, 7.63 and 7.99W, respectively.

In order to charge the battery efficiently, a DC-DC converter is needed to steady the voltage output due to the fluctuation caused by the varying external conditions. The selection depends on the range of power output. In many situations, the available voltage from the system is not suitable for direct battery charging. An efficient DC-DC converter is required to increase adjust the voltage output from the system to the input requirement of the charged device due to a better charging performance [160]. The input and output conditions of the electrical converter may vary with changes in thermoelectric power generation or the operating condition of charged device. In order to achieve an efficient charging over a wide range of operating conditions, the converter needs to be correctly designed. Single-ended primary inductance converter is a common type of dc-dc converter. A typical circuit diagram is shown in Figure

6-24. It has three dynamic energy storage elements,  $L_1$ ,  $L_2$  and  $C_1$ . The ratio of voltage output and the duty cycle are defined as:

$$M = \frac{V_{output}}{V_{input}} \tag{6-22}$$

$$D = \frac{t_{on}}{T} \tag{6-23}$$

Where  $D = \frac{M}{M + 1}$ , substituting it into Eq.(6-22) and Eq.(6-23), the voltage output can be expressed as:

$$V_{output} = \frac{D}{1 - D} V_{input} \tag{6-24}$$

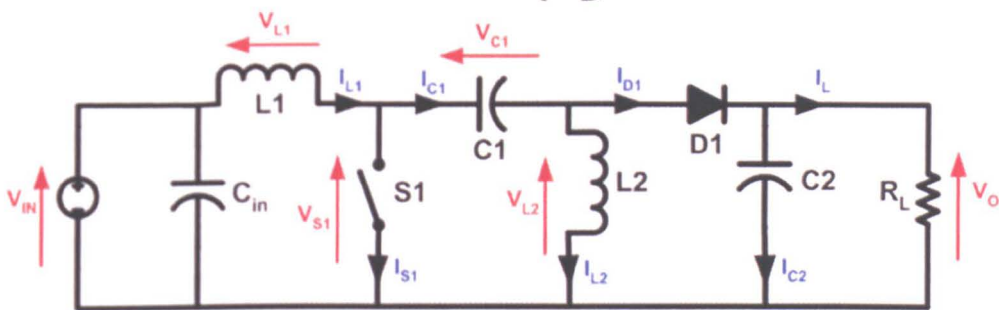


Figure 6-24 Schematic of Single-ended primary inductance converter (SEPIC)

The typical method is shown in Figure 6-25, the charging unit consists of three parts: thermoelectric generator, converter and battery set. The power output from thermoelectric generator is converted to the voltage level which is nominal for charging the battery set.

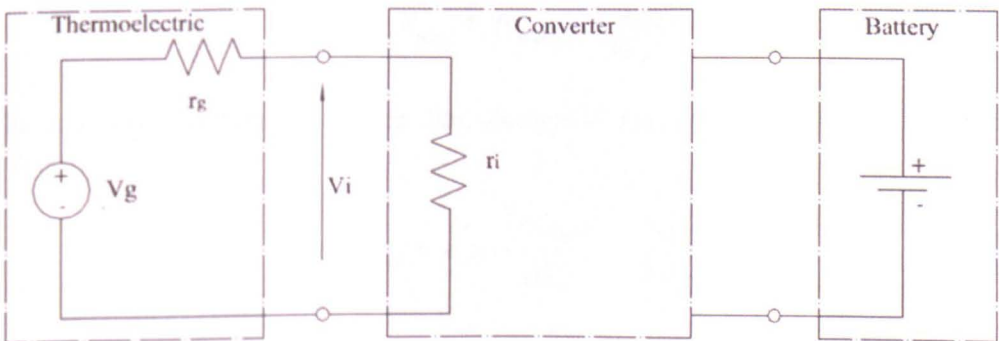


Figure 6-25 Schematic of typical battery charging setting

In the past few years, much work has been reported on the TE power generator. In [130], a MAX642 step-up switching regulator was used to work in the range of 5mW to 10W. Four modules were used to operate at the temperature difference of 160°C with a 7W power output. A 6V/4Ah valve regulated lead acid battery set was chosen for energy storage. The floating voltage is about 6.75V with a charging current at 0.75A. Anders [161] developed a stove-top generator using two modules, model HZ-20. During the operating time, the average output of the generator was about 10W



and supplied the battery with a net input from 1 to 5 W. A charging unit for laptop has been developed by Rahman [162] using thermoelectric generator powered by butane gas, which has a potential power output of 13.5W. A DC-DC step-up converter was used to stabilize the fluctuating voltage output for battery charging. The unit produces power output of 5 watts, which was said to double the life of the laptop's internal batteries. Roth et al. [163] developed and tested a photovoltaic/thermoelectric hybrid system as a power supply for a mobile telephone repeater. The developed system supplies enough for 50 W permanent loads. All of the above research uses the converter to boost-up the output voltage to charge the battery. The battery charging goal can be achieved but the power output is not maximally charged into the battery due to the fluctuation characteristics of power output.

An efficient charging method needs to be explored to charge the electrical power output into the battery to its possible full extent. The maximum power output is obtained when the external resistance load matches with the internal load. The thermal operating condition of the system varies with the condition of external condition of heat source. The availability and the amount of the heat that is provided by the heat source vary with time and condition. Consequently, the internal resistance load changes with the thermal condition as well. The external load resistance needs to be dynamically matched with the varying internal load resistance to make sure the power output can be obtained from the system.

In real application, the maximum power point varies with the temperature. A maximum power point tracking control method is introduced for the system. The maximum power transfer to the battery normally occurs when the input impedance of the converter is equal to the output impedance of thermoelectric generator. The input impedance of the dc-dc converter can be controlled by changing the duty cycle of gate driving signal, then the maximum power point of the power chargeable to the battery can be found. The rate change of the input power with respect to the input voltage and input resistance can be described by:

$$P_{input} = P_{output} = \frac{U_{input}^2}{R_{ex}} \quad (6-25)$$

At the maximum power point, the rate change of the input power should be zero. Therefore,

$$\partial P_{input} = 0 \Rightarrow \frac{\partial U_{input}}{\partial R_{ex}} = \frac{U_{input}}{2R_{ex}} \quad (6-26)$$

Where  $U_{input}$  and  $R_{ex}$  are voltage input and load resistance at the maximum power point respectively.

Koutroulis [164] introduced a method which used a feed-forward MPPT( maximum power point tracking) to control the battery-charging current directly by applying the duty cycle of the PWM control signal to the dc-dc converter in the battery charging process. An output power increase results in both a higher current output and a higher PWM control signal duty cycle, until the maximum power is charged to the load.

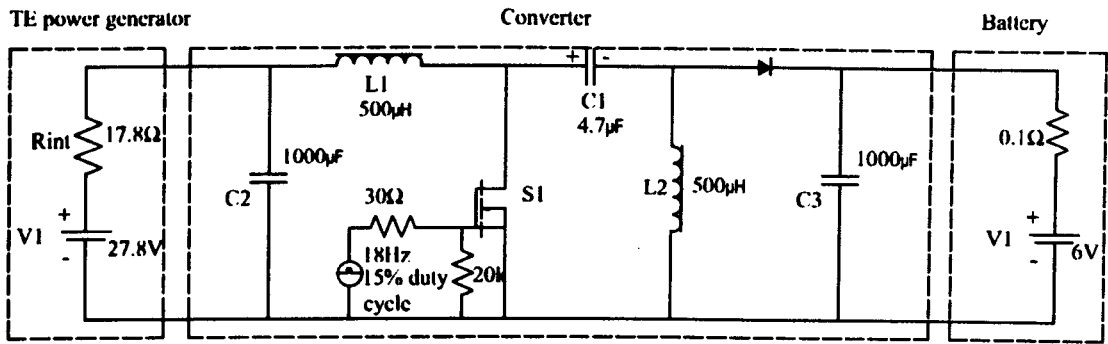


Figure 6-26 Schematic diagram of battery charging by TE power generator

Marcel [160] used the circuit diagram shown in Figure 6-26. A SEPIC dc-dc converter was used to transfer the power from thermoelectric generator to the battery set and track the maximum power point. The used battery was charged at the nominal voltage at 6V with 12Ah output. The thermoelectric generator consisted of 6 modules which were connected in series, giving a 27.8V open-circuit voltage at 120°C temperature difference and 60°C cold side temperature.

The stored electrical power can be used to power LED lamps or charge devices such as mobile devices. The storage of electrical power produced by the TCS has been only discussed based on the efforts made by previous research. It is intended to shed light to the future work on the electrical management for the specific system.

## 6.5. Mechanical assembly

### 6.5.1 Assembly introduction

Generally, a temperature gradient is obtained by supplying heat on one side and dissipating the heat from the other side. The electricity is generated when the heat flux flows through the thermoelectric element. The performance of thermoelectric generator is affected by the quality of thermoelectric assembly, which connects the modules and the heat exchangers at the hot and cold side. The assembly quality is determined by the surface quality of heat exchangers, the quality of thermal interface material, the surface quality and thickness variance of the module, the pressure load and washer configuration.

Each individual component can be easily checked for the quality with individual test. However, it is difficult to inspect the thermoelectric assembly quality due to the invisibility. The thermal junctions are buried in the assembly making it difficult to do accurate visual inspection. It is also very difficult to justify whether the correct compression force is applied even though the torque applied to each assembly screw is correct.

In order to decide which assembly methods are beneficial for thermoelectric performance, the system performance under each assembly configuration is measured. The results are compared to assess the quality of each assembly configuration.

Generally speaking, the thermal management is favourably directed to the achievement of the maximum temperature difference across the thermoelectric power generator. This leads to two important thermal treatments in thermoelectric

applications—thermal insulation and thermal interface enhancement. In some application assemblies where the heat source is not directly assembled to the heat dissipation devices, thermal insulation is unnecessary. However, in other assemblies where the heat source and the heat dissipation have to be connected by screws due to the limitations of heat exchanger category and system structure, the thermal insulation must be considered to avoid thermal bridge which directs the heat flux from heat source to heat sink directly without going through the module. Meanwhile, the thermal enhancement at the module interfaces must be considered in all types of thermoelectric applications. The importance of thermal enhancement at the module interfaces lies in minimizing the thermal resistance of the system and establishing a higher temperature difference across the module under the thermal condition of the given heat source.

The recommended compression for a thermoelectric assembly is 10 to 21 kilograms per square centimetre (150-300psi) of module surface area. Using the following equation, the torque per screw can be solved by Eq.(6-27) [165]:

$$T = (C \times D_{screw} \times P_f \times A_m) / N_{screw} \quad (6-27)$$

$T$  =torque per screw (Nm);

$C$  =torque coefficient (0.20 as received, 0.15 lubricated);

$D_{screw}$  =nominal screw size (M3=0.003, M4=0.004, M5=0.005);

$P_f$  =Force (N/m<sup>2</sup> or psi);

$A_m$  =module surface area (length×width);

$N_{screw}$  =screw quantity;

Using stainless steel screws, fibre insulating shoulder washers, and steel spring (Belleville or split lock type) washers, the suitable torque per screw can be calculated by using  $C=0.20$ ,  $A=0.0016\text{m}^2$ ,  $D_{screw}=0.004$ ,  $P_f=150\text{-}300\text{psi}$ , 4 screws are used in the assembly. The torque range lies in  $T=0.33\text{Nm}\text{-}0.66\text{Nm}$ . To ensure good thermal grease performance, there should be no bowing of either surface in the torquing process. To prevent bowing, less torque should be applied when the thickness of one or both surfaces are less than 3.18mm for the copper or 6.35 mm for the aluminium.



Figure 6-27 Torque wrench for thermoelectric assembly

For the assembly of thermoelectric module, the assembling method that has been mostly used is shown in Figure 6-27. The screw driver in this figure is a torque

wrench which can load customized pressure on the thermoelectric module by adjusting the torque to the stainless steel screw. The specification details are listed in Table 6-3.

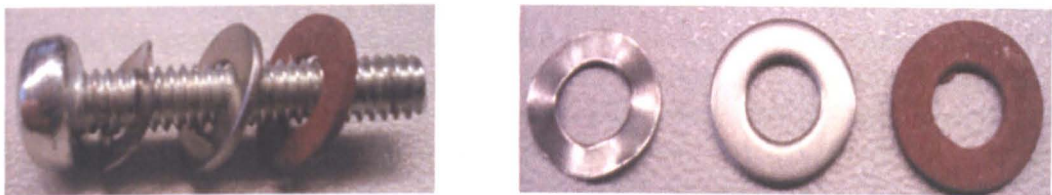



Figure 6-28 The most common thermoelectric assembly method (left to right: crinkle washer, flat metal washer and fibre washer)

The crinkle washer (sometimes Belleville washer or spring washer) is used to accommodate the thermal expansion caused by temperature change. The flat metal washer is used to bridge the crinkle washer and the fibre washer. The fibre washer is used to thermally insulate the thermal path between the hot side heat exchanger and the cold side heat exchanger to prevent the heat flux to go through the screws.

Table 6-3 Specifications of torque wrench

Torque screwdriver	
Accuracy	±6%
Drive Type	Hex
Length	155mm
Torque range	0.3 to 1.2Nm
Type	Quick Release

In the commercial practice, the cost for building a thermoelectric product is one of the important factors that need to be considered. With the precondition of delivering expected system performance, the simplicity is more favoured for the system structure because it can maintain the system building cost at the possibly lowest level due to less material use and less manual related work. Meanwhile, the simplicity of the system can also eliminate or reduce the maintenance working load because of the accessible and user friendly structure.

As discussed in the previous section, four screws are used to sandwich the thermoelectric module between the hot side and cold side heat exchangers. In this circumstance, certain amount of heat will go from the hot side heat exchanger to the cold heat exchanger via the four screws. Theoretically, the thermal bypass through these four screws is unbeneficial for the system performance in terms of energy conversion because of the heat goes through the unintended path rather than the module. Therefore, according to this analysis, a fibre washer is needed to reduce the negative impact that the screws have on the amount of energy that is used for conversion. In a typical thermoelectric application, the crinkle washer and fibre washer are commonly used to accommodate the thermal expansion and reduce thermal bypass through the screws with a flat metal washer to mechanically bridge these two washers. However, this study also introduces the experimental tests to the system without fibre washer and flat washer in an attempt to identify a simpler assembly, without compromising to the performance.



6.5.2 The optimum pressure load

In order to investigate the impact that the washers have on the system performance and evaluate the necessity of using those washers, tests have been carried out to investigate the system performance under two different assembling configurations: 1. A crinkle washer, a flat metal washer and a fibre washer; 2. A crinkle washer. This experimental study is designed to develop a simple system assembling configuration without significantly affecting the system performance. The benefit lies in keeping the cost for building up the system at the lowest level.

Before the test for different mechanical configurations, a test for exploring the impact that the pressure load has on the system performance has been conducted to identify the optimum pressure load on the module for the sake of the best energy conversion. In the test, a 47W power was supplied to the hot side heat exchanger by two cartridge heaters which were evenly installed in internal space of the oil tank. On the cooling side, a cooling plate is used to take the heat away from the cold side surface of the module. A 0.3Nm torque was used to tighten the four screws in the pressure load, and then the torque was loaded at an increment of 0.05Nm until 0.5Nm, the corresponding pressure load of each torque value is shown in Table 6-4.

Table 6-4 The pressure loads used for the test

Torque (Nm)	0.3	0.35	0.40	0.45	0.50
Pressure(psi)	136	159	181	204	227

The system was firstly heated up until the output stabilized. Then the pressure load was adjusted according to Table 6-4 using a torque wrench, the details are shown in Table 6-3. The voltage output at different pressure load has been measured and the result is shown in Figure 6-29. The voltage increases when the load pressure increases from 136psi to 181psi, and decreases when the load increases further from 181psi to 227psi. Hence, the optimum pressure load can be located at 181psi whose corresponding torque value is 0.40Nm. A possible explanation for this phenomenon is that the thermal contact between the module and heat exchangers improves as the pressure load increases in the range of 136psi to 181psi. When the pressure load further increases in the range of 181psi to 227psi, the thermal resistance of the washers decreases to the level where the thermal bypass effect is enhanced to an influential level.

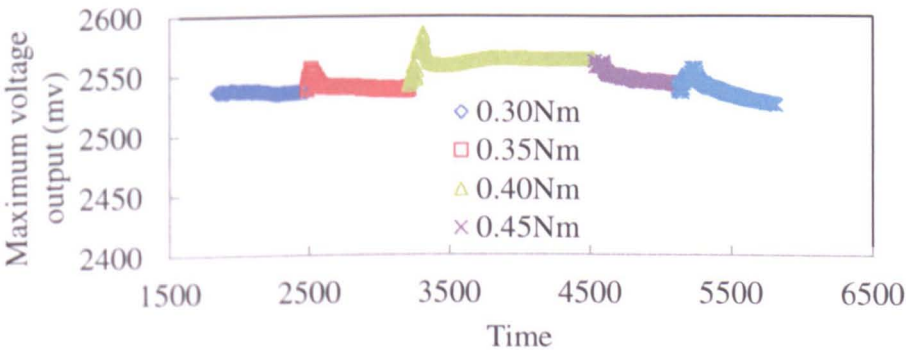


Figure 6-29 Maximum voltage output under different pressure load

Figure 6-30 and Figure 6-31 show the power output and heat output under different pressure load. Same as the maximum voltage output, the maximum power output is

given when the load pressure is at 181psi or the torque value is 0.40Nm. However, the variation of pressure load in this range does not influence the heat output significantly.

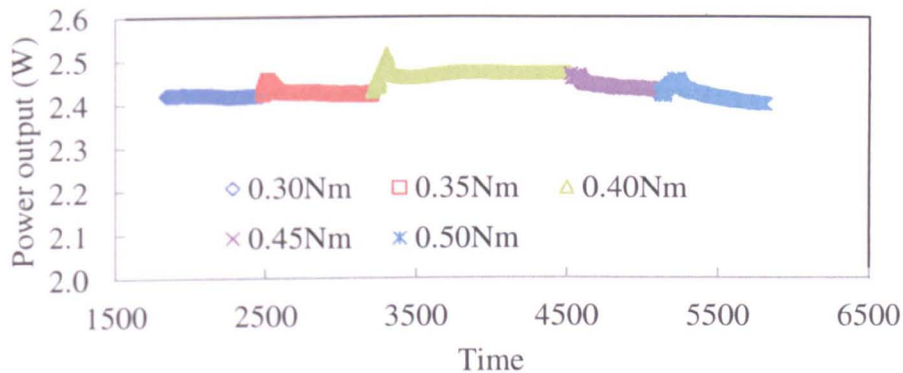


Figure 6-30 Power output under different pressure load

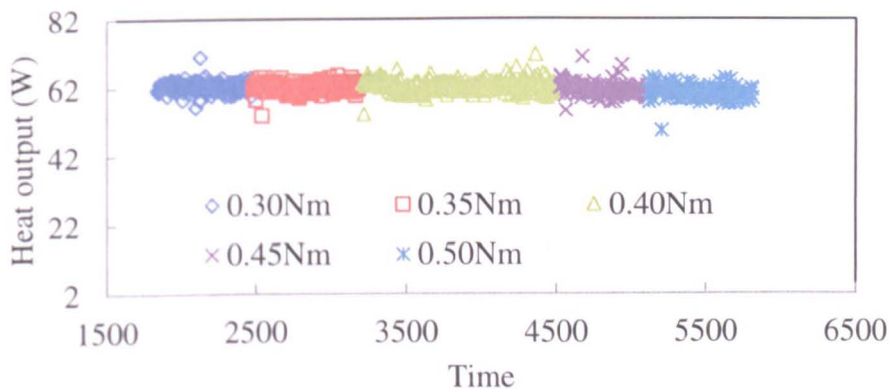


Figure 6-31 Heat output under different pressure load

6.5.3 Washer configuration

As shown in Figure 6-32, the two washer configurations, which include three washers (crinkle washer, flat metal washer and fibre washer) and one washer (crinkle washer). They are used to assemble the system and the corresponding test has been conducted to investigate the system performance with each assembly.



Figure 6-32 Washer configurations in the assembling procedure (from left to right, crinkle washer, flat metal washer and fibre washer)

Denoting the two washer configurations as “one crinkle washer” and “three washers”, they represent the assemblies with only crinkle washer and three washers, respectively. The impact of these two configurations has been experimentally investigated with the precondition of being reproducible. The results are shown in Figure 6-33 and Figure 6-34.



Figure 6-33 shows the removal of fibre washer and flat metal washer decreases the conversion efficiency slightly, whilst the thermal efficiency has been increased, which is shown in Figure 6-34. The removal of fibre washer and flat metal washer has decreased the thermal resistance of the assembling part. This diverts more heat to the assembling part.

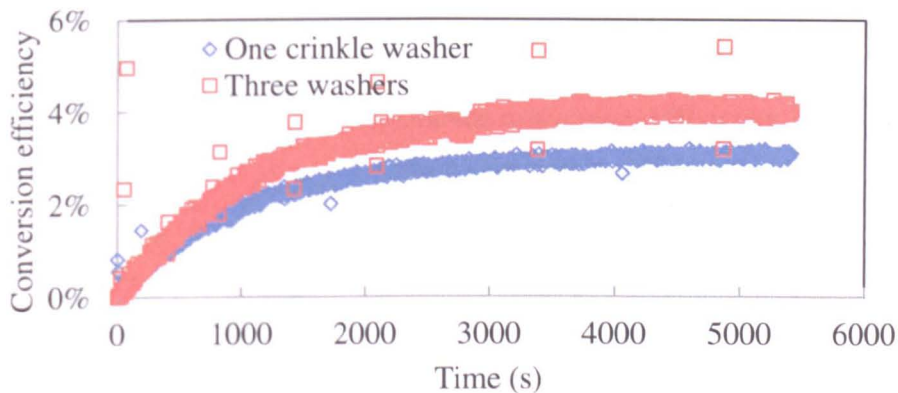


Figure 6-33 Conversion efficiency change caused by the removal of fibre washer and flat metal washer

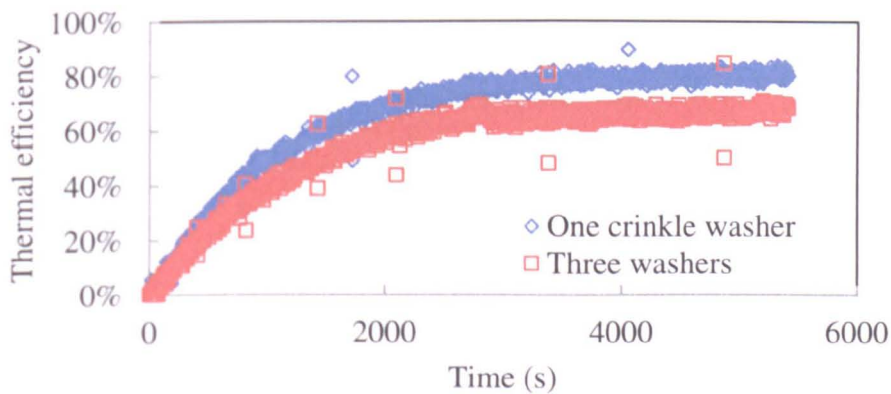


Figure 6-34 Thermal efficiency when the unit is assembled with one crinkle washer and three washers

For this thermoelectric cogeneration system, the use of fibre washer and flat washer is a double edged sword. Compared to the removal of them, the use of them can enlarge the temperature difference across the thermoelectric generator. Meanwhile, the thermal efficiency of the system without the fibre washer and flat metal washer is bigger than that when they are used. This can be attributed to the characteristics of this system which produces dual products during operation: electrical power and thermal energy. The output of electrical power can be enhanced by the use of fibre washer and flat metal washer, whilst the output of thermal energy can be enhanced by the removal of them at the investigated temperature (170°C). In the real application, the necessity of using them in the assembling configuration can be determined by the priority of electrical power or thermal energy.

#### 6.5.4 Uneven assembling

Uneven pressure load has been deliberately introduced in the assembly. Four screws have been tightened to the heat exchangers with the three washers. Three of them have been loaded with pressure given by the torque value of 0.4Nm and the fourth

one was loaded at the torque value at 0.3Nm. A test has been carried out to investigate the impact that an uneven assembling has on the system performance in comparison with the system with even assembly.

The conversion efficiency and thermal efficiency are used to characterize the performance and analyze the change caused by this uneven pressure load. The results are shown in Figure 6-35 and Figure 6-36.

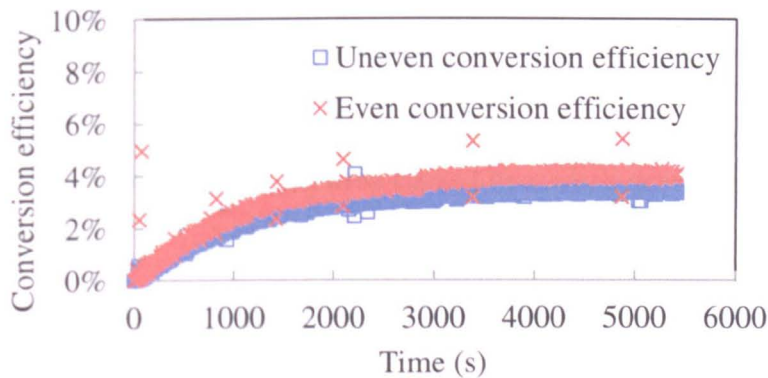


Figure 6-35 The impact on conversion efficiency from uneven pressure load

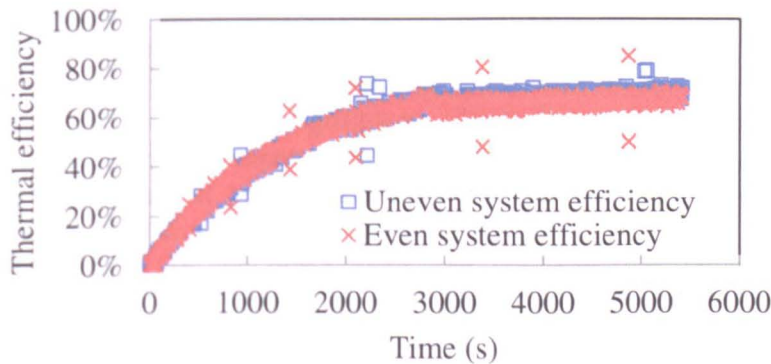


Figure 6-36 The impact on thermal efficiency from uneven pressure load

Up to 20% drop in conversion efficiency was caused by an uneven assembling. The possible reason is the increased thermal resistance which deteriorates the thermal contact at the interface between the module surfaces and the heat exchanger surfaces. It consequently directs more of the heat flux to the assembling route and decreases the temperature difference across the module. Consequently, the conversion efficiency is lowered. However, the thermal efficiency is not significantly affected by the uneven assembling despite of a slight increase (the minus value represents the efficiency increase), shown in Figure 6-37. This is because most of diverted heat flux flows to the cooling plate through the assembling set when the thermal resistance through the module is increased by the uneven assembling.



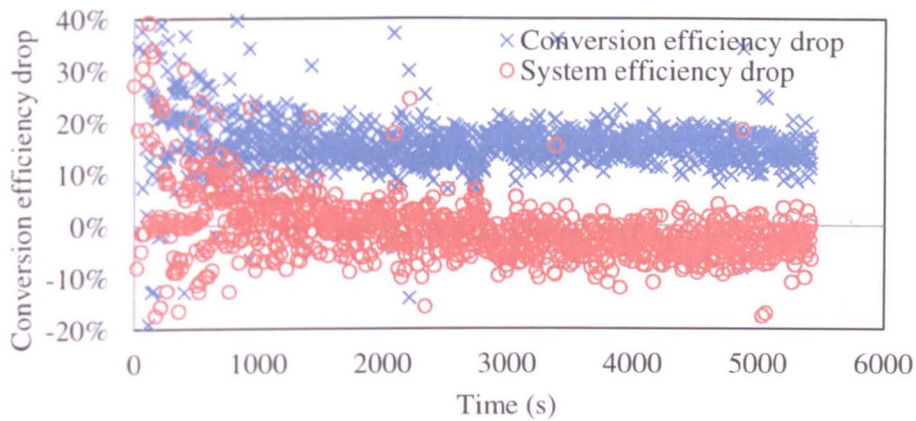


Figure 6-37 Efficiency drop caused by uneven assembling

### 6.5.5 Conclusion

Analyzing the influence to the system performance from different reproducible assembling configurations, the following conclusions can be drawn:

1. The pressure load on the thermoelectric module in the assembly has a significant impact on the performance of TCS. The optimum pressure load is 181psi given by the torque value 0.40Nm;
2. The system performance is influenced by the washer configuration. The conventional washer configuration, which uses a fibre washer, a crinkle washer (Belleville washer or spring washer) and a flat metal washer, can weaken the thermal bypass effect by reducing thermal conductance of the assembly set compared to the case of the removal of fibre washer and flat metal washer. On the other hand, the simplification of the assembly by removing the fibre washer and flat metal washer is able to enhance the thermal efficiency although the conversion efficiency has been decreased.
3. The uneven assembly affects the performance by worsening the thermal contact at the interface between the module surfaces and the heat exchanger surface and thus thermal resistance from the surface of hot side heat exchanger to the surface of the cold side heat exchanger is increased. It is essential to load even pressure on each thermoelectric module to achieve the optimal thermal contact and harmless thermal assembly.
4. Assembling the thermoelectric applications by torque wrench is feasible method because it can load the pressure with a reasonable accuracy and makes the assembly reproducible.

### 6.6. Summary

In this chapter, the theoretical models for the domestic TCS of one-stage and two-stage have been introduced. Corresponding experimental studies have been introduced in comparison with each other. The experimental study of one-stage TCS has been introduced with more details in various performances. The factors that affect the system performance from the construction's point of view including the pressure load, distribution and washing configuration have also been introduced.

It shows the one-stage TCS produces more power than the two-stage TCS does when the heat input is supplied at 47W and 60W. As the heat input increases, the power output of two-stage TCS gets closer to that of one-stage TCS.

In the system construction and assembly, uneven assembly can lead to conversion efficiency drop even module damage/failure when the load is excessive. The pressure load at 181psi gives the highest power output out of five load values: 136psi, 159psi, 181psi, 204psi and 227psi. In comparison with individual assembly, module thickness difference in whole assembly degrades the system conversion efficiency.

The output of electrical power can be enhanced by the use of fibre washer and flat metal washer, whilst the output of thermal energy can be enhanced by the removal of them at the investigated temperature (170°C).

## **Chapter 7 Discussion, conclusion and future work**

This chapter discusses a potential candidate concept that, on the basis of the result of current work, has been modified and introduced. The economic impact of deploying the domestic TCS in residential house in the UK has been evaluated in a case study. The environmental impact has also been discussed. Final insight has been shed onto the conclusion of this current work and suggestions for future work.

### **7.1. Discussion**

This system basically has two products, which are electrical power and thermal energy in the form of preheated water. The amount of power generation is determined by the temperature difference across the thermoelectric generators. The temperature level of the preheated water is determined by the heating period in the cooling plate. It can be adjusted according to the need by varying the flow rate in the economic range. When the temperature level of the preheated water needs to be higher, the feed water into the cooling system can be supplied at a smaller flow rate, vice versa. As shown in the results of previous experimental study, the power output hardly had any change when the flow rate of feed water reduces. This is because the temperature difference across the module does not have obvious fluctuation when the cold side temperature changes. However, the heat output is increased when the water feed velocity is decreased.

Due to the characteristic of this domestic TCS, it largely relies on the amount and temperature level of the heat. Its operation can be fulfilled by using the available heat in the domestic environment. The available heat includes the waste heat from domestic facilities, solar power or purposely designed heat source. It can either be used as a parasitic application which recovers the waste heat given out by other facilities, or as a main power generator by using the purposely designed heat source. The former concept is suitable for the areas or regions where the electricity supply is not scarce. It can be used as a supplemental power generation method to partially supply the electrical power. The parasitic application concept helps improve the energy efficiency of the host facilities. The latter concept is suitable for the regions where lacks of electricity or has no electricity supply. A facility, relying on the local sufficient sources, can be built to provide heat for power generation, e.g. remote mountain areas where the wood is of great abundance.

The purpose of this system is to recover the waste heat existing in domestic environment and use solar energy at the same time. More boiler waste or solar energy means more electrical power and thermal energy can be produced. This does not necessarily mean a more inefficient boiler or domestic heating device is rewarding. The goal is to improve the energy utilisation efficiency by recovering the waste heat in residential house and meanwhile utilise the solar energy to reinforce the system viability in domestic environment.

#### **7.1.1. Candidate design**

Based on the system introduced in this research, a modified concept is proposed as the candidate design for possible domestic applications in the purpose of pointing the direction of future research work. The system concept is shown in Figure 7-1. It

distinguishes itself by adopting a different system structure, is discussed in this section with more details due to its structural advance over other concepts. The aforementioned system establishes the temperature difference by exchanging the heat with the heat source and coolant indirectly through the heat exchangers at the two sides of the module. This new concept is designed to enable the module to exchange heat with the coolant directly. This direct heat exchange aims to reduce the thermal resistance of heat flow from the heat source to the coolant.

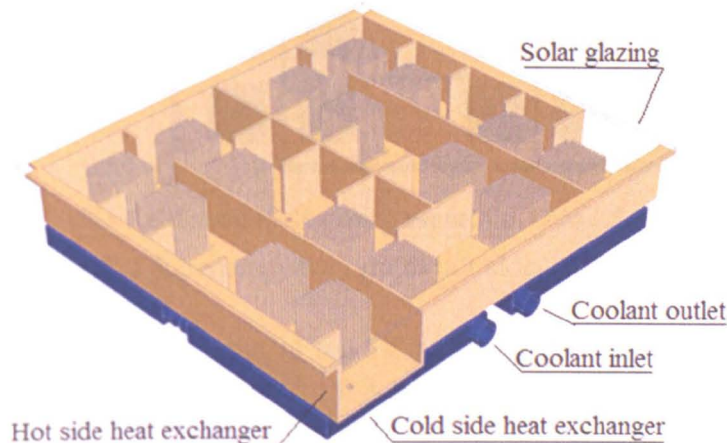


Figure 7-1 Improved system concept for domestic TCS

The hot side heat exchanger is designed to accommodate the existence of boiler waste heat and solar energy by being exposed to the solar radiation and flue gas. The flue gas exhausted from the boiler enters the flow channel to exchange heat with the heat sink which consequently heats TE module hot side surface, part of which is heated by the base board which is partially attached to the TE hot side surface. The TE hot side surface is heated by the flue gas and bottom wall. Heat sinks absorb heat from flue gas and solar radiation and transfer the absorbed heat to the module hot side surface.

The heat exchanger is enclosed by a 5mm glazing top which allows solar radiation to get through and heat up the inner surface which consists of channel walls and heat sinks. The material of glazing top is transparent glass ceramic which stands the temperature up to  $700^{\circ}\text{C}$ , allowing high temperature operation. It is coated with reflective coating on the interior surface which prevents the heat in the form of long wavelength to escape to outside. A glazing insulation, which prevents significant heat loss through the solar glazing and also allows the solar radiation to get through, needs to be installed on top of the solar glazing. such as acrylic sheet which is installed on top of the solar glazing leaving an air gap.



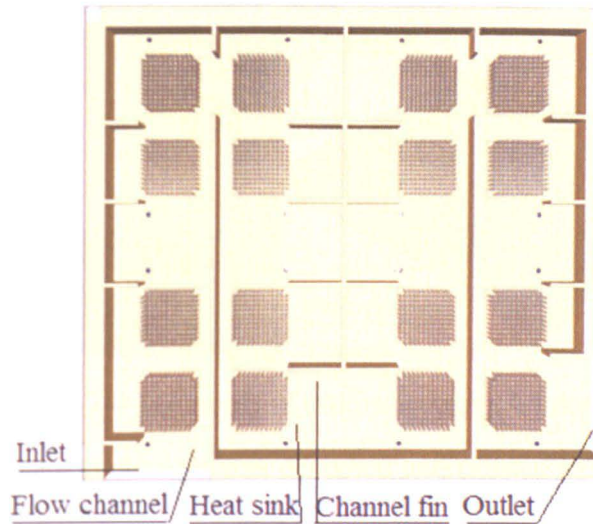


Figure 7-2 Schematic diagram of hot side heat exchanger

Figure 7-3 shows the cooling unit of the TE building block. It consists of four cold side heat exchangers. Each cold side heat exchanger accommodates four thermoelectric modules, which are connected in series, shown in Figure 7-4. The system assembly is a combination of whole assembly and individual assembly to obtain even pressure load on the modules and enhance system simplicity.

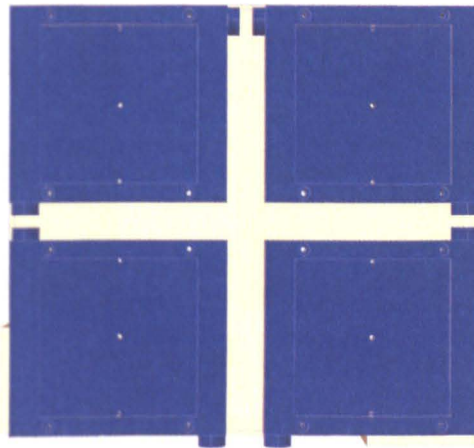


Figure 7-3 Cooling unit of thermoelectric cogeneration system

The cold side heat exchanger is made by 3D printer which is able to print it out with the designed features in 3D modelling software. The material that is used to print the model is ABS (Acrylonitrile butadiene styrene, chemical formula  $(C_8H_8)_x \cdot (C_4H_6)_y \cdot (C_3H_3N)_z$ ), which is a common thermoplastic. Its glass transition temperature (ABS is amorphous and therefore has no true melting point) is approximately  $105^\circ\text{C}$ , which is much higher than the temperature level ( $10\text{-}40^\circ\text{C}$ ) required by the cooling side of the system.

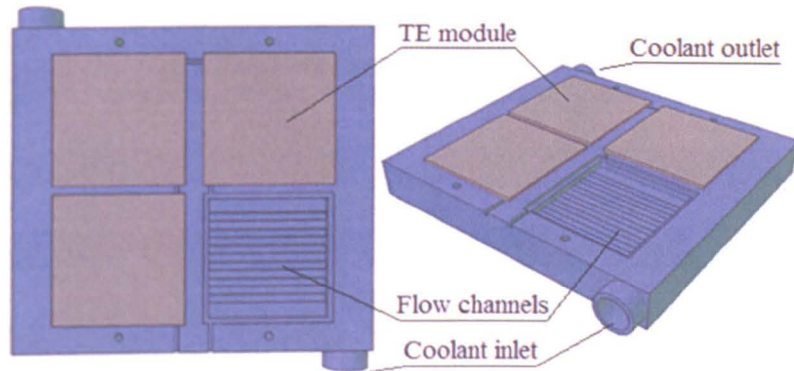


Figure 7-4 3D model of cold side heat exchanger

A sample cold side heat exchanger was designed and printed to see physical quality. Checking through the surface flatness and rigidity, the quality is good enough for being used in this system. Hence, it is technically possible to produce cold side heat exchanger by 3D printing technology, which is able to make the features that are difficult to achieve by the conventional method easy to do. The sample is shown in Figure 7-5. The feasibility of fabricating cold side heat exchanger using 3D printing gives this system the following advantages.

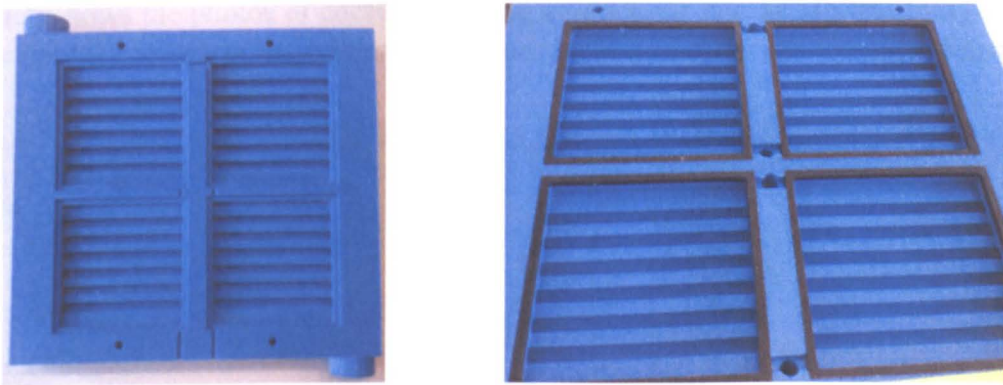


Figure 7-5 3D printed sample of cold side heat exchanger

1. The sophisticated structure is possible to be made, which can reduce the thermal resistance between the module and coolant by establishing direct contact between the module cold side surface and the coolant;
2. The system weight can be significantly reduced by using ABS instead of the conventional aluminium;
3. The good fabrication accuracy enables the system to be assembled with the optimal pressure load, which can achieve a good system performance;
4. Its design is combined with the merits of individual assembly and whole assembly; high module density and even pressure load.
5. Due to the use of silicone rubber gasket, the modules are allowed to adjust themselves to find the best position to attach to the surface of hot side heat exchanger. In this way, a good thermal contact can be achieved.

The integration with the domestic boiler is shown in Figure 7-6.



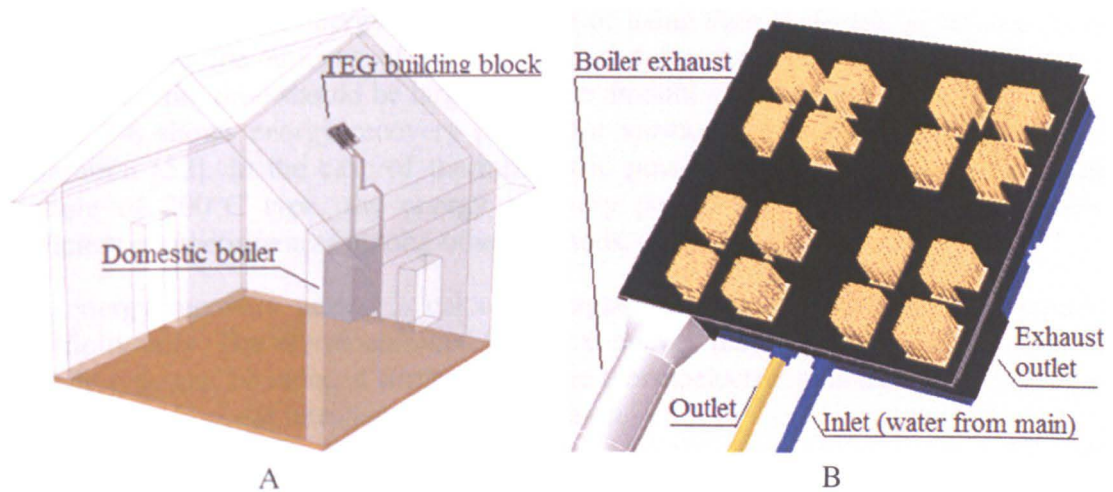


Figure 7-6 Schematic diagram of the integration with domestic boiler, A: distant view; B: near view;

Distant view and near view of the system integrated in a domestic space are shown. In Figure 7-6 B, the colour of heat sinks is set as gold to highlight their presence out of the black enclosure. In real application, it should be black due to a better absorption of sun light. The details of real prototype can be referred in Figure 7-7, which shows the photos of cooling side and heat source side of TEG building block. The detailed results of experimental and numerical studies are not introduced here.

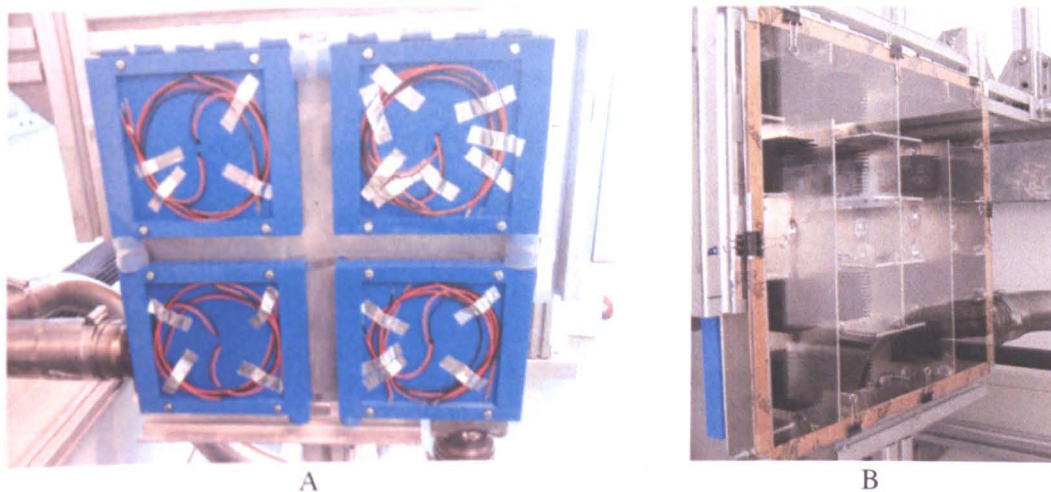


Figure 7-7 Photos of TEG building block, A: Cooling side; B: Heat source side

### 7.1.2. Economic analysis

There are a large amount of existing boilers that are operating highly inefficiently in the UK, leading to massive energy waste. When we discuss about the potential methods of solving this issue, the boiler retrofit always seems to be on top of the list. However, it requires a large amount of upfront capital and puts the home owners off from a boiler replacement. It does not meet the ROI (return of investment) thresholds for energy efficiency retrofit, although it saves a considerable amount of money over the expected lifetime of the boiler. The economic viability of domestic TCS is discussed in this section to demonstrate its economic viability in the purpose of proposing an alternative option to measures of improving home energy efficiency.

When considering the energy saving benefit of using thermoelectric generators, it is important that the amount of energy produced by the thermoelectric generators during their life time should be larger than the amount of energy for fabricating them. Figure 7-8 shows energy recovery period for various methods of electrical power generation [52]. In the case of thermoelectric power generation by a Bi-Te-based module of 200°C type, the energy recovery period is 0.85 year which shows sufficient competitiveness among other methods.

The energy recovery period is calculated against the application which generates electricity only. The aforementioned 0.85 year energy recovery period for the 200°C module type can be reduced further when the thermoelectric generator is used in the cogeneration concept introduced in this research.

To more accurately evaluate the economic benefit that the use of this system concept can bring to the residential house which uses conventional domestic or old inefficient boiler, the amount and availability profile of the heat sources along the timeline of whole year and the temperature of boiler flue should be understood.

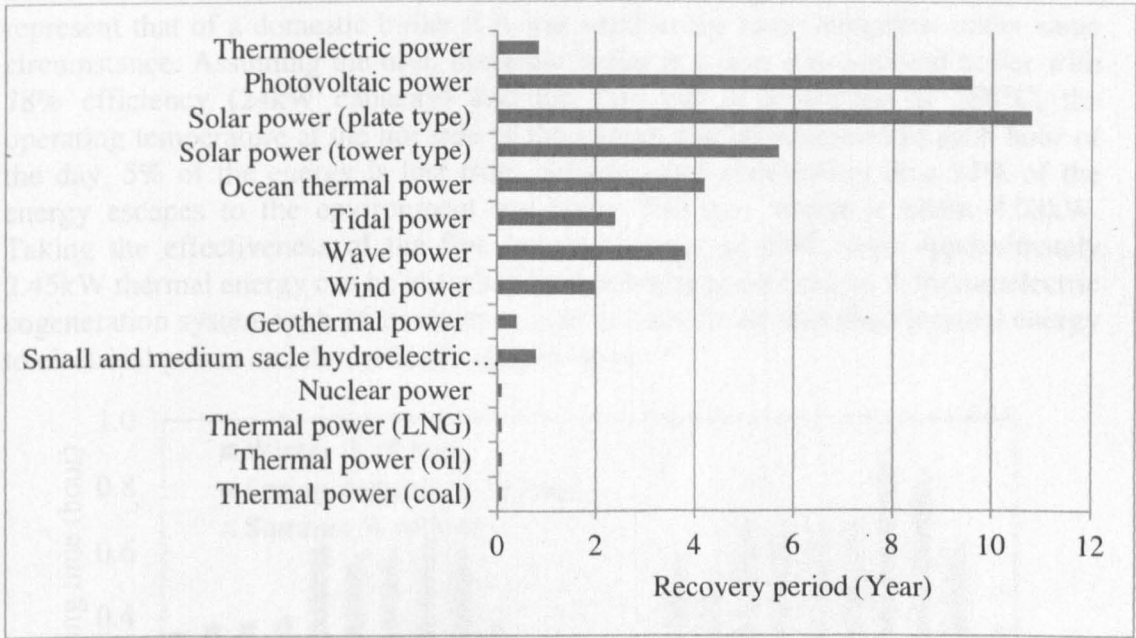


Figure 7-8 Comparison of energy recovery period

For the UK, a comprehensive study conducted on the solar energy arriving at the surface of the Earth has been carried out by the Institute for Environment and Sustainability of European Commission [166]. It is cited here to show the solar availability in different regions and countries. The amount of available solar energy depends on the geographical variability, weather conditions and time dynamics. The analysis to the availability helps us understand the contribution that TCS could make to the improvement of domestic power conditions.

Taking a two-bed bungalow in Northampton as an example, the average daily solar irradiance of each month is shown in Figure 7-9.



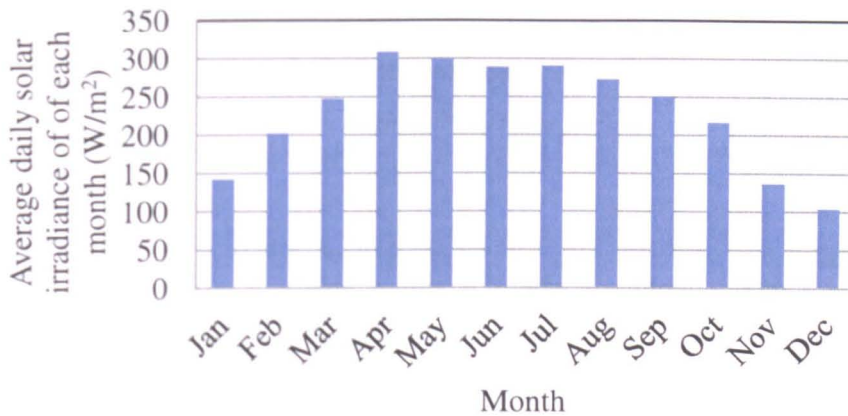


Figure 7-9 Average daily solar irradiance of each month in Northampton

The profile of boiler waste heat is determined by the outdoor temperature and the user demand. The heating demand of the two-bed bungalow in the whole year is shown in Figure 7-10 based on the operating time in each hour of the day. The data is based on the air source heat pump, whose operating pattern should be able to represent that of a domestic boiler if it was used in the same bungalow under same circumstance. Assuming the used domestic boiler is a new conventional boiler with 78% efficiency (24kW capacity) and the flue gas is exhausted at 180°C, the operating temperature at the hot side of the system can be estimated in each hour of the day, 5% of the energy is lost from radiation and conduction, then 17% of the energy escapes to the environment via boiler flue gas, which is about 4.08kW. Taking the effectiveness of the flue heat exchanger as 60%, then approximately 2.45kW thermal energy can be absorbed by the flue heat exchanger. A thermoelectric cogeneration system with 16 modules is used to convert the absorbed thermal energy to electrical power and domestically useable heat.

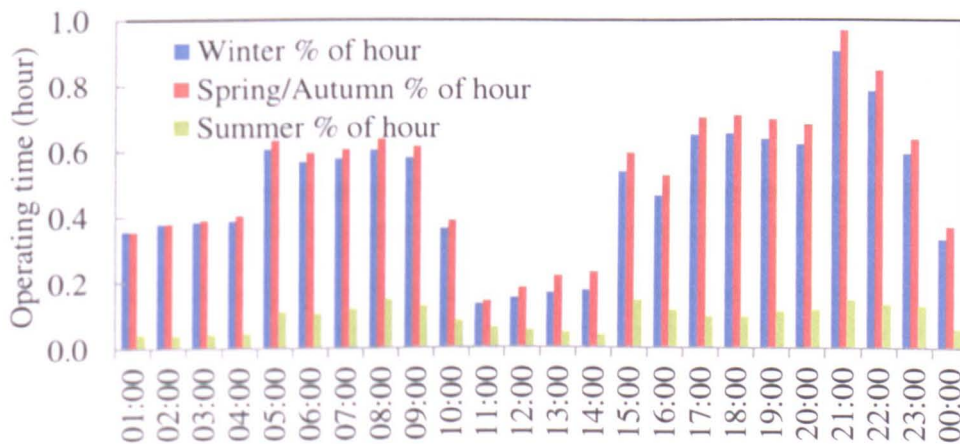


Figure 7-10 Hourly heating demand of a UK two-bed bungalow in a year

Taking one set of experiment as an example, the heat input is given at 93W by cartridge heater which simulates the heat source. The power output and open voltage of a single cell thermoelectric cogeneration system under different operating temperature difference is shown in Figure 7-11. When the temperature difference across the thermoelectric generator is 130°C, the power output and heat output of the single module system is 2.5W and 59.4W. The conversion efficiency and thermal efficiency is 4% and 67%, respectively.

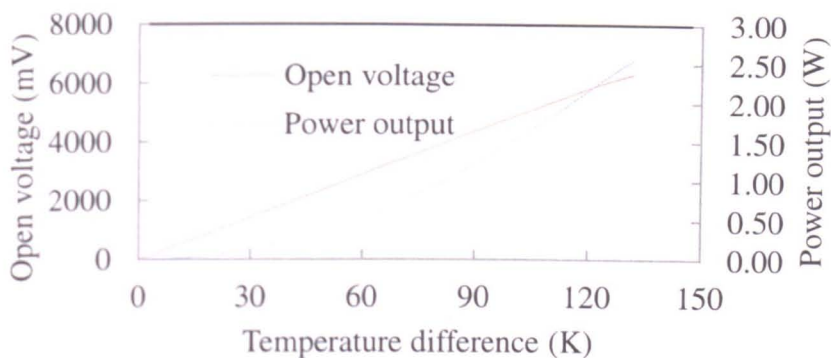


Figure 7-11 Open voltage and power output of a single cell thermoelectric cogeneration system

The heat output and open voltage of a single cell thermoelectric cogeneration system under different operating temperature difference is shown in Figure 7-12. The few abrupt fluctuations in the curve of heat output could be caused by equipment error and can be omitted.

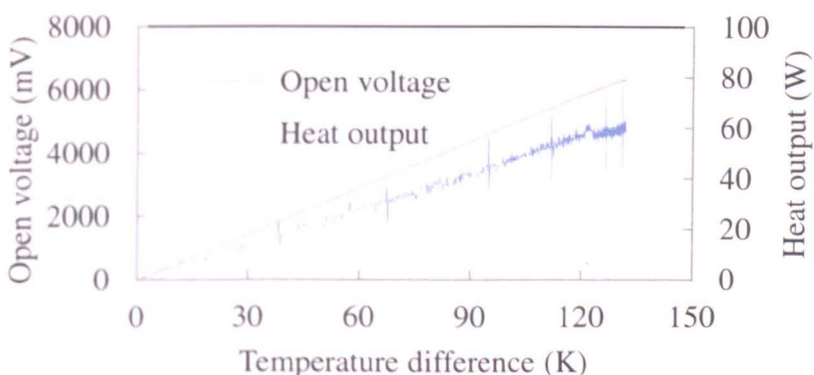


Figure 7-12 Open voltage and power output of a single cell thermoelectric cogeneration system

For a domestic TCS using 16 thermoelectric modules, the cost recovery and energy recovery period is estimated on the assumption that the same conversion efficiency and thermal efficiency is achieved by adopting the reproducible assembly technique and configuration used in the single thermoelectric cogeneration system.

Table 7-1 Cost estimation of a TCS with 16 thermoelectric modules

Component	Modules	Heat transfer oil	Hot side x	Cold side x	TIM	Installation and operation	Total cost
Quantity	16	0.4litre	1	16	1	1	£467
Cost	£200	£1.20	£82	£22	£12	£150	
Type	First (Electricity668kWh/ Gas148kWh)						Rest
Electricity	22.765p						9.88p
Gas	6.621p						3.05p
For electricity and gas, the rates are 22.765p and 6.621p per unit for the first 668 kWh and 148 kWh, the rest is 9.879p and 3.05p per unit, respectively.							

The economic impact is analysed as follow: The users are normally concerned about the time of recovering the system cost when they justify the economic benefit of

turning to utilising this system. Here the cost recovery period will be evaluated to provide the information for assessments. The cost for establishing this system is estimated and shown in Table 7-1 as below:

Considering the low temperature drop of heat pipe heat exchanger, let's conservatively assume there is a 20°C temperature drop from the flue gas to the module hot side surface and the average temperature of cold side is 30°C, then the operating temperature difference is 130°C. With the conversion efficiency and thermal efficiency is 4% and 67% at 130°C temperature difference, the 24kW house can produce 98W electricity and 1640W useable heat when the boiler is running. To include the contribution from the solar energy, the availability of solar energy based on a 1m<sup>2</sup> solar collector is overlapped with that of boiler waste heat, shown in Table 7-2.



Table 7-2 Hourly availability of solar energy and boiler waste heat in the two-bedroom bungalow of each month in a whole year in Northampton (kW)

Time	01:00	02:00	03:00	04:00	05:00	06:00	07:00	08:00	09:00	10:00	11:00	12:00	13:00	14:00	15:00	16:00	17:00	18:00	19:00	20:00	21:00	22:00	23:00	00:00
W	0.36	0.38	0.38	0.39	0.61	0.57	0.58	0.60	0.58	0.37	0.13	0.15	0.17	0.17	0.54	0.47	0.65	0.65	0.64	0.62	0.90	0.78	0.59	0.33
Jan	2.45	2.45	2.45	2.45	2.45	2.45	2.45	2.56	2.56	2.56	2.56	2.56	2.56	2.56	2.56	2.56	2.45	2.45	2.45	2.45	2.45	2.45	2.45	2.45
Feb	2.45	2.45	2.45	2.45	2.45	2.45	2.61	2.61	2.61	2.61	2.61	2.61	2.61	2.61	2.61	2.61	2.61	2.45	2.45	2.45	2.45	2.45	2.45	2.45
Mar	2.45	2.45	2.45	2.45	2.45	2.65	2.65	2.65	2.65	2.65	2.65	2.65	2.65	2.65	2.65	2.65	2.65	2.65	2.45	2.45	2.45	2.45	2.45	2.45
S/A	0.36	0.38	0.39	0.40	0.63	0.59	0.61	0.64	0.61	0.39	0.14	0.18	0.22	0.23	0.60	0.53	0.70	0.71	0.70	0.68	0.97	0.85	0.64	0.37
Apr	2.45	2.45	2.45	2.45	2.45	2.70	2.70	2.70	2.70	2.70	2.70	2.70	2.70	2.70	2.70	2.70	2.70	2.70	2.70	2.70	2.45	2.45	2.45	2.45
May	2.45	2.45	2.45	2.45	2.69	2.69	2.69	2.69	2.69	2.69	2.69	2.69	2.69	2.69	2.69	2.69	2.69	2.69	2.69	2.69	2.69	2.45	2.45	2.45
Jun	2.45	2.45	2.45	2.45	2.68	2.68	2.68	2.68	2.68	2.68	2.68	2.68	2.68	2.68	2.68	2.68	2.68	2.68	2.68	2.68	2.68	2.45	2.45	2.45
Oct	2.45	2.45	2.45	2.45	2.45	2.45	2.62	2.62	2.62	2.62	2.62	2.62	2.62	2.62	2.62	2.62	2.62	2.62	2.45	2.45	2.45	2.45	2.45	2.45
Nov	2.45	2.45	2.45	2.45	2.45	2.45	2.56	2.56	2.56	2.56	2.56	2.56	2.56	2.56	2.56	2.56	2.45	2.45	2.45	2.45	2.45	2.45	2.45	2.45
Dec	2.45	2.45	2.45	2.45	2.45	2.45	2.45	2.53	2.53	2.53	2.53	2.53	2.53	2.53	2.53	2.53	2.45	2.45	2.45	2.45	2.45	2.45	2.45	2.45
S	0.04	0.04	0.04	0.05	0.11	0.11	0.12	0.15	0.13	0.08	0.06	0.05	0.05	0.04	0.14	0.12	0.10	0.10	0.11	0.12	0.15	0.13	0.13	0.06
Jul	2.45	2.45	2.45	2.45	2.68	2.68	2.68	2.68	2.68	2.68	2.68	2.68	2.68	2.68	2.68	2.68	2.68	2.68	2.68	2.68	2.68	2.45	2.45	2.45
Aug	2.45	2.45	2.45	2.45	2.45	2.67	2.67	2.67	2.67	2.67	2.67	2.67	2.67	2.67	2.67	2.67	2.67	2.67	2.67	2.67	2.45	2.45	2.45	2.45
Sep	2.45	2.45	2.45	2.45	2.45	2.65	2.65	2.65	2.65	2.65	2.65	2.65	2.65	2.65	2.65	2.65	2.65	2.65	2.65	2.45	2.45	2.45	2.45	2.45

\*W, S/A and S represent winter, spring/autumn and summer, respectively. The number in the same row represents the period of operation in each hour.

The hourly availability of solar energy and boiler waste heat is shown in Table 7-2. The gold part represents the period when both the solar energy and boiler waste heat are available.

With the aforementioned operational condition, the power output of this system can be predicted according to the availability of heat source in Table 7-2.



Table 7-3 Hourly output of electrical power of each month in a whole year in Northampton (kWh)

W	01:00	02:00	03:00	04:00	05:00	06:00	07:00	08:00	09:00	10:00	11:00	12:00	13:00	14:00	15:00	16:00	17:00	18:00	19:00	20:00	21:00	22:00	23:00	00:00	Subtotal
Jan	34.9	37.0	37.7	38.0	59.4	55.7	56.6	62.0	59.6	37.5	13.8	15.7	17.2	17.9	55.2	47.7	63.8	64.0	62.5	60.8	88.7	76.8	58.1	32.6	35.8
Feb	34.9	37.0	37.7	38.0	59.4	55.7	60.4	63.2	60.7	38.2	14.0	16.0	17.5	18.2	56.2	48.6	68.0	64.0	62.5	60.8	88.7	76.8	58.1	32.6	36.2
March	34.9	37.0	37.7	38.0	59.4	60.2	61.2	64.0	61.5	38.7	14.2	16.2	17.7	18.5	57.0	49.3	68.9	69.2	62.5	60.8	88.7	76.8	58.1	32.6	36.7
S/A																									
Apr	34.8	37.1	38.2	39.6	61.9	64.2	65.4	68.7	66.3	41.9	15.3	19.6	23.7	24.9	64.3	56.7	75.9	76.6	75.1	73.5	94.9	83.0 3	62.4 1	36.2 2	40.3
May	34.8	34.8	34.8	34.8	38.2	38.2	38.2	38.2	38.2	38.2	38.2	38.2	38.2	38.2	38.2	38.2	38.2	38.2	38.2	38.2	38.2	34.8	34.8	34.8	27.7
Jun	34.8	37.1	38.2	39.6	67.8	63.8	65.0	68.3	65.9	41.7	15.3	19.5	23.6	24.8	63.9	56.4	75.4	76.1	74.7	73.1	104	83.0	62.4	36.2	40.6
Oct	34.8	37.1	38.2	39.6	61.9	58.3	63.6	66.8	64.5	40.8	14.9	19.1	23.1	24.2	62.5	55.2	73.8	74.5	68.3	66.8	94.9	83.0	62.4	36.2	39.2
Nov	34.8	37.1	38.1 6	39.5 9	61.9 3	58.2 9	62.0 6	65.2 2	62.9 3	39.8 1	14.5 6	18.5 9	22.5	23.7	61.0	53.8	68.9	69.6	68.3	66.7	94.9	83.0	62.4	36.2	38.6
Dec	34.8	37.1	38.2	39.6	61.9	58.3	59.4	64.6	62.3	39.4	14.4	18.4	22.3	23.4	60.4	53.3	68.9	69.6	68.3	66.8	94.9	83.0	62.4	36.2	38.4
S																									
July	4.15	3.80	4.06	4.45	12.0	11.3	12.9	15.9	13.7	9.03	6.57	5.72	4.95	4.10	15.5	12.4	10.3	10.3	12.0	12.5	15.7	13.0	12.5	5.53	7.2
Aug	4.15	3.80	4.06	4.45	11.0	11.3	12.8	15.8	13.7	8.98	6.54	5.69	4.93	4.07	15.4	12.3	10.2	10.2	11.9	12.4	14.3	13.0	12.5	5.53	7.1
Sep	4.15	3.80	4.06	4.45	11.0	11.2	12.7	15.7	13.6	8.93	6.50	5.65	4.90	4.05	15.3	12.2	10.1	10.2	11.8	11.4	14.3	13.0	12.5	5.53	7.0
																								Tota l	355

\*W, S/A and S represent winter, spring/autumn and summer, respectively.

Hence, the annual output of electrical power of this system is 355kWh. The annual heat output can be calculated as 5941 kWh.

One of the tariffs of the electricity and gas from British Gas is shown in Table 7-1. Then the cost recovery period of this system can be calculated according to this tariff scheme. The annual saving by the electrical power and gas is £80.8 and £186.5, respectively. The labour hours are comprised of the time spent on fabricating the hot side and cold side heat exchanger, which are 10 hours and 16 hours, respectively. The labour cost is calculated as £650 in total using the pay rate of technicians in the Faculty of Engineering of the University of Nottingham at £25/hour. The total cost of building the system can be calculated as £1117. Therefore, the cost recovery period can be calculated as  $\text{£1117}/(\text{£267}/\text{year})=4.18$  years. Here a clarification needs to be made that the costs are estimated in research laboratory environment, where the material cost and labour cost is higher than that could be realized in industrial environment. The reasons mainly lie in the higher material cost due to small purchase and likely ineffective material sourcing as well as lower efficiency in material use due to weak integration in laboratory environment. Namely, in the commercial case, the total cost can be reduced further which also means the cost recovery period could be less than 4.18 years.

The carbon emission from natural gas and grid electricity is 0.18523kg per kWh and 0.53909kg per kWh. The saving of carbon emission in the use of electricity and gas can be calculated as 65.8kg and 3202.7kg, respectively. Hence, the total annual saving of carbon emission is 3268.5kg.

### **7.1.3. Environmental impact**

Bismuth telluride is a compound of bismuth and tellurium, a gray powder. It is a semiconductor which is an efficient thermoelectric material for refrigeration or power generator. Bismuth telluride comprises some of the best performing room temperature thermoelectrics. The single crystalline bismuth telluride compounds can be grown by using the Czochralski method and obtained with directional solidification from melt or powder metallurgy processes.

It is prepared by sealing a sample of bismuth and telluride metal in a quartz tube under vacuum and heating it to 800°C in a muffle furnace. Exposure (at 15mg/m<sup>3</sup> for 6 hr/day, 5 days/week) to the dust of undoped bismuth telluride (0.4micron) does not impose adverse influence on animals like dogs, rabbits and rats [167]. For human being, exposure to undoped bismuth telluride can occur through inhalation, eye/skin contact and ingestion. Acute exposure to undoped bismuth telluride can cause local irritation of eyes and skin [168]. No signs or symptoms of chronic exposure to the undoped bismuth telluride have been reported. However, suggestions have been given on avoidance and rescue in case of exposure to it [169].

When it is used in residential house, the long lifespan of continuous operation of thermoelectric generator (up to 11 years) makes sure the system operate for a considerably long time. The ability of recovering the waste heat from the boiler flue gas improves the fuel utilisation efficiency of domestic boiler and at the same time utilise the free solar energy. The thermoelectric cogeneration system partially offsets the need of electrical power and thermal energy.

## 7.2. Conclusion

Thermoelectric generators have found wide applications in different areas due to reliable operation, no-moving parts and compact structure. The thermoelectric cogeneration of electrical power and hot water designed for residential houses in country/regions with temperate climate is proposed and tests have been carried out on a bench scale prototype to investigate its performance. Its viability has been discussed based on the availability of domestic boiler waste heat and solar radiation. The benefit of employing thermoelectric generators in domestic environment has been evaluated on the basis of experimental studies. The results prove that the thermoelectric cogeneration concept is able to deliver much higher energy utilisation efficiency by generating electrical power and producing thermal energy. The essential issues in this cogeneration concept, including heat sourcing, heat dissipation, mechanical assembly, economic operating zone and system performance, have been investigated along with the design, test and modification of heat exchanger.

The heat sourcing design has been investigated using the numerical simulation method which simplifies the heat pipe into pipe flow based on four comparisons. With the simplifications, the suitable model of flue heat exchanger has been identified and further modified on basis of four variables: heat pipe layout, cross section of flue heat exchanger, heat pipe pitch and joint style. It was found that:

1. In the square-cross sectioned flue heat exchanger installed amid the boiler flue pipe, the flue heat exchanger with inline layout shows better performance than that with staggered layout due to improvements in both thermal and hydraulic performance;
2. Bigger cross section (1.19A) achieved an obvious decrease in pressure drop compared to the model with cross section at 0.91A. Without compromising to the thermal performance, a better overall performance has been achieved by adopting the model with bigger cross section;
3. Smaller pitch (2d) improves the overall performance by enhancing the heat transfer between flue gas and heat pipes but without causing significant change in pressure drop;
4. The flue heat exchanger with gradual junction shows worse performance when the flue gas velocity is 1m/s due to smaller value of effectiveness caused by the “inducing effect” along the near-wall region from the gradual constriction, a slight improvement in overall performance can be found in the model with gradual junction due to decreased pressure drop when the velocity is 2m/s, 3m/s, 4m/s and 5 m/s; whereas the effectiveness does not show any improvement. It implies a better overall performance could be achieved by adopting sudden junction and gradual junction at inlet and outlet junction respectively.

The model with sudden expansion and gradual constriction has been identified gives the most suitable structure of flue gas heat exchanger. Based on this, modified models have been established. Among them, M4 and M5 show better overall performance than other models do. However, M4 shows better performance than in the velocity range of 3.6m/s-5m/s, whilst M5 shows better performance between 0-3.6m/s.

M4 and M5 are selected to be studied with the use of heat transfer enhancement design-fins; the thermal performance is improved at 1m/s, 2m/s and 3m/s (the enhancement in heat transfer rate is 3.9%, 3.8% and 2.7%). For the velocity at 4m/s and 5m/s, no enhancement has been shown. Meanwhile, the pressure drop has been increased by using the heat enhancement method at 1m/s, 2m/s, 3m/s, 4m/s and 5m/s, the corresponding pressure drop increase is 145%, 102%, 69.7%, 54.3% and 42%, respectively.

In the numerical simulations, the working mechanism of heat pipes has been simplified into the pipe flow. The results of heat transfer result can't be used to represent the thermal performance of heat pipe heat exchanger in real applications. Therefore, it is improper to make the final decision whether the installation of fins on the heat pipes is beneficial to the overall system performance. Future effort needs to be made to investigate the real impact of fin designs to the flue heat exchanger based on experimental studies and numerical simulations that accommodates the real mechanisms of heat pipe.

The system performance has also been investigated experimentally with the use of cooling plates with different branch channel dimension which are purposefully designed for the cogeneration system. The comparison result of numerical and experimental studies has shown a satisfactory consistency in hydraulic and thermal performance of the three cooling plates.

It shows the larger the pumping power, the smaller the thermal resistance is. This also reflects the correlation between the flow velocity and thermal resistance that the larger the flow velocity, the smaller the thermal resistance is. The cooling plates are located in two groups. The ones with 3mm, 4mm and 5mm branch channels are in the high thermal resistance region, whilst the rest locate in the low thermal resistance region. In the higher thermal resistance region, for the same pumping power, the cooling plate with 4mm branch channel has the lowest thermal resistance with the 3mm one taking the second place and the 5mm one showing the largest thermal resistance. In the lower thermal resistance region, for the same pumping power, the cooling plate with 6 branch channels shows the lowest thermal resistance, followed by the one with 45° angle, 60° angle and 90° angle. However, the one with 45° angle has the lowest pumping power in the whole velocity range. The net energy gain of cooling plates under different Reynolds number ( $Re$  is calculated according to the main channel). The cooling plates that deliver the net energy gain in ascending order are single channel cooling plate (SC), the plate with 5mm branch channel or 8 branch channels, the plate with 45° channel angle, the plate with 60° channel angle, the plate with 4mm branch channel, the plate with 6 branch channels, the plate with 3mm branch channel and the plate with 4 branch channels, respectively.

Experimental studies have also been conducted to investigate the one-stage system and two-stage system separately to evaluate the pros/cons of the multi-stage thermoelectric cogeneration system in comparison with the one-stage system. Together with the mathematical models, it has been found that the one-stage TCS produces more power than the two-stage TCS does when the heat input is supplied at 47W and 60W. As the heat input increases, the power output of two-stage TCS gets closer to that of one-stage TCS. However, it doesn't exceed the power output of one-stage TCS in the experimental range.



Analyzing the influence to the system performance from different reproducible assembling configurations, the following conclusions can be drawn:

1. The pressure load on the thermoelectric module in the assembly has a significant impact on the performance of TCS. In the even assembly, the pressure load at 181psi gives the highest power output out of five load values: 136psi, 159psi, 181psi, 204psi and 227psi.
2. The system performance is influenced by the washer configuration. The conventional washer configuration, which uses a fibre washer, a crinkle washer (Belleville washer or spring washer) and a flat metal washer, can weaken the thermal bypass effect by reducing thermal conductance of the assembly set compared to the case of the removal of fibre washer and flat metal washer. On the other hand, the simplification of the assembly by removing the fibre washer and flat metal washer is able to enhance the thermal efficiency although the conversion efficiency has been decreased.
3. The uneven assembly affects the performance by worsening the thermal contact at the interface between the module surfaces and the heat exchanger surface and thus thermal resistance from the surface of hot side heat exchanger to the surface of the cold side heat exchanger is increased. It is essential to load even pressure on each thermoelectric module to achieve the optimal thermal contact and harmless thermal assembly.
4. In the system construction and assembly, uneven assembly can lead to about 20% drop in conversion efficiency. It shows the importance of even assembly to the electrical performance of the system.
5. In comparison with individual assembly, module thickness difference in whole assembly degrades the system conversion efficiency up to 54% when care is not taken in the module selection and installation.
6. Assembling the thermoelectric applications by torque wrench is feasible method because it can load the pressure with a reasonable accuracy and makes the assembly reproducible.

The cost recovery period of deploying this system in a residential house installed with a 24kW boiler and 1m<sup>2</sup> solar collector has been evaluated. Based on the conversion efficiency and thermal efficiency is 4% and 67% at 130°C temperature difference, the house can produce 98W electricity and 1640W useable heat when the boiler is running and the contribution from the solar energy is included. It takes less than 4.2 years to recover the system cost.

### **7.3. Future work**

This research has been looking into the issues associated with adopting the thermoelectric technology in an economically viable way by studying the single cell thermoelectric cogeneration system. This allows a better accuracy of understanding the fundamental characteristics of cogeneration system, and the factors that influence the system performance. The intention is to provide the important information for constructing the real scale system and pave the way to further work of tackling the issues in the development and integration of real scale system to onsite applications.

In section 7.1.1, the prototype that consists of 16 TEG modules, 3D printed cold side heat exchanger and boiler flue heat exchanger have been introduced. Further work needs to be conducted to investigate the performance of this real scale domestic TCS

prototype in both laboratory and onsite environment. Due to the use of 3D printed cold side heat exchanger, the system is endowed with advantages such as: light weight due to the use of ABS and lower thermal resistance due to direct contact between the coolant and cold side surface of TEG module. In order to maximize these advantages for lower cost and better performance, extra work needs to be done to push the material use of 3D printing to a lower level and modify the channel structure for a better temperature distribution on the module cold side surface. Insight also needs to be shed into the application of solar concentrator which is designed to increase the temperature level on the module hot side.

## Reference

- 
- [1]. Department of Energy and Climate Change, UK ENERGY IN BRIEF 2010, National Statistics. Available from:  
<http://www.decc.gov.uk/assets/decc/statistics/publications/brief/190-uk-energy-in-brief-2010.pdf>.
- [2]. Bass, J.C., Elsner, N.B., and Leavitt, F.A., 1995, "Performance of the 1 kW Thermoelectric Generator for Diesel Engines," 13th International Conference on Thermoelectrics, Kansas City, MO, American Institute of Physics, New York.
- [3]. K. Matsubara and M. Matsuura, 'Thermoelectric applications to vehicles' Chapter 52, Thermoelectric Handbook, Macro to Nano, CRC Press, 2005.
- [4]. Ewert, Michael K. Terrestrial and Aerospace Solar Heat Pump Development: past, present and future, ASME paper at Solar '98, Albuquerque, NM; 1998.
- [5]. D.M. Rowe, United States Thermoelectric Activities in Space, Proceedings VIII Int Conf on Thermoelectric Energy Conversion, 10-13 July 1989, Nancy, France, pp. 133-142.
- [6]. G. Bennett, Space applications Chapter 41 CRC Handbook of Thermoelectrics, Ed. D.M. Rowe, CRC Press.
- [7]. Department of Trade and Industry, Energy consumption in the United Kingdom, National statistics.
- [8]. U.S. Department of Energy, Energy Loss Reduction and Recovery in Industrial Energy Systems,  
[http://www1.eere.energy.gov/industry/intensiveprocesses/pdfs/reduction\\_roadmap.pdf](http://www1.eere.energy.gov/industry/intensiveprocesses/pdfs/reduction_roadmap.pdf).
- [9]. DM Rowe. Thermoelectric conversion of waste heat from redundant oil wells. Proceedings Mediterranean Petroleum Conf, 1992, pp.556-563.
- [10]. T. Kajikawa, I Makoto Ito, I Katsube and E Shibuya, 'Development of Thermoelectric power generation Utilising Heat of Combustible Solid Waste'. Proc. 13 Int. Con. On Thermoelectrics, Kansas City Mo. Ed B Mathiprakasam, pp314-318. 1994.
- [11]. T. Kajikawa. Thermoelectric power generation systems recovering heat from combustible solid waste in Japan. Proc. 15th Inter. Conf. On Thermoelectrics, Pasadena, USA, pp. 343-351, 1996.
- [12] Rowe, D.M., CRC Handbook of Thermoelectrics, CRC Press, 1995.
- [13] Ziman JM, Electrons and Phonons, Cambridge University Press, London.
- [14] Callen, HB, Phys. Rev., 73, 1349, 1948.
- [15] Drabble JR and Goldsmid HJ, Thermal Conduction in Semiconductors, Pergamon Press, Oxford, 1961.
- [16]. A. Killander, J. Bass. A stove-top generator for cold areas. 15th Int. Conf. on Thermoelectrics.
- [17]. D. Mastbergen, B. Willson, S. Joshi. Generating Light from Stoves using a Thermoelectric Generator,  
[http://www.vrac.iastate.edu/ethos/files/ethos2005/pdf/mastbergen\\_paper.pdf](http://www.vrac.iastate.edu/ethos/files/ethos2005/pdf/mastbergen_paper.pdf).
- [18]. R.Y. Nuwayhid, DM. Rowe , G. Min, Low cost stove-top thermoelectric generator for regions with unreliable electricity supply, Renewable Energy 28 (2003) 205-222.
- [19] K. Qiu, A.C.S. Hayden. A Natural-Gas-Fired Thermoelectric Power Generation System. Journal of ELECTRONIC MATERIALS, Vol. 38, No.7, 2009.

- 
- [20] Rowe D.M., Min G. Evaluation of thermoelectric modules for power generation. *J Power Srouces* 1998; 73:193-198.
- [21]. Bell. L., Accelerating the commercialization of promising new thermoelectric materials, *Materials Science & Technology 2008 Conference and Exhibition*, October 2008, pages 418-428.
- [22] Park, D., *Thermoelectrics Market Study*. 2008.
- [23] Bell, L.E., Addressing the challenges of commercializing new thermoelectric materials, in *International Conference on Thermoelectrics*. 2008: Corvallis, Oregon USA.
- [24]. Bell, L., *Accelerating the Commercialization of Promising New Thermoelectric Materials*, BSST LLC: Irwindale, California USA.
- [25]. Bell, L.E., Addressing the challenges of commercializing new thermoelectric materials, in *International Conference on Thermoelectrics*. 2008: Corvallis, Oregon USA.
- [26]. Mahan G., Sales B. and Sharp J., 1997, "Thermoelectric Materials: New Approaches to an Old Problem", *Physics Today*, (3)42.
- [27]. Yang R. and Chen G., *Nanostructured Thermoelectric Materials: From Superlattices to Nanocomposites*, *Materials Integration*, 2006.
- [28]. G. Chen, *Smicond. Semimetals* 71 (2001) p.203.
- [29]. B.Moyzhes and V. Nemchinsky, *Appl. Phys. Lett.* 73 (2001) p.175.
- [30]. A. Shakouri and J.E. Bowers, *Appl. Phys. Lett.* 71 (1997) p.1234.
- [31]. B. Yang, and G. Chen, *Thermal Conductivity: Theory, Properties and Applications* (Ed: T.M. Tritt), Kluwar Press (2005), pp.167-186.
- [32]. *Proc. 1st Natl. Thermogenic Cooler Workshop*, edited by S. B. Horn (Center for Night Vision and Electro-Optics, Fort Belvoir, VA, 1992).
- [33]. D. Hicks and M.S. Dresselhaus, *Phys. Rev. B* 47(1993) p.12727.
- [34]. H.Beyer, A. Lambrecht, E.Wagner, G. Bauer, H.Boettner, and J. Nurnus, *Physica E* 13 (2002) p.965.
- [35]. T.C. Harman, P. Taylor, M.P. Walsh, and B.E. LaForge, *Science* 297 (2002) p.2229.
- [36]. R. Venkatasubramanian, E. Siivola, T.Colpitts, and B. O'Quinn, *Nature* 413 (2001) p.597.
- [37]. T.C. Harman, D.L. Spears, and M.P. Walsh, *J. Electron. Mater.* Lett. 28 (1999) p. L1.
- [38]. Boettner H., Chen G. and Venkatasubramanian R., *Aspects of thin-film superlattice thermoelectric materials, device and applications*, *Mrs Bulletin*. Vol.31, March 2006.
- [39]. L.D. Hicks and M.S. Dresselhaus, *Phys. Rev. B* 47, 16631 (1993)
- [40]. G. Chen, *Phys. Rev. B* 57, 14958 (1998).
- [41]. B. Yang, and G. Chen, *Thermal Conductivity: Theory, Properties and Applications* (Ed: T.M. Tritt), Kluwar Press (2005), pp. 167-186.
- [42]. T.C. Harman, P.J. Taylor, M.P. Walsh, and B. E. LaForge, *Science* 297, 2229 (2002).
- [43] R. Venkatasubramanian, E. Silvona, T. Colpitts, and B. O'Quinn, *Nature* 413, 597 (2001).
- [44]. H. Beyer, A. Lambrecht, E. Wagner, G. Bauer, H. Böttner, and J. Nurnus, *Physica E* 13 (2002)p. 965.



- 
- [45] A. Mzerd, D. Sayah, G. Brun, J.C. Tedenac, and A. Boyer, *J. Mater. Sci. Lett.* 14 (1995) p. 194.
  - [46] A. Mzerd, D. Sayah, J.C. Tedenac, and A. Boyer, *Int. J. Electron.* 77 (1993) p. 291
  - [47] Y.A. Boikov, V.A. Danilov, T. Claeson, and D. Erts, in *Proc. ICT'97* (IEEE, New York, 1997) p. 89.
  - [48] R. Venkatasubramanian, T. Colpitts, B. O'Quinn, M. Lamvik, and N. El-Masry, *Appl. Phys. Lett.* 75 (1999) p. 1104.
  - [49] H. Zou, M. Rowe, and G. Min, in *Proc. ICT'00* (IEEE, Piscataway, NJ, 2002) p. 251.
  - [50] L.W. Da Silva, M. Kaviani, A. DeHennis, and J.S. Dyck, in *Proc. ICT'03* (IEEE, Piscataway, NJ, 2003) p. 665.
  - [51] XIE Zhen, YANG Junyou, etc. *Progress in Wet Chemical Synthesis of Bi<sub>2</sub>Te<sub>3</sub> Based Thermoelectric Nanomaterials*. *Material Review*, 2002, 11 (20), VII:33-35.
  - [52] Sano S., Mizukami H., Kaibe H., *Development of High-Efficiency Thermoelectric Power Generation System*, KOMAI'SU TECHNICAL REPORT, 2003 vol.49 No.152.
  - [53] Fleurial, J. -P., A. Borshchevsky, and T. Caillat (1997a) "New Thermoelectric Materials and Devices for Terrestrial Power Generators", in *Proceedings of the 1st Conference on Synergistic Power and Propulsion Systems Technology*, M.S. El-Genk editor, American Institute of Physics, New York, AIP Conf. Proc. No. 387, 1:293-298.
  - [54] Swanson, B. W., E.V. Somers, and R.R. Heikes (1961) "Optimization of a Sandwiched Thermoelectric Device", *Journal of Heat Transfer*, 77-82.
  - [55] Fleurial J., Borshchevsky A., Caillat T., and Ewell R., *New Materials and Devices for Thermoelectrics applications*, IECEC-97.
  - [56] Kat suyama S, Kanayama Y, Ito M, et al. *J Appl Phys*, 2000, 88 :3484
  - [57] G. Chen, D. Borca-Tasciuc, and R.G. Yang, "Nanoscale Heat Transfer" in *"Encyclopedia of Nanoscience and Nanotechnology"*, eds. H.S. Nalwa, American Scientific Publishers (2004), Vol.7, pp. 429-459.
  - [58] Worlock J M. *Phys Rev*, 1996, 147 :636
  - [59] Vining C B. *Mater Res Soc Symp Proc*, 1991, 234 :95
  - [60] G. Chen, *Semiconductors and Semimetals* 71, 2003 (2001).
  - [61] R.G., Yang and G. Chen, *Phys. Rev. B* 69, 195316 (2004).
  - [62] Hicks L D, et al. *Phys Rev B*, 1993, 47 (19) :12727
  - [63] Heremans J, et al. *Phys Rev B*, 1999, 59 (19) :12579
  - [64] Behnke J F, Prieto A M. 18th International Conference on Thermoelectric USA : IEEE, 1999. 451
  - [65] Yong Peng, et al. *Mater Sci Eng*, 2000, B77 :246
  - [66] Prieto A M, Sander M S, Stacy A M. International Symposium on Circuits and Systems, 2001, 4 :Z1411
  - [67] Wang Wei. *J Inorganic Mater*, 2004, 19 :127
  - [68] Huber T E, Onakoya O. *J Appl Phys*, 2002, 92 (3) :1337
  - [69] Dresselhaus M S, Lin Y M. 18th International Conference on Thermoelectric USA : IEEE, 1999. 92
  - [70] Cronin S B, Lin Y M, Koga T, et al. 18th International Conference on Thermoelectrics, 1999. 554

- 
- [71] J i X H , Zhao X B , et al. 23rd International Conference on Thermoelect ric , Aust ralia , 2004
- [72] Tritt T M. Science , 1999 ,283 :804
- [73] Hillhouse H W, Tuominen M T. Microporous Mesoporous Mater , 2001 ,47 :39
- [74]. Yadav A, Pipe KP, Shtein M. Fiber-based flexible thermoelectric power generator. J Power Sources 2008; 175: 909-913.
- [75] Min G, Rowe DM, Ring-structured thermoelectric module, Semicond Sci Technol 2007; 22: 880-883.
- [76]. Lofy, J., & Bell, L.E., Paper presented at the 21st International Conference on Thermoelectrics, Long Beach, CA, 25-29 August 2002.
- [77] Bell, L. E., Broader Use of Thermoelectrics Systems in Vehicles, Proceedings of the 1st Thermoelectric IAV Conference, Berlin, Germany, October 2008.
- [78]. Fairbanks J. Thermoelectric application in vehicles of status 2008, available from:  
<http://ect2008.icmpe.cnrs.fr/Contributions/0-PL-00-Fairbanks.pdf>
- [79]. Lon E. Bell, Broader Use of Thermoelectric Systems in Vehicles, 1st Thermoelectric IAV Conference (23-24 October 2008, Berlin)
- [80]. Nihal Fatma Gueler, Rasit Ahiska, Design and testing of a microprocessor-controlled portable thermoelectric medial cooling kit, Applied Thermal Engineering 22 (2002) 1271-1276.
- [81]. Stephen L. Coffee. Thermoelectric cooler and warmer for food. U.S. Patent, Oct. 27, 1998, D400053.
- [82]. David Joseph Najewicz. Thermoelectric icemaker and control. U.S. Patent, May 18, 2004, 6735959.
- [83]. R.H. Redus et al., Improved thermoelectrically cooled X/  $\gamma$  -ray detectors and electrobnics, Nuclear Instruments and Methods in Physics Research SectionA: Accelerators, Spectrometers, Detectors and Associated Equipment 458 (2001) 214-219.
- [84]. G. Bale et al., Cooled CdZnTe detectors for X-ray astronomy, Nuclear Instruments and Methods in Physics Research Section A: Accelerators, Spectrometers, Detectors and Associated Equipment 436 (1999) 150–154.
- [85]. M.K. Scruggs et al., Thermal-electrically cooled photodetector, United States Patent Application, 20010032922, kind code, A1, October 25, 2001
- [86]. Mark Najarian and Erik Garnett, Thermoelectrics and Photovoltaics: Integration Challenges and Benefits, MSE 226, 12/13/06.
- [87] LaGrandeur J, Crane D, Eder A. Vehicle fuel economy improvement through thermoelectric waste heat recovery. Available at:  
<http://mediag.com/preview/bsst/121109/pdfs/LaGrandeur.Vehicle%20Fuel%20Economy%20Improvement%20through%20TE%20Waste%20Heat%20Recovery.DEER2005.pdf>
- [88]. John LaGrandeur, Doug Crane, Andreas Eder, Vehicle Fuel Economy Improvement through thermoelectric Waste Heat Recovery, 2005 DEER Conference.
- [89]. J.L. Creveling, A thermoelectric generator to use waste heat, US Patent No 1118269, 1914.
- [90]. Birkholz, E. Grob, U. Stohrer and K. Voss, Conversion of waste exhaust heat in automobiles using FeSi<sub>2</sub> thermoelements, Proceedings of 7th International

- Conference on Thermoelectric energy conversion, University of Texas, March 16-18 1988, pp.124-128
- [91]. Bass, J.C., Elsner, N.B., and Leavitt, F.A., 195, "Performance of the 1 kW Thermoelectric Generator for Diesel Engines," 13th International Conference on Thermoelectrics, Kansas City, MO, American Institute of Physics, New York.
- [92]. Birkholz, U., Grob, E., Strohrer, U., Voss, K., Gruden, D.O., and Wurster, W., 1988, "Conversion of Waste Exhaust Heat in Automobiles Using FeSi<sub>2</sub> Thermoelements," Seventh International Conference on Thermoelectric Energy Conversion, University of Texas at Arlington, Arlington, TX.
- [93]. Embry, B.L., and Tudor, J.R., 1968, "A Thermoelectric Generator Powered by Engine Exhaust Heat," Intersociety Energy Conversion Engineering Conference, Boulder, CO, IEEE, New York.
- [94]. Menchen, W.R., Osmeyer, W.E., and McAlonan, M., 1990, "Thermoelectric Conversion to Recover Heavy Duty Diesel Exhaust Energy," Society of Automotive Engineers Proceedings of the Annual Automotive Technology Development Contractors' Meeting, Dearborn, MI, SAE, Warrendale, PA.
- [95]. K. Matsubara, Proc. 15th Int. Conf. Thermoelectrics, Ed. T. Caillat, CA, pp. 418, 2002.
- [96]. K. Matsubara and M. Matsuura, 'Thermoelectric applications to vehicles' Chapter 52, Thermoelectric Handbook, Macro to Nano, CRC Press, 2005.
- [97]. Rowe, D.M., Review thermoelectric waste heat recovery as a renewable energy source, International Journal of Innovations in Energy Systems and Power, Vol.1, No.1(2006).
- [ 98 ]. J.C. Bass, R.J. Campana and N.B. Elsner, Proc 10th Int. Conf. on Thermoelectrics, Ed. Rowe D.M. UK pp.127, 1991
- [99]. J. Bass, N.B. Elsner and F.A. Leavitt, Proc. 13th Int.Conf. Thermoelectrics, Ed. Mathiprakisam B., AIP Conf. Proc New York, pp. 295 1995.
- [ 100 ]. K. Matsuura and D.M. Rowe, 'Thermoelectricity to hydrogen energy conversion for waste heat recovery' Proc Third European Workshop on Thermoelectrics Sept 16-17 1996, Cardiff UK, pp. 22-27, ISBN 0-9519286-3-5
- [101]. Eder, A., et. al. Vision of Possible Thermoelectrics for Vehicle Application, in DOE/EPRI High Efficiency Thermoelectrics Wrokshop, 2004. San Diego.
- [ 102 ]. E. Takanase and H. Tamakoshi,, 'The development of thermoelectric generator for passenger car' Proc 12th Int Conf Thermoelectrics, Ed. Matsuura K., pp. 46 1994.
- [103]. K. Ikoma, M. Munkiyo, K. Furuiya, M. Koyayashi, H. Komatsu and K.J. Shinohara, 'Thermoelectric generator for gasoline engine using Bi<sub>2</sub>Te<sub>3</sub> modules', Japan Inst. Metals, 63 (11), 1475, 1999.
- [104]. LaGrandeur, J., Crane, D., and Eder, A., Vehicle fuel economy improvement through thermoelectric waste heat recovery, DEER Conference, Chicago, IL, August 25, 2005.
- [105]. Ewert, Michael K. Terrestrial and Aerospace Solar Heat Pump Development: past, present and future, ASME paper at Solar '98, Albuquerque, NM; 1998.
- [106]. Department of Trade and Industry of National Statistics, Energy Consumption in the United Kingdom, UK.
- [107] U.S. Department of Energy, Energy Loss Reduction and Recovery in Industrial Energy Systems,  
[http://www1.eere.energy.gov/industry/intensiveprocesses/pdfs/reduction\\_roadmap.pdf](http://www1.eere.energy.gov/industry/intensiveprocesses/pdfs/reduction_roadmap.pdf).

- [108]. Thierry Caillat, Jean-pierre Fleurial and Alex Borshchevsky, Development of high efficiency thermoelectric generators using advanced thermoelectric materials, <http://hdl.handle.net/2014/23015>.
- [109]. Rowe, D.M., An introduction to thermoelectric energy conversion and an assessment of its potential for the large scale recovery of waste heat', Pub. Babrow Press, ISBN 0951 9286, 19, pp.1-35.
- [110]. Rowe, D.M., 'Thermoelectric conversion of waste heat from redundant oil wells', Proceedings Mediterranean Petroleum Conference, 19-22 Jan. Tripoli, Libya, 1992, pp.556-563.
- [111]. T. Kajikawa, I Makoto Ito, I Katsube and E Shibuya, 'Development of Thermoelectric power generation Utilising Heat of Combustible Solid Waste'. Proc. 13 Int. Con. On Thermoelectrics , Kansas City Mo. Ed B Mathiprakasam, pp314-318. 1994.
- [ 112 ]. Takenobu Kajikawa, Tsujido nishikaigan, Fujisawa Kanagawa, Thermoelectric power generation systems recovering heat from combustible solid waste in Japan, 15th International Conference on Thermoelectrics.
- [113]. T. Kajikawa, 'Thermoelectric power generation systems recovering heat from combustible solid waste in Japan' Proc. 15th Int Conf. On Thermoelectrics, Pasadena, USA, pp. 343-351, 1996.
- [114]. Naughton, A. G., 1995 "Commercially Available Generators," in CRC Handbook of Thermoelectrics, CRC Press, 459.
- [115]. F. Volklein, V.Baier, U. Dillner, E.Kessler, Thin solid films 187 (1990) 253.
- [116]. A. Lopez-Otero, Thin solid films 49 (1978) 1.
- [117]. H. Noro, K. Sato, H. Kagechika, J. Appl. Phys. 73 (1993) 1252.
- [118]. A. Giani, F. Pascal-Delannoy, A. Boyer, A. Foucaran, M. Gschwind, P. Ancy, Thin Solid Films 303 (1997) 817.
- [119]. A. Boyer, E. Cisse, Mater. Sci. Eng. B 13 (1992) 103.
- [120]. Helin Zou, D.M.Rowe, Gao Min, Growth of p- and n-type bismuth telluride thin films by co-evaporation, Journal of Crystal Growth 222 (2001) 82-87.
- [121]. A.F. Ioffe, Semiconductor Thermoelements and Thermoelectric Cooling, Infosearch, London, 1957.
- [122]. Creveling JL. A thermoelectric generator to use waste heat, US Patent No 1118269, 1914.
- [123]. James W. Stevens, Optimal design of small delta T thermoelectric generation systems, Energy Conversion and Management 42 (2001) 709-720.
- [124] Department of Trade and Industry, Energy consumption in the United Kingdom, National statistics, July 2002. Available from: <http://webarchive.nationalarchives.gov.uk/+http://www.berr.gov.uk/files/file11250.pdf>.
- [125].J. Thurlwell, C. Davis, S. Mohamed, British Gas Home Energy Report 2011, An assessment of the drivers of domestic natural gas consumption Available from [https://www.centrica.com/files/pdf/BG\\_Home\\_Energy\\_Report\\_110202.pdf](https://www.centrica.com/files/pdf/BG_Home_Energy_Report_110202.pdf)
- [126]. M. Suri, T.A. Huld, E. Dunlop, H.A. Ossenbrink. Potential of solar electricity generation in the European Union member states and candidate countries. Solar Energy 81 (2007) 1295-1305.
- [127] Che DF, Liu YH, Gao CY. Evaluation of retrofitting a conventional natural gas fired boiler into a condensing boiler. Energy Conversion and Management 45(2004) 3251-3266.



- [128]. Department of Trade and Industry of National Statistics, Energy Consumption in the United Kingdom, UK.
- [129]Anozie AN, Bakare AR, Sonibare JA, Oyebisi TO. Evaluation of cooking energy cost, efficiency, impact on air pollution and policy in Nigeria. *Energy*. 2007;32:1283–90.
- [130] D.Champier et al. Thermoelectric power generation from biomass cook stoves. *Energy* 35 (2010) 935-942.
- [131] K.Qiu, A.C.S. Hayden. Development of a thermoelectric self-powered residential heating system. *Journal of Power Sources* 180 (2008) 884-889.
- [132] R. Schuitema, N.C. Sijp heer, E.J. Bakker. Energy performance of a drainwater heat recovery system. Proc of the CIBAT conference, Lausanne 2005. Available from:  
<http://www.ecn.nl/docs/library/report/2005/rx05178.pdf>
- [133] Liu L.B, Fu L., Jiang Y. Application of an exhaust heat recovery system for domestic hot water. *Journal of Energy*, volume 35, issue 3, March 2010, pages 1476-1481.
- [134] Baek, N.C. A study on the design and analysis of a heat pump heating system using waste water as a heat source.
- [135] KIER. Feasibility study on heat pump system using waster thermal hot water as a heat source. Deajeon: Korea Institute of Energy Research (2001) [Internal report]
- [136]. Nuwayhid R.Y., Rowe D.M., Min G., Low cost stove top thermoelectric generator for regions with unreliable electricity supply. *Renewable Energy* 2003; 28:205-222.
- [137] D.T. Allen, W.C. Mallon. Further development of “self-powered boilers”. 18th International Conference on Thermoelectrics (1999).
- [138] D.T. Allen, J. Wonsowski. Thermoelectric self-powered hydronic heating demonstration. 16<sup>th</sup> International Conference on Thermoelectrics (1997).
- [139]. Rowe DM. Thermoelectric waste heat recovery as a renewable energy source. *Int J Innov Energy System Power* 2006; 1: 13-23
- [140] Marcel Suri, Thomas A. Huld, Ewan D. Dunlop, Heinz A. Ossenbrink, Potential of solar electricity generation in the European Union member states and candidate countries, *Solar Energy* 81 (2007) 1295-1305.
- [141] J. Caillat, T., Fleurial, J.P. and Borshchevsky, A., Development of high efficiency thermoelectric generators using advanced thermoelectric materials, Albuquerque, New Mexico, USA.
- [142] Zheng XF, Yan YY, Simpson K. A potential candidate for the sustainable and reliable domestic energy generation-Thermoelectric cogeneration system. *Applied Thermal Engineering* (2012), doi:10.1016/j.applthermaleng.2012.03.020.
- [143] L.D. Shorrock, J.I. Utley. Domestic energy fact file 2003. BRE Housing Centre. Available from : <http://projects.bre.co.uk/factfile/BR457prtnew.pdf>.
- [144] Ralph L.W. and Nae-Hyun K., 2005. Principles of Enhanced Heat Transfer (Second Edition). Taylor & Francis Group.
- [145] Braucer. H., 1964. Compact heat exchanger, *Chem. Prog. Symp. Ser.*, No.41, 59, 1-10.
- [146] Rabas, T.J. and Huber, F.V., 1989. Row number effects on the heat transfer performance of inline finned tube banks, *Heat Transfer Eng.*, 10(4), 19-29.
- [147] L.D Shorrock, J.I Utley. Domestic energy fact file 2003.

---

Available from: <https://www.breem.org/filelibrary/pdf/rpts/BR457prtnew.pdf>

- [148] Zumdahl, Steven S. (2005). Chemical Principles (5th Edition ed.). Houghton Mifflin College Division. ISBN 0-618-37206-7.
- [149] B. Zohuri. Heat Pipe Design and Technology-A Practical Approach. CRC Press, Taylor and Francis Group, 2011.
- [150] Fritz JD, Grubb JF, Polinski RE. Choosing the right material: Reactive metals versus stainless steels or nickel alloys. Available from: <http://www.atimetals.com/businesses/business-units/wahchang/Documents/Tech-Serv-Library/1999-Conf-Proceedings/1999027.pdf>
- [151] Mastbergen D. *et al* 2005 Producing Light from Stoves using a Thermoelectric Generator, available from: [http://www.vrac.iastate.edu/ethos/files/ethos2005/pdf/mastbergen\\_paper.pdf](http://www.vrac.iastate.edu/ethos/files/ethos2005/pdf/mastbergen_paper.pdf).
- [152] Nuwayhid R.Y. *et al* 2003 Low cost stove-top thermoelectric generator for regions with unreliable electricity supply, *Renewable Energy* 28 205–222.
- [153] Champier D. *et al* 2010 Thermoelectric power generation from biomass cook stoves. *Energy* 35 935-942.
- [154] Nuwayhid R.Y. *et al* 2005 Design and testing of a locally made loop-type thermosyphonic heat sink for stove-top thermoelectric generators *Renewable Energy* 30 1101-1116.
- [155] X F Zheng *et al* 2012 *J. Phys.: Conf. Ser.* 395 012062;
- [156] Khan WA, Culham JR, Yovanivich MM. Optimization of microchannel heat sinks using entropy generation minimization method. *IEEE Transactions on Components and Packaging Technologies* 32 (2009) 243-251.
- [157] W.M. Kays and A. L. London. Compact Heat Exchangers, The National Press, Palo Alto, CA, 1964.
- [158] Steudle E. Water transport across plant tissue: Role of water channels. *Biology of the Cell* (1997) 89, 259-273.
- [159] C.Y. Yang, C.T. Yeh, W.C. Liu. Advanced Micro-Heat Exchangers for High Heat Flux. *Heat Transfer Engineering*, 28 (8-9): 788-794, 2007.
- [160] J. Eakburanawat, I. Boonyaroonate. Development of a thermoelectric battery-charger with microcontroller-based maximum power point tracking technique. *Applied Energy* (2006) Volume: 83, Issue:7, Pages: 687-704.
- [161] Anders Killander, John C Bass. A stove-top generator for cold areas. In: *Proceedings of the IEEE 15<sup>th</sup> international conference on thermoelectrics*; 1996. p. 390–393.
- [162] Mahmudur R, Roger S. Thermoelectric power-generation for battery charging. In: *Proceedings of the IEEE conference on energy management and power delivery*, vol. 1; 1995. p. 186–191.
- [163] Roth W, *et al*. Grid-independent power-supply for repeaters in mobile radio networks using photovoltaic/thermoelectric hybrid systems. In *Proceedings of the 16th international conference on thermoelectrics*; 1997.p. 582–585.
- [164] Koutroulis Eftichios, Kalaitzakis Kostas, Voulgaris NC. Development of a microcontroller-based, photovoltaicmaximum power point tracking control system. *IEEE Trans Power Electron* 2003;16(1):717–24. 46–54,2001.
- [165] Laired technology. Thermoelectric handbook. Available from: <http://www.knap.at/datenblaetter/pel/assembling-lapped-te.pdf>

- 
- [166] M. Suri, T.A. Huld, E. Dunlop, H.A. Ossenbrink. Potential of solar electricity generation in the European Union member states and candidate countries. *Solar Energy* 81 (2007) 1295-1305.
- [167] Cralley LJ, Cralley LV. *Patty's industrial hygiene and toxicology*. 1985, 2nd ed. Vol.3. New York, NY: John Wiley and Sons.
- [168] NJDH [1985]. Hazardous substance fact sheet: bismuth telluride. Trenton, NJ: New Jersey Department of Health.
- [169] U.S. Department of Health and Human Services. Occupational safety and health guideline for bismuth telluride, undoped, available at:  
<http://www.cdc.gov/niosh/docs/81-123/pdfs/0056.pdf>